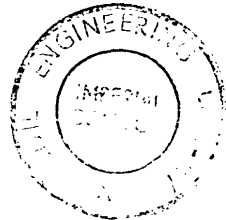


Thesis submitted for the Ph.D. degree in
the Faculty of Engineering of the
University of London.

FLOW IN NESTS

OF

TUBES.



R.Pendennis Wallis, M.Sc.,
King's College, London.

October 1937.

FLOW IN NESTS OF TUBES.

CONTENTS

BRIEF ACCOUNT OF RESEARCH AND RESULTS.

SCOPE AND AIM OF THE RESEARCH.

LIST OF SYMBOLS.

1. INVESTIGATION OF THE HYDRAULIC RESISTANCE OF NESTS.
 - 1.1 Description of the nest of tubes.
 - 1.2 Method and result of testing with water.
 - 1.3 Method and result of testing with air.
 - 1.4 Comparison between results with water and with air.
 - 1.5 Analysis of total resistance, - relative importance of the various rows of tubes.
 - 1.6 Alternative method of expressing resistance of nest.
 - 1.7 Comparison with the results of previous investigators.

Contents

(Continued)

2. INVESTIGATION OF THE LACK OF SYMMETRY OF FLOW
OBSERVED IN STAGGERED NEST.
 - 2.1 Discovery of asymmetry during experiments with
water.
 - 2.2 Asymmetry of the form drag diagrams.
 - 2.3 Asymmetrical polar diagrams.
 - 2.4 Asymmetry unchanged by reversal of nest.
 - 2.5 Asymmetrical flow with air.
 - 2.6 General conclusions with regard to instability
of staggered nests.

3. MEASUREMENT OF VELOCITY DISTRIBUTION ON A CROSS
SECTION BETWEEN 1st AND 2nd ROWS OF TUBES WITH
RECTANGULAR SPACING OF TUBES. PITOT TUBE
CHARACTERISTICS.
 - 3.1 Type of Pitot tube used and total energy curves
obtained.
 - 3.2 Search for a suitable static tube.
 - 3.3 Transverse velocity distribution. - Apparent
lateral shift of Pitot tube.

Contents
(Continued)

4. MEASUREMENT OF THE LONGITUDINAL VELOCITY
DISTRIBUTION THROUGH THE NEST.
 - 4.1 Type of static tube used.
 - 4.2 Description of improved Pitot-static tube.
 - 4.3 The observed longitudinal variation of velocity.

5. INVESTIGATION OF THE FORM DRAG OF THE INDIVIDUAL
TUBES.
 - 5.1 Aim of the investigation.
 - 5.2 Experimental arrangements and typical results of
form drag investigations.
 - 5.3 Anomalous behaviour of front of second row of
tubes.
 - 5.4 The effect of variation of air speed on the mean
ordinate of the form drag curves.
 - 5.5 Relation between "central ordinate" and "mean
ordinate" of form drag diagrams.
 - 5.6 Mean ordinates of form drag curves.
 - 5.7 Estimate of the relation between form drag and
total drag.
 - 5.8 The effect of initial turbulence in the air stream.
 - 5.9 Connection between tangential drag and heat transfer.

Contents

(Continued.)

6. EXPERIMENTS IN ORDER TO MAKE THE AIR FLOW VISIBLE.
 - 6.1 Design of transparent box.
 - 6.2 Experiments with low air speed.
 - 6.3 Experiments with high air speed.

7. EXPERIMENTS IN THE AHLBORN TANK. PHOTOGRAPHS OF TYPICAL FLOW PATTERNS.
 - 7.1 Description of the tank and method of use.
 - 7.2 Investigation to determine the reliability of the results and the range of usefulness of such experiments.
 - 7.21 Indications of general flow pattern. Surface tension ripples restrict range to below $R_e = 2,000$.
 - 7.22 Experiments with a single cylinder.
 - 7.23 Flow pattern at bottom of tank.
 - 7.24 Surface tension effects caused by temperature differences.
 - 7.3 Flow pattern with various arrangements of groups of tubes.
 - 7.4 Flow pattern as seen by observer moving relative to nest.
 - 7.5 Analysis of individual eddies.
 - 7.6 Determination of the velocity in eddies between successive rows of tubes.

Contents

(Continued)

- 7.
 - 7.7 Diffusion from the surface of a cylinder.
 - 7.8 General conclusions of the effects of longitudinal and transverse spacing on the flow pattern.
 - 7.9 The formation and dissipation of eddies.
 - 7.91 Formation of eddies.
 - 7.92 Dissipation of eddies.

- 8. EXPERIMENTS WITH THE ELECTRIC TRAY.
 - 8.1 Analogy between frictionless fluid flow and electric flow.
 - 8.2 Description of apparatus.
 - 8.3 Verification of the method.
 - 8.4 Velocity distribution across the tray at a distance of 1.3 tube diameters upstream.
 - 8.5 Representation of fluid with friction.
 - 8.6 Velocity at the tube surface.
 - 8.7 Estimation of the effective thickness of the boundary layer.
 - 8.8 Distribution of velocity in the boundary layer and the tangential drag.
 - 8.81 Velocity distribution in boundary layer in gap of nest of tubes.

Contents

(Continued)

- 8. 8.82 Comparison with the velocity distribution for
 an isolated cylinder.
- 8.83 Variation of thickness of the boundary layer.
- 8.84 Total drag up to point of breakaway.
- 8.9 Summary of results of the electric tray.

- 9. INTERPRETATION OF RESULTS AND EXPOSITION OF FLOW
 PATTERN OF PARALLEL ARRANGEMENT.
- 9.1 Analysis of form drag diagrams for first row of
 tubes.
- 9.2 The dispersion of the stream after passing through
 the gap.
- 9.3 Comparison of the shape of form drag diagrams for
 the subsequent rows of tubes.
- 9.4 Pressure recovery after the constrictions and the
 point of breakaway.
- 9.5 Form drag diagrams in their relation to each other.
- 9.51 Distribution of kinetic energy through the nest.
- 9.52 Estimation of the velocity in the eddies at the
 rear of the tubes.
- 9.53 Recovery of pressure after passing the last row
 of tubes.

Contents

(Continued)

9.
 - 9.6 Dissipation of energy in the dead water region.
 - 9.7 Shear stresses on the dead water region.

10. INTERPRETATION OF RESULTS OF THE STAGGERED
ARRANGEMENT AND COMPARISON OF THE TWO ARRANGEMENTS.
 - 10.1 Comparison of form drag diagrams.
 - 10.2 Loss of energy throughout the nest.
 - 10.3 Estimation of the tangential drag for the staggered
nest.
 - 10.4 Effect of speed on form drag diagram.
 - 10.5 Comparison of the form drag resistance of the first
row of tubes with that of a single cylinder in a
wind tunnel.
 - 10.6 Influence of speed on the later rows.
 - 10.7 Comparison between later rows in parallel and
staggered arrangements.

11. CONFIRMATION THAT THE REYNOLDS' NUMBER CHOSEN FOR
THE MAJOR PORTION OF THE EXPERIMENTS WAS NOT A
CRITICAL NUMBER.
 - 11.1 Considerations necessary to confirm that the
experiments and results are of a general nature.

Contents

(Continued)

- 11.
 - 11.2 Form drags on the fourth row of tubes at varying air speeds - parallel arrangement.
 - 11.3 Form drags on the sixth row of tubes at varying air speeds - staggered arrangement.

- 12. THE DEPOSITION OF SOLIDS ON THE OUTSIDE OF THE TUBES.
 - 12.1 Position of dust deposits and explanation of the cause.
 - 12.2 Experiments with the deposition of soot.

REVIEW

APPENDICES.

- No.1. Effect of changes of atmospheric temperature, pressure and humidity. (Section 1.3)
- No.2. Pressure registered by a cylindrical Pitot when placed at an angle to the direction of flow. (Section 3.2)
- No.3 Flow of an inviscid fluid between pairs of cylinders. (Section 8.3).
- No.4 Estimation of the thickness of the boundary layer (Section 8.7).

Contents

(Continued)

Appendices (Continued).

No.5. Calculation of theoretical position of breakaway
from the pressure recovery at the rear of a tube.

(Section 9.3).

TABLES.

BIBLIOGRAPHY.

INDEX.

FLOW IN NESTS OF TUBES

BRIEF ACCOUNT OF RESEARCH AND RESULTS

Experiments were carried out with nests of cylindrical tubes arranged in rectangular and staggered formation.

Curves showing the variation of total resistance of a nest with varying velocities were obtained for the flow of air and of water. By the aid of specially designed Pitot tubes the hydraulic loss through a nest was explored and curves were obtained showing the longitudinal and transverse distribution of velocity of the fluid between rows of tubes. The pressure distribution at the surface of several of the tubes was determined and the form drag on tubes of various rows compared. From these curves an estimate of the total form drag was obtained and this is compared with the total hydraulic resistance.

In some of the experiments a transparent box with the air flow coloured with smoke was used to study the formation of eddies at the back of the tubes and the general flow pattern of the fluid stream between the tubes. These results were confirmed and studied in greater detail with the aid of an Ahlborn tank using aluminium dust as an

indicator. By the latter method the effect of rectangular and staggered arrangements of tubes was studied and the effect of variation of spacing of the tubes explored. An insight into the nature of the eddying motion was derived and in one case the difference of using tubes of elliptical instead of circular cross-section was examined.

The theoretical velocity distribution of the fluid as it converged between the first row of tubes was investigated. This was carried out in a shallow electric tray with a uniform drop of E.M.F. from one end to the other. Large discs of paraffin wax were used to represent the tubes and the longitudinal and transverse velocity distributions in the gap were ascertained.

The results were correlated with the work of other investigators in the various problems encountered.

SCOPE AND AIM OF THE RESEARCH

The research was carried out in the Engineering Laboratories of King's College, Strand, and The City and Guilds, Imperial College of Science and Technology, South Kensington, from 1931 to 1936. The work was carried out under the guidance and with the collaboration of Dr.C.Masey White.

The object of the research was to investigate the flow of fluid over the outside of tubes arranged in a nest; to determine the distribution of the velocities and hydraulic losses and to ascertain the effect of variation of spacing of the tubes. It was also desired to obtain some knowledge of the "flow pattern" of the fluid as it traversed between and around the tubes and to gain some insight into the structure of the eddies formed at the back of the tubes.

The field covered has a bearing on the design of nests of tubes used for the transfer of heat. The data obtained should be of assistance in striking that compromise between excessive pumping losses on the one hand and high intensity of heat transfer on the other, which is so essential in most heat transfer plant. Further, the information, particularly that regarding the flow pattern, may be suggestive in the design of plant for air and flue gas purification by film washing and in the control of soot deposition.

The experimental work falls naturally into three sections:

- (a) Exploration of static pressure and total energy with the aid of Pitot tubes.
- (b) Efforts to render the flow visible: examination of the eddies through the walls of a celluloid box and investigation of eddies and the determination of flow pattern in an Ahlborn tank.
- (c) Determination of the longitudinal and transverse velocity distribution of the fluid as it converged between the first row of tubes. This was carried out in a shallow electric tray.

As far as possible the simpler deductions and conclusions from the experimental data are given immediately following the data, but a great deal of the more general discussions is based upon the whole of the experimental evidence and so appears in later sections.

To facilitate cross references from section to section, the decimal system of paragraphing is used. All diagrams and tables are numbered in a matter similar to the paragraph in which they are first mentioned, the diagrams appearing in the text while the various tables are placed together at the end of the thesis.

List of symbols.

A list of symbols is given together with the dimensions in c.g.s. units.

Appendices.

Explanatory work which would distract from the main theme has been relegated to appendices.

Bibliography.

A bibliography of the outstanding literature on the subject is included. This is arranged alphabetically under a subject index, the simpler treatments of the subject being mentioned first.

Index.

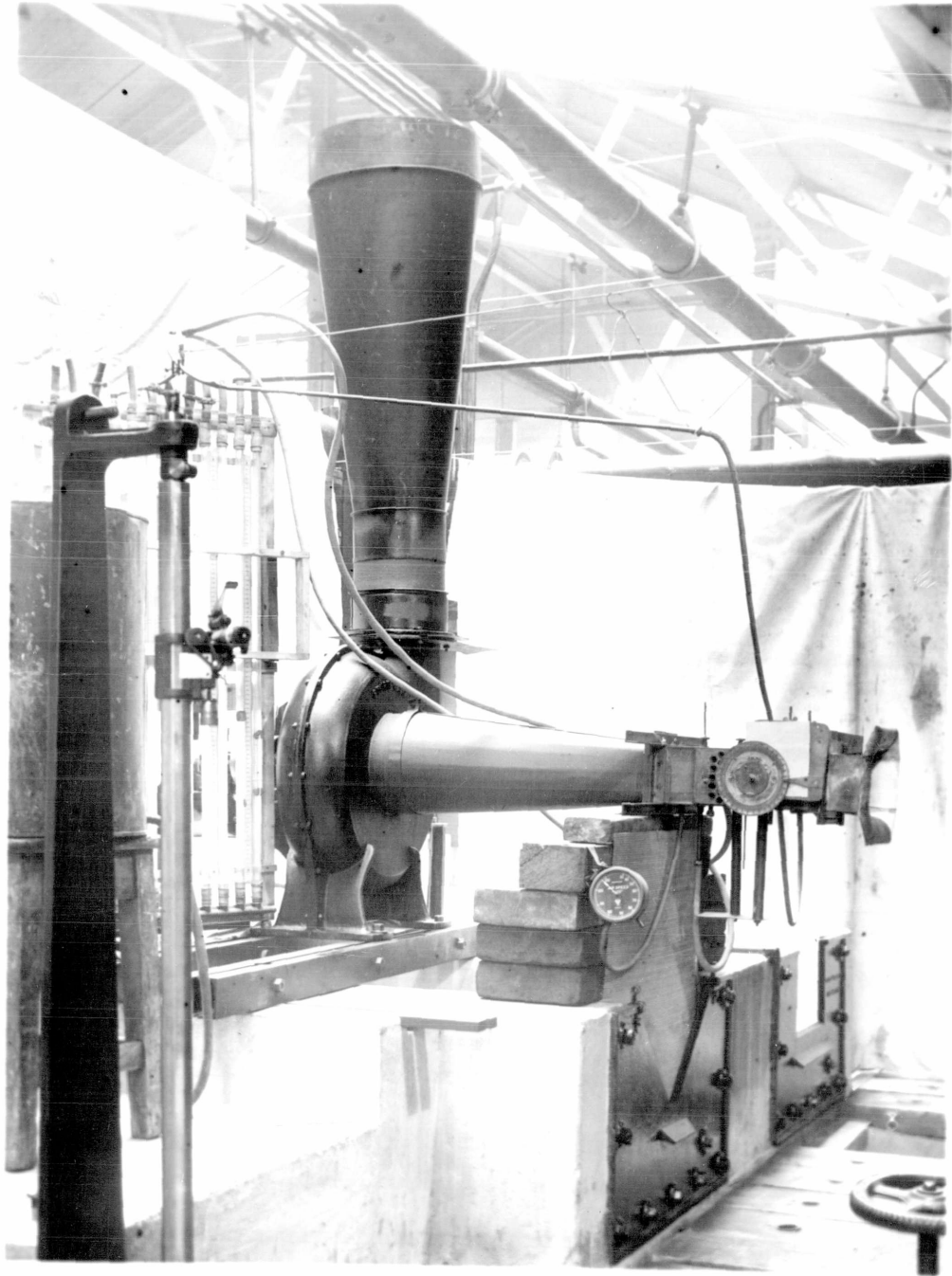
The work finishes with a brief index.

LIST OF SYMBOLS

- A = area - Cms²
- a = distance of P₁ from K₁ - Cms
- b = " " P₁ " K₂ - Cms Appendix No.3
- B = Length shown on figure Appendix No.5 - Cms.
- C (Chezy formula) = a friction coefficient-Cms^{1/2} Sec.⁻¹
- C = a dimensionless turbulence coefficient defined by
 $\ell = C \times$ where ℓ is Prandtl's "mischungsweg"
- c = $\frac{P}{\rho V_{N,max}^2}$ coefficient of resistance - dimensionless. Identical with $\frac{P}{\rho V_{N,max}^2}$ the average form drag coefficient.
- d = diameter of tube (1.27 Cms. for tubes in the nest)
- d_i = internal diameter of standard Pitot - Cms
- d_o = external " " " " - Cms Section 3.3
- G = length of gap = 0.648 Cm.
- g = acceleration due to gravity - Cms Sec.⁻²
- H_g = barometric pressure in inches of mercury
- h = head of water - Cms.
- i (Chezy formula) = energy slope-dimensionless.
- K = circulation - Cms.² Sec.⁻¹
- l = length of tubes 15.24 Cms.
- l = Prandtl's Mischungsweg - Cms.
- m (Chezy formula) = hydraulic mean depth - Cms.
- n = number of tubes in nest 24 for parallel arrangement
42 " staggered "

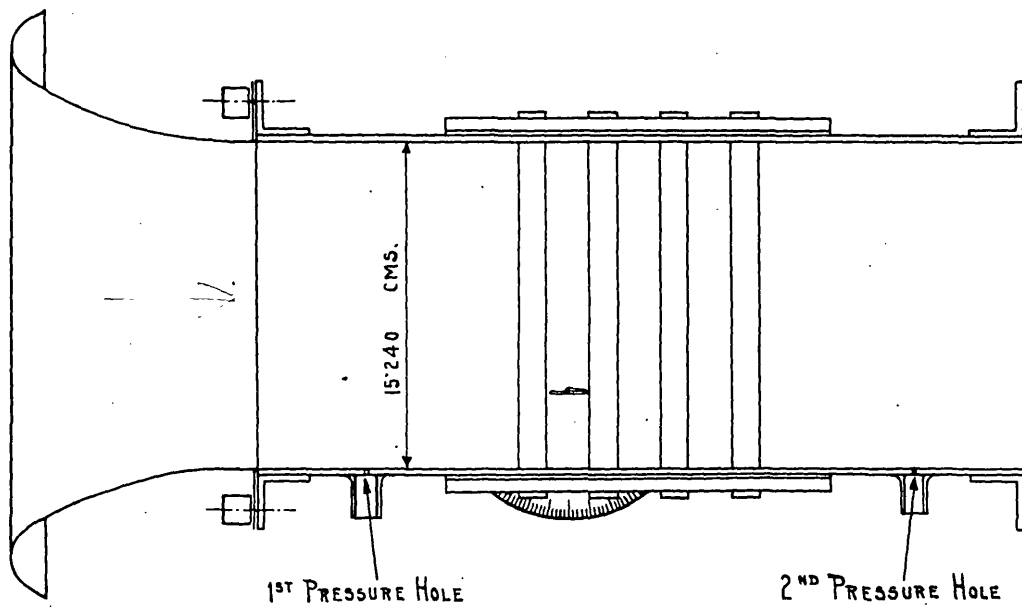
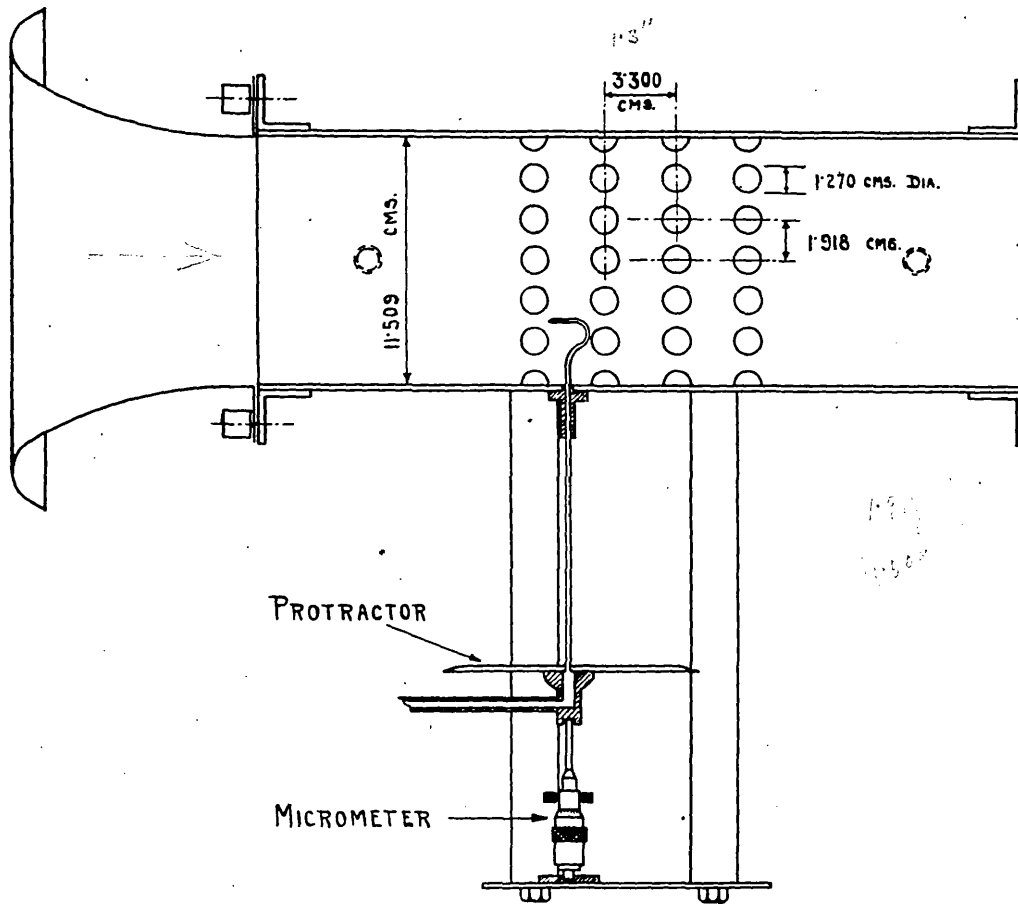
- P = Force exerted on tubes - Grams.Cms.Sec.⁻²
 p = Pressure intensity - Grams.Cms.⁻¹ Sec.⁻²
 p_f = longitudinal pitch - Cms.
 P_t = transverse pitch - Cms.
 Q = volume of fluid flowing through the gap per second
 Cms.³ Sec.⁻¹ - Appendix No.4
 q = velocity - Cms. Sec.⁻¹
 R = radius of a circle - Cms.
 Re = Reynolds' number $\equiv \frac{V_{N,max}.d}{\nu}$ or $\frac{V_o d}{\nu}$ - dimensionless
 S = length shown on figure Appendix No.5 - Cms.
 U = velocity - Cms.Sec.⁻¹
 U = velocity in main stream outside boundary layer - Cms.Sec.⁻¹
 u = velocity within boundary layer - Cms.Sec.⁻¹
 V = velocity - Cms.Sec.⁻¹
 V_o = $V_{minimum}$ = original velocity in the undisturbed
 stream - Cms.Sec.⁻¹
 $V_{N,max}$ \equiv Nominal maximum velocity in gap - Cms.Sec.⁻¹
 $= V_o \cdot \frac{\text{Transverse pitch}}{\text{Gap}}$
 V_m = mean velocity in the gap - Cms.Sec.⁻¹ Appendix No.4
 V_H = $\sqrt{\frac{\tau_{dw}}{\rho}}$ where τ_{dw} is the shear stress on the dead water
 This has the dimensions of velocity Cms.Sec.⁻¹
 x = distance on surface of tube from upstream generator - Cms.
 x = distance downstream from origin where mixing begins - Cms.
 y = distance measured across the stream - Cms.

- α = an angle in figure. Appendix No.2 - dimensionless.
 α = a very small fraction - Appendix No.5 - dimensionless
 α = distance of P₂ from K₁ - Cms
 β = " " P₂ " K₂ - Cms Appendix No.3
 γ = resistance coefficient in alternative formula Section 1.6
 - dimensionless.
 δ = thickness of the boundary layer - Cms.
 δ^* = effective thickness of boundary layer - Cms.
 θ = angle, generally measured from upstream generator -
 dimensionless.
 μ = viscosity - Grams Cms.⁻¹ Sec.⁻¹
 ν = kinematic viscosity - Cms.² Sec.⁻¹
 π = 3.1416
 ρ = density of fluid - Grams Cms.⁻³
 τ = tangential drag - Grams. Cms.⁻¹ Sec.⁻²
 $\bar{\tau}$ = average tangential drag - Grams.Cms.⁻¹ Sec.⁻²
 τ_{dw} = tangential drag on dead water region - Grams.Cms.⁻¹ Sec.⁻²
 ϕ = velocity potential - Cms.² Sec.⁻¹
 ϕ = an angle - dimensionless
 ψ = stream function - Cms.² Sec.⁻¹
 ψ = an angle - dimensionless.



DETAILS OF NEST OF TUBES.

FIG. 11.



1. INVESTIGATION OF THE HYDRAULIC RESISTANCE OF NESTS.

1.1 Description of the nest of tubes.

Figure 1.1 shows the details of the nest of tubes. With the staggered arrangement this consisted of 38 tubes and 8 half tubes. The tubes were 1.270 cms. diameter and 15.240 Cms. long. They were arranged at the apices of equilateral triangles thus forming seven rows of six tubes each. The parallel arrangement shown in Figure 1.1 was obtained by removing the second, fourth and sixth rows. The tubes were contained in a box composed of brass plates. The internal cross-section of the box was 15.240 Cms. by 11.509 Cms. The tubes pass through holes in the tube plates and the joints were made water tight with rubber anchor rings secured by an outer brass plate.

The box was of sufficient height to ensure the flow being parallel to the walls when the stream impinged on the tubes.

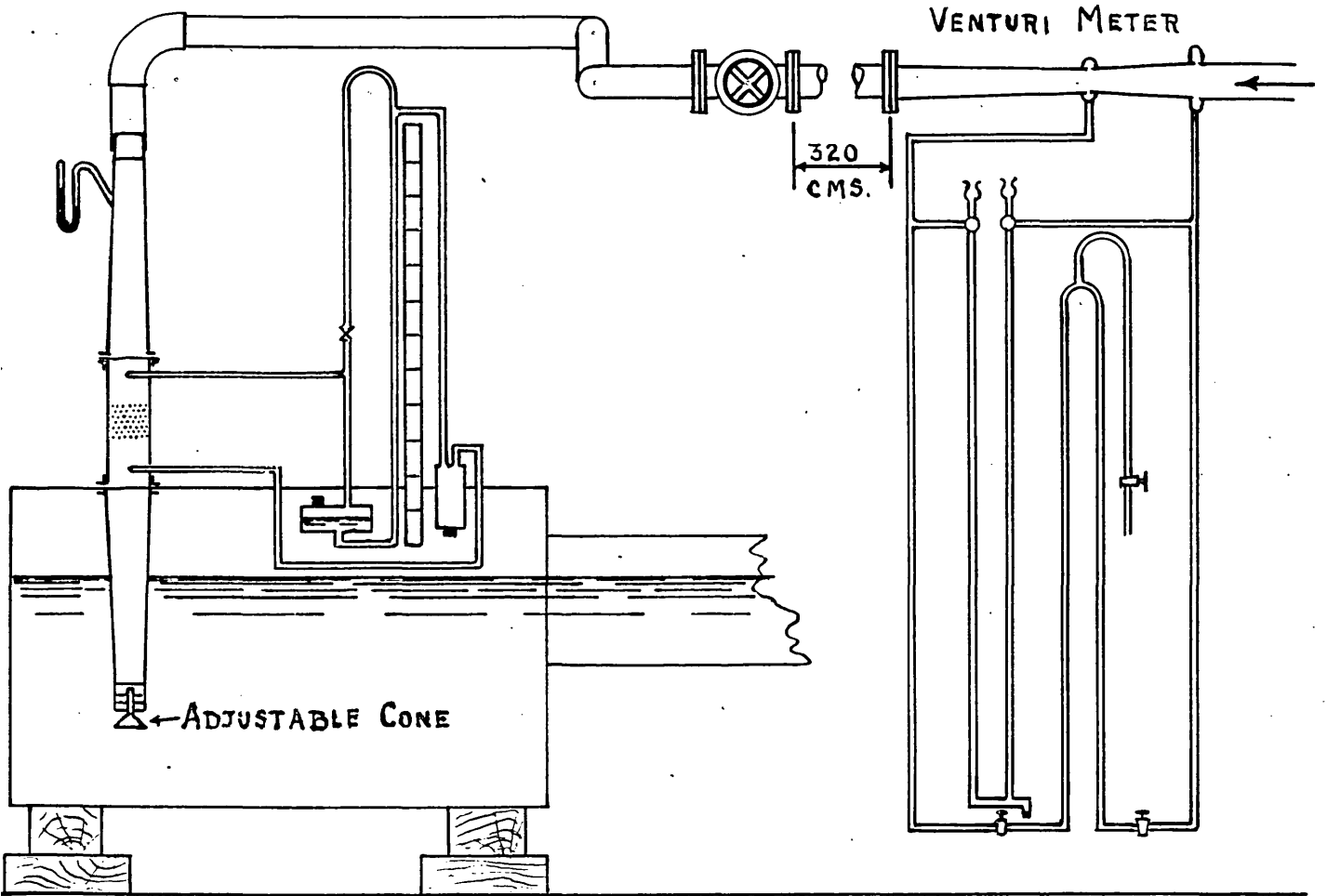
1.2 Method and result of testing with water.

Figure 1.2A shows the arrangement of the nest when prepared for testing on water.

The water passed through the Venturi meter and then vertically downwards over the nest of tubes. With this

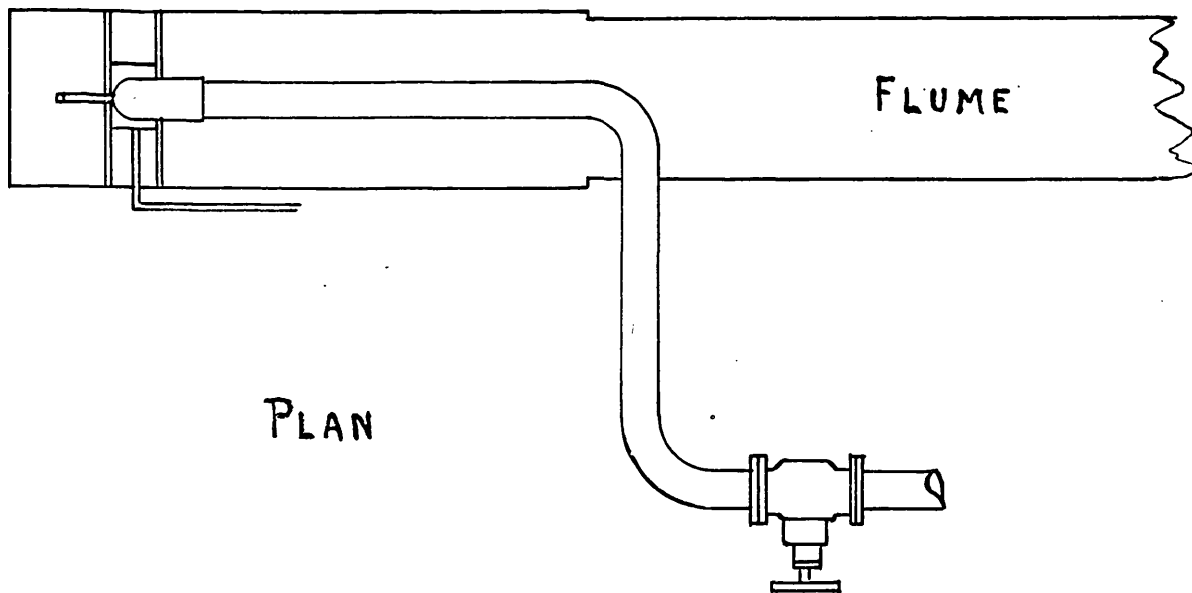
TESTS ON HYDRAULIC RESISTANCE

FIG. 1'2 A.



SECTIONAL ELEVATION.

100 CMS.



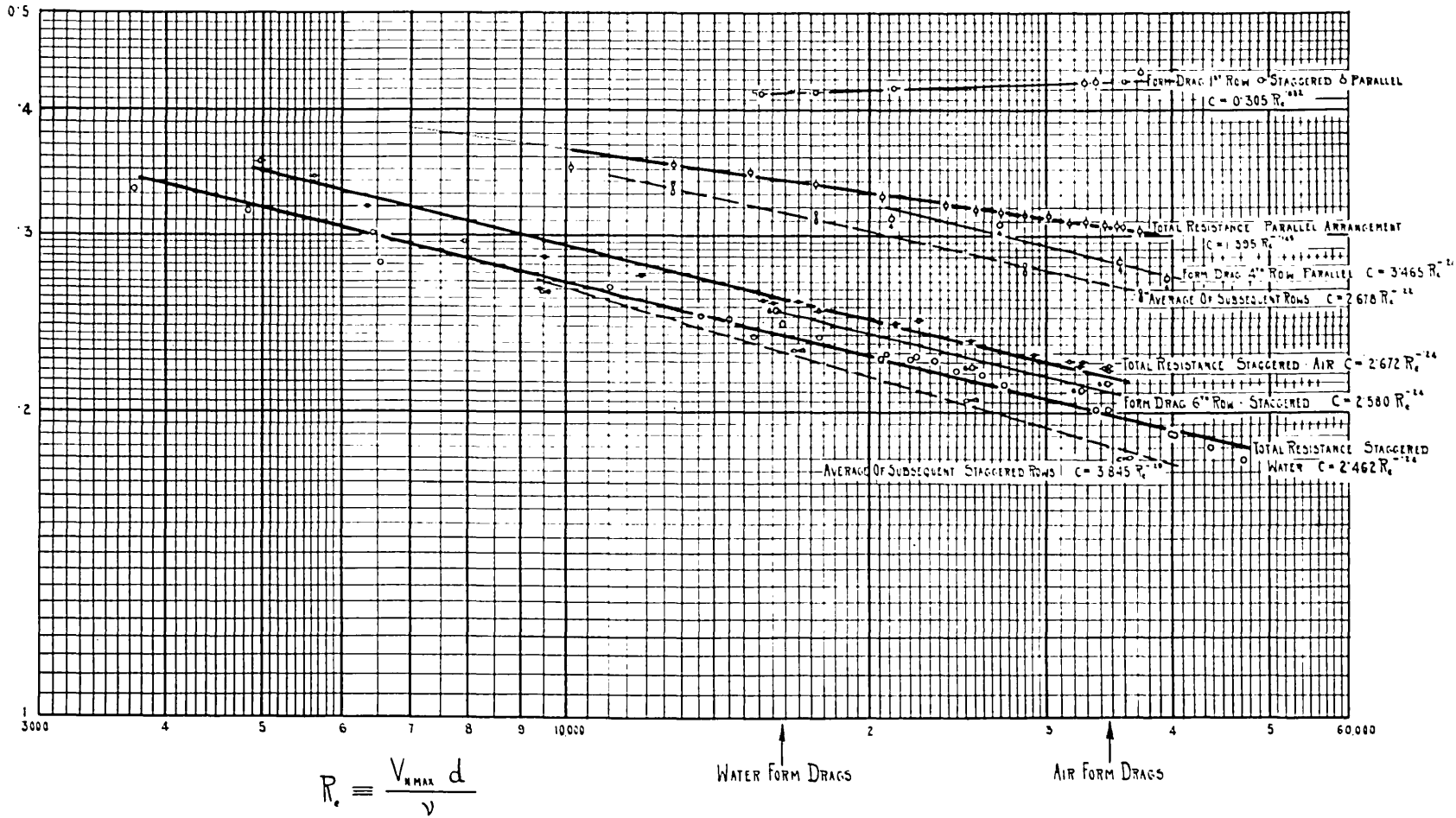
PLAN

ANALYSIS OF TOTAL RESISTANCE OF NESTS.

FIG. 1-2 B.

$$C = \frac{P}{n d l \rho V_{n,MAX}^2} =$$

AVERAGE FORM DRAG
COEFFICIENT $\frac{\rho}{\rho V_{n,MAX}^2}$



arrangement it was possible on low rates of flow to create a partial vacuum inside the nest. This resulted in air being drawn into the apparatus. In order to prevent this an adjustable cone was fitted in the outlet pipe and a manometer tube containing mercury was fitted to the inlet tube as shown on Figure 1.2A.

Small pressure holes (0.081 Cm. diameter) were drilled in the side of the box in front of and behind the nest of tubes. Short lengths of brass tube were soldered to the wall of the box over these holes and they were connected by rubber tubing to a differential manometer tube.

The results are given in Table 1.2B and are plotted in Figure 1.2B. In this figure the logarithm of the

coefficient of resistance "c"
$$= \frac{P}{n d l \rho V_{N.max}^2}$$

is plotted against the logarithm of the

Reynolds' number
$$R_e = \frac{V_{N.max} d}{\nu}$$

where P is the total hydraulic resistance

n is the number of tubes. viz. 24 for the parallel arrangement and 42 for the staggered arrangement.

l is the length of the tubes. viz. 15.25 Cms.

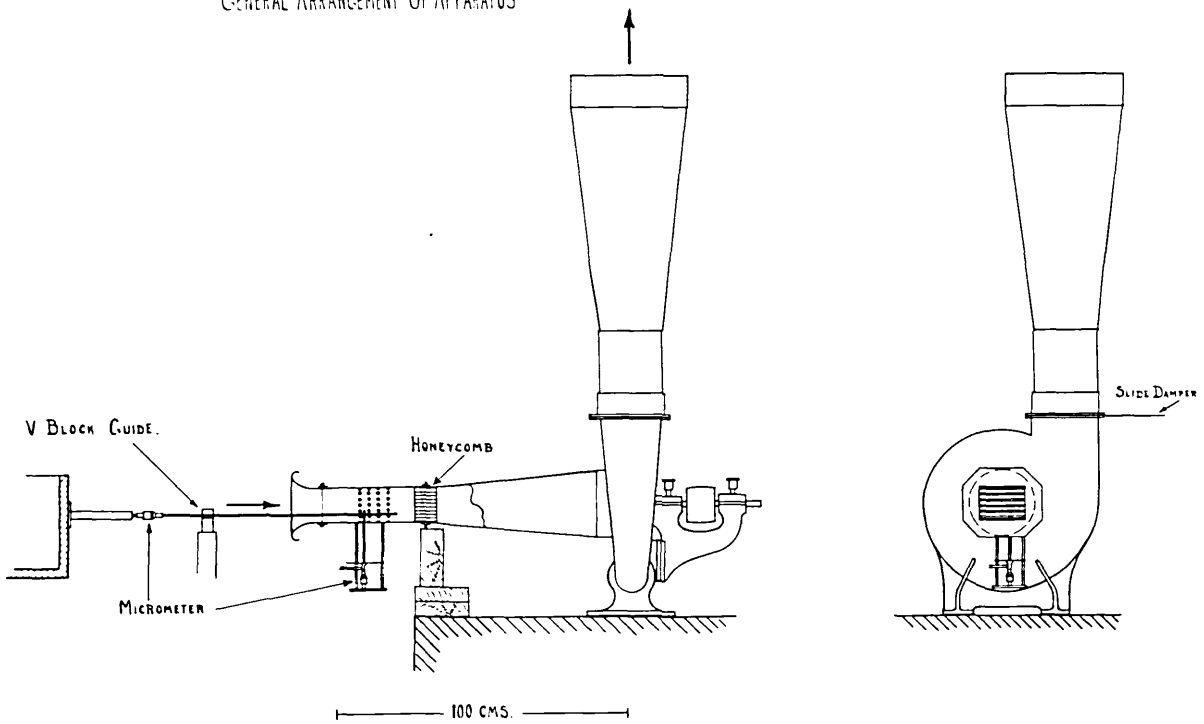
ρ is the density of fluid

$V_{N.max}$ is the nominal maximum velocity. i.e. original velocity of stream multiplied by 2.96

AIR FLOW OVER NEST OF TUBES

FIG. 13A.

GENERAL ARRANGEMENT OF APPARATUS



d is the diameter of the tubes 1.27 Cms.

ν is the kinematic viscosity of fluid.

This curve is represented by $c = 2.462 R_e^{-.24}$

The hydraulic resistance and the flow pattern will largely be determined by the maximum velocity in the gap between adjacent tubes. The actual maximum velocity will depend upon the thickness of the boundary layer on the surface of the two tubes. This thickness is not usually known and therefore a term called the nominal maximum velocity has been introduced. This is the assumed velocity in the gap, based on the assumption that the velocity distribution across the gap is constant. This is represented by $V_{N.max}$ and is the initial velocity of the stream multiplied by the ration $\frac{\text{transverse pitch}}{\text{width of gap}}$.

1.3 Method and result of testing with air.

Figure 1.3A shows the general arrangement of the experimental plant when investigating with air flow.

The air was drawn into the apparatus through a converging mouth-piece by a No.3 high pressure Sturtevant fan. The rate of flow of air through the apparatus was measured by the difference in pressure of the atmosphere and that at the first pressure hole ahead at the nest of tubes. This pressure point was connected to a glass manometer tube of

1.4 Cms. bore through a four-way cock and the pressure difference when the manometer tube was open to the atmosphere or to the pressure hole was read by means of a cathetometer.

This method was found satisfactory for the numerous experiments at constant air speed, corresponding to a cathetometer reading of 1.17 Cms. of water, but for the variable speed tests where much lower air velocities were used the head was determined with a Chattock tilting gauge.

Although the distance between the outlet of the nest and the inlet of the fan was 58 Cms., it was thought that the angle of the vanes of the fan might have an effect on the direction of flow in the nest. In order to obviate this possibility a honeycomb 8 Cms. long was inserted in the outlet of the nest. This divided the exit air into streams 1.27 Cms. x 1.27 Cms. cross section.

The total resistance of the nest when containing seven rows of tubes with the staggered arrangement and also of four rows with parallel or rectangular arrangement was determined. The results are given in tables 1.3A and B. Minor adjustments are involved due to changes in the atmosphere temperature, pressure and humidity. These are explained in detail in appendix No.1.

To assist in comparison, the results are plotted on

Figure 1.2B. The curve for the staggered arrangement with air flow is represented by the equation:

$$c = 2.672 R_e^{-.24}$$

while that for the parallel arrangement with air flow

$$c = 1.395 R_e^{-.145}$$

1.4 Comparison between results with water and with air

From Figure 1.2B it is seen that the test points for a test with water and those with air definitely do not conform to a single curve. There is no reason to doubt the actual measurements since in each case results were confirmed by independent repetition at different periods of the research. The nest of tubes used was the same for both fluids though naturally it was taken apart from time to time for cleaning and inspection. It would seem that the different inlet arrangement in the two cases caused the discrepancy between the air and water results. With the latter fluid the arrangement shown in Figure 1.2A was far from ideal. Nevertheless it is surprising that it should cause a difference so large as 7.9% of the air resistance. Further, any effect of inlet conditions might, at first sight, have been expected to be confined to the first row of tubes. Actually it was found that the water value for the first row of tubes agreed very satisfactorily with the air values and the discrepancy

appears to be mainly in later rows.

Whatever the explanation it seems advisable to restrict attention to the air experiments which were much more comprehensive and also contained much self-checking evidence.

1.5 Analysis of total resistance, relative importance of the various rows of tubes.

At a later stage it is shown by measurements of the pressure distribution around individual tubes that the first row behaves in an anomalous manner and its resistance coefficient did not vary appreciably with Reynolds' number. Its value was about 0.42 both for the staggered and rectangular arrangements. The resistance for the first row is seen plotted towards the top of Figure 1.2B. This row is seen to have a resistance very much greater than the average for the whole nest.

The other rows, notably the second and third, also had individual characteristics, but the deviations in these cases were of a small order. It is convenient therefore to subdivide the resistance of the nest into two main parts; that due to the first row and that due to subsequent rows. On subtracting the value of the first row from the total for the whole nest an average value for the later rows is obtained and this could be used in estimating the resistance

of a nest with a different number of rows of tubes.

The results are approximately represented by the following

where $c \equiv \frac{P}{n d l \rho V_{N,max}^2}$ for the total resistance of the

nest and the average form drag coefficient $\frac{p}{\rho V_{N,max}^2}$
for the various rows.

| | <u>Parallel</u> | <u>Staggered</u> |
|----------------------------|------------------------|-----------------------|
| First row | $c = 0.305 Re^{.032}$ | $c = 0.305 Re^{.032}$ |
| Average of subsequent rows | $c = 2.678 Re^{-.22}$ | $c = 3.845 Re^{-.29}$ |
| Fourth row | $c = 3.465 Re^{-.24}$ | |
| Sixth row | | $c = 2.580 Re^{-.24}$ |
| Average of four rows | $c = 1.395 Re^{-.145}$ | |
| " " seven " air | | $c = 2.672 Re^{-.24}$ |
| " " " " water | | $c = 2.462 Re^{-.24}$ |

The range over which these experimental laws apply can be seen from Figure 1.2B.

It is rather surprising to find that the exponent for the subsequent rows of the staggered nest is so similar to that for the parallel arrangement. In both cases the influence of the Reynolds' number is much larger than experiments with roughened pipes would suggest, particularly in the case of the parallel arrangement which may be regarded as an extreme case of a rough pipe. In a roughened

pipe, however, the protuberances are arranged in a non-systematic manner and the possibility of major pressure recoveries behind them hardly exists. In the present case, as shown later in Figure 4.2, such recoveries do take place and play a large part in determining the general pressure gradient through the nest.

The resistance of "subsequent rows" for the staggered arrangement is 30% less than that for the parallel. This is later shown to be almost entirely due to differences on the upstream faces of the tubes.

1.6 Alternative method of expressing resistance of nest.

The method of reduction utilised in the preceding subsections follows the well-known idea of reducing frictional forces to a dimensionless coefficient of the type $\frac{p}{\rho V^2}$ and studying the dependence of this coefficient upon the Reynolds' number. During the past thirty years this method has been universally adopted for fluid friction problems. It is convenient from the experimenter's point of view since in the laboratory "V" is usually one of the known independent variables. In engineering practice the permissible pressure drop is the known factor, while "V" becomes one of the unknown dependent variables. For this reason it is desirable to adopt some

method in which "V" appears in one only of the two dimensionless arguments.

In the very early days the Chezy resistance formulae $V = C \sqrt{m i}$ was widely used and possessed the above advantage. This form is again appearing in connection with the Pradtl-Karman theory of pipe resistance. This leads to a resistance law of the type.

$$V = \gamma \sqrt{8 g m i} \dots\dots\dots(1)$$

where γ is a resistance coefficient depending upon a Reynolds' number formed out of the pressure gradient rather than out of the velocity. e.g. for flow in circular pipes

$$\gamma = 2 \log_{10} \rho \sqrt{\frac{8 \tau d}{\rho \mu}} - 0.8 \dots\dots(2)$$

where τ is the tangential drag per unit area of the wetted surface. It will be observed that "V" does not appear on one side of the formula.

For purposes of transformations it may be noted that equation (2) is conveniently written

$$\gamma = 2 \log_{10} \frac{Re}{\delta} - 0.8$$

To adapt this line of thought to the resistance of a nest of tubes it is merely necessary to define the resistance coefficient as

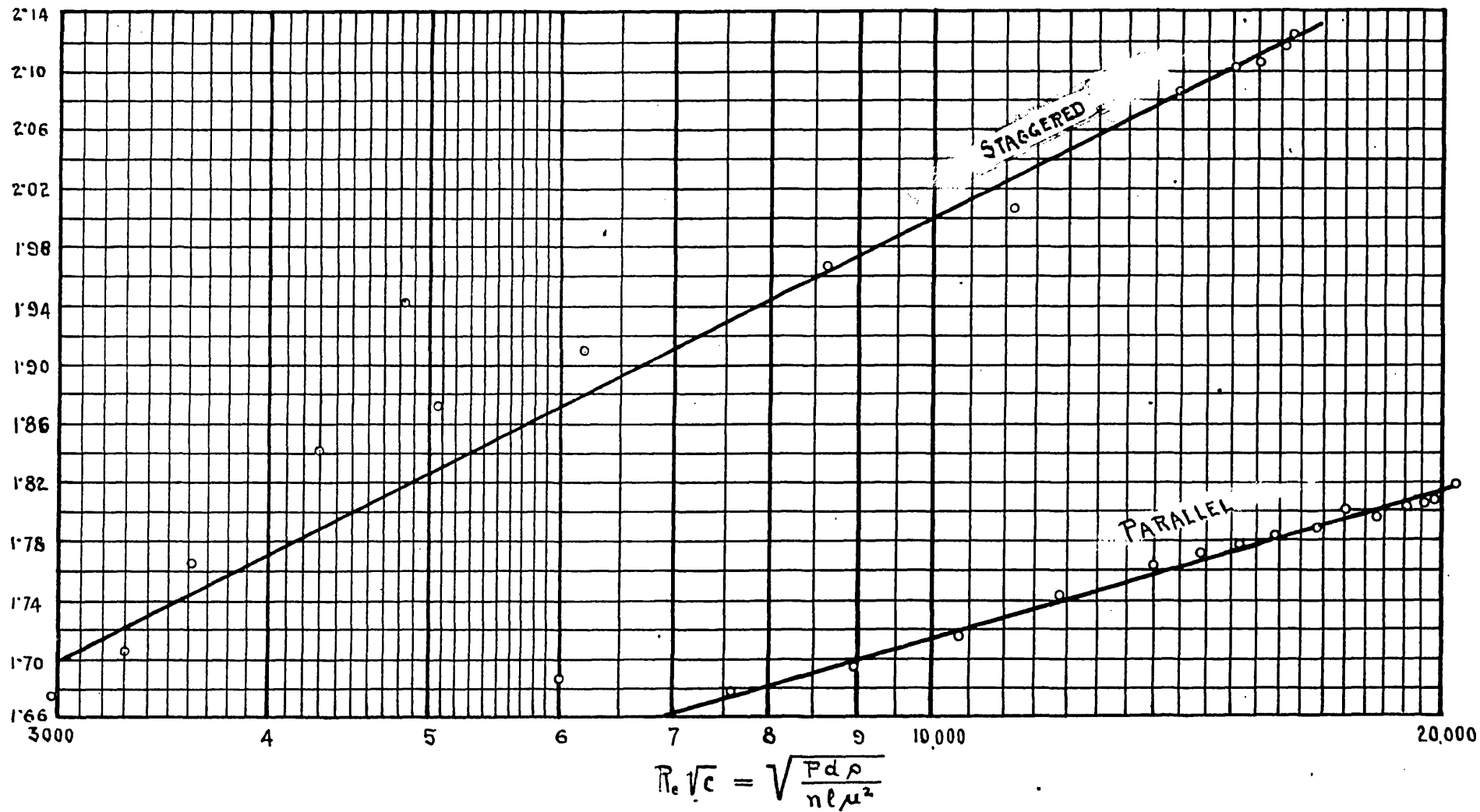
$$v. \sqrt{\frac{n d l \rho}{P}}$$

which is $\frac{1}{\sqrt{c}}$ in Figure 1.2B.

ALTERNATIVE METHOD OF EXPRESSING RESISTANCE OF NEST

FIG. 1'6.

$$\frac{1}{\sqrt{c}} = V_{N.MAX} \sqrt{\frac{nd\rho}{P}}$$



STAGGERED $\frac{1}{\sqrt{c}} = \frac{1}{1.732} \log_{10} Re \sqrt{c} - 0.31$

PARALLEL $\frac{1}{\sqrt{c}} = \frac{1}{3.02} \log_{10} Re \sqrt{c} + 0.39$

The necessary change in "Reynolds' Number" is to multiply by \sqrt{c} giving $\frac{V_{N.\max} d}{\nu} \times \sqrt{\frac{P}{n d l \rho V_{N.\max}^2}}$

which equals $\sqrt{\frac{P d \rho}{n l \mu^2}}$ and this is used as the abscissa in Figure 1.6.

Here an approximate linear relation is observed and the resistance laws are conveniently written as.

Parallel arrangement:

$$\begin{aligned} \frac{1}{\sqrt{c}} &= \frac{1}{3.02} \log_{10} Re \sqrt{c} + 0.39 \\ &= \frac{1}{6.04} \log_{10} Re^2 c + 0.39 \end{aligned}$$

i.e.

$$V_{N.\max} \sqrt{\frac{n d l \rho}{P}} = \frac{1}{6.04} \text{LOG}_{10} \frac{P d \rho}{n l \mu^2} + 0.39$$

Staggered arrangement:

$$\begin{aligned} \frac{1}{\sqrt{c}} &= \frac{1}{1.732} \log_{10} Re \sqrt{c} - 0.31 \\ &= \frac{1}{3.464} \log_{10} Re^2 c - 0.31 \end{aligned}$$

i.e.

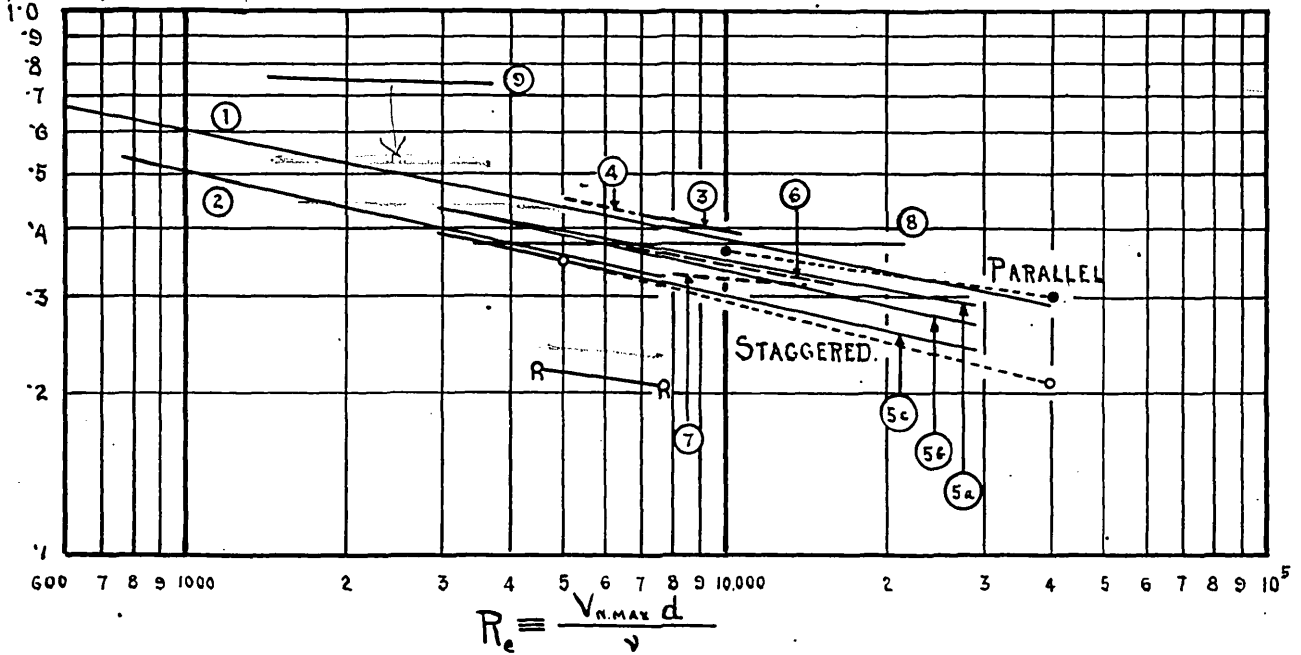
$$V_{N.\max} \sqrt{\frac{n d l \rho}{P}} = \frac{1}{3.464} \log_{10} \frac{P d \rho}{n l \mu^2} - 0.31$$

It will be noticed that in Figures 1.2B and 1.6 linear relations have been adopted. In both cases it is probable that the true relations should be represented by curves,

COMPARISON OF RESISTANCE OF NESTS WITH THE RESULTS

OF PREVIOUS INVESTIGATORS FIG. 17.

$$C = \frac{P}{nd\rho V_{n,MAX}^2}$$



$$Re = \frac{V_{n,MAX} d}{\nu}$$

| INVESTIGATOR | Nº OF ROWS | INVESTIGATOR | Nº OF ROWS |
|--------------|-------------|--------------|-------------------------|
| ① | SIEDER I 24 | ⑥ | SOULE |
| ② | " II 20. | ⑦ | ALLEN |
| ③ | REIHER II 5 | ⑧ | CARRIER 4 |
| ④ | " III 4 | ⑨ | DEHN 6 |
| ⑤a | RIETSCHEL 2 | R—R | REIHER PARALLEL |
| ⑤b | " 3 | •-•- | PRESENT WORK - PARALLEL |
| ⑤c | " 4 | ○-○- | " " STAGGERED. |

but it is more probable that the curvature is less in Figure 1.6. If it is necessary to extrapolate beyond the experimental points, it is safer to use equations associated with Figure 1.6.

1.7 Comparison with the results of previous investigators.

A survey of this subject has been made by Chilton and Genereaux,⁽¹⁾ who attempted to correlate the results of seven investigators. These experimenters had all worked with staggered arrangements but with different pitch - diameter ratios. Chilton and Genereaux were unable to obtain a perfect correlation although they had tried a wide variety of different forms of coefficients and basis for Reynolds' numbers.

They do not appear to have considered the present method which appears to be slightly more logical and satisfactory than the one they recommend.

Chilton and Genereaux recommend a coefficient which is, in fact, given by

$$f \text{ (Chilton)} = c \times \frac{d}{2p} \quad \text{where } d = \text{diameter of tube}$$

$$p = \text{transverse pitch}$$

and they express this as a function of $R_e \times \frac{\text{gap}}{\text{tube diameter}}$

(1) Chilton and Genereaux. Contribution No. 127. Experimental Station. E.1. du Pont de Nemours & Co.

Figure 1.7 shows the results of the seven investigators quoted by Chilton and Genereaux when reduced to the present method as used in Figure 1.2B. The "scatter" seen appears to be due to uncertainties of measurement rather than to geometrical arrangement or number of rows. In particular the values given by Dehn seem inexplicably high. In fact they are greater than that of an isolated cylinder and this appears to be sufficient ground for discounting his results.

The results of the several investigators are somewhat high, in some cases partly due to the few rows of tubes and possibly also to the different geometrical arrangements, but mainly, no doubt, to the difficulties of experimental measurement.

It may be noted that the present resistance values are independently checked by the form drag diagrams. Further, the rate of air flow received independent confirmation, at least with the rectangular arrangement, by the values of the pressure observed at the points of maximum constriction, which may be regarded as miniature venturi meters.

With regard to the rectangular arrangement, Reiher with five rows of tubes obtained the very low value of $c = 0.21$. This is not supported by the present results,

where "c" is well in excess of 0.3 even at higher Reynolds' numbers. This is definitely higher than with the staggered arrangement. It appears to show that the conclusion drawn by Chilton, Genereaux and others, that rectangular arrangements have less resistance than staggered arrangements, is erroneous, or at least applicable only in particular cases.

2. INVESTIGATION OF THE LACK OF SYMMETRY OF FLOW OBSERVED
IN STAGGERED NEST.

2.1 Discovery of asymmetry during experiments with water.

It was thought that the determination of the pressure distribution around the surface of the various tubes would prove a suitable starting point for the investigation of the pressure and velocity distribution throughout the nest.

The experiments were carried out in a manner similar to those of Fage⁽¹⁾ on a circular cylinder in a wind tunnel. A hole 0.0865 Cm. in diameter was drilled radially in the centre of a length of the same brass tubing from which the nest of tubes was constructed. One end of this tube was closed and a graduated scale reading to 0.5 of a degree was attached to indicate the angular position of the hole. The open end was attached to a manometer tube. This exploration tube could be made to replace any of the original tubes in the nest and it was of such a length that the pressure hole could be near the front or back wall of the nest or placed in any intermediate position.

(1) Fage. R. & M. No. 106 - 1913-14. p.65.

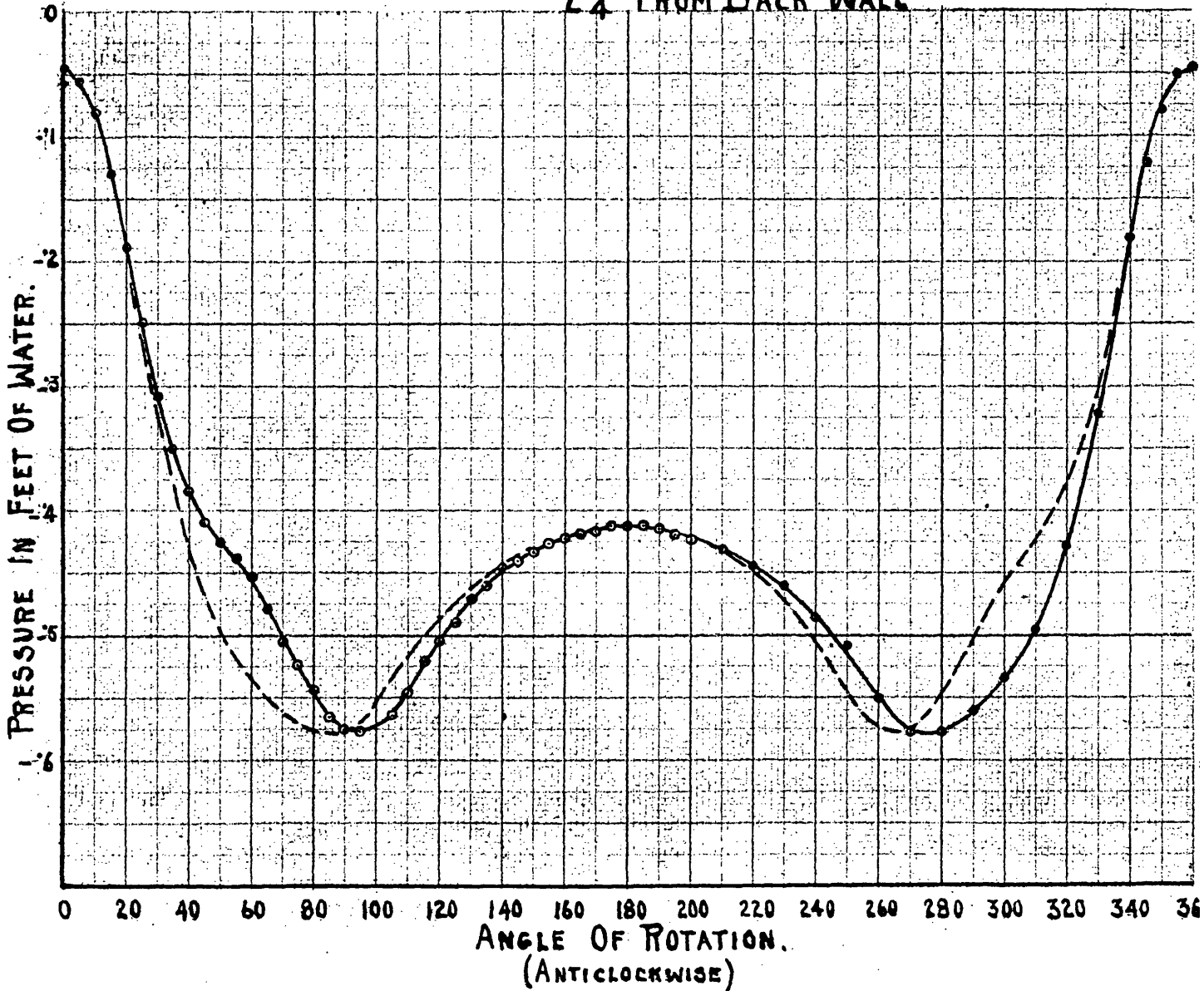
(Note: R. & M. refers to Reports & Memoranda
of the Aeronautical Research Committee.)

NORMAL PRESSURE AT SURFACE OF TUBE. FIG. 2.1A.

STAGGERED ARRANGEMENT.

3RD ROW CENTRE TUBE

2 $\frac{3}{4}$ " FROM BACK WALL



VENTURI METER 2.10' OF WATER

WATER VELOCITY $V_{N.MAX.}$ 140 CMS/SEC.

15°C. $\frac{V_{N.MAX.} \cdot d}{\nu} = 15,470$

Since the angle subtended by the diameter of the hole at the centre of the tube is about 8° , there arose the question whether it was sufficiently accurate to assume that the pressure recorded in the manometer tube was that at the centre of the hole. Thom⁽¹⁾ has suggested that it would be more correct to assume that the pressure inside the exploration tube is not the pressure at the centre of the hole, but that at a point half-way along the hole radius towards the front of the cylinder. This would make a difference of 2° in the various readings.

When a very small exploration hole is used there is a considerable time lag between the rotation of the tube and the water in the manometer attaining the correct level corresponding with the pressure at the surface of the exploration hole. This causes uncertainty and possible inaccuracy and it was considered advisable to use a hole of 0.0865 Cm. diameter and to make the necessary correction on the area of the form drag diagrams.

While determining the pressure distribution at the surface of the centre tube of the third row from the top, with the pressure hole 7 Cms. from the back wall of the nest, a marked asymmetry was discovered in the curve. Figure 2.1 A shows the pressure distribution. The continuous

(1) Thom. R. & M. No. 1194 - 1928, p. 183.

line is plotted from the pressure records (Table 2.1 A) and the dotted line is the "mirror image" of this curve. This shows clearly the lack of symmetry. Since the holes in the tube plates of the nest were only marked off and drilled, and not jigged, it was realised that slight inaccuracies in the spacing of the tubes would exist. It was thought possible that these slight differences in spacing might make a large difference in the velocity of the water between the various tubes and this might be the cause of the unequal distribution of pressure.

In order to test this, the exploration tube was removed from its original position and placed in the adjacent hole on the left, the pressure hole being again positioned 7 Cms. from the back wall. It was anticipated that any irregularity which had been apparent in the first position of 90° would now be rendered visible at 270° . Contrary to expectation, the pressure distribution curve was very similar to that of the centre tube and showed the same lack of symmetry.

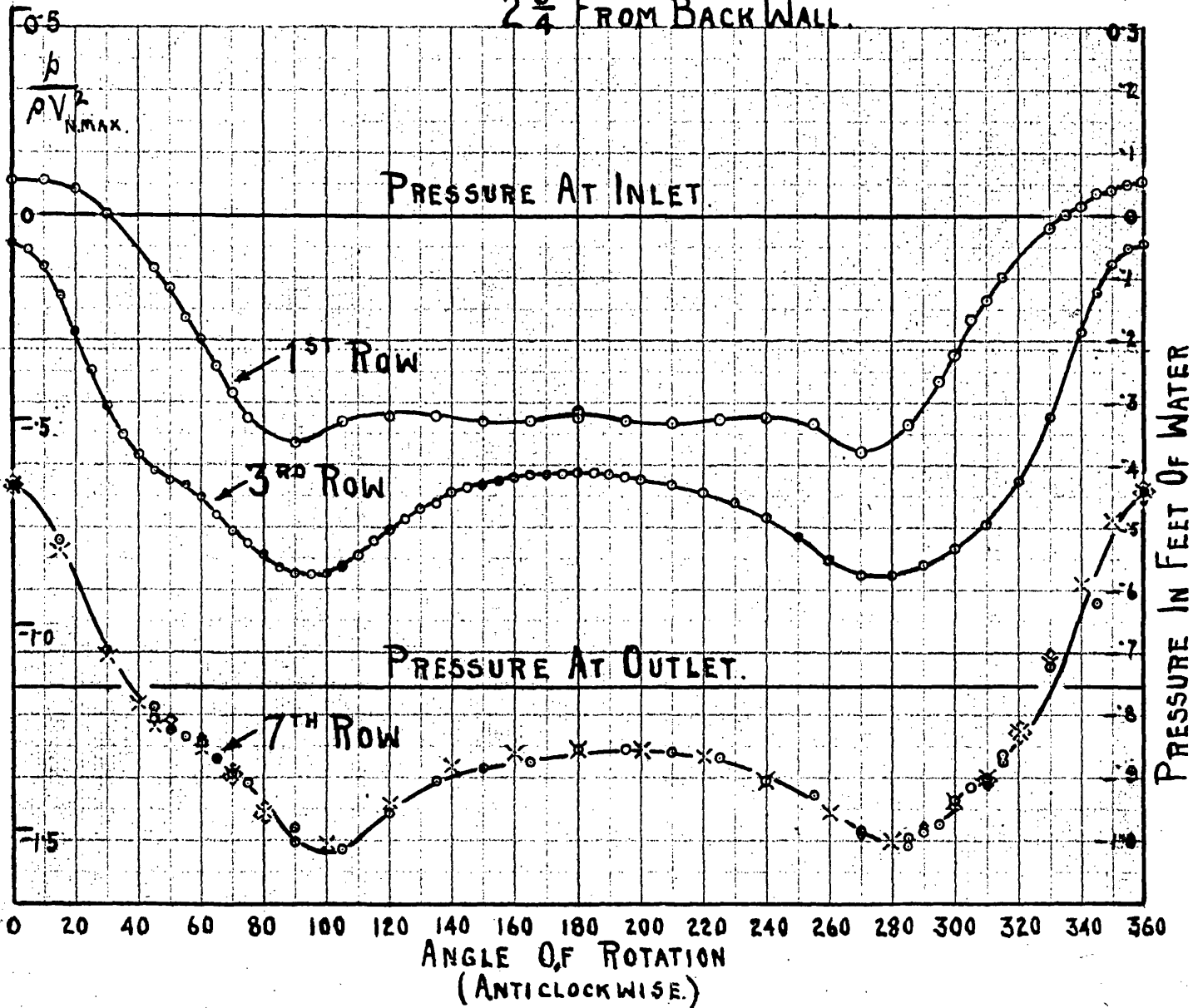
2.2 Asymmetry of form drag diagrams.

Since slight variations in the spacing of the tubes was not the cause of asymmetry, experiments were carried out to see if the degree of asymmetry was the same throughout the nest of tubes.

If the components of the normal pressure in the direction

NORMAL PRESSURE AT SURFACE OF TUBE FIG. 2·2 A.

STAGGERED ARRANGEMENT.
 1ST, 3RD & 7TH ROWS. CENTRE TUBES.
 2 $\frac{3}{4}$ " FROM BACK WALL.



○ ORIGINAL EXPERIMENTS

× AFTER ADJUSTMENT OF CONE

◇ WITH BENT CONE

WATER VELOCITY $V_{N.MAX.} 140 \text{ CMS/SEC.}$

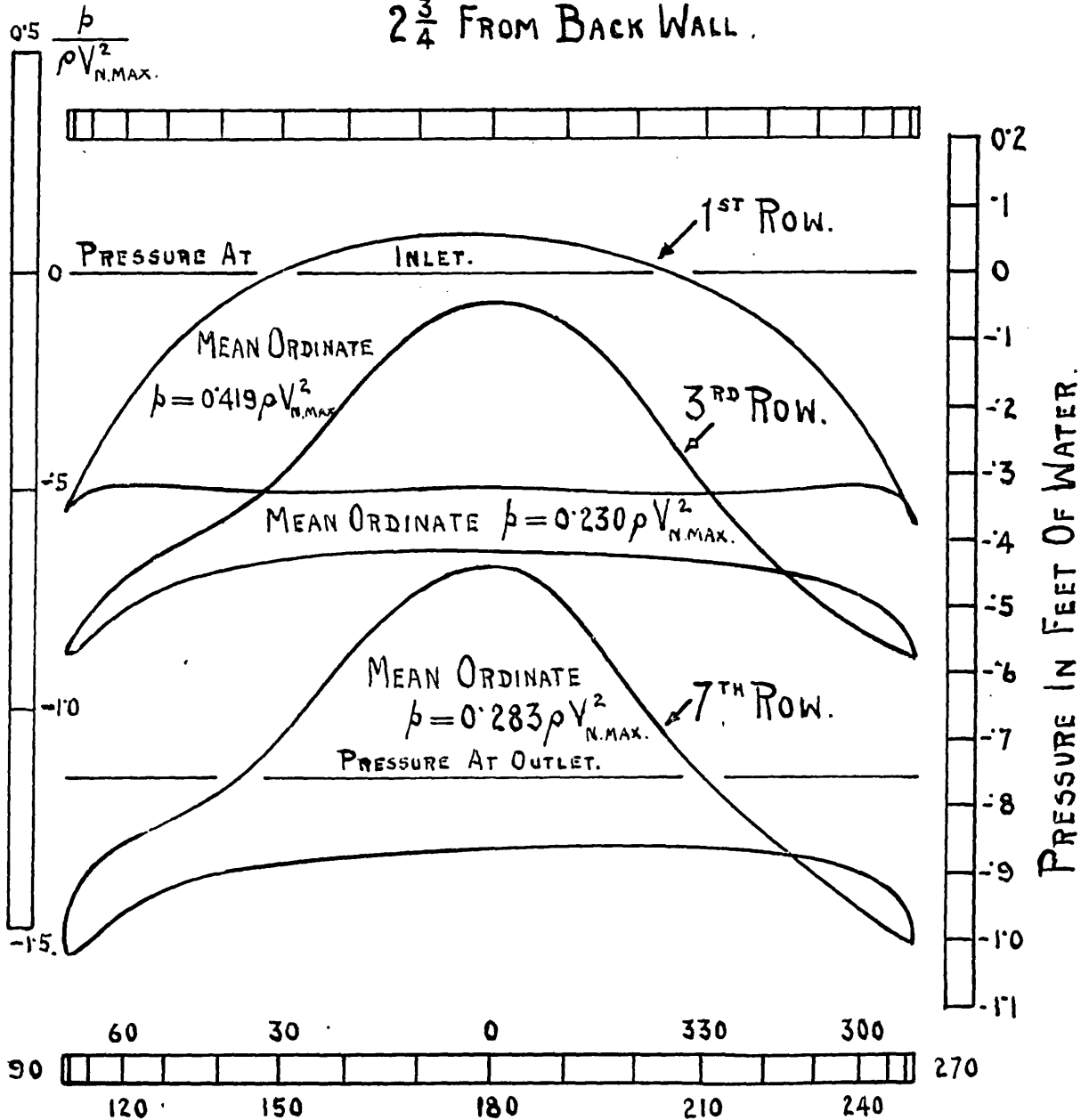
17°C $\frac{V_{N.MAX.} d}{\nu} = 16,380.$

FORM DRAG FIG. 2·2 B.

STAGGERED ARRANGEMENT.

1ST, 3RD & 7TH ROWS CENTRE TUBES.

2 $\frac{3}{4}$ " FROM BACK WALL.



WATER VELOCITY $V_{N.MAX.}$ 140 $\frac{CMS}{SEC.}$

$$17^{\circ}C \quad \frac{V_{N.MAX.} d}{\nu} = 16380.$$

of flow are plotted on the projected diameter of the tube, this gives the form drag curve.

It was found that the asymmetry was more clearly seen on the form drag curves than on the curves of pressure distribution on an angular basis.

Figures 2.2 A and B show the pressure distribution and form drag curves for the centre tubes of the 1st, 3rd, and 7th rows, with the pressure hole in each case at a distance of 7 Cms. from the back wall.

It will be seen that although the form drag of the centre tube of the 1st row is almost perfectly symmetrical, there is an increasing degree of asymmetry in the tubes of the 3rd and 7th rows.

2.3 Asymmetrical polar diagrams.

If the stream of water as it passed through the nest became deflected towards the right or left side of the box, it would not impinge vertically on the tubes but at a slight angle to the vertical. If this deflection steadily increased with the passage of the water through the nest, the angle at which the stream would impinge on successive rows of tubes would increase progressively also. This would be discerned clearly if the pressure distributions were plotted on a polar diagram.

NORMAL PRESSURE AT SURFACE OF TUBE. FIG. 2:3.

POLAR DIAGRAM.

STAGGERED ARRANGEMENT.

1ST, 3RD & 7TH ROWS .CENTRE TUBES.

2 $\frac{3}{4}$ " FROM BACK WALL

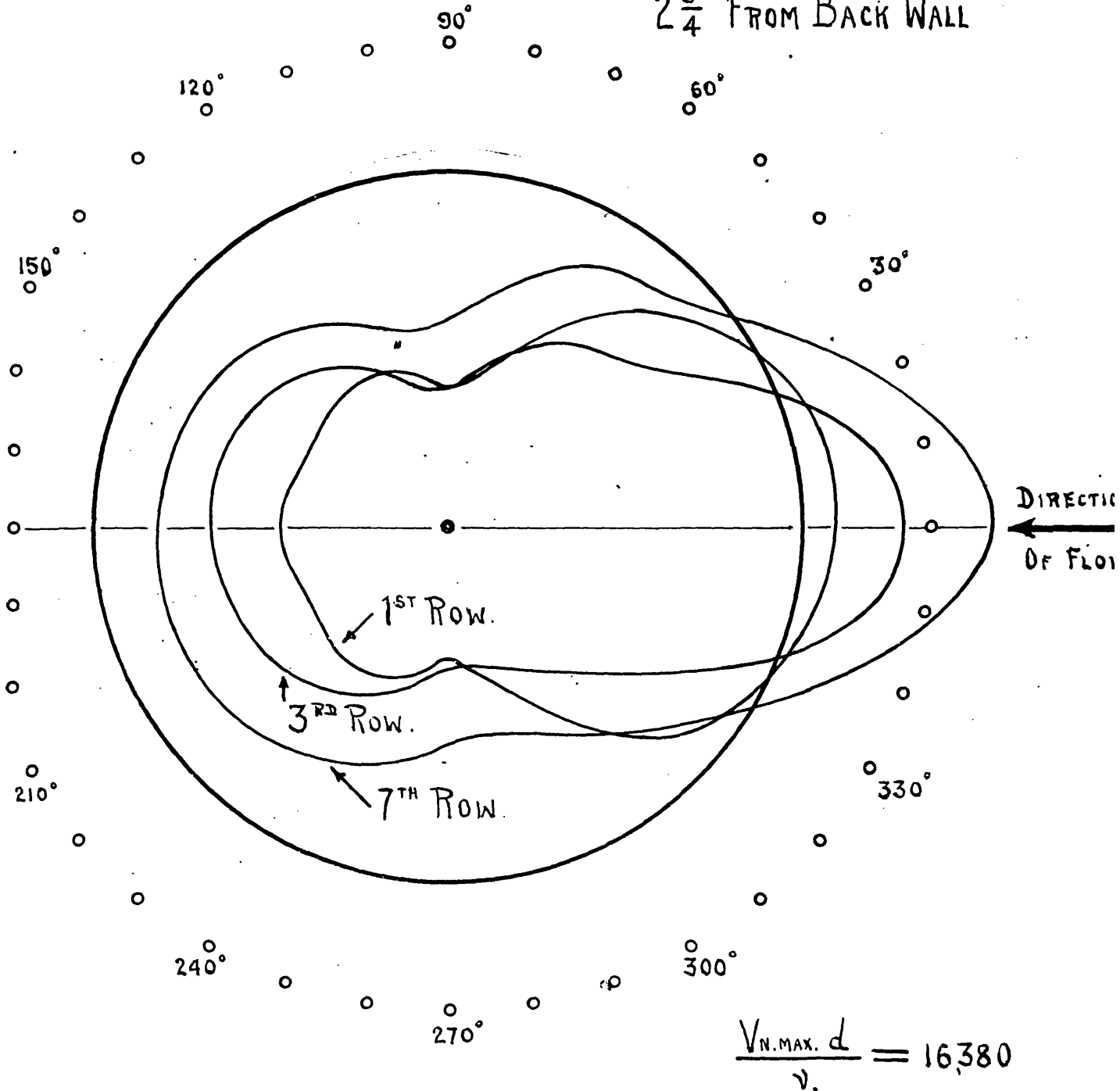


Fig. 2.3 shows such a diagram. In the case of the centre tube, 1st row, pressures in excess of that at the first pressure hole at the inlet of the nest are regarded as positive and are plotted outside the base circle. Pressures lower than this are regarded as negative and plotted inside the base circle.

With regard to the tubes of the 3rd and 7th rows, a difficulty arises in that the true static pressure of the fluid in the neighbourhood of these tubes is not known. It was therefore assumed that base pressure for the 3rd row of tubes was the pressure at the top of the apparatus minus $2/7$ of the total hydraulic resistance, and that the base pressure for the 7th row was the pressure at the bottom of the apparatus.

It was appreciated that, while these assumptions probably would be not far from the truth, there was no scientific evidence in their support. However, the reason for plotting the polar diagram was the determination of the angular displacement of the respective curves and this is independent of the actual pressure values.

From Fig. 2.3 it will be seen that while the pressure distribution for the centre tube of the 1st row is symmetrical about the line $0^\circ - 180^\circ$, the pressure distribution for the

3rd row shows a slight angular displacement and the pressure distribution at the rear of the tube of the 7th row is displaced 10° , the stream apparently leaving the tube at 190° . This progressive increase in the degree of asymmetry from the first to the last row of tubes suggested some lack of uniformity at the outlet of the apparatus. The cone at the outlet (See Fig. 1.2 A) was very carefully adjusted so that it was concentric with the centre line of the nest and that the annular opening was of uniform width all round. The experiment on the centre tube of the 7th row was repeated and the pressures recorded are marked with crosses on Fig. 2.2 A. This appeared to have no appreciable effect on the pressure distribution.

The outlet cone was bent so as to give a definite irregularity at the outlet. Further observations of the pressure were taken and these are marked with diamonds on Fig. 2.2 A. All the points lie on the same curve. It was concluded that whether the outlet cone was adjusted to give an annular orifice of uniform width or not, or even if it were bent to give a definite irregularity, it had no appreciable effect on the pressure distribution on the centre tube of the bottom row.

2.4 Asymmetry unchange by reversal of nest.

The next possible cause of the asymmetry which suggested

itself was in the general arrangement at the inlet of the apparatus. From Fig. 1.2 A it will be seen that immediately over the top of the inlet there is a sharp right angle bend. It was thought that the effect of the centrifugal force on the water as it passed round this bend might result in a non-uniform velocity distribution across the inlet of the nest. As the stream encountered the major hydraulic resistance in the nest, the distribution would tend to become more uniform and this would necessitate a flow of water from left to right in Fig. 1.2 A. Since this process of equalisation of the velocity would be progressive throughout the nest, so, it might be expected, would be the progressive increase in the transverse component of the velocity.

The direction of the angular displacement in the polar diagram gave support to this possible explanation.

In order to test this hypothesis, the nest of tubes was rotated through 180° with respect to the inlet. It was anticipated that exactly similar asymmetry would be present, but on the various curves it would be to the opposite hand. For example, on the polar diagram it was anticipated that the displacement at the rear of the last row of tubes would be 10° before the 180° instead of 10° after that position.

NORMAL PRESSURE AT SURFACE OF TUBE

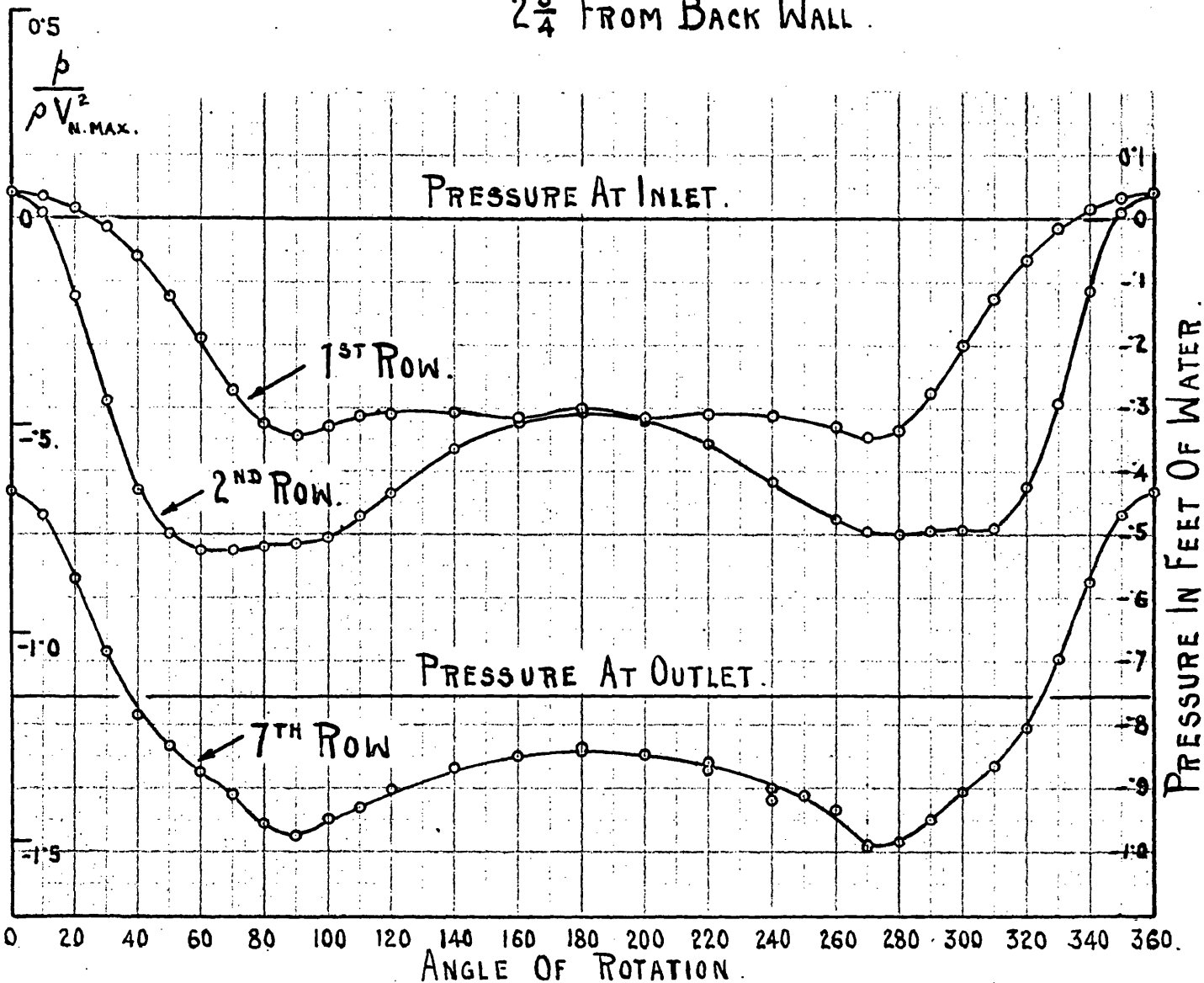
FIG. 2.4 A.

NEST ROTATED THROUGH 180°

STAGGERED ARRANGEMENT.

1ST, 2ND & 7TH ROWS CENTRAL TUBES.

2 $\frac{3}{4}$ " FROM BACK WALL.



WATER VELOCITY $V_{N,MAX} 140 \frac{CMS}{SEC}$.

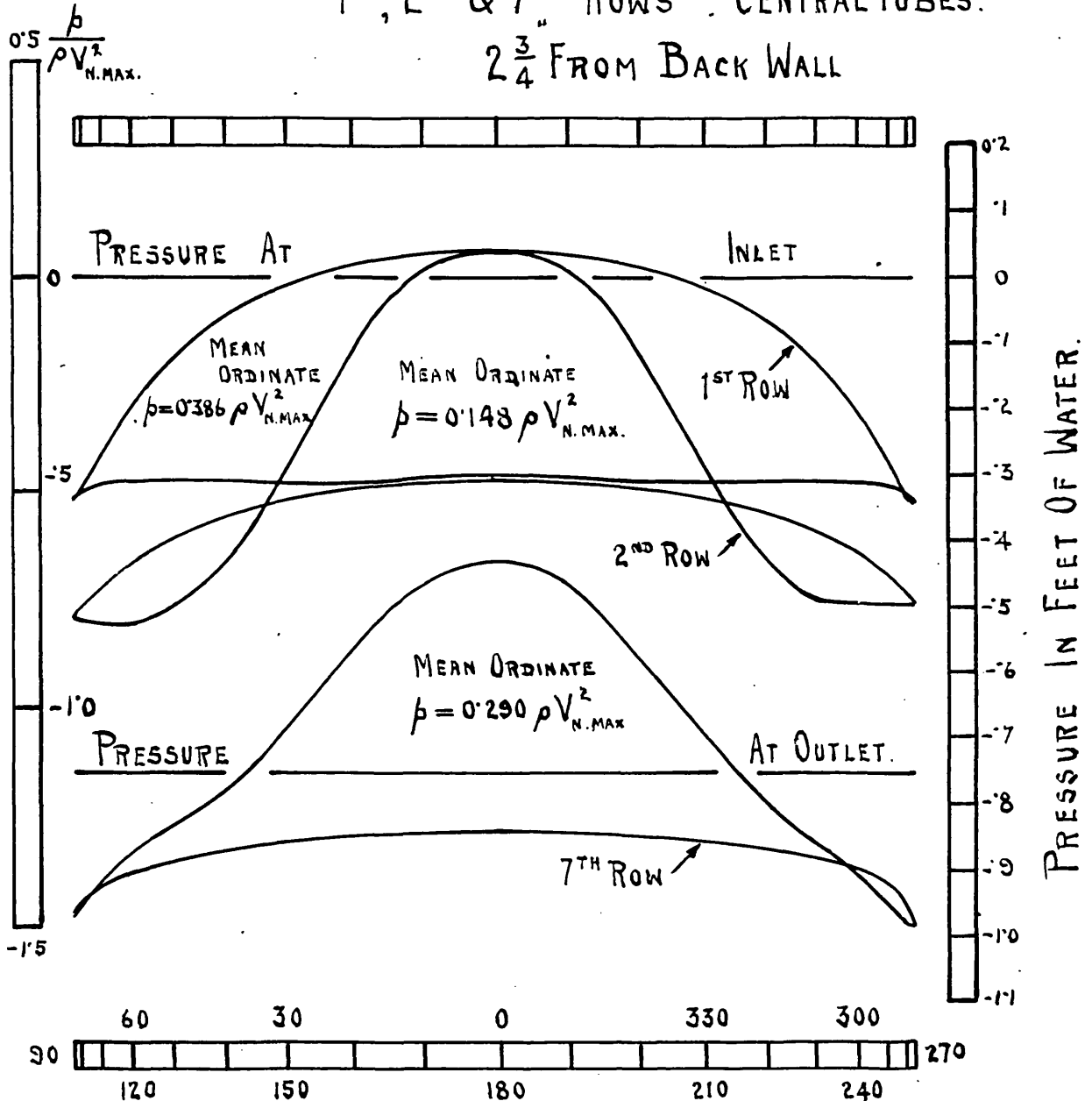
18.3°C $\frac{V_{N,MAX} d}{\nu} = 16,950.$

FORM DRAG DIAGRAMS. FIG. 2.4B.

NEST ROTATED THROUGH 180°

STAGGERED ARRANGEMENT.

1ST, 2ND & 7TH ROWS . CENTRAL TUBES.
 $2\frac{3}{4}$ " FROM BACK WALL



WATER VELOCITY $V_{N.MAX} 140 \frac{CMS}{SEC}.$

$18.3^\circ C.$

$$\frac{V_{N.MAX.} d}{\nu} = 16,950.$$

Figs. 2.4 A and B show the pressure distribution and form drag curves for the centre tube of the 1st and 7th rows with the pressure hole 7 Cms. from the back wall of the apparatus.

Since on the previous results the pressure distribution on the centre tube of the 3rd row always showed characteristics between those of tubes of the 1st and 7th rows, it was considered unnecessary to carry out further experiments on this row.

The distribution of pressure on the 1st tube to the right of the centre-line of the 2nd row, at a plane 7 Cms. from the back wall, is included in these diagrams and further reference is made to this when discussing the subject of form diagrams in detail in section 5.

From Figs. 2.4 A and B it will be seen that while the curves for the centre tube of the 1st row are symmetrical, the curves for the 7th row still show asymmetry. This asymmetry is not so marked as before but it has not changed from right to left hand as was expected.

Since all the experiments in this section were carried out with the pressure hole of the exploration tube at 7 cms. from the back wall of the apparatus, it was realised that with respect to the arrangements for the inlet of the water

two variables had been changed simultaneously. Firstly, the apparatus had been rotated through 180° and, secondly, the plane of exploration had been moved from 0.62 Cm. on one side of the mid-length of the tubes to 0.62 Cm. on the other side. If the plane of exploration were to remain unchanged with respect to the inlet arrangements of the complete water circuit, the observations should have been made with the pressure hole 7 Cms. from the front wall instead of that distance from the back wall. If this relatively small movement of the plane of exploration were the cause of appreciable change in the conditions of asymmetry, then it was certain that the flow through the staggered arrangement of tubes could not be considered to be generally in the direction of the axis of the nest. It would be probable that the mid-length of the tubes would be a point of instability, or at any rate a position where a small movement to the right or the left might make appreciable changes in the angle of impingement of the stream upon the tubes. That this was so was proved by experiments with air instead of water flowing over the tubes.

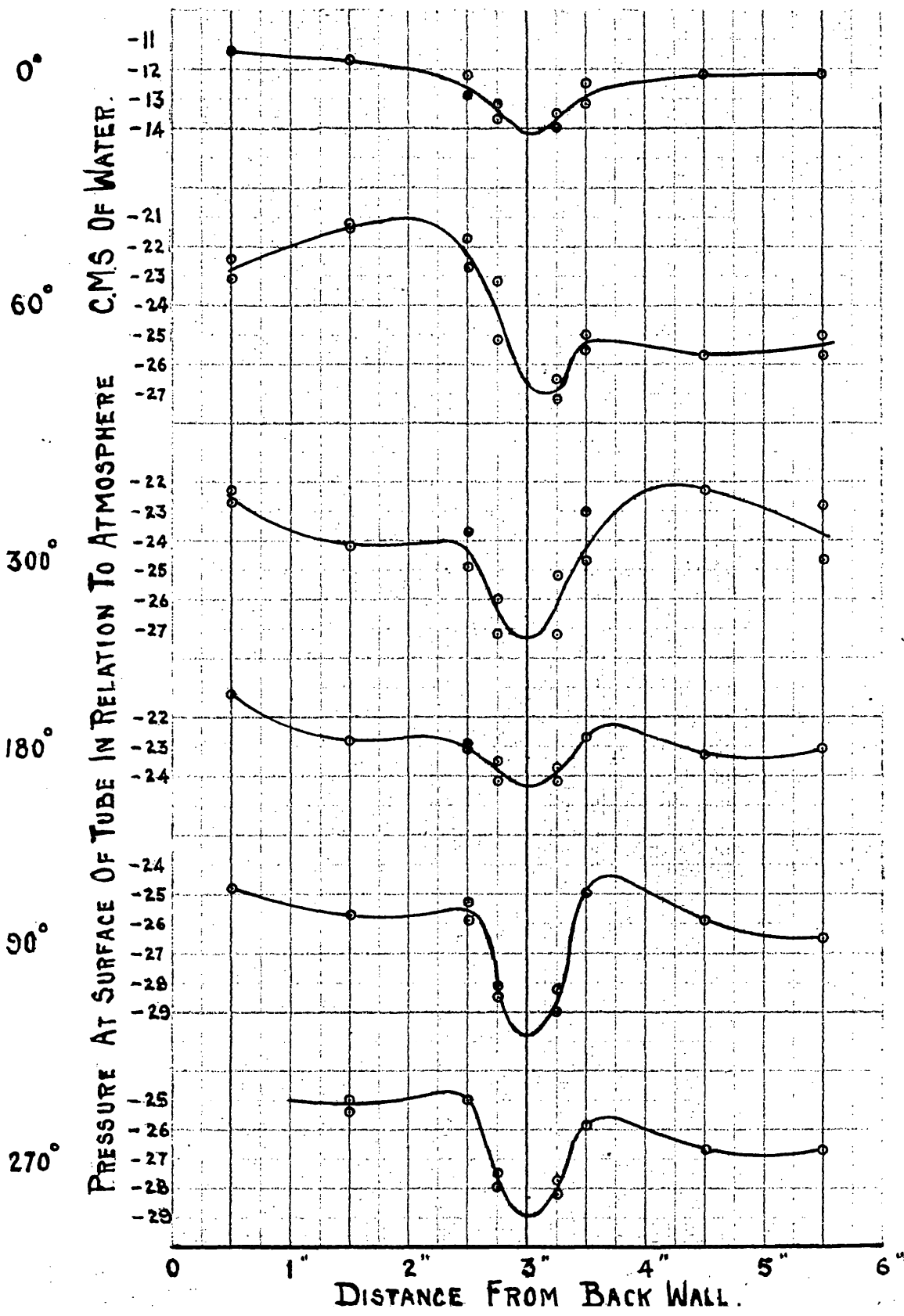
2.5 Asymmetrical flow with air.

Due to the increased convenience with which experiments could be carried out with air flow, it was decided to

INVESTIGATION OF CAUSE OF ASYMMETRY. FIG. 2.5A.

STAGGERED ARRANGEMENT.

7TH ROW CENTRE TUBE.



investigate further the causes of asymmetry of flow with this fluid. For this purpose the nest was arranged horizontally as shown in Figure 1.1.

Since the asymmetry was most marked on the last row of tubes, the centre tube of the 7th row was particularly examined.

Pressure readings at 0° , 60° , 90° , 180° , 270° and 300° were taken at planes 1.27, 3.81, 6.35, 6.98, 8.25, 8.89, 11.43, and 13.97 Cms. from the back wall. These are given in Table 2.5 A and plotted in Fig. 2.5A.

By considering together the curves for 60° and 300° and the curves for 90° and 270° , it appears that the air in the nest has divided into two streams of practically equal width. One of the streams is flowing over half the length of the tubes with a slight upward angle, while the other stream is flowing over the other half length of the tubes with an equal but downward angle.

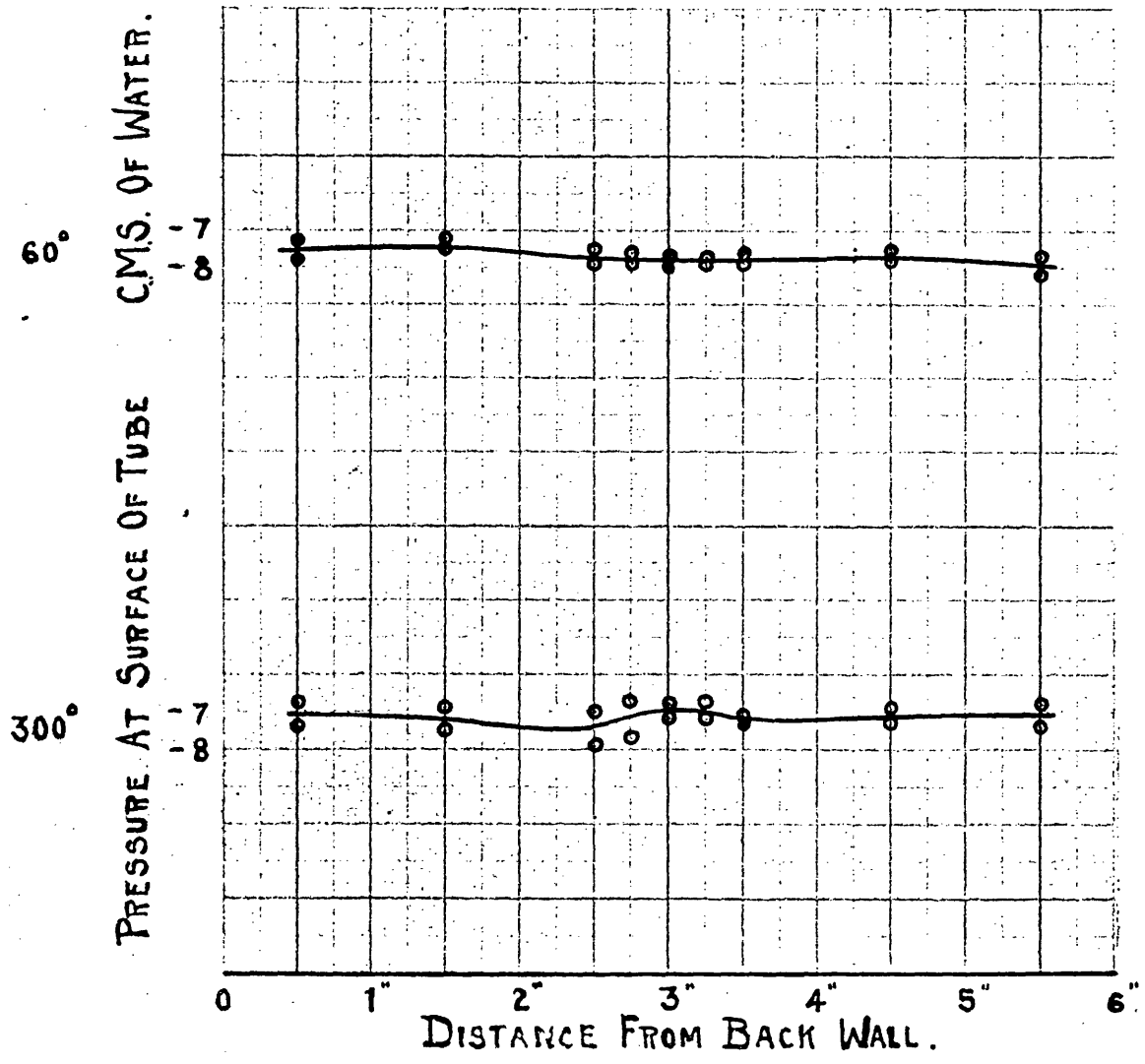
On the curves the maximum and minimum pressure readings have been plotted. From these it will be seen that there exists considerable instability at the centre of the tube and stable conditions at the two ends.

In order to make certain that this dividing of the stream was caused by the flow through the nest of tubes and

INVESTIGATION OF CAUSE OF ASYMMETRY. FIG. 2.5B.

STAGGERED ARRANGEMENT

1ST ROW CENTRE TUBE.



that the asymmetry did not exist in the original stream as it entered the nest, experiments were carried out with the centre tube of the 1st row. Pressure readings across the length of the tube were taken at angles of 60° and 300° , and these are given in the Table 2.5 B and plotted in Fig. 2.5 B. These prove that there was no initial irregularity in the stream and that the asymmetry at the outlet was caused by the flow through the nest.

2.6 General conclusions with regard to instability of staggered nests.

It had been hoped that the flow through the nest would have been two dimensional and that the velocity across any tube would have been approximately constant throughout a large portion of the centre part of the tube. Due to the boundary layer on the sides of the box, it was expected that the velocity of the stream at the ends of the tubes would be less than that over the central portion. Apart from this, it was anticipated that somewhat constant conditions would prevail along the major portion of each tube and that the exploration of any one plane near the mid-length of the tubes would suffice, and that the results obtained on this plane would be typical of all planes except those near to the front and back walls. The previous experiments had proved that this was not so, and the problem now to be

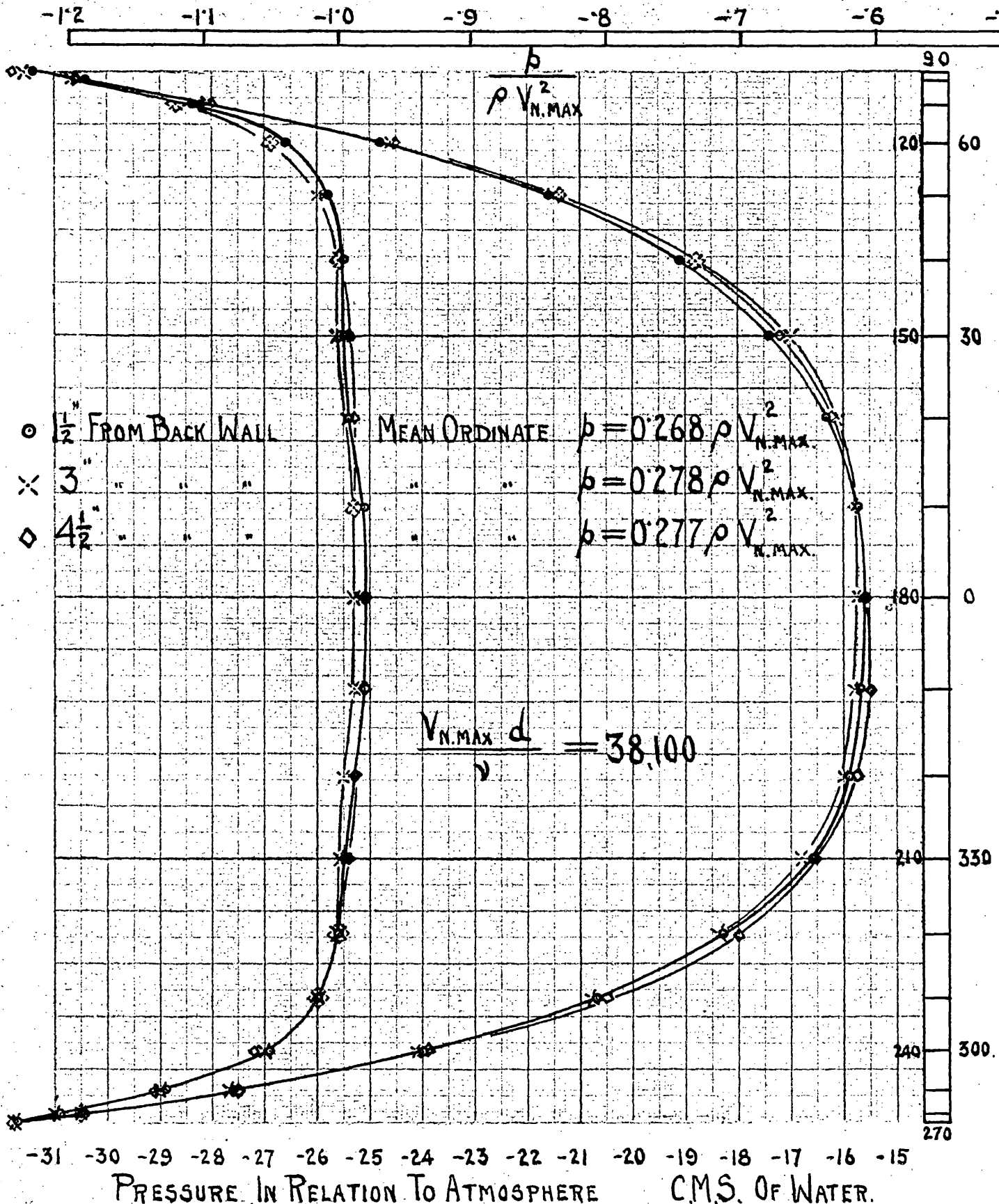
determined was whether this tendency for the stream to divide was inherent in all staggered arrangements or whether the particular spacing of tubes which had been chosen was conducive to this form of asymmetry. Experiments in the Ahlborn tank described in section 7 were carried out with spacing of these particular proportions and with more closely packed and also more open spacing of tubes in staggered formation, but in no case could it be said that the photographs showed that the main direction of the stream as it impinged upon the last row of tubes was different from the original direction of flow.

Here a fundamental difference should be noted between the conditions of the experiments with the air flow over the nest of tubes and those of the Ahlborn tank. In the air experiments the ratio of length to diameter of tubes was 12 to 1, whereas in the Ahlborn tank the ratio was 1.8 to 1. With such a small length to diameter ratio there would naturally be much less tendency for the stream to divide even if the Reynolds' numbers had been the same.

It was realised that with the staggered arrangement and divided flow, the work of determining the pressure and velocity distribution throughout the nest would be prohibitive. It was therefore decided to reduce the nest to one of rectangular tube arrangement. This was achieved

FORM DRAG PARALLEL ARRANGEMENT FIG. 2.6A.

4TH ROW CENTER TUBE.



PRESSURE IN RELATION TO ATMOSPHERE C.M.S. OF WATER.

by removing the 2nd, 4th and 6th rows of tubes and filling the holes in the tube plates with small button-shaped discs of brass.

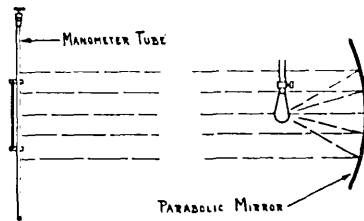
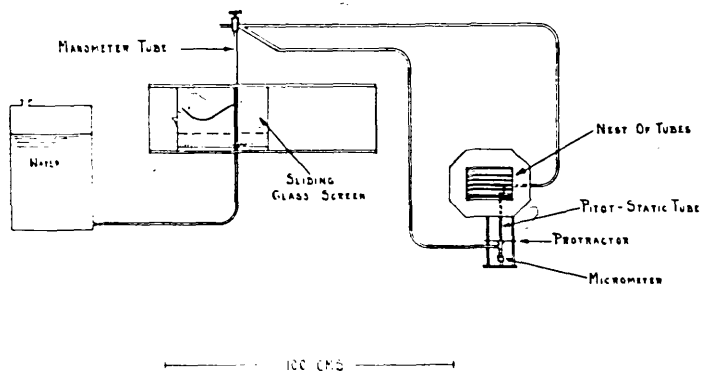
Experiments were repeated on the centre tube of the last (now the 4th) row. The results are given in Table 2.6. Fig. 2.6 A shows the form drag curves at distances of 3.8, 7.6 and 11.4 Cms. from the back wall. These curves are practically alike and symmetrical. From this it is seen that with the rectangular or parallel arrangement of tubes the general flow is always parallel to the axis of the nest and there is no tendency for the stream to divide.

In much work of this nature, where large numbers of pressure readings have to be taken and subsequently plotted, the labour of recording the readings is considerable, and the time involved necessarily great. In the present instance the pressure records were made directly in the form of curves without the intermediate recording of the readings. This was achieved by means of the following device. (See Fig.2.6 B.)

In front of the manometer tube was mounted a glass screen capable of being moved horizontally. To the surface of the glass screen squared paper was attached. At a distance of 500 Cms. behind the manometer tube a parabolic mirror and a 100 watt lamp were erected. The light falling

DIRECT METHOD OF RECORDING PRESSURE READINGS.

FIG. 2-6 B.



11 20 20 20
29

on the empty manometer tube cast an ordinary shadow on the squared paper. When the manometer tube was partially filled with water the lower portion acted as a cylindrical lens and focussed a vertical streak of light on to the squared paper. By moving the glass screen sideways until this streak of light fell on the appropriate ordinate and marking in each case the top of the streak of light, any set of pressure readings could be permanently recorded.

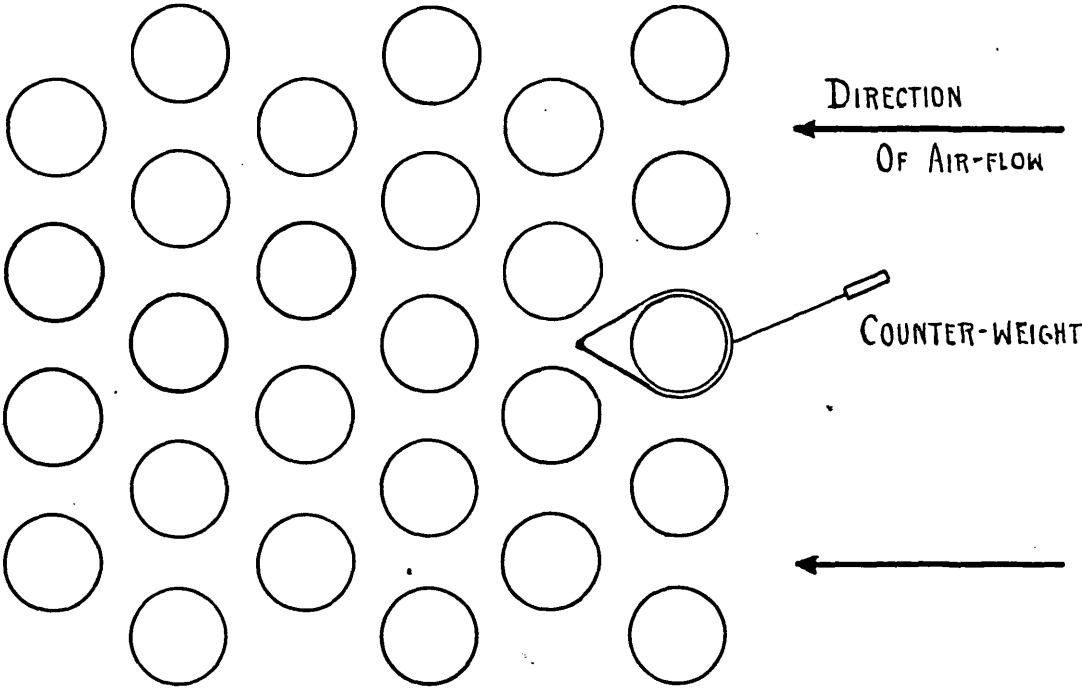
This greatly facilitated the investigation of pressure distribution on the surface of the tubes and after the completion of the form drag diagrams for the parallel arrangement a renewed attack was made on the form drags with staggered arrangement.

While the foregoing explanation of the stream dividing satisfies to some extent the observed asymmetry of pressure distribution, it leaves unexplained the reason why the stream does not take the obvious direct path. From the later experiments there was evidence of a tendency for the asymmetry to be of the same hand from end to end of one tube. This seemed too consistent to be explained as being due to the fortuitous change-over of flow from one experiment to the next. To test this, two form drag diagrams were taken simultaneously at the two ends of the same tube, which was suitably equipped with duplicate pressure holes. Definite

INSTABILITY OF DEAD WATER REGION WITH STAGGERED

ARRANGEMENT OF TUBES.

FIG. 2-6C.



evidence was obtained of the simultaneous existence of left-handed asymmetry at each end of the tube.

In the light of this the Ahlborn tank photographs were re-examined and it was noticed that the dead water region lay in a position of instability between the two adjacent tubes of the succeeding row. It seemed possible that a slight displacement of the dead water region would cause a higher stream velocity and therefore a lower pressure at the side to which it was displaced and the converse on the other side. As a matter of interest an experiment was made in which a tin plate dummy replaced the dead water region as shown in Fig. 2.6 C. As expected, a very definite instability existed and it was only with great difficulty that the dummy could be persuaded to remain central. The stable condition was with the dummy well over to one or the other side.

This experiment was carried out on the first row of tubes and such instability of the dead water region may be accepted in complete explanation of the observed asymmetry in all subsequent rows. The difference of pressure is of less than 20% of the velocity head. This corresponds to a difference of 10% in the stream velocity, an amount hardly noticeable in the Ahlborn tank photographs.

Thus the complete picture of the cause of asymmetry is

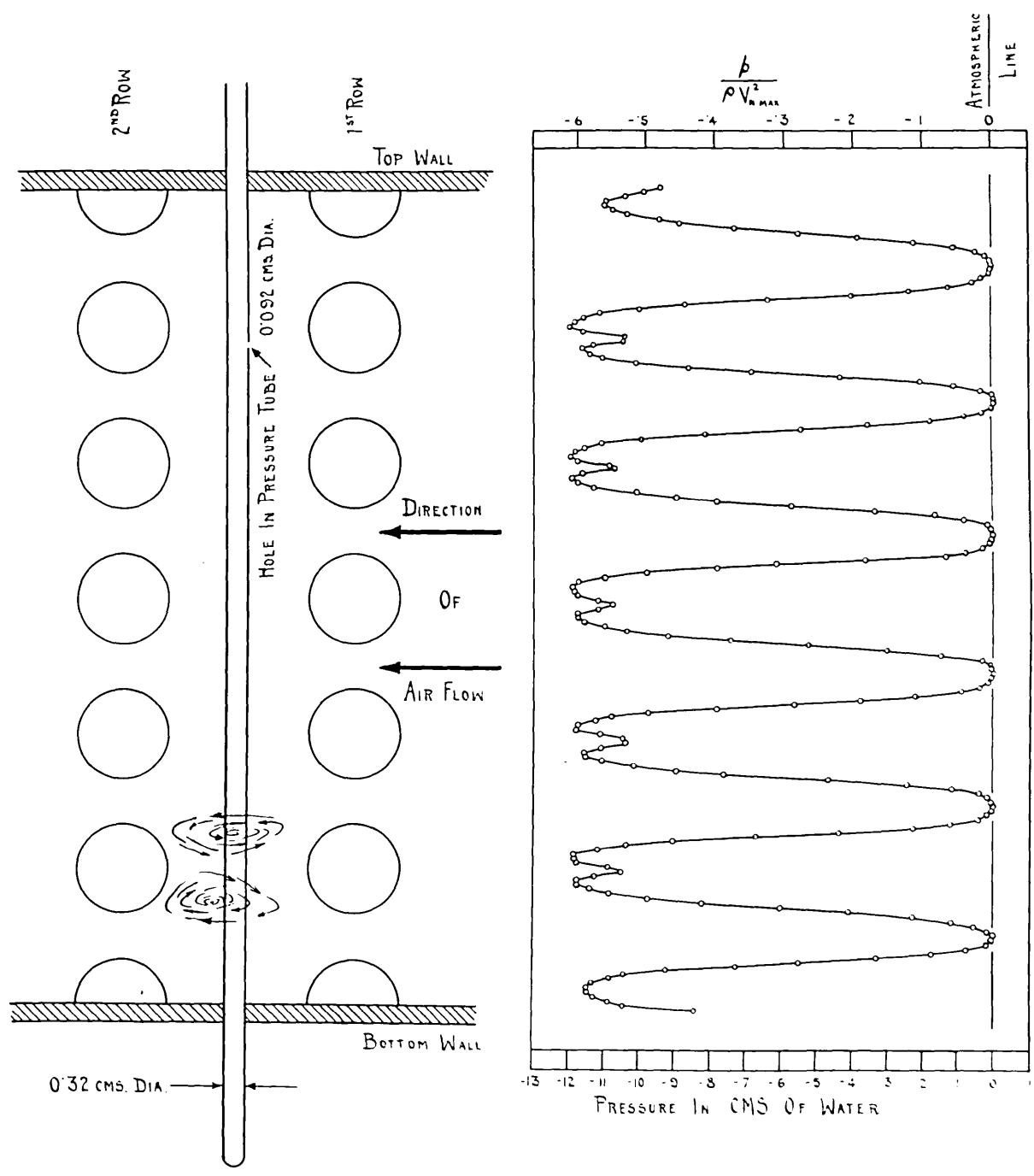
this instability, which in its turn may lead either to a division of the stream or cause the stream to take a zig-zag path throughout the nest.

TOTAL ENERGY AT SECTION BETWEEN 1ST & 2ND ROWS OF TUBES. FIG. 3.1A.

PARALLEL ARRANGEMENT.

$V_0 = 1,340 \text{ CMS/SEC}$ $V_{N,MAX} = 3,966 \text{ CMS/SEC}$

$\frac{V_{N,MAX} d}{\nu} = 35,000.$



3. MEASUREMENT OF VELOCITY DISTRIBUTION ON A CROSS SECTION
BETWEEN 1st AND 2nd ROWS OF TUBES WITH RECTANGULAR
SPACING OF TUBES. PITOT TUBE CHARACTERISTICS.

3.1 Type of Pitot tube used and total energy curves obtained.

The experiments were initiated with the simplest possible design of Pitot tube, viz. a straight tube of 0.320 Cm. diameter placed normal to the stream, with a pressure hole 0.092 Cm. diameter facing up-stream. Theoretically⁽¹⁾ in an inviscid fluid the pressure excess at the up-stream generator of such a cylindrical tube is $\frac{1}{2}\rho V^2$ and the corresponding recorded pressure represents the total energy of the stream. In actual fluids the effect of viscosity is to increase this pressure, but the experiments of Thom⁽²⁾ show that provided the Reynolds' number exceeds 100 there is no detectable deviation.

This arrangement is particularly convenient in problems where the exact location of the Pitot opening is important. As an illustration of this, the curve of total energy Fig. 3.1 A is given. In this case the Pitot tube was traversed in a vertical line with its axis midway between the 1st and 2nd rows of tubes. From the figure it will be seen that

(1) Glauert "The Elements of Aerofoil and Airscrew Theory". p.31

(2) Thom. R. & M. No. 1194 - 1928. p.183.

the position of the pressure hole can be varied without in any way altering the obstructive effect of the tube itself. Further, this arrangement permits the side walls to be reached and in this respect possesses the advantage of the specially designed Pitot tubes of Stanton.⁽¹⁾

The high total energy in the middle of the gaps was in accordance with expectation, but the recovery of pressure immediately behind each of the tubes required further examination, and it was not until after the work on the Ahlborn tank had been carried out that the cause for this recovery of pressure was discerned.

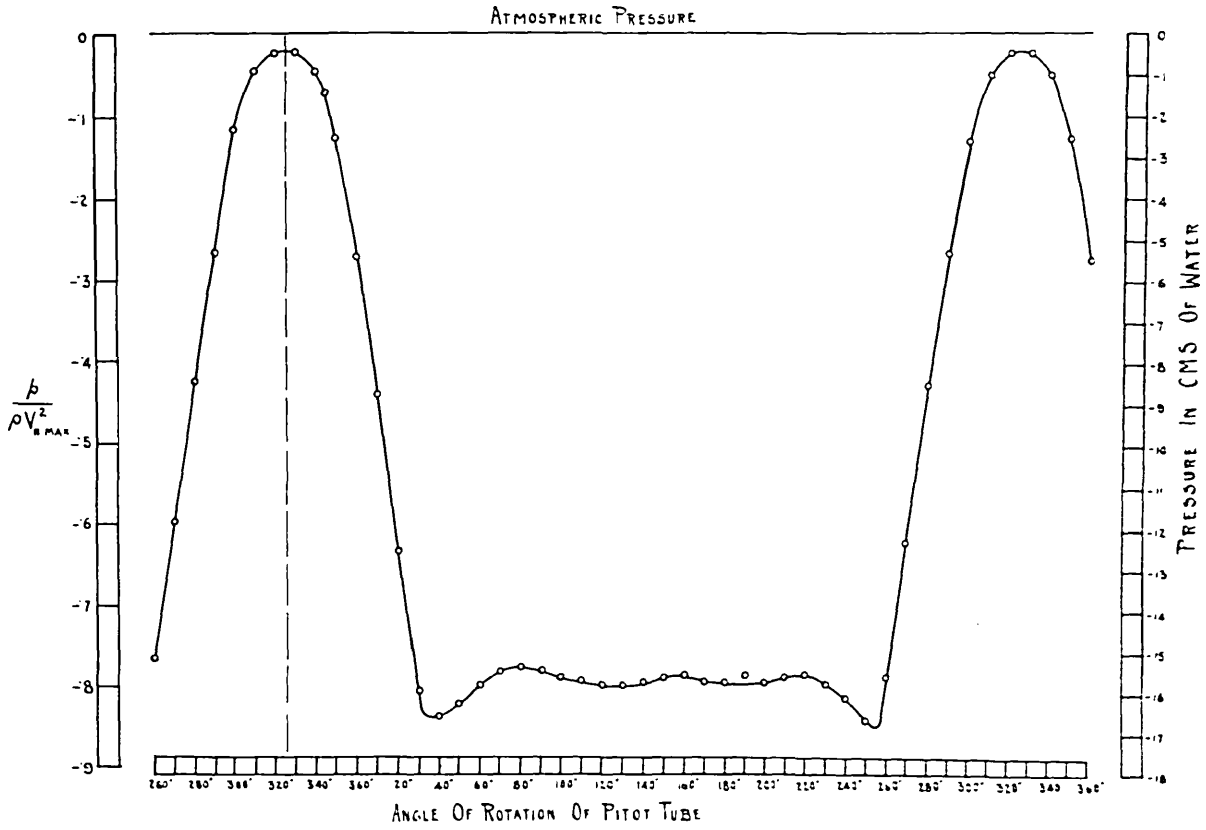
In 1923 Nisi and Porter⁽²⁾ carried out experiments on the velocity distribution in eddies behind a cylinder in a stream of air. From their experiments it was realised that immediately behind the tubes of the first row there is a region of quiescent air. This is followed by an area usually containing two eddies. The eddies have their highest velocity at or near their periphery. Two typical eddies have been drawn on Fig.3.1 A. From this illustration it will be seen that as the Pitot tube is traversed across the first eddy the velocity of the eddy is, at first, in the same direction as the general stream; a little later the pressure

⁽¹⁾Stanton, Marshall and Bryant. Proc. Roy. Soc. A.
Vol. 97 (1920) p. 413.

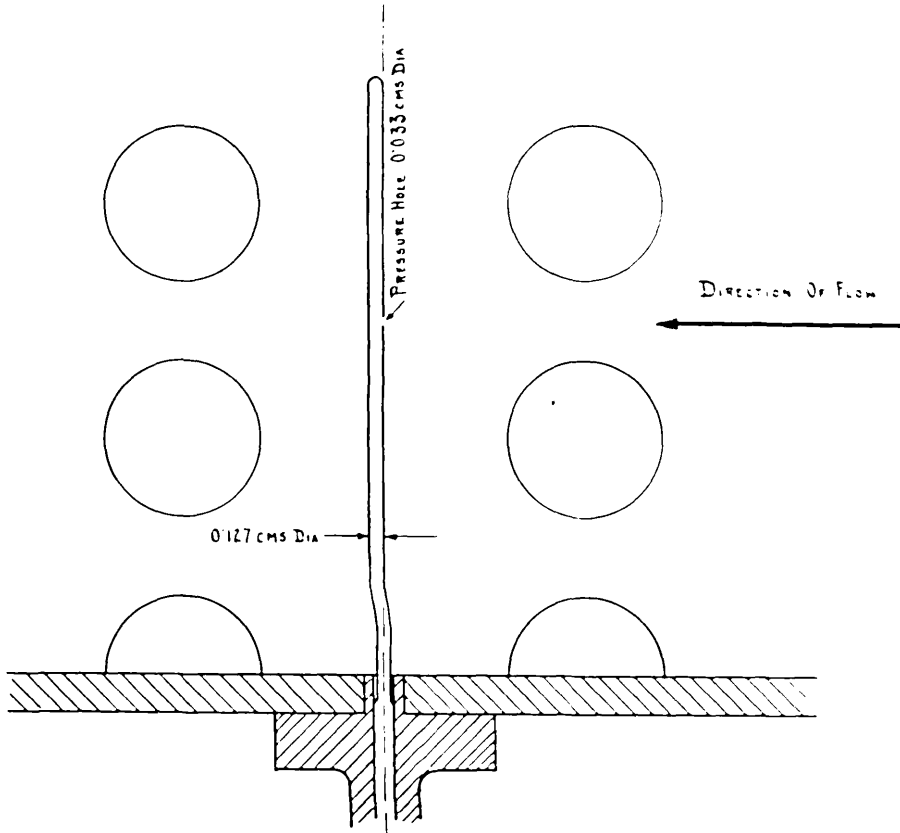
⁽²⁾Nisi and Porter. Phil. Mag. Vol. 46. (1923) p. 754.

METHOD OF ORIENTATION OF PITOT TUBE.

FIG 3'B.



PRESSURE HOLE FACES UPSTREAM WHEN ANGLE = 325°



hole is opposite a portion of the eddy where the velocity is in the opposite direction to the general stream and reaches its maximum velocity in this direction. At this point the maximum negative pressure is registered. As the Pitot tube is traversed still further, the pressure hole passes through the region of quiescent air. Here the air is at rest or moving at extremely slow speed. There is therefore no negative velocity and the pressure as recorded in the manometer tube recovers. If it could be assumed that the air in this region were absolutely at rest the maximum recovery of pressure would indicate the true static pressure at the back of the tubes of the first row. This subject is referred to later in Section 7.5 on the analysis of eddies.

It was thought that the relatively large Pitot tube may have acted as an obstacle to the flow and increased the size of the quiescent air region. It was therefore decided to repeat the experiment with a Pitot tube 0.127 Cm. external diameter (Fig. 3.1 B). A short length of copper tube of this diameter was soldered into a brass tube 0.159 Cm. diameter. The end of the copper tube was closed and a hole 0.033 Cm. diameter was drilled about 2 Cms. from the closed end. The brass tube was arranged to pass through a bush in order to keep the motion vertical. It was appreciated that in the case of the first Pitot tube of diameter 0.318 Cm. the pressure

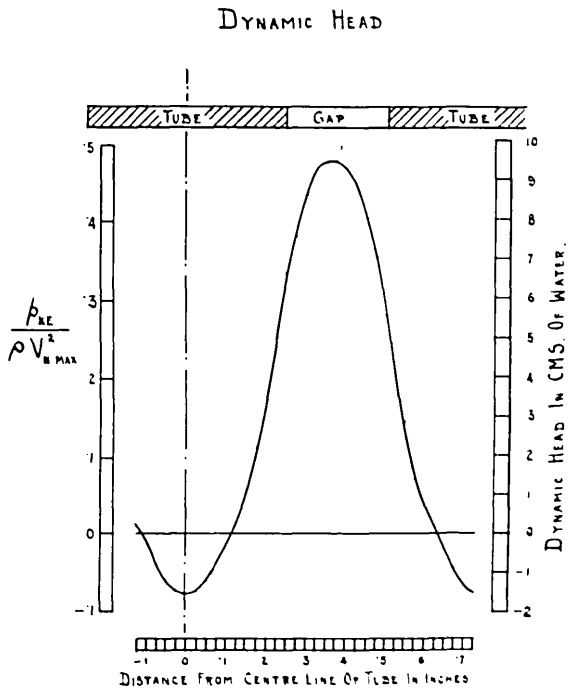
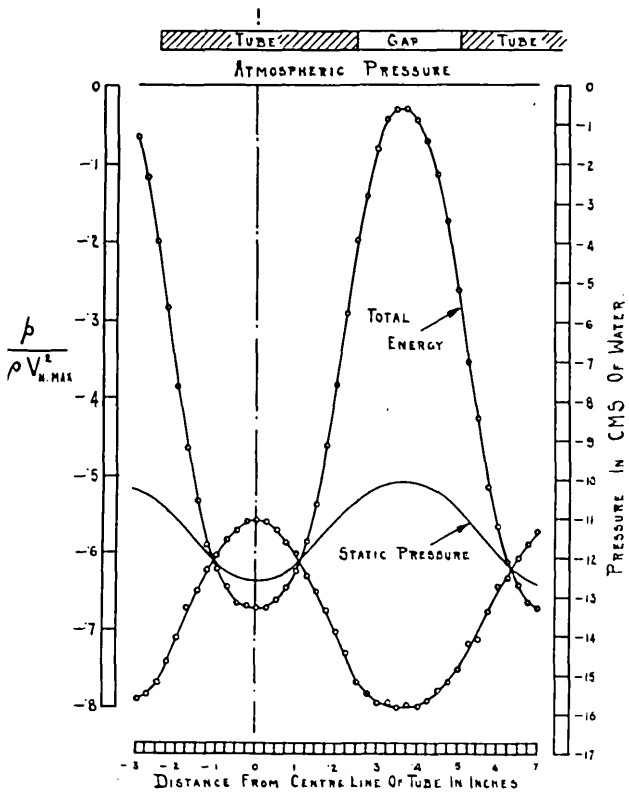
hole in the face of the tube traversed a line $\frac{d}{2}$ or 0.159 Cm. up-stream of the section midway between the 1st and 2nd rows of tubes: and that in the case of the copper tube 0.127 Cm. diameter the pressure hole in the up-stream face would traverse a line 0.0635 Cm. up-stream of the required section. In order that the same transverse section should be explored, no matter what diameter of Pitot tube was used, the copper tube was bent backwards as illustrated in Fig. 3.1 B. With this arrangement the vertical diameter of the pressure hole was on the vertical axis of the Pitot tube and remained stationary when the Pitot tube was revolved.

At the lower end of this Pitot tube was attached a graduated disc 12 Cms. diameter as shown in Figures 1.1 and 1.3 A. The Pitot tube was raised or lowered by means of a micrometer screw until the pressure hole was at the same height as the centre of the gap between two tubes of the nest. The orientation when the pressure hole was facing directly up-stream was determined by rotating the Pitot tube and recording the pressure. Fig. 3.1 B shows such a determination from which the pressure hole is found to face directly up-stream when the graduation on the horizontal disc reads 325° .

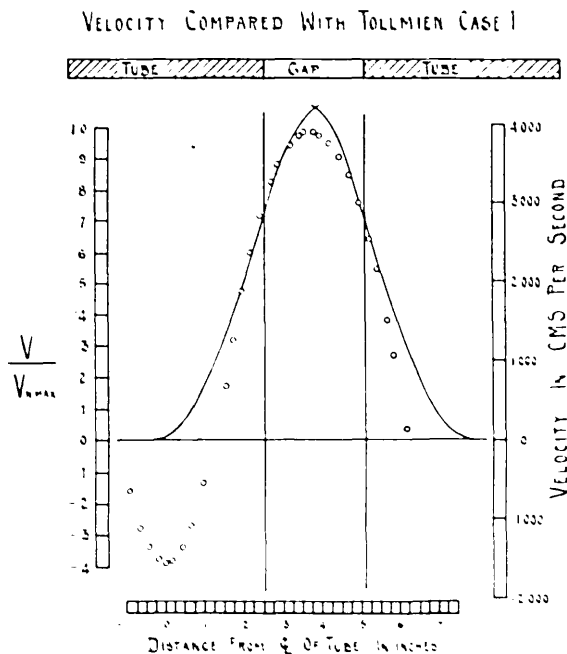
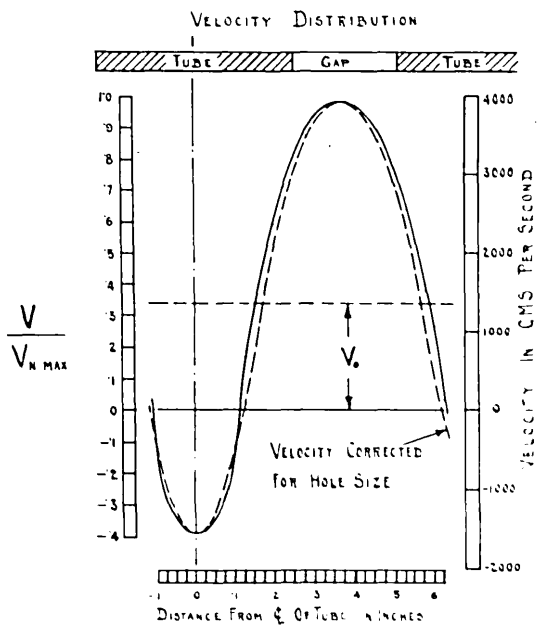
Fig. 3.1 C shows the pressure recorded with this Pitot tube with the pressure hole facing up-stream and also with it

TRANSVERSE VELOCITY DISTRIBUTION

FIG. 31C.



$$\frac{V_{N,MAX} d}{\nu} = 35,000$$



facing directly down-stream. The second curve was added to assist in assessing the negative velocity in the eddies at the back of the tubes. In order to reduce the time taken for the level in the manometer tube to come to rest, four readings of the up-stream pressure were taken and then four readings with the pressure hole facing downstream.

Comparing this curve with 3.1 A it will be seen that there is no recovery of pressure immediately behind the tubes. This is probably due to this traverse being taken 0.159 Cm. further down-stream than 3.1 A and the fact that the smaller diameter Pitot tube would have less tendency to increase the natural size of the quiescent area at the back of the tube.

It will be noticed that in curve 3.1 A the curves rise to a height equal to the atmospheric pressure whereas in curve 3.1 C the maximum height is about 0.5 Cm. below this pressure. Curve 3.1 C is probably the more correct value as this is confirmed by the longitudinal pressure distribution considered in section 4.

3.2 Search for a suitable static tube.

As instanced by Gibson (1) it has always been easier to

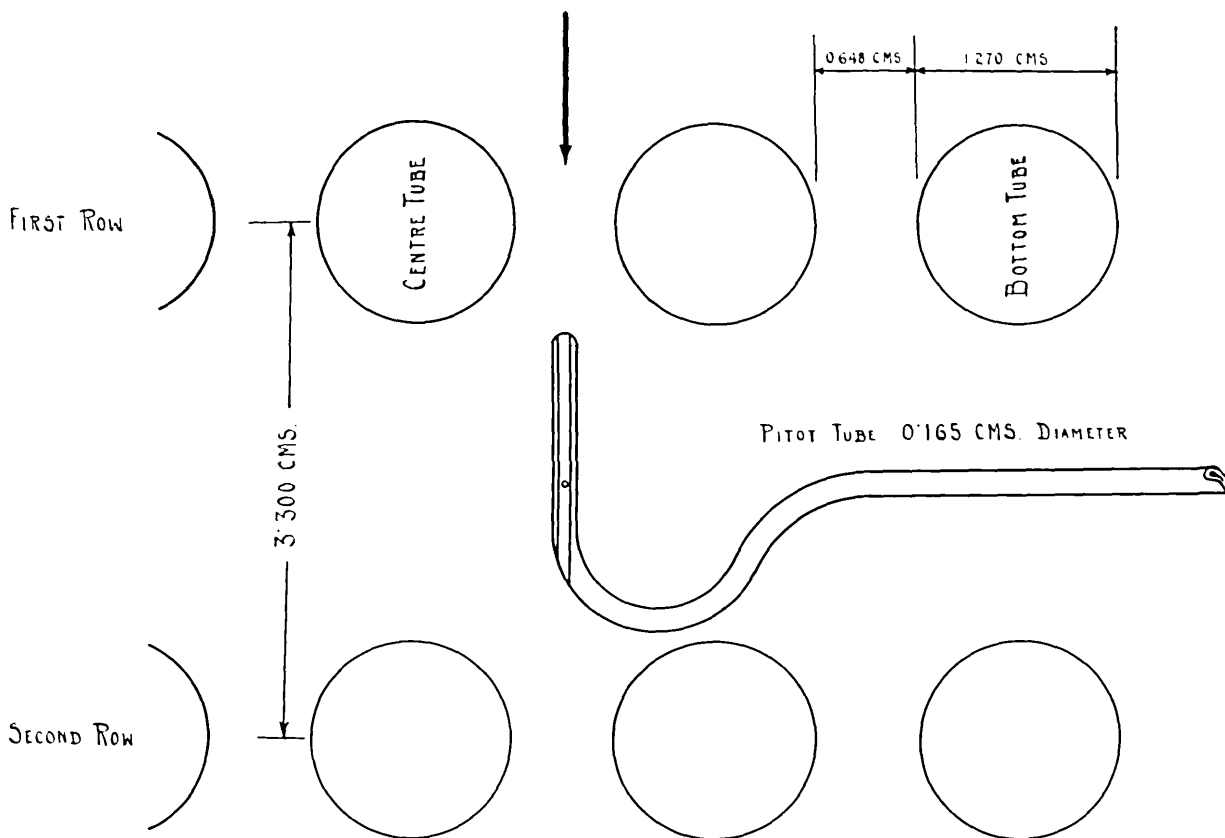
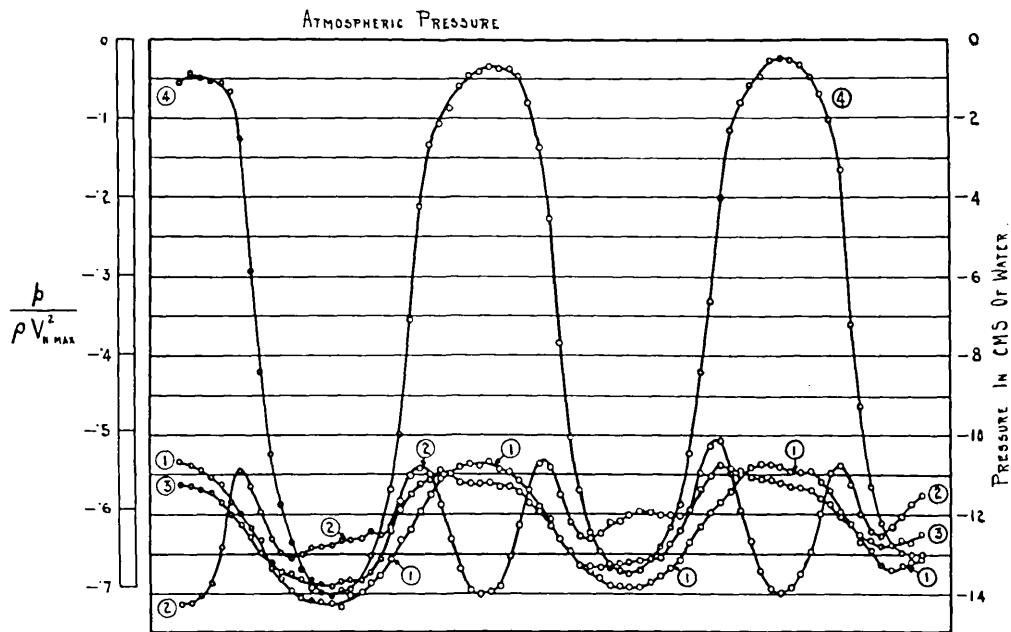
(1) Gibson. The Engineer. July 10th, 1914. p.29.

DISTRIBUTION OF STATIC & TOTAL PRESSURE AT SECTION MIDWAY BETWEEN 1ST & 2ND ROWS.

$V_0 = 1350 \text{ CMS/SEC}$
 $V_{R, \text{MAX}} = 3997 \text{ CMS/SEC}$
 $\frac{V_{R, \text{MAX}} d}{\nu} = 35,100$

FIG. 32 A.

LARGE PITOT



DISTRIBUTION OF STATIC & TOTAL PRESSURE AT SECTION MIDWAY BETWEEN 1st & 2nd ROWS

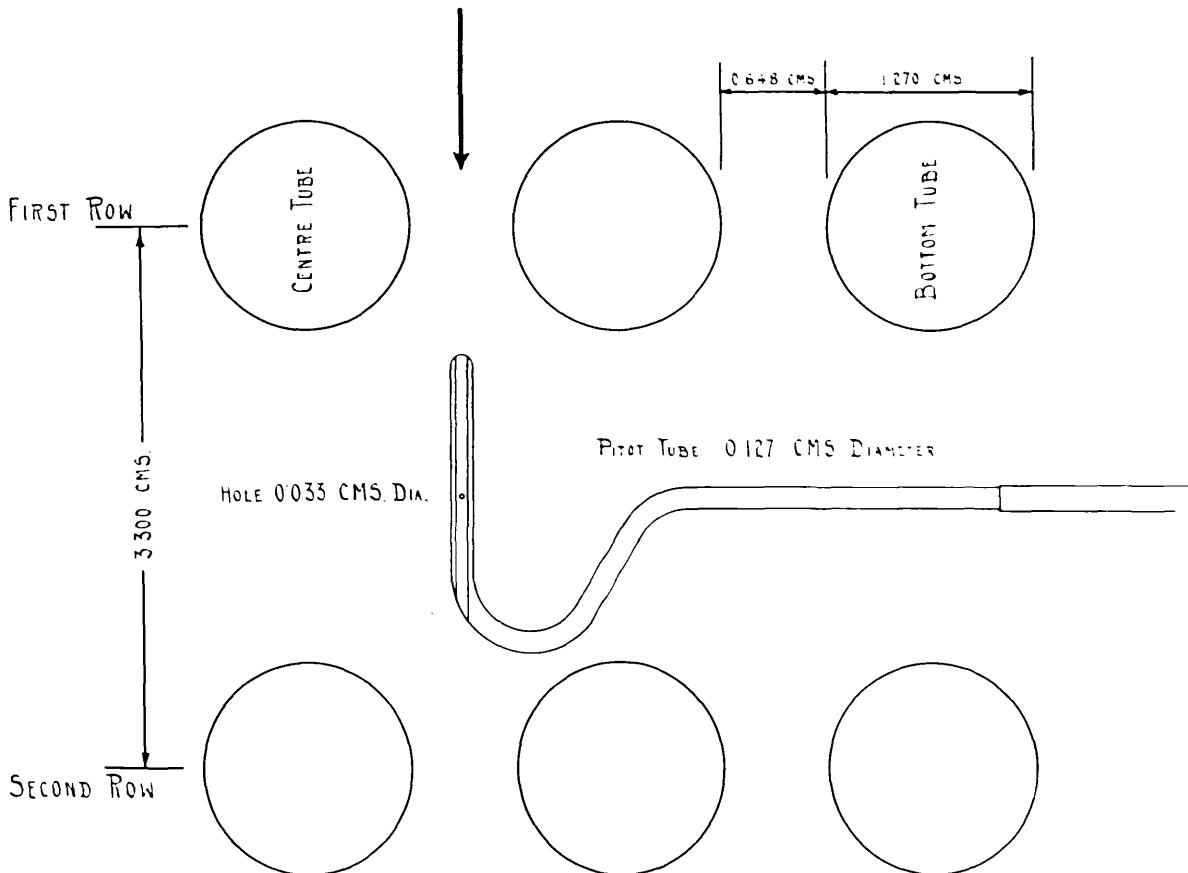
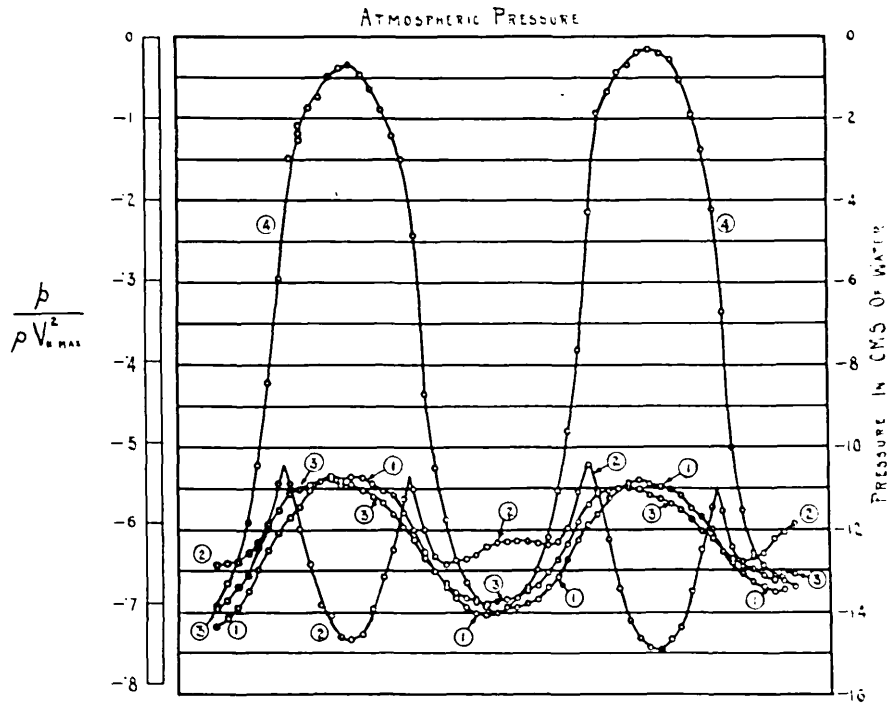
$$V_0 = 1,368 \text{ CMS/SEC}$$

$$V_{\text{max}} = 4,048 \text{ CMS/SEC}$$

$$\frac{V_{\text{max}} d}{\nu} = 33,930$$

FIG 3.2 B.

SMALL PITOT

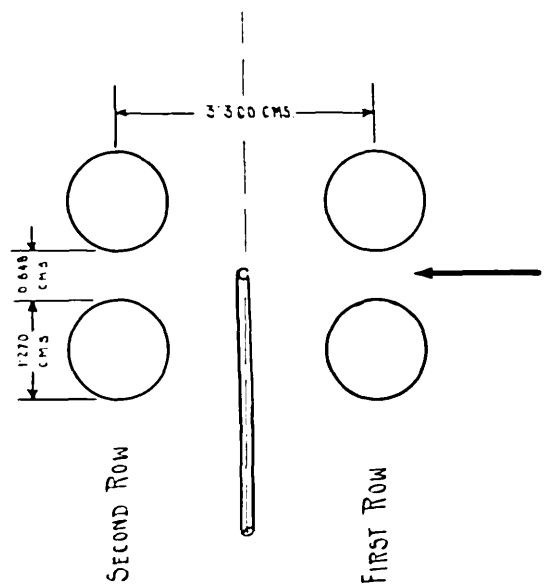
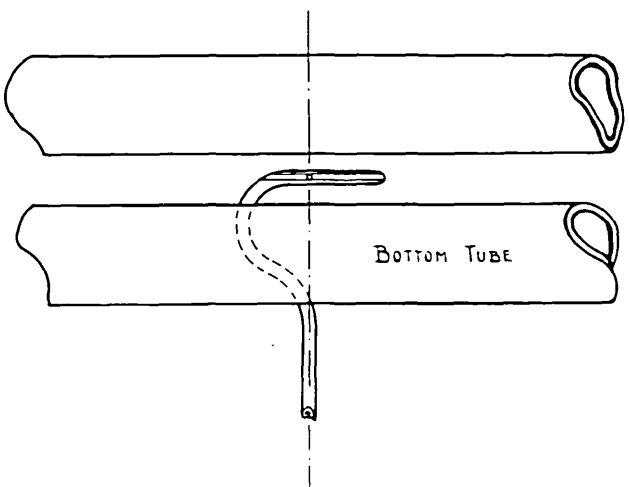
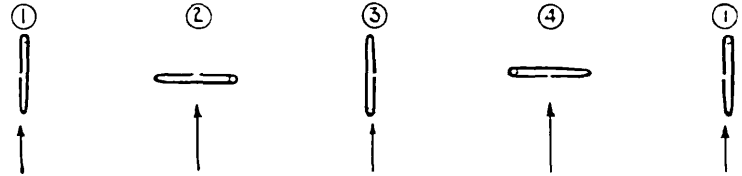
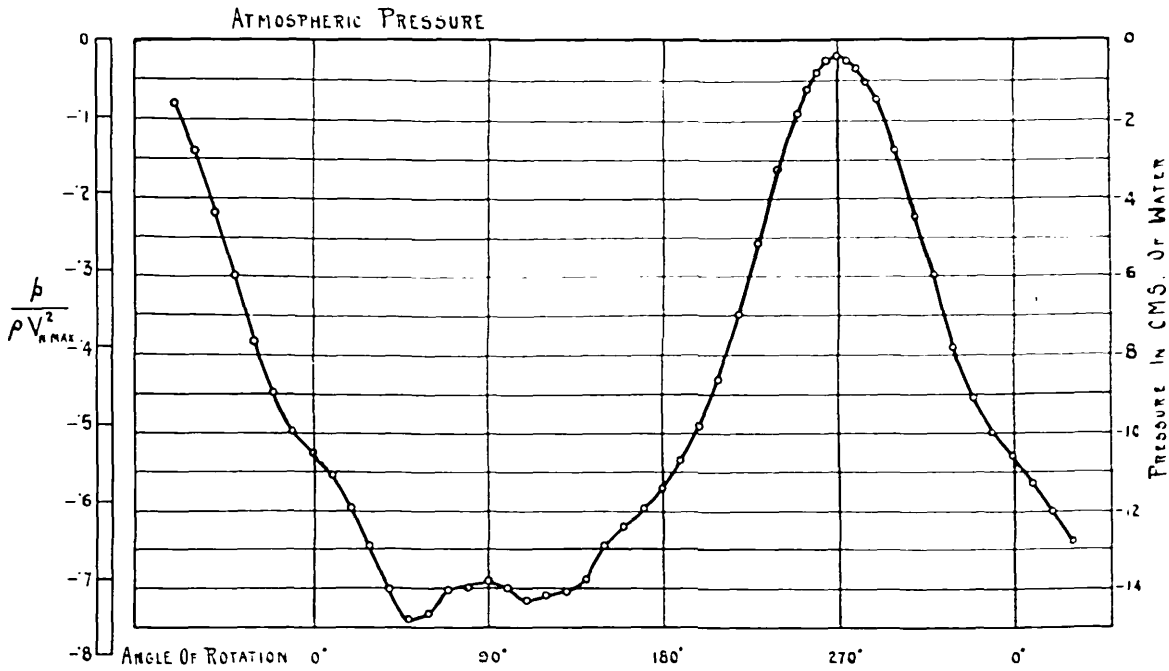


ascertain the total energy of a stream than the true static pressure. More particularly is this the case when both the pressures and velocities are varying rapidly.

The first efforts at the determination of the static pressure were carried out with the hooked-shaped tubes as illustrated in Fig. 3.2 A and B. As in the case of the Pitot tube in Fig. 3.1 B, the head of the hook is bent slightly backwards so that the vertical diameter of the face of the pressure hole remains stationary in space when the tube is revolved. It was thought that such tubes might be used both for Pitot and also for static tubes. When the face of the tube was normal to the stream and facing upstream the total energy would be recorded, but when the tube was revolved through 90° so that the face was in the plane of the stream the static pressure would be registered. When determining the orientation of these hooked Pitot tubes an opportunity was afforded to investigate the pressure recorded by a cylindrical tube when placed at an angle to the stream. The results of this investigation are of interest and have been recorded in appendix No.2.

Fig. 3.2 C shows the curve for the determination of the orientation of the hooked Pitot static tube of 0.165 Cm. diameter. Figs. 3.2 A and B give the results of the transverse exploration with these two tubes. Four curves

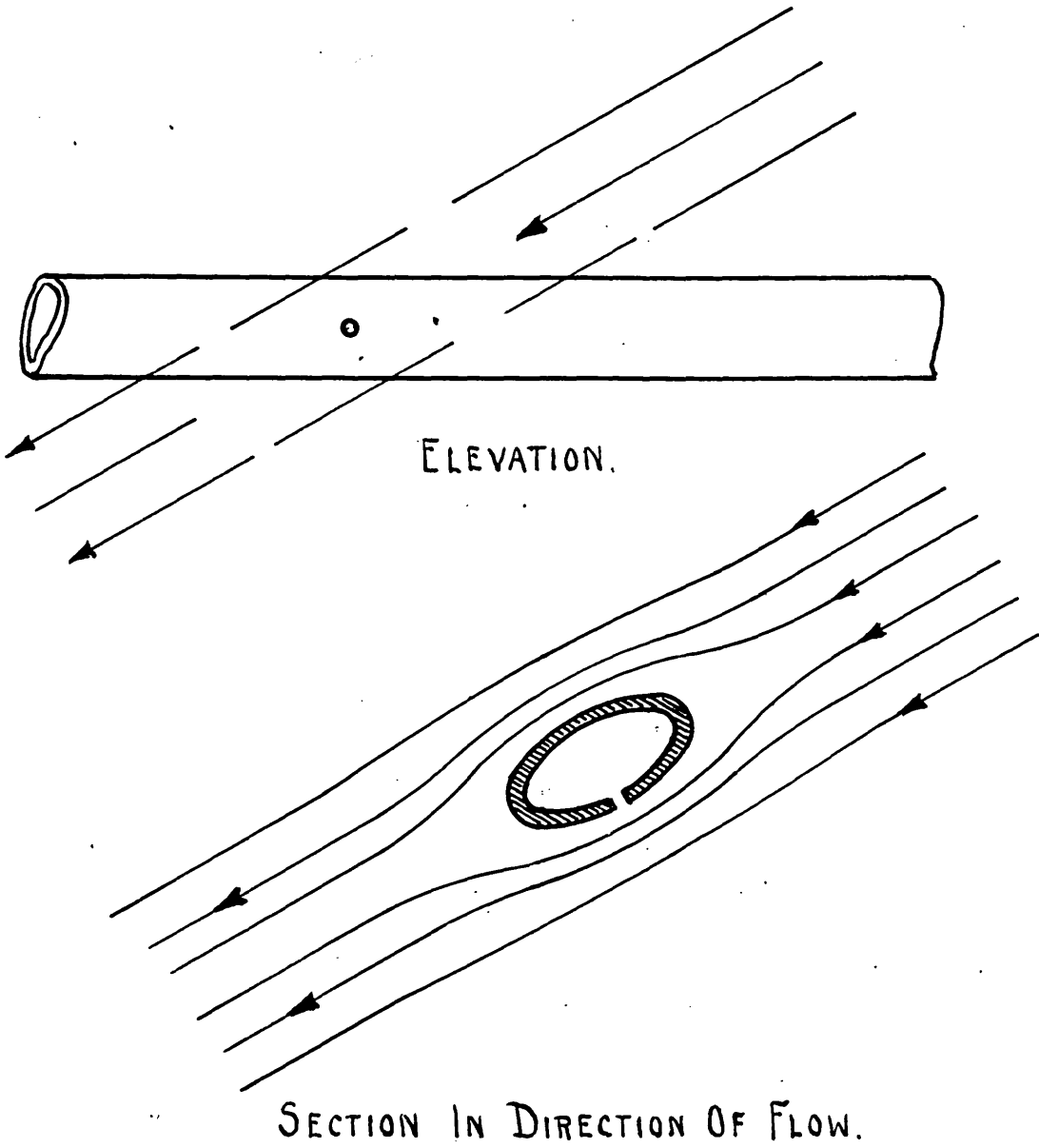
VARIATION OF PRESSURE WITH ANGLE OF ROTATION OF HOOK-SHAPED
 PITOT-STATIC TUBE 0.165 CMS. DIAMETER FIG. 3.2 C.



EFFECT OF STREAM PASSING OBLIQUELY.

OVER STATIC TUBE.

FIG. 3·2 F.



are shown in each case, two static and two total energy. The curves (1), (2), (3) and (4) in Figs. 3.2 A and B are taken with the hooked Pitot tubes in the positions marked (1), (2), (3) and (4) in Fig. 3.2 C respectively. The four positions were considered necessary since complete reversal of flow occurs at the rear of the tubes of the nest.

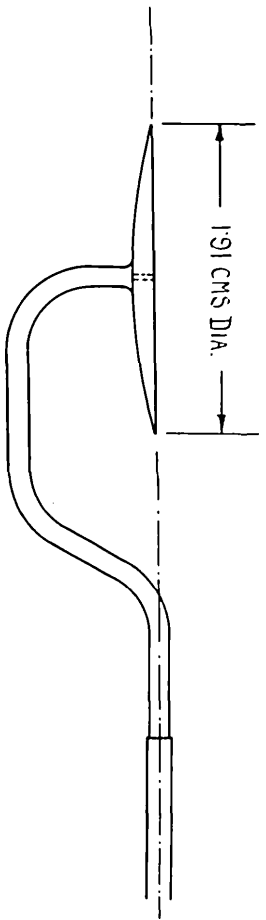
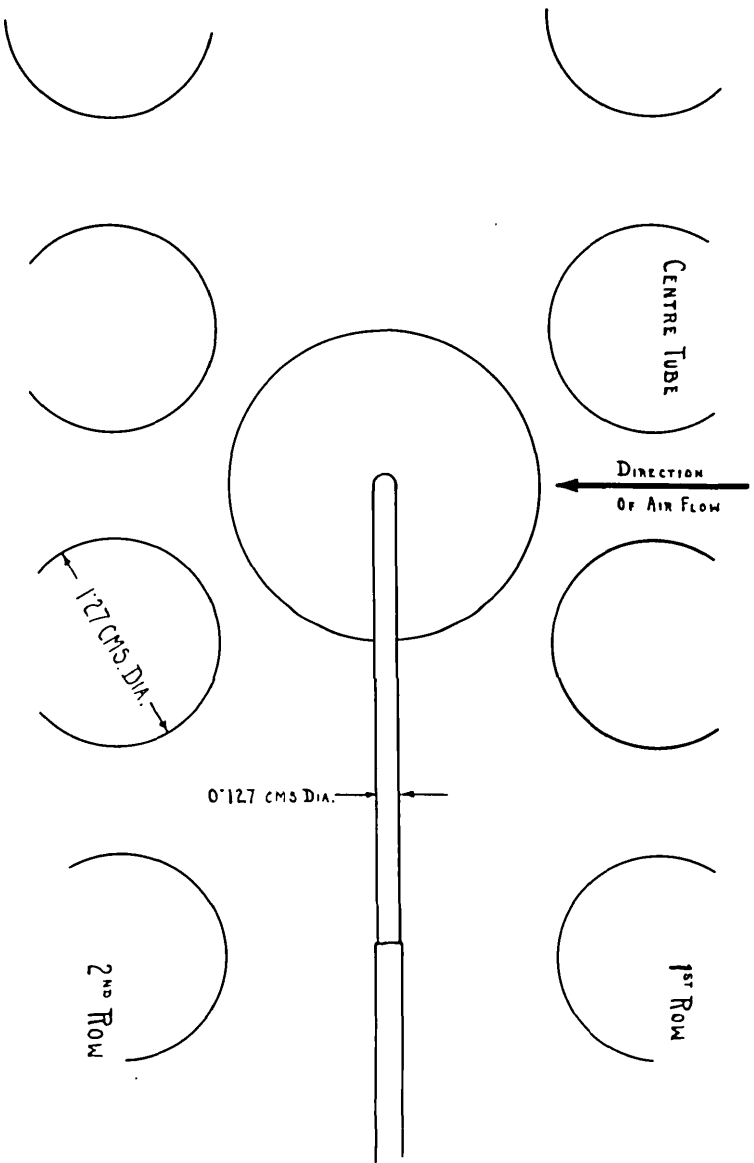
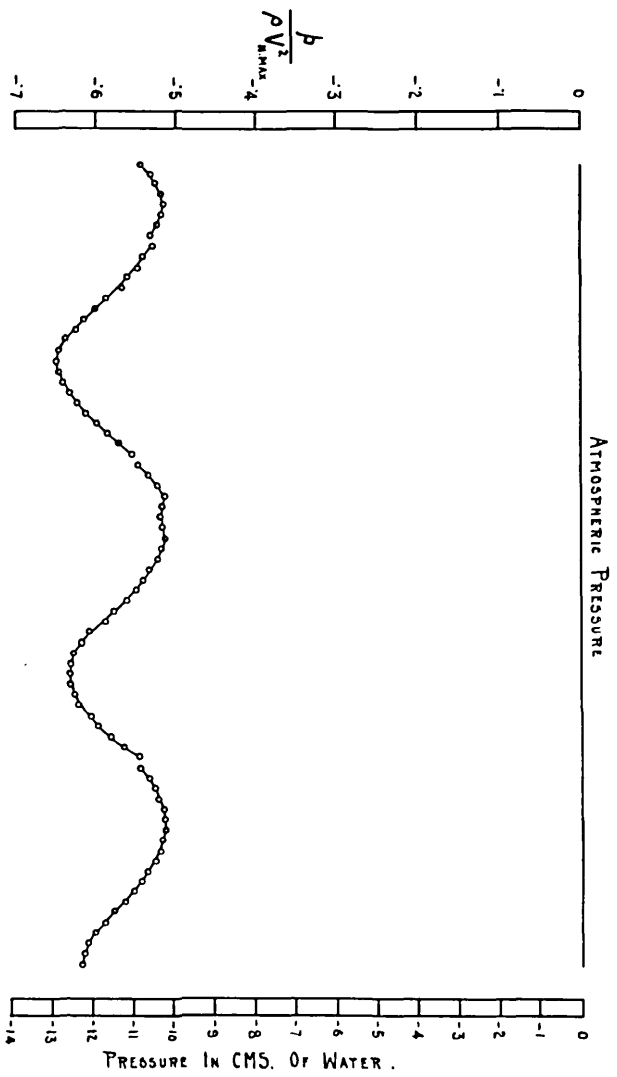
A particular feature noticeable in these figures is that there is an appreciable discrepancy between the two static curves (1) and (3) at the points where the two dynamic curves (2) and (4) intersect, i.e. at the points presumably of zero velocity.

Further consideration showed that a static tube of this type, i.e. one of the conventional type, cannot be used satisfactorily in this investigation. Due to the existence of the eddies, the lines of flow at the back of the tubes are curved and it is difficult, if not impossible, to arrange for the static tube to lie in the direction of the flow. Any tendency for the flow to pass obliquely over this type of static tube will result in a fictitiously low pressure being recorded.

Instead of the flow being in lines parallel to the walls of the static tube as it passes the pressure hole, it is curved outwards as shown in Fig. 3.2 F. This creates a

DETERMINATION OF TRANSVERSE STATIC PRESSURE

FIG. 3-2 G.

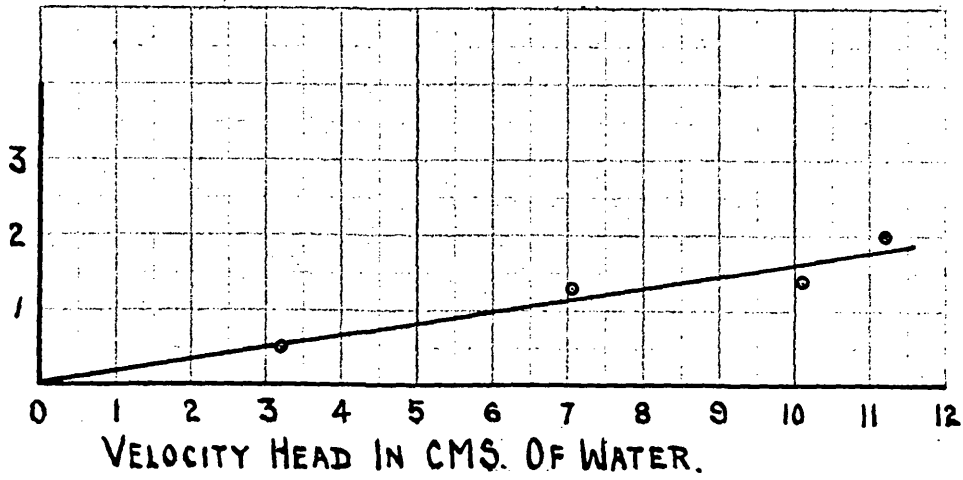


SIDE ELEVATION OF STATIC TUBE.

CALIBRATION OF DISC STATIC TUBE.

FIG. 3-2 H.

AMOUNT BY WHICH DISC STATIC TUBE
READS LOW IN MMS. OF WATER.



centrifugal force which tends to lower the pressure in layers adjacent to the pressure hole.

Since the actual direction of flow varied from point to point across the traverse and was unknown, it was realised that the ideal static tube was one in which the pressure reading was independent of the direction of flow across the pressure hole. This condition was obtained by making the head of the static tube in the form of a disc. (Fig. 3.2 G).

In order to calibrate this disc static tube, all the tubes (except the half-tubes) were removed from the nest and the apparatus used as an ordinary wind tunnel.

The static pressure as indicated by the disc was compared with the static pressure as indicated by a tube of 0.32 Cm. diameter with a closed end and a small hole drilled in the side of the tube. This static tube was held with its axis in the direction of air flow against the front wall of the apparatus, with the hole directly opposite to the hole in the disc. The results are plotted in Fig. 3.2 H and it will be seen that the disc tube indicates a pressure which is lower than the true static pressure by 1.6% of the velocity head $\frac{\rho v^2}{2}$. Fig. 3.2 G shows the static pressure as determined with the disc tube.

3.3 Transverse velocity distribution. Apparent lateral shift of Pitot tube.

In Fig. 3.1 C this static curve has been corrected in accordance with the calibration of the disc and then superimposed to the total energy curve.

From this composite diagram the curve of dynamic head has been obtained. By taking the square root of the heights of the ordinates of this curve the velocity curve has been plotted.

From other experiments when exploring a steep velocity gradient with a standard type of Pitot tube it was known that the pressure recorded by the Pitot tube was not that at its geometrical centre but that at a point $\frac{d_i + 2d_o}{10}$ from the geometrical centre towards the region of higher pressure.

(where d_i = inside diameter of Pitot tube
 d_o = outside " " " ")

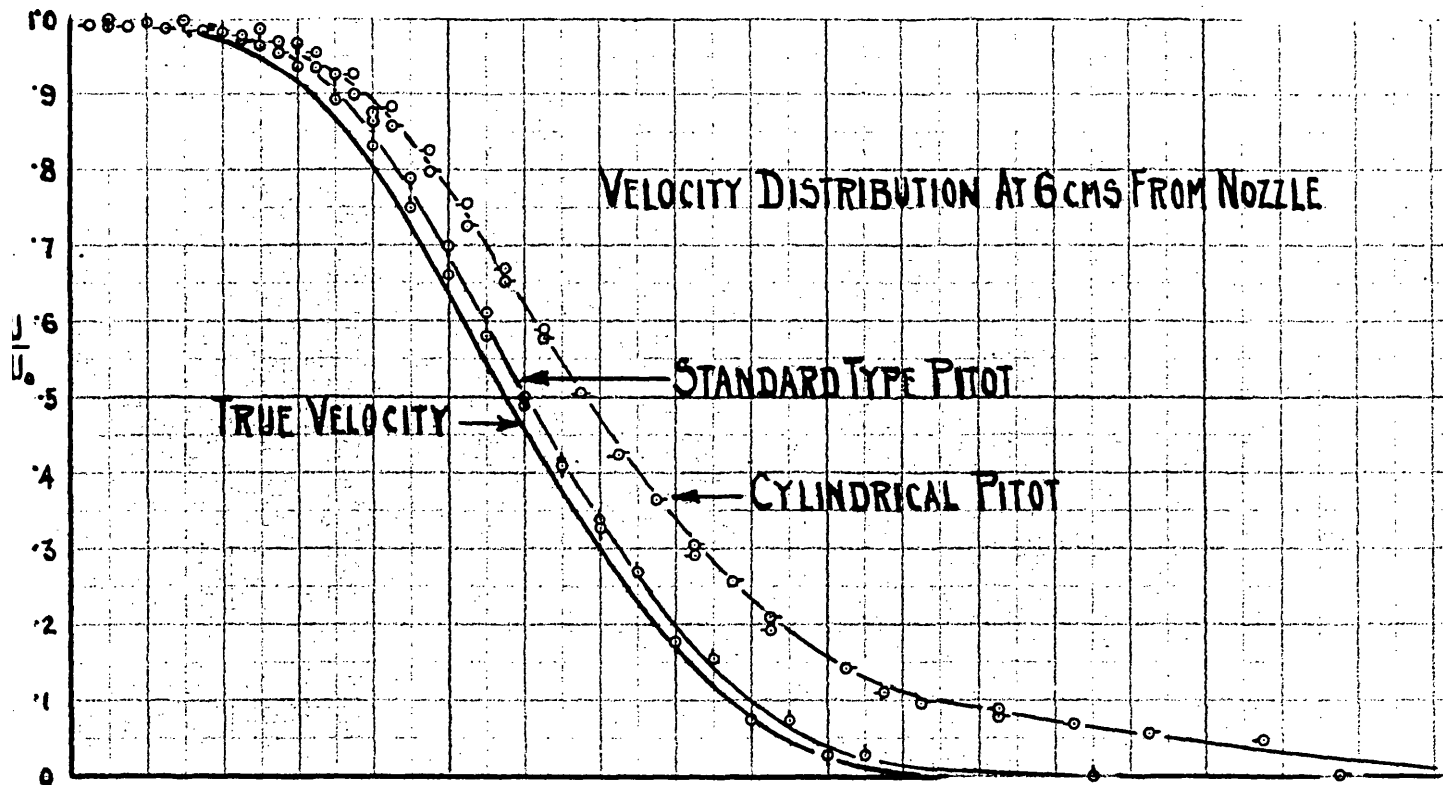
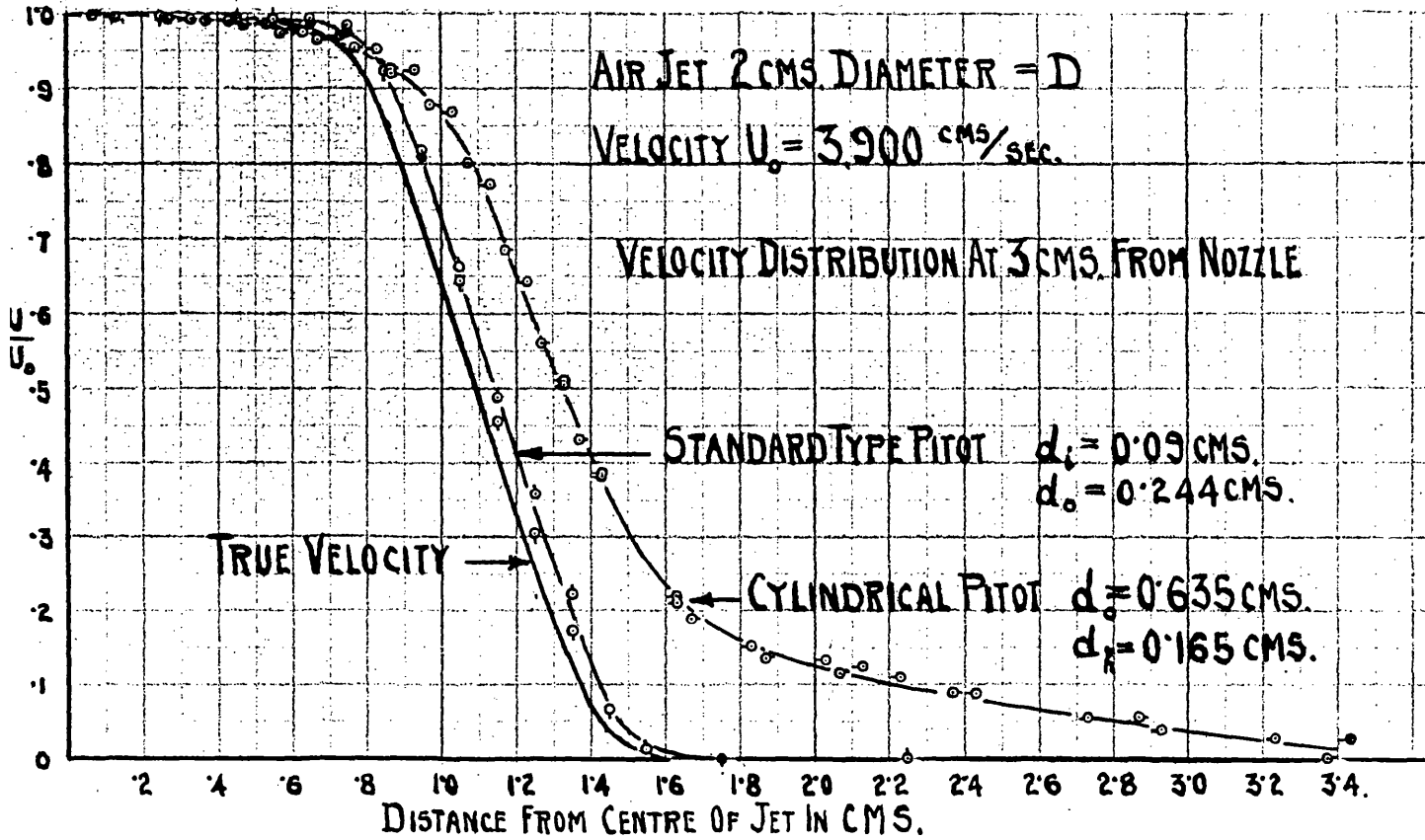
From this it was realised that some correction would have to be applied to the velocity distribution curve to allow for the displacement of the curve due to the size of the cylindrical Pitot tube.

In order to determine the amount of this correction a cylindrical Pitot tube was constructed to the same proportions but five times as large as that used in the nest of tubes.

DETERMINATION OF "SHIFT" OF VELOCITY DISTRIBUTION CURVE

FOR CYLINDRICAL PITOT TUBE

FIG. 3.3.



The velocity distribution across the diameter of a jet of air 2 Cms. diameter was first determined with a standard Pitot tube 0.09 Cm. internal diameter and 0.244 Cm. external diameter at distances of 3 Cms. and 6 Cms. from the face of the nozzle. These are plotted on Fig. 3.3. The above correction for a standard type Pitot was applied to the results and the true velocity distribution is shown by a continuous line in the two diagrams.

The same velocity distributions were then determined with the large scale model of the cylindrical Pitot tube and these are also shown on Fig. 3.3. From this the extent of the "shift" of the velocity distribution line was determined and 1/5 of this amount represented the appropriate correction to apply to Fig. 3.1 C.

The corrected velocity is shown by the broken line in the diagram at the bottom left-hand corner of Fig. 3.1 C. On integrating this curve it was found that mean velocity was 1390 Cms. per second, or 3% greater than the mean entering velocity. This result can be considered to be within the accuracy of the experiments.

4. MEASUREMENT OF THE LONGITUDINAL VELOCITY DISTRIBUTION THROUGH THE NEST.

4.1 Type of static tube used.

A preliminary exploration of the longitudinal variation in static pressure was carried out with the simple static tube described at the end of Section 3.2 and used to calibrate the disc static tube.

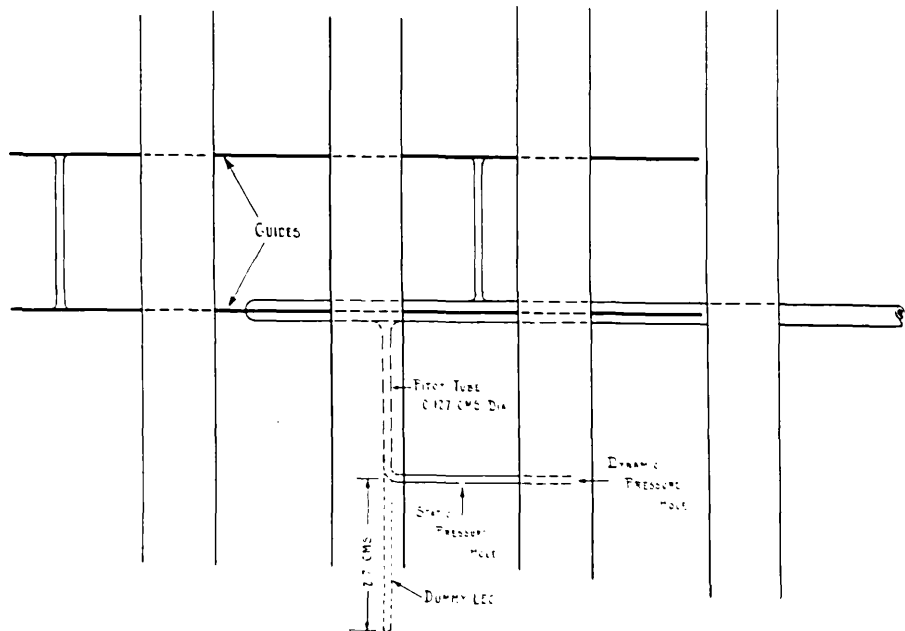
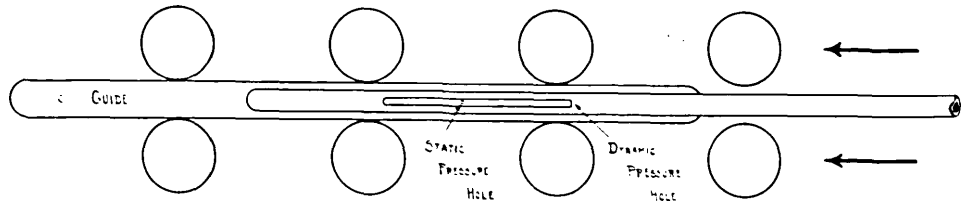
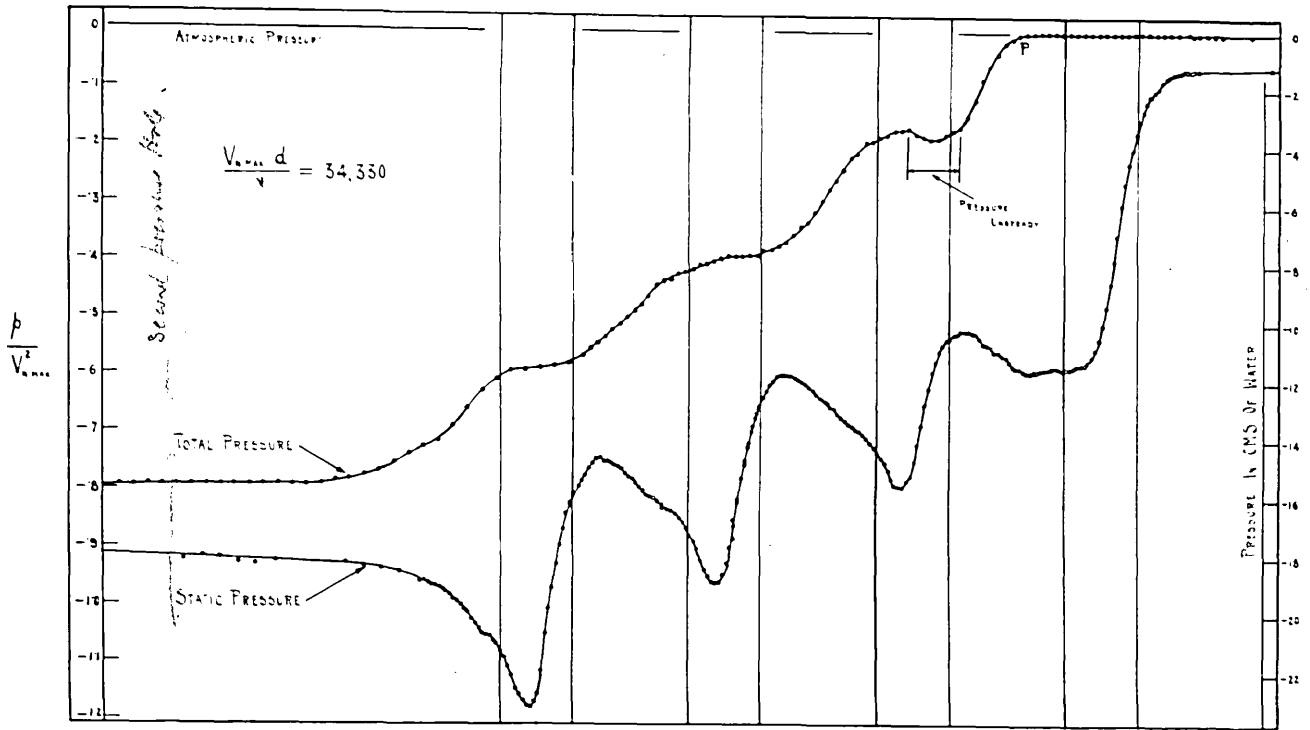
The distance which the tube had entered into the nest was accurately determined with a micrometer as illustrated in Fig. 1.3 A.

Since the gap between any pair of tubes was 0.648 Cm. and the diameter of the static tube was 0.317 Cm. it was evident that some further refinement was necessary before the pressure hole could be allocated exactly between the tubes.

While making this improvement the instrument was adapted so that it would be used to register both the static and the total energy of the stream along a longitudinal section.

4.2 Description of improved Pitot-static tube.

To the simple static tube used in the preliminary work, was fitted a pair of guides somewhat in the form of a sledge and shown in Fig. 4.2. These guides had the effect of



definitely locating the tube midway between the layers of tubes in the nest.

On the side of the tube remote from the sledge was soldered a copper tube of 0.127 Cm. diameter bent into the form of an "L". The end of the "L"-shaped tube was left open and since it faced directly up-stream it could be used as a Pitot tube.

On the outside of the copper tube was drilled a small hole 0.05 Cm. diameter. When this was used for the pressure hole to determine the static pressure, the end of the copper tube was sealed with a small hemispherical blob of plasticine.

When the open end of the copper tube was used to determine the total energy, the static hole was covered with a small piece of adhesive tape.

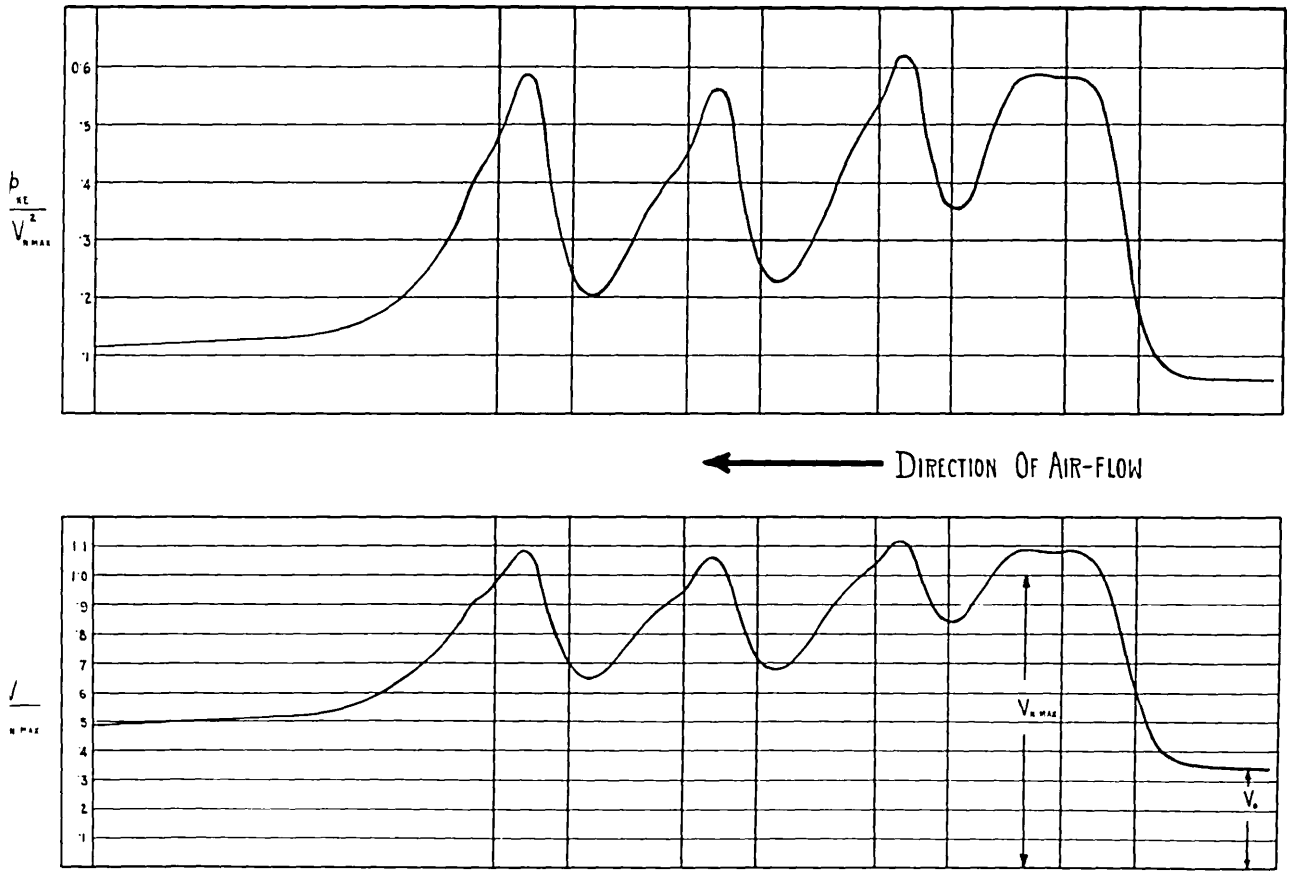
To determine the exact position of the static hole in relation to the centre line of the first row of the nest the Pitot tube was inserted part way into the nest and nicked with a flat knife blade bevelled on one side only. This knife blade was firmly pressed against the upstream faces of the first row of tubes so ensuring that the nick corresponded to this plane. The micrometer was simultaneously read and the relatively position of the nick and Pitot hole subsequently determined by a travelling microscope.

LONGITUDINAL VELOCITY DISTRIBUTION

FIG. 4-3 A.

$V_{max} = 4,000 \text{ cms/sec}$

$\frac{V_{max} d}{\nu} = 34,260.$



4.3 The observed longitudinal variation of velocity.

This Pitot tube when traversed longitudinally between the bottom and next to bottom layers of tubes yielded the curves shown in Fig. 4.2 from which the non-dimensional curves in Fig. 4.3 A have been constructed to show the pressure and velocity variations in the axial direction.

Unfortunately at the time of carrying out these experiments the author had not read Ower and Johansen's⁽¹⁾ work on Pitot tubes in which is discussed the effect of curvature of the boundary layer at the nose of the instrument in reducing the indicated static pressure and also the effect of the stem of the instrument in increasing the indicated static pressure.

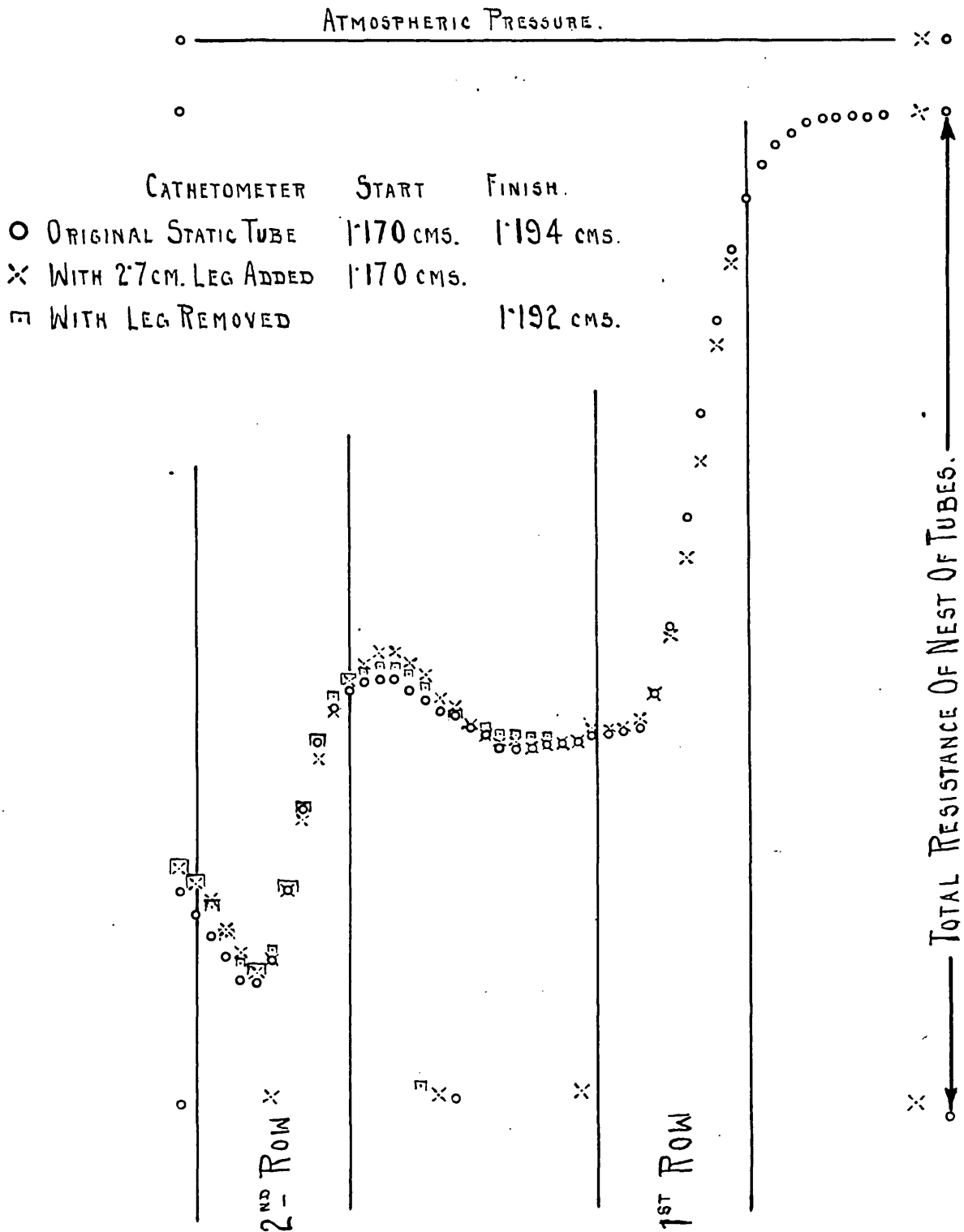
Ower and Johansen suggest that for a round-nosed tube with seven holes equally spaced around the circumference, these holes should be placed 6 diameters from the base of the hemispherical end and 15 diameters from the stem.

From Fig. 4.2 it will be seen that the distance (14 diameters) of the static hole from the nose of the instrument is sufficient and the curvature of the lines of flow in the boundary layer should not cause any appreciable depression of the reading.

(1) Ower & Johansen. R. & M. No. 981 - 1925. p.985.

ACCURACY OF LONGITUDINAL STATIC PRESSURE.

FIG. 4·3B.



On the other hand, in the light of Ower and Johansen's work it is seen that the distance of 10 diameters between the static hole and the stem is somewhat too small.

Since in the sledge Pitot-static tube there was only one static hole and that was drilled on the side remote from the stem, it is probable that the influence of the proximity of the stem would not be so great as in Ower and Johansen's tube. To test whether the stem did influence the readings a second stem or leg 2.7 Cms. long was soldered on the opposite side of the static tube as shown dotted in Fig. 4.2.

Fig. 4.3 B shows the results. The longitudinal traverse was first made with the original design of sledge Pitot-static tube and the results are plotted, 0 on the figure. The second leg was then soldered to the tube and the results are plotted X.

It will be seen that when the static pressure is falling the second leg appears to make the pressure lower by about 0.5 Cm. and when the static pressure is rising it appears to make the pressure from 0.2 to 0.5 Cm. higher.

The second leg was then removed and the results are plotted □. These are found to be within a few millimetres of the previous readings.

From the recorded pressures of the total resistance of the nest, it will be seen that the above results are within the accuracy with which it was possible to keep the air speed constant. The maximum variation of the total resistance was 0.5 Cm.

5. INVESTIGATION OF THE FORM DRAG OF THE VARIOUS TUBES.5.1 Aim of the investigation.

It is well known⁽¹⁾ that the resistance of any obstacle in a fluid stream can be divided into two parts: firstly, the tangential drag of the boundary layer between the surface of the obstacle and the main stream, and, secondly, the form or pressure drag of the obstacle.

On the analogy first propounded by Osborne Reynolds⁽²⁾ there is a definite relationship between the change of momentum in the boundary layer and the heat transferred from the obstacle to the stream, if the obstacle is at a higher temperature. It was thought that if the form drag of each of the tubes could be determined, it would be possible to separate the total hydraulic resistance in the nest into its constituent parts and to state what proportion of this resistance was due to tangential drag and what proportion was due to form drag.

If this could be done it was anticipated that a scientific basis would be obtained for the study of heat transfer in nests of tubes.

(1) White, C.M. Inst. Chem. Eng. Vol.10 - 1932. p. 66.

(2) Osborne Reynolds. Scientific Papers. Vol. I.

5.2 Experimental arrangements and typical results of form drag investigations.

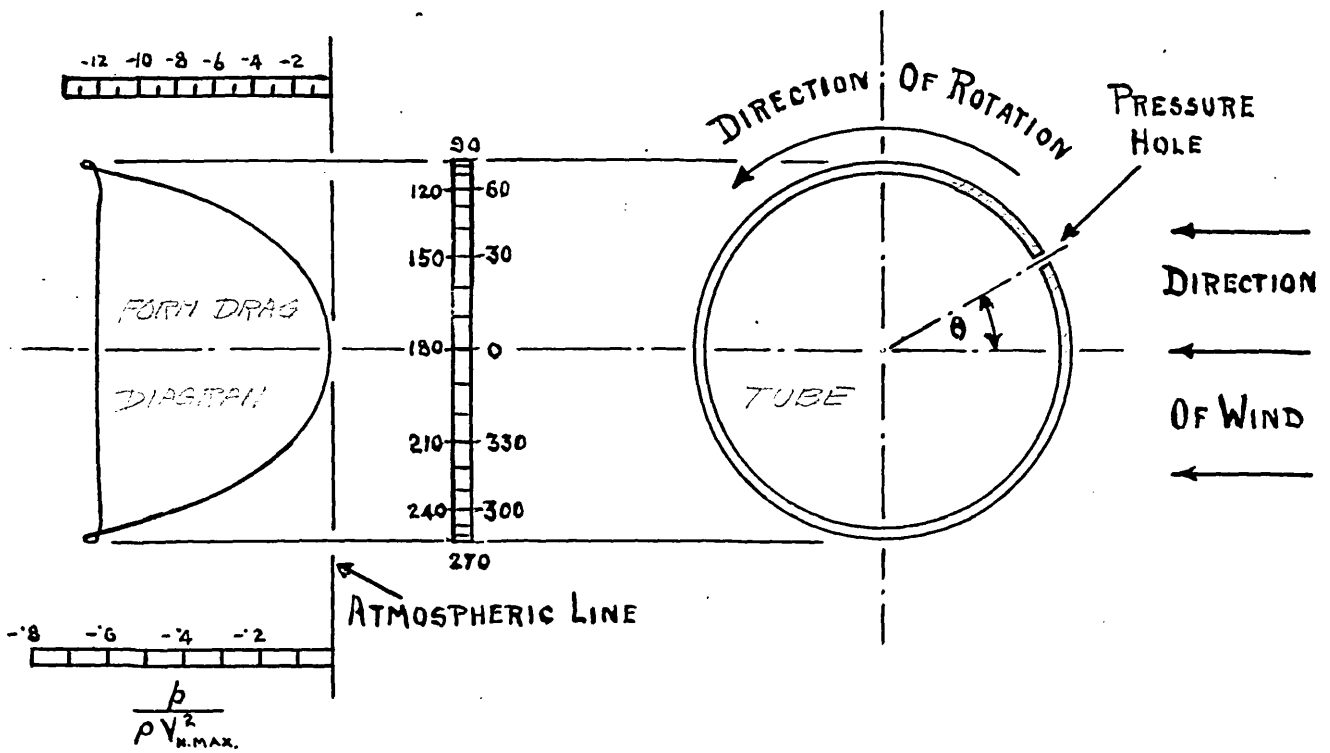
The method of carrying out form drag experiments has been briefly referred to in Section 2.2. The exploration tube could be arranged to replace any of the tubes of the nest.

The Sturtevant fan, which was used for drawing the air through the nest, was driven from the coupling of a hydraulic pump and, assisted by the inertia of the pump, it was possible to keep the speed reasonably constant. The speed of the fan could be varied by varying the position of the rheostat in circuit with the pump motor, and also by varying the opening of the discharge valve on the pump outlet and by opening or closing an improvised slide valve on the fan discharge. The pump was fitted with a tachometer which proved a useful guide to the correct speed when starting the apparatus. This usually indicated 2100 r.p.m. The air speed was measured by the difference in pressure of the atmosphere and that at the first pressure hole in the back wall of the apparatus ahead of the first row of tubes. The difference of the height of the water in the manometer tube was measured by the aid of a cathetometer before and after every form drag curve was obtained. This difference of pressure was kept as constant as possible at 1.17 Cms. of water.

FORM DRAG DIAGRAM

FIG. 5.2A.

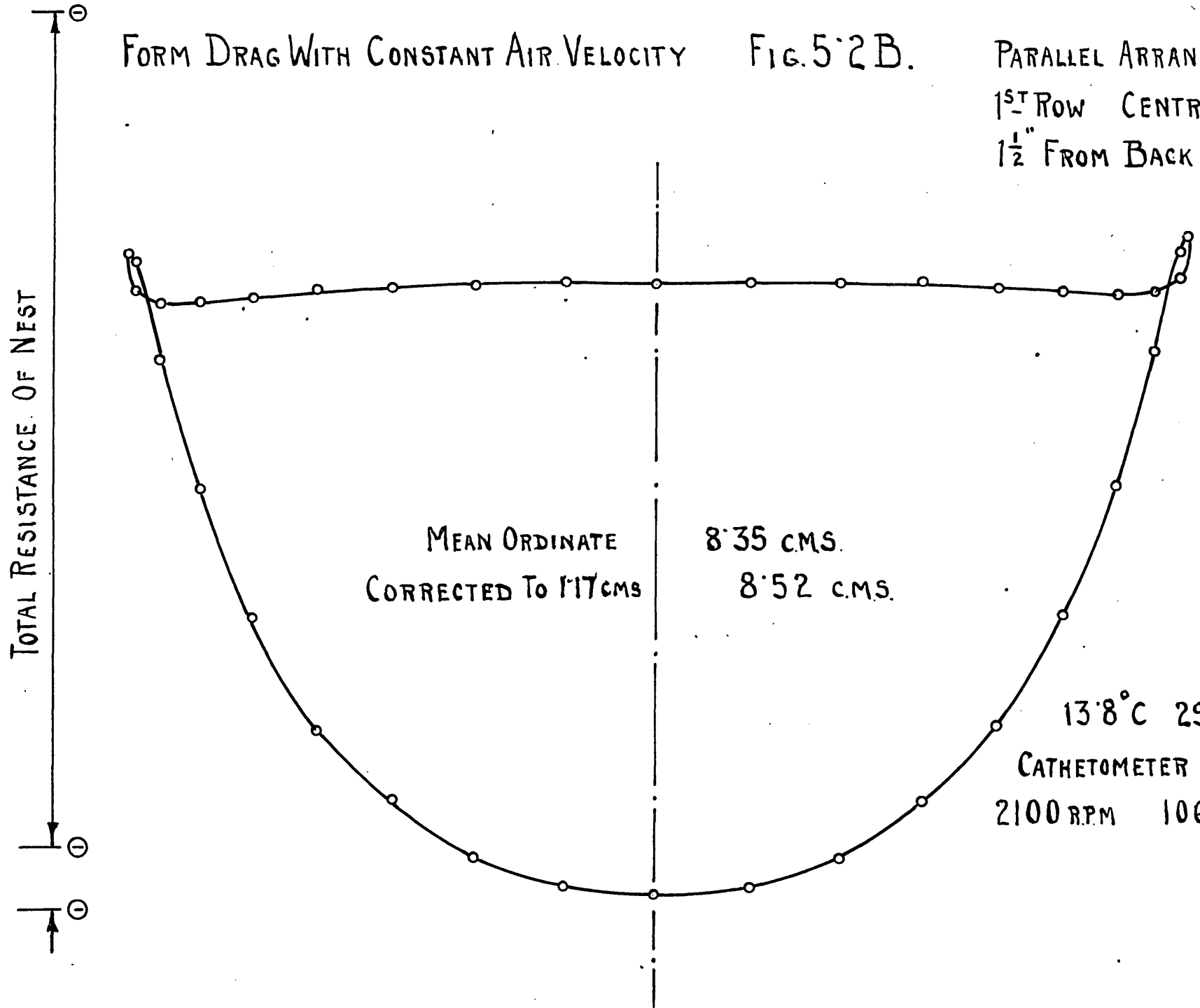
PRESSURE IN CMS. OF WATER.



FORM DRAG WITH CONSTANT AIR VELOCITY

FIG. 5.2 B.

PARALLEL ARRANGEMENT.
 1ST ROW CENTRE TUBE
 1 1/2" FROM BACK WALL.



MEAN ORDINATE
 CORRECTED TO 117 CMS

8.35 CMS.

8.52 CMS.

13.8° C 29.15" Hg.

CATHETER 1.147 CMS

2100 RPM

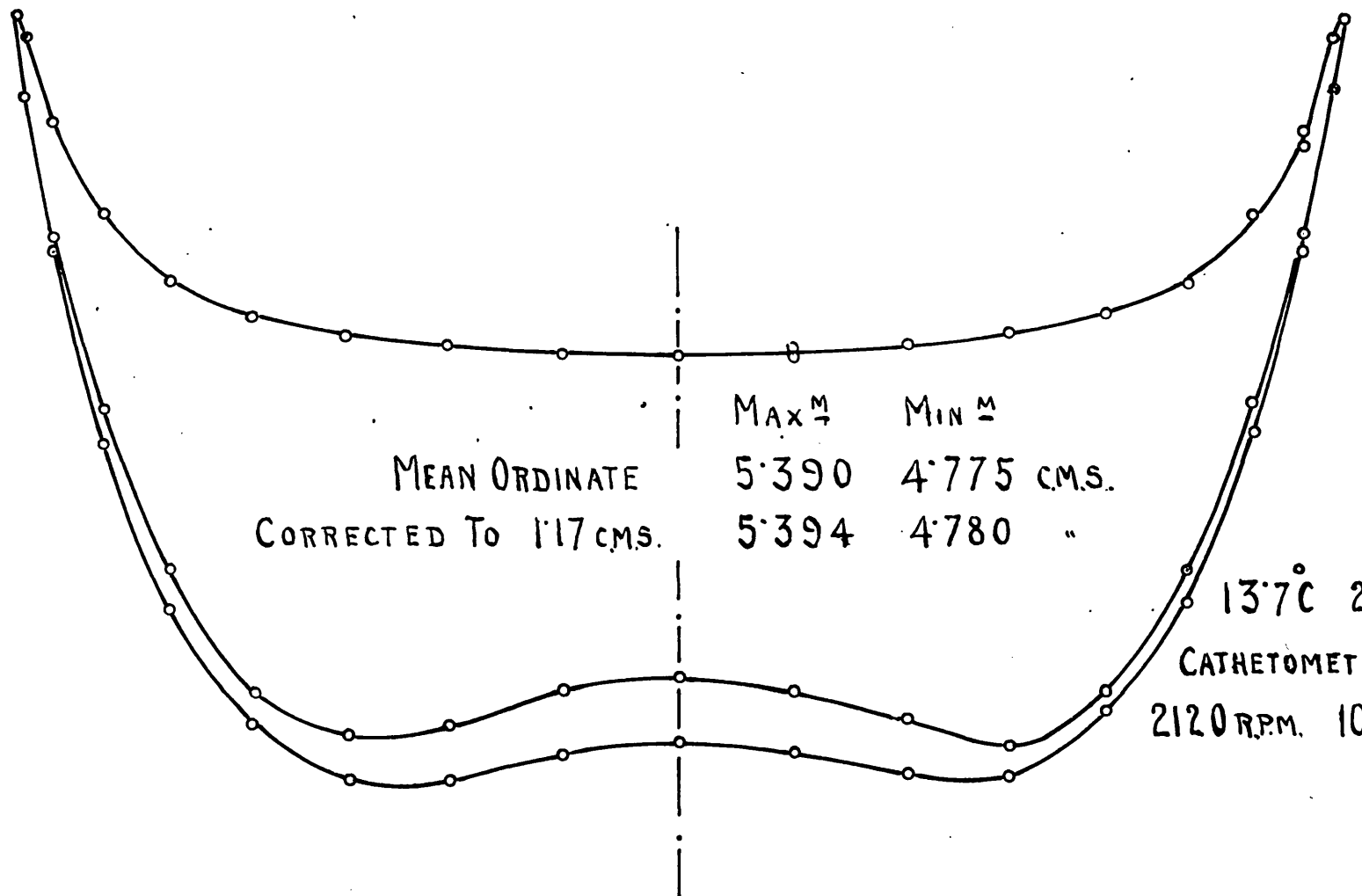
106.5 M.P.H.

FORM DRAG WITH CONSTANT AIR VELOCITY

FIG. 5.2C.

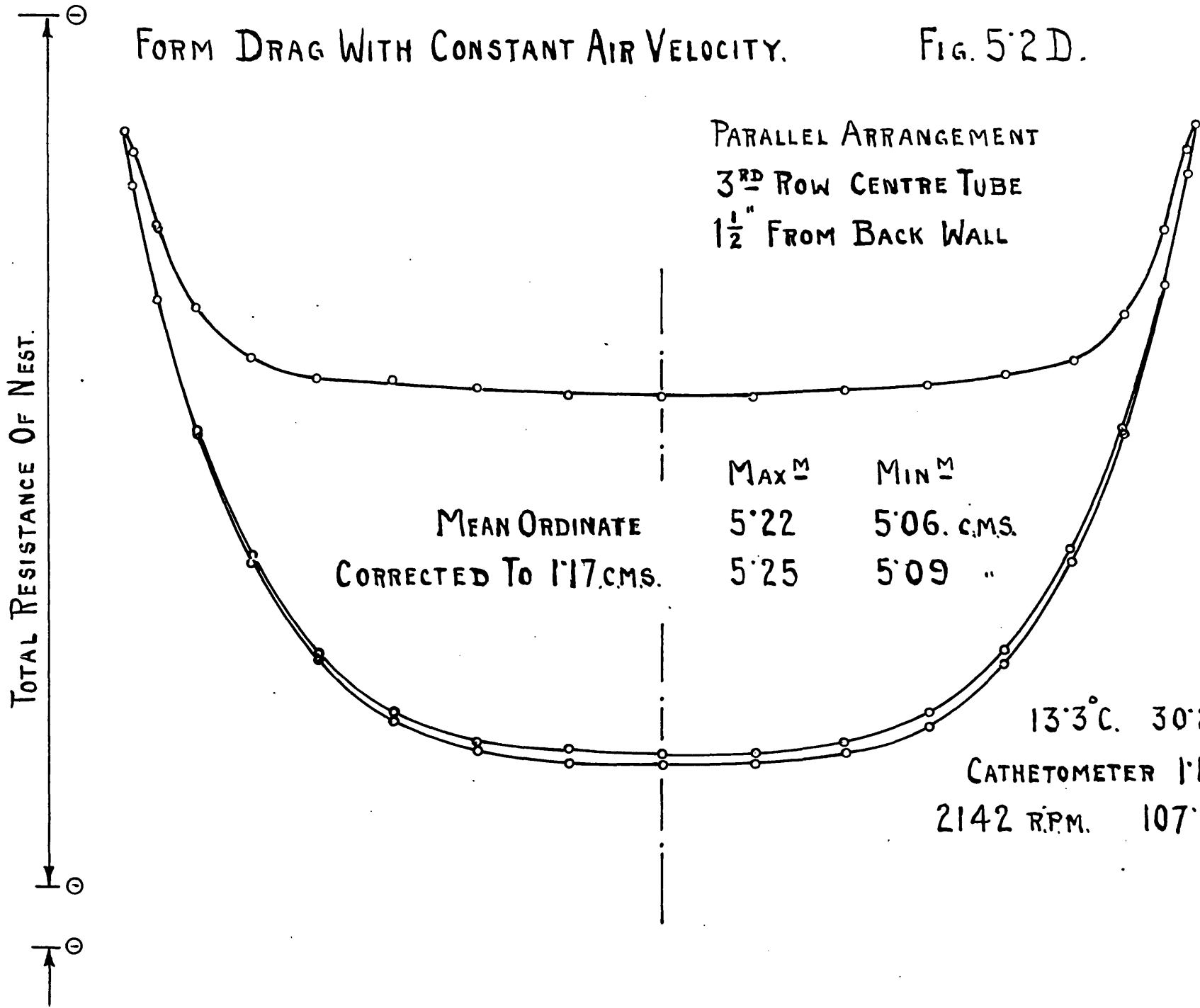
PARALLEL ARRANGEMENT
 2ND ROW CENTRE TUBE
 1 1/2" FROM BACK WALL.

TOTAL RESISTANCE OF NEST.



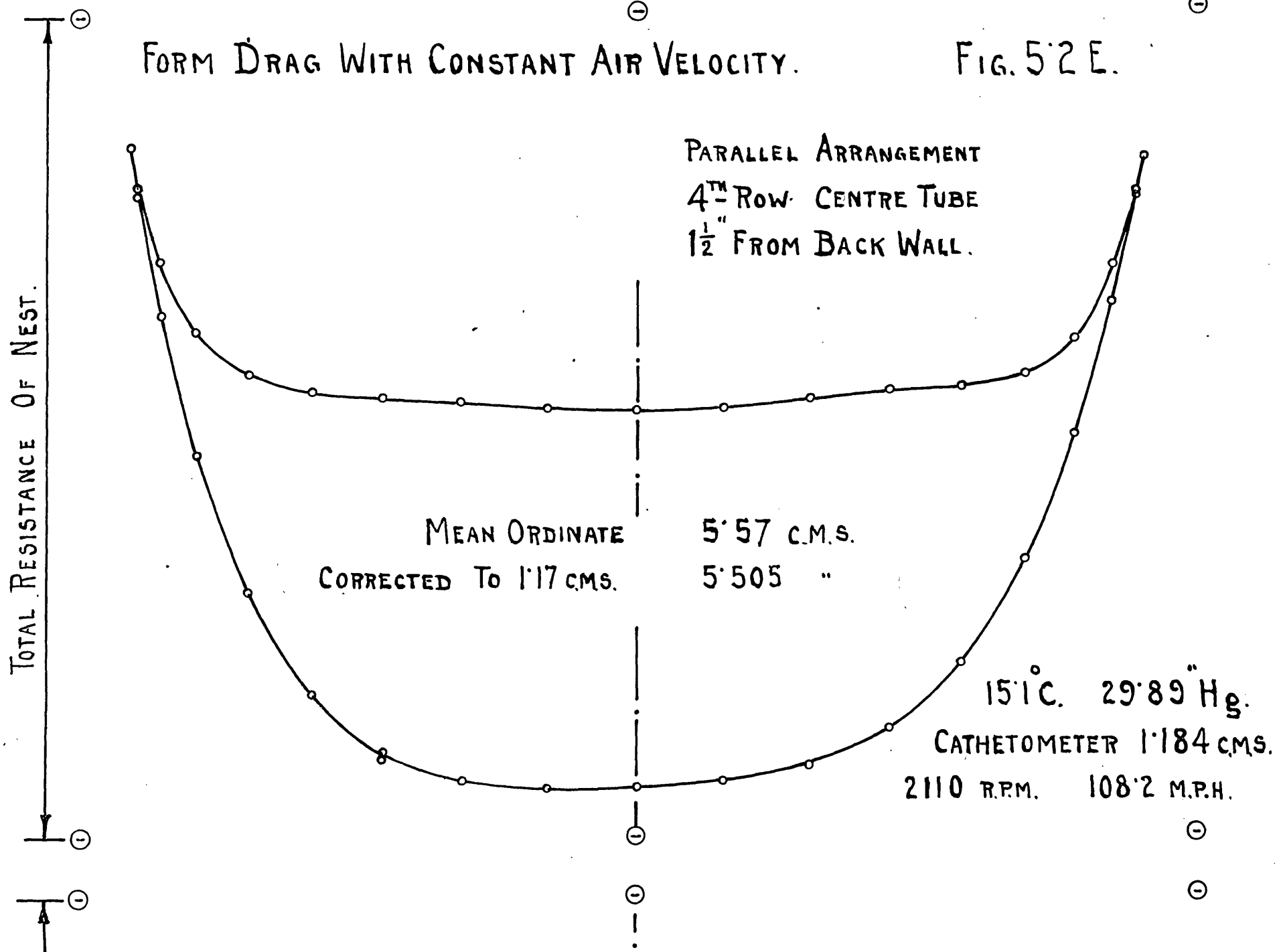
FORM DRAG WITH CONSTANT AIR VELOCITY.

FIG. 5'2 D.



FORM DRAG WITH CONSTANT AIR VELOCITY.

FIG. 5.2 E.



In order to give the observer an opportunity of noting any variation in speed which did take place during a run, an anemometer calibrated in miles per hour was attached to the down-stream end of the apparatus and normally read about 107 miles per hour. This instrument was conveniently placed and could be seen while the other data were being obtained. It was not used as an absolute measurement, but, since its reading was a measure of the total hydraulic resistance of the nest, it proved a convenient indicator of any change of air speed.

In the determination of the form drag, the quantity that is required is the integral of the components of the normal pressure at the surface, in the direction of the stream. This was obtained by plotting the various pressure readings not on an equally spaced scale of angles of rotation but on a scale graduated to the sine of the angle of rotation, as illustrated in Fig. 5.2 A. This shows the form drag diagram for the centre tube of the first row.

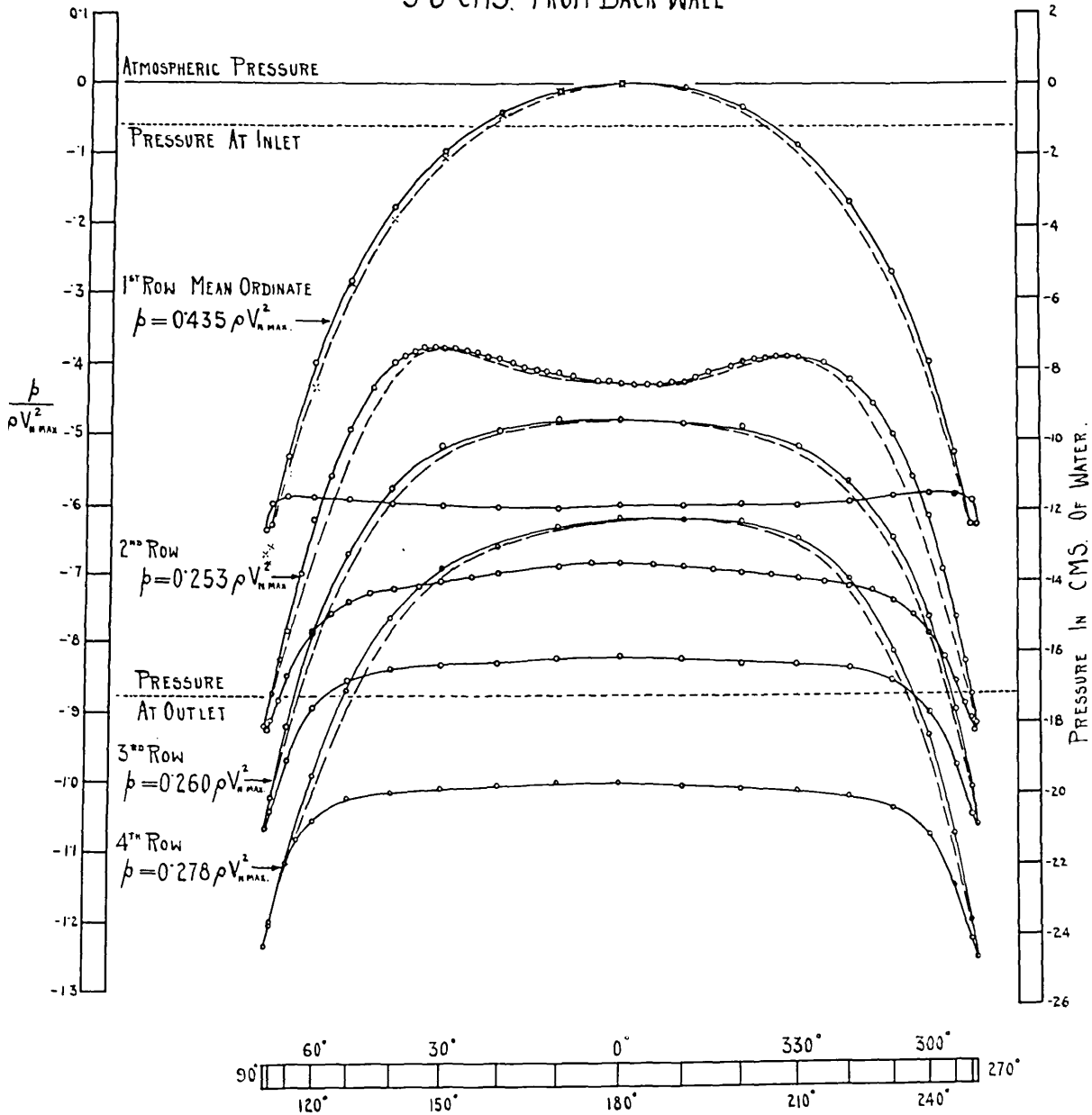
On completion of the experimental curve the diagram was divided into two by a line joining the points 0° and 180° , and the area of each side determined separately with a planimeter. From this area the mean ordinate was determined.

Figs. 5.2 B, C, D and E are typical charts exactly as

FORM DRAG DIAGRAMS

FIG. 5.2 F.

PARALLEL ARRANGEMENT 1ST, 2ND, 3RD & 4TH ROWS CENTRE TUBES
3.8 CMS. FROM BACK WALL



$$\frac{V_{n, \text{MAX}} d}{\nu} \approx 35,000.$$

BROKEN LINES SHOW DIAGRAMS CORRECTED FOR SIZE OF PRESSURE HOLE

FORM DRAG DIAGRAMS

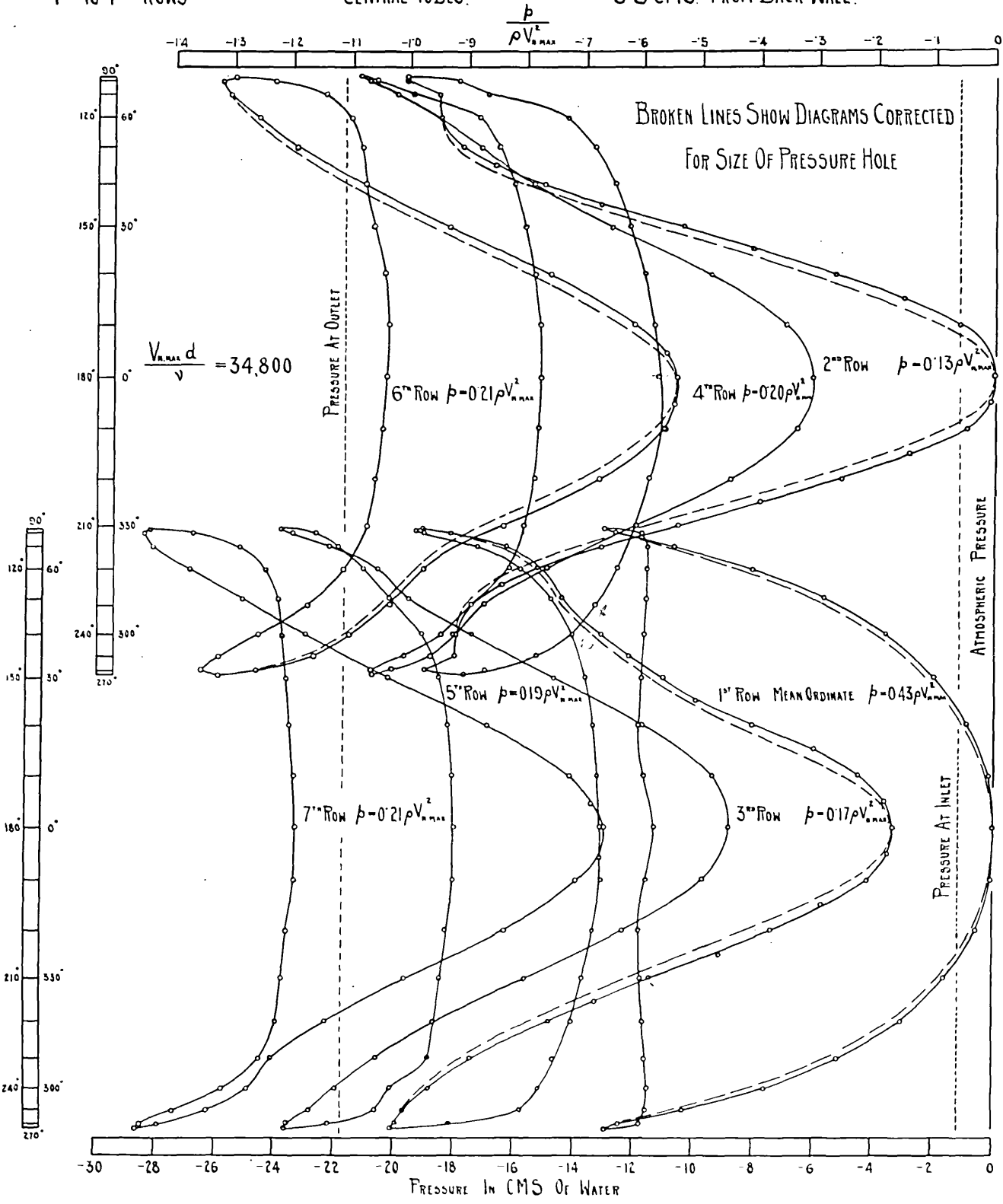
STAGGERED ARRANGEMENT.

FIG. 5'2 G.

1ST TO 7TH ROWS

CENTRAL TUBES.

3.8 CMS. FROM BACK WALL.



they were obtained from the experimental apparatus. They are the form drag curves for the centre tubes of the 1st, 2nd, 3rd and 4th rows at a distance of 3.8 Cms. from the back wall.

The pressure at the front of the tubes of the 2nd row showed considerable instability and therefore the maximum and minimum readings are shown on the diagram. This instability was also present on the front of tubes of the 3rd row, but not to such a marked degree. Figures 5.2F and G show a series of form drag diagrams in their correct relation to the atmospheric pressure. The inner dotted lines show the diagrams corrected for the size of the pressure hole as suggested by Thom and referred to in Section 2.1. The numerical values of the form drag mean ordinates are for the uncorrected diagrams. The appropriate corrections are given in the tables below.

Parallel Arrangement. Figure 5.2F.

| | Area of original diagram | Area of Correction | % Correction |
|---------|-----------------------------|-----------------------|-----------------|
| 1st Row | 170.4 | 4.9 | 2.88 |
| 2nd Row | 99.2 | 5.35 | 5.39 |
| 3rd Row | 101.8 | 3.9 | 3.83 |
| 4th Row | <u>109.0</u> | <u>4.1</u> | 3.76 |
| | <u>480.4</u> | <u>18.25</u> | |

Percentage correction on total nest $\frac{18.25 \times 100}{480.4} = 3.80$

Staggered Arrangement. Figure 5.2 G

| | Area of original diagram | Area of Correction | % Correction. |
|--|-----------------------------|-----------------------|------------------|
| 1st Row | 169.5 | 4.85 | 2.86 |
| 2nd Row | 53.0 | 10.50 | 19.81 |
| 3rd Row | 66.9 | 8.90 | 13.31 |
| Estimation for Rows 4 to 7 based on 6th Row | 322.5 | 30.40 | 9.43 |
| | <hr/> 611.9 <hr/> | <hr/> 54.65 <hr/> | |

Percentage correction on total nest $\frac{54.65 \times 100}{611.9} = 8.93$

5.3 Anomalous behaviour of front of second row of tubes

It was thought that the cause of this instability might be that the air, as it left the back of a tube in the front row, was deflected first over the top and a moment later under the bottom of the corresponding tube in the second row. If this were so, equidistant points on either side of the direction of the stream would have maximum and minimum values simultaneously i.e. if the pressure at 30° were at its maximum value, the pressure at 330° would, at the same instant, be at its minimum.

INVESTIGATION OF PERIODICITY OF PRESSURE VARIATION.

FIG. 5.3.

PARALLEL ARRANGEMENT.

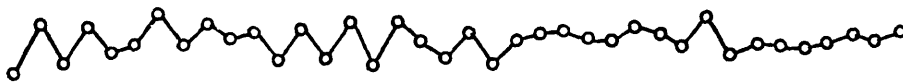
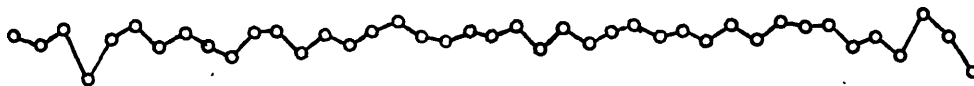
2ND ROW

CENTRE TUBE

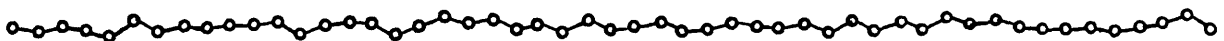
TIME INTERVAL 2 SECONDS.

OSCILLATIONS DAMPED.

PRESSURE TUBE WITH TWO SMALL HOLES AT 30° & 330°



PRESSURE TUBE WITH HOLES AT 150° & 210°



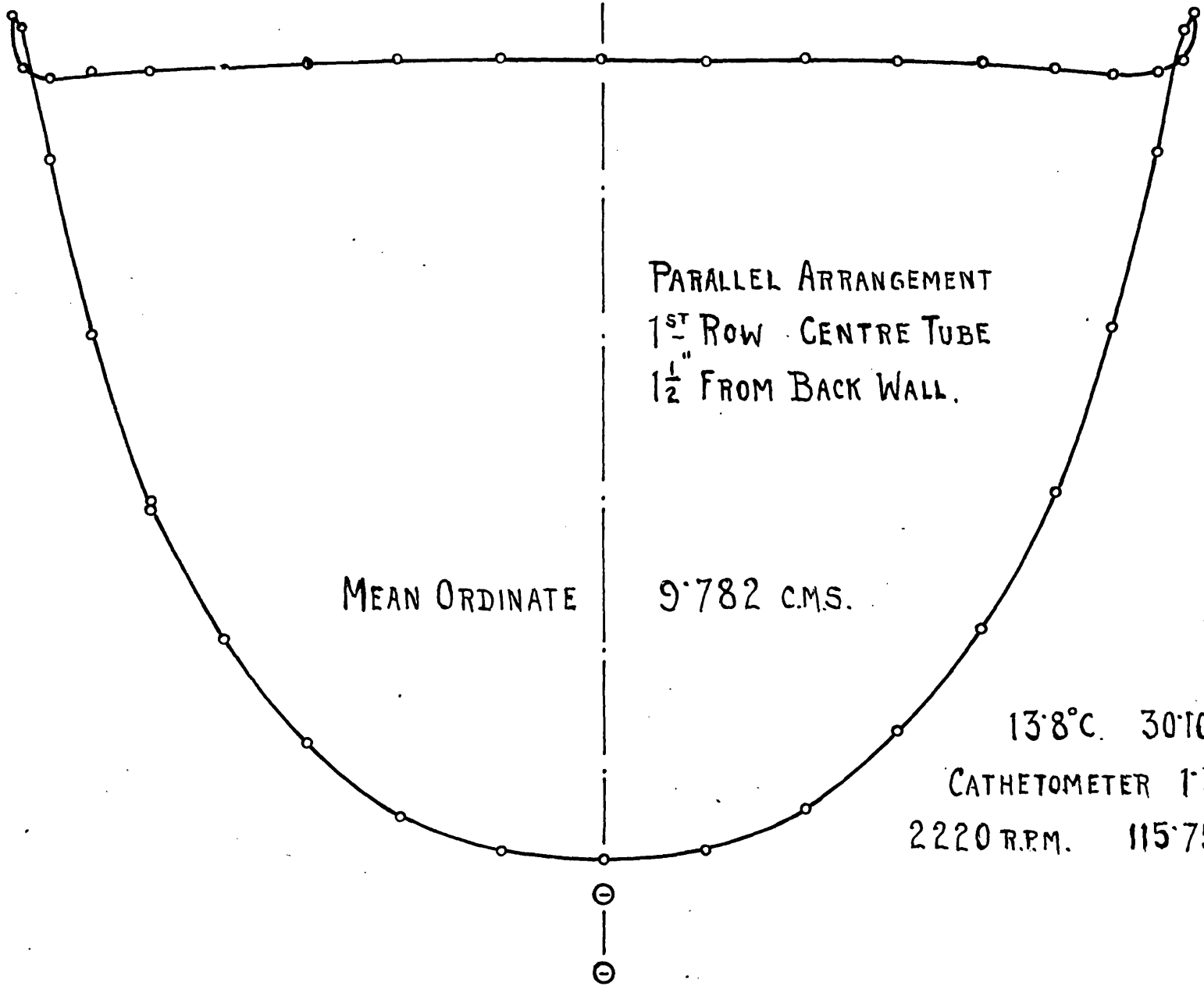
In order to test if this were true, a test was made with a pressure tube in which had been drilled two holes in the same plane and at an angle of 60° .

With this tube, the pressure indicated by the manometer would be the average of the pressures at two points on the surface of the tube 60° apart, and if the above assumptions were correct, the reading should be very much more steady and the variations in pressure considerably less. When this experiment was tried it was found that the fluctuations in pressure were of the same magnitude as before, thus indicating that it was possible to have maximum pressures at 30° and 330° at the same instant. The pressure tube was then turned through 180° so that the holes corresponded to angles of 150° and 210° . Here the fluctuations of pressure were small, but they were of the same magnitude as those observed when using the pressure tube with the single hole. Observations were made to see if it were possible to detect any regular periodicity in the variations of pressure. The glass screen was moved sideways 0.32 Cm. each interval of 2 seconds, and the height of the water in the manometer tube recorded on the paper on the front of the glass screen.

From Fig. 5.3 it was impossible to detect any regular cycle of variation of pressure and the opinion was formed that the variations were due to innumerable chance circumstances,

FORM DRAG WITH VARYING AIR VELOCITY FIG. 5.4 A.

TOTAL RESISTANCE OF NEST 18.04 C.M.S.



PARALLEL ARRANGEMENT
1ST Row CENTRE TUBE
1/2" FROM BACK WALL.

MEAN ORDINATE 9.782 C.M.S.

13.8°C. 30.10" Hg.

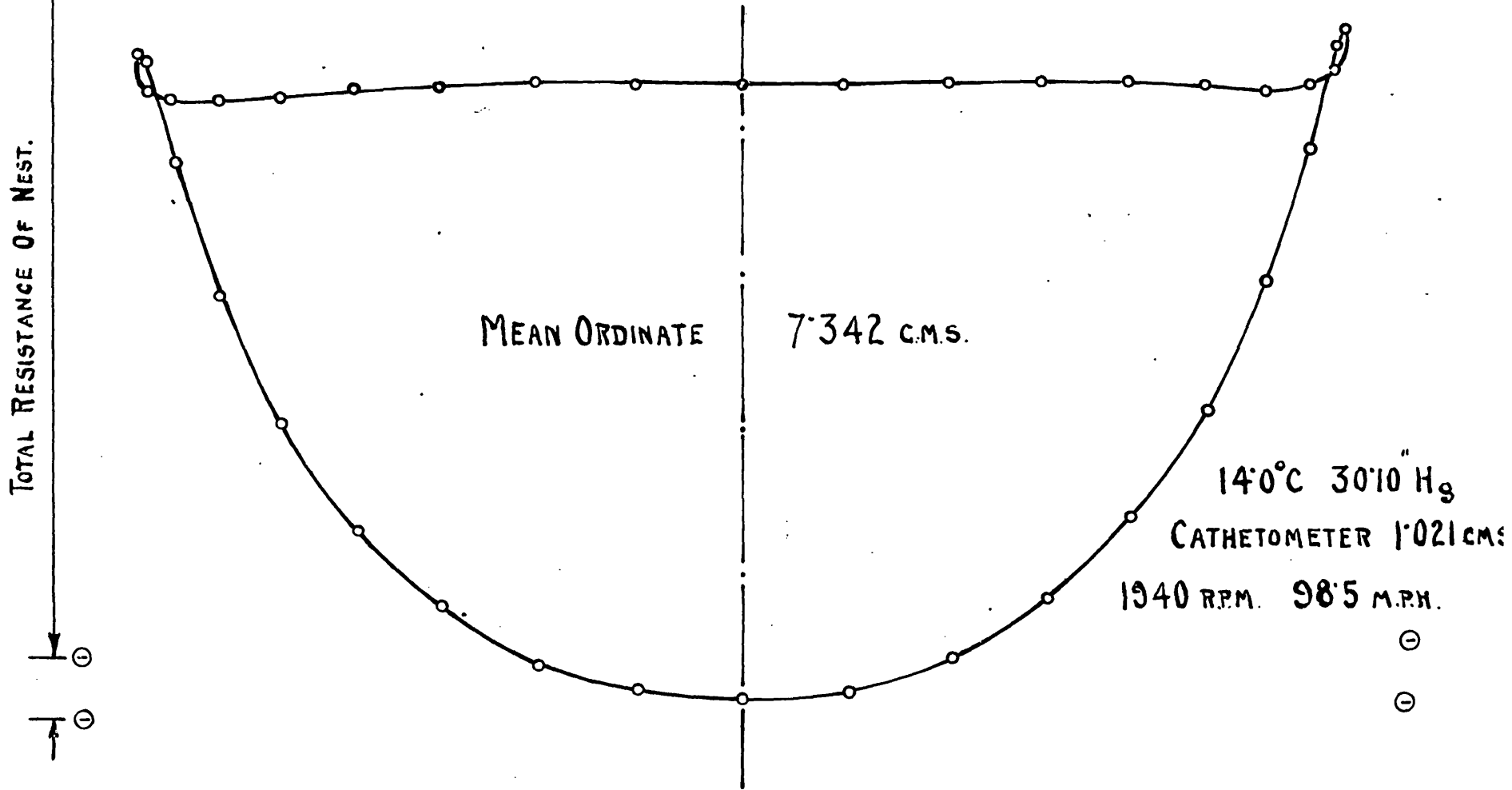
CATHETOMETER 1.325 C.M.S.

2220 R.P.M. 115.75 M.P.H.



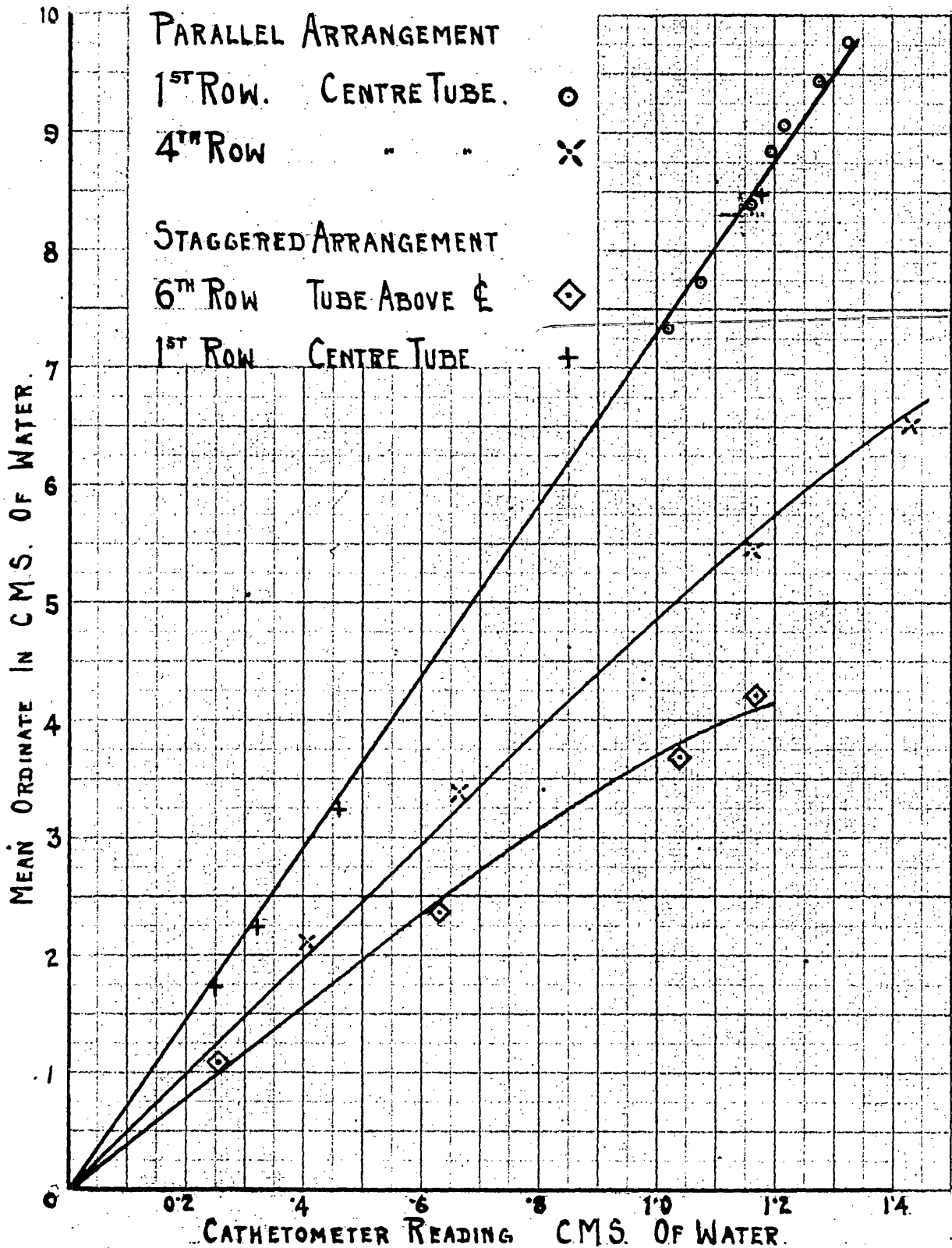
FORM DRAG WITH VARYING AIR VELOCITY FIG. 5.4 B.

PARALLEL ARRANGEMENT
1ST ROW CENTRE TUBE
1 1/2" FROM BACK WALL.



EFFECT OF VARIATION OF AIR SPEED ON DRAG MEAN ORDINATE

FIG. 5.4C.



not the least important of which would be slight initial movements in the air as it entered the mouthpiece of the apparatus.

The probable cause of the instability and the general shape of the form drag curves are discussed in Section 9, after the experimental work on the Ahlborn tank and electric tray has been described: the results of these researches being utilised in the interpretation of the form drag curves.

5.4 The effect of variation of air speed on the mean ordinate of the form drag curves.

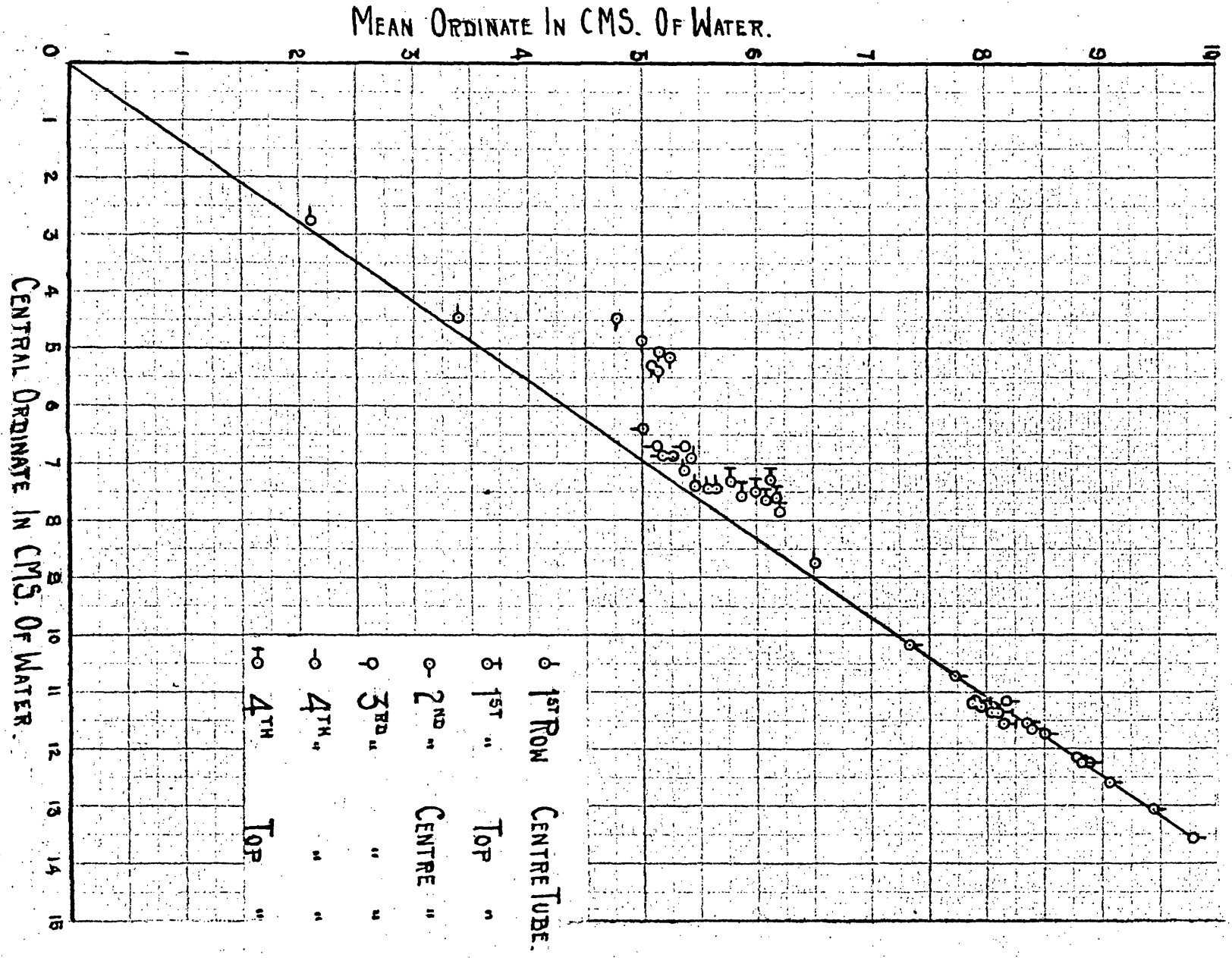
It was found impossible always to carry out the form drag experiments at an air speed corresponding exactly to 1.17 Cms. of water. A series of tests was therefore carried out to ascertain how the mean ordinate varied with varying air speed.

These tests were made on the centre tube of the 1st row at a distance of 3.8 Cms. from the back wall.

The largest and smallest form drag diagrams are reproduced in Figs. 5.4 A and B, and the results of the seven experiments are given in Table 5.4 C and plotted in Fig. 5.4 C. From this figure it is seen that for the minor corrections that were necessary, due to the slight deviations of air speed from that corresponding to 1.17 Cms. W.G., it

RELATION BETWEEN "CENTRAL" & "MEAN" ORDINATES. FIG. 5.5.

PARALLEL ARRANGEMENT.



can be taken that the height of the mean ordinate of the form drag curve is proportional to the cathetometer reading. This necessary minor correction was therefore made on the mean ordinate of each individual form drag curve if the cathetometer reading was not exactly 1.17 Cms.

5.5 Relation between "central ordinate" and "mean ordinate" of form drag diagrams.

The results obtained in the previous section presented the possibility of comparing the height of the "mean ordinate" with that of the "central ordinate", i.e. the ordinate $0^\circ - 180^\circ$.

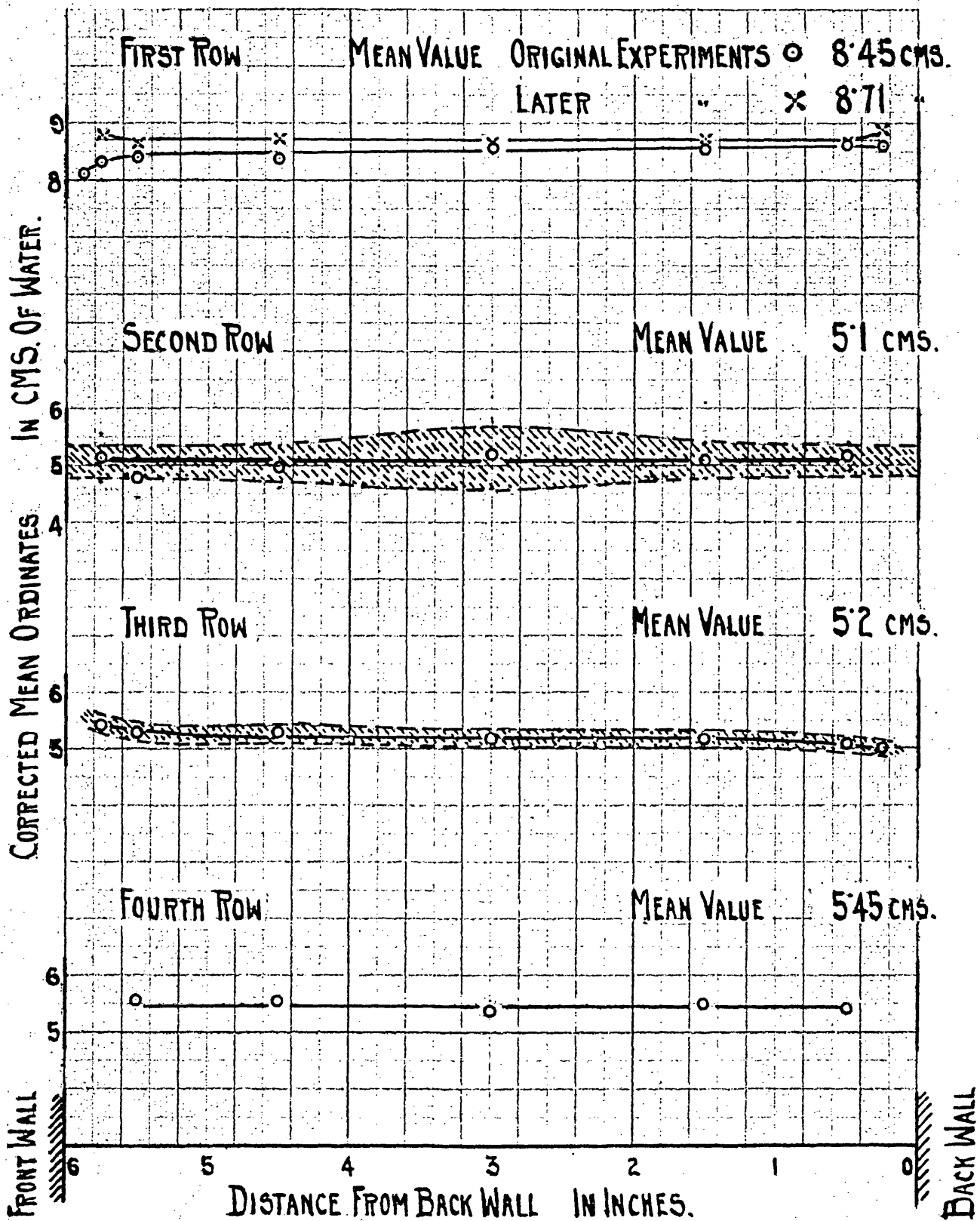
A comparison of the seven form drag diagrams, from which curve 5.4 C was obtained, showed that they all possessed the same characteristic features and appeared to differ only in the heights of the various ordinates.

If a relation between the height of the "mean" and the "central" ordinate could be established, it would reduce greatly the amount of work involved, at any rate in preliminary investigations. The relation between these two ordinates is plotted in Fig. 5.5, and it is seen that as far as the variable speed test on the centre tube of the 1st row is concerned, there is a well-defined relationship. The mean ordinate is 0.72 of the central ordinate. This was a useful approximation and was used in the investigation of the effect of initial turbulence in the air stream (Section 5.8).

DISTRIBUTION OF FORM DRAG ACROSS CENTRE TUBES. FIG. 5.6 A.

PARALLEL ARRANGEMENT.

$$\frac{V_{N. MAX} d}{v} = 34,800$$



It was borne in mind, however, that all the above data were obtained on the centre tube of the 1st row at a plane 3.8 Cms. from the back wall. The relationship for other lateral positions of the same tube and for various positions of the top tube of the 1st row were added to Fig. 5.5. Within the range of experimental error the same relationship holds true. It was decided to see whether the relationship could be extended to the tubes of other rows, and the necessary data have been given in Table 5.5 and added to the figure.

While for the tubes of the other rows the points are more scattered, there still appears to be an approximate relationship.

5.6 Mean ordinate of form drag curves.

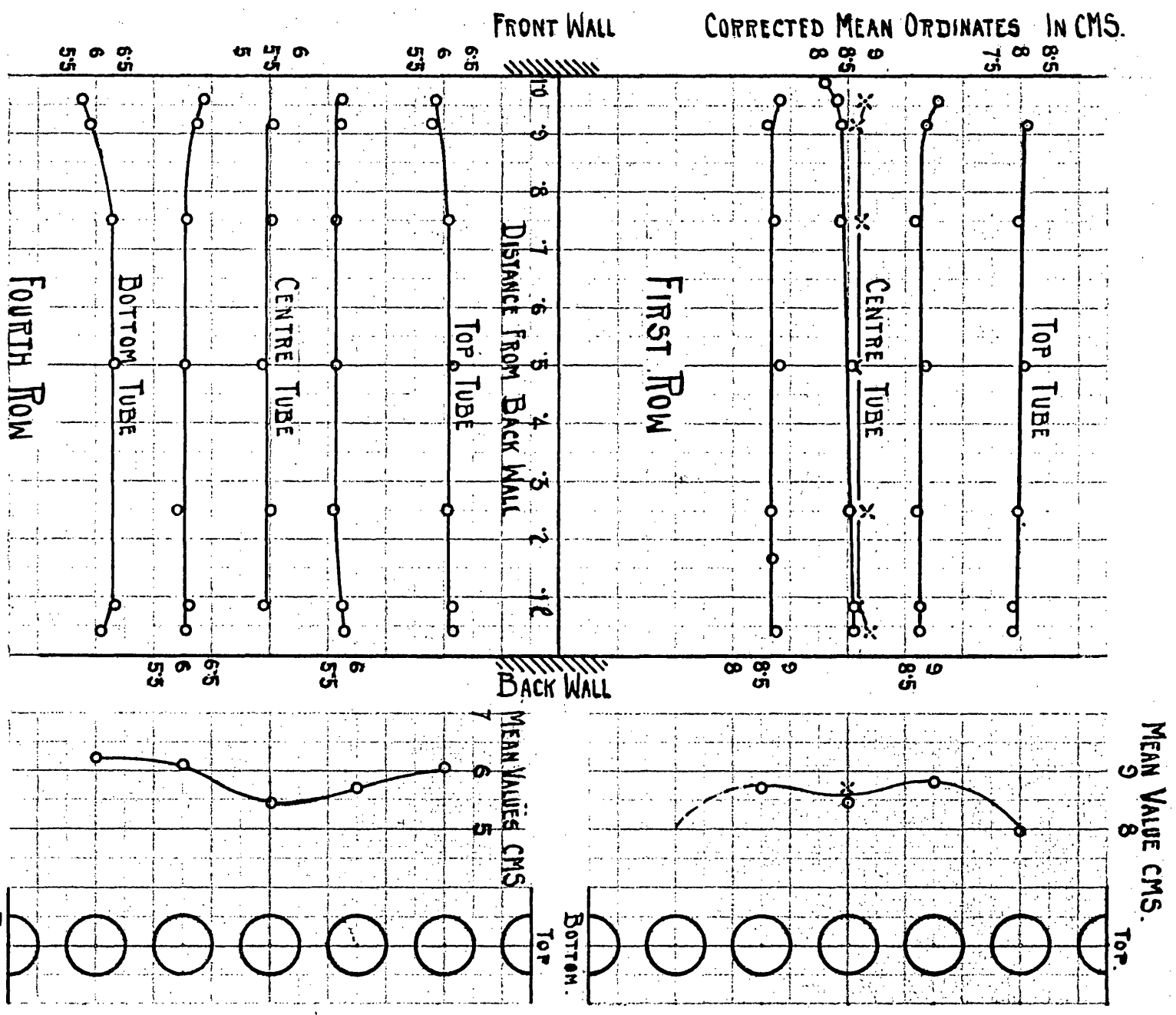
Fig. 5.6 A shows the distribution of form drag across the centre tubes of the 1st, 2nd, 3rd and 4th rows. In the case of the 2nd and 3rd rows, the pressure was variable and the maximum and minimum values of the ordinate are indicated. In the 3rd row the band is of uniform width, indicating a constant degree of instability across the length, whereas in the second row the instability appears to be greater at the mid-length.

Fig. 5.6 B shows the value of the form drag ordinate

DISTRIBUTION OF FORM DRAG ACROSS TUBES OF THE 1ST & 4TH ROWS.

FIG. 5.6B. PARALLEL ARRANGEMENT.

$$\frac{V_{r,max}}{v} d = 34,800.$$



across four of the tubes in the 1st row and all the tubes in the 4th row. From these it is seen that, with the exception of about 5% of the length at each end, the ordinate of the form drag is practically constant throughout the length of each tube. The mean value of the ordinate is marked on each curve in Fig. 5.6 A and plotted as a separate curve on the right-hand side of Fig. 5.6 B.

5.7 Estimation of the relation between form drag and total drag.

At this stage it was decided to make a preliminary estimate of the relation between the form drag and the total drag in the nest.

In carrying out the experiments on the form drags of the various tubes and the total resistance of the nest, the varying atmospheric temperatures and pressures were recorded as well as the cathetometer readings. If "p" is the intensity of drag in dynes per sq. Cm., either on an individual tube or the whole nest:

$$p = g \rho_{\text{air}} h_{\text{air}} = g \rho_{\text{air}} \frac{\rho_{\text{water}}}{\rho_{\text{air}}} \cdot h'_{\text{water}}$$

where h' is the mean ordinate of the form drag diagram or the total resistance of the nest in Cms. of water gauge. Therefore "p" is independent of ρ_{air} and since ρ_{water} varies only slightly with temperature, it is seen that "p" is not affected by changes of atmospheric temperature and pressure.

The drag mean ordinates were obtained from the areas of the form drag diagrams and these were corrected to a standard cathetometer reading of 1.17 Cms. of water.

As explained in Sections 2.1 and 5.2 a correction was also applied to compensate for the size of the pressure hole and the results obtained were as follows:-

Value of Drag Mean Ordinates in Cms. of Water
(Parallel Arrangement).

| No. of Tube | Top | | Centre | | Bottom | Uncor- rected Average. | Average corrected for hole size. |
|----------------|------|------|--------|------|--------|------------------------------|---|
| | 1 | 2 | 3 | 4 | 5 | | |
| 1st row. | 7.97 | 8.80 | 8.45 | 8.70 | | 8.48 | 8.24 |
| 2nd row | | | 5.10 | | | 5.10 | 4.83 |
| 3rd row | | | 5.20 | | | 5.20 | 5.00 |
| 4th row | 6.04 | 5.70 | 5.45 | 6.10 | 6.22 | 5.90 | <u>5.68</u> |
| | | | | | | | 23.75 |

Average mean ordinate per tube = 5.94 Cms. = h' .

Average pressure in dynes per square Cm. = $\rho_{\text{water}} h'$ =

$981 \times 1 \times 5.94 = 5825$. Length of each tube = 15.24 Cms.

Diameter of tube = 1.27 Cms. Therefore average force on each

tube = $5825 \times 15.24 \times 1.27 = 112,700$ dynes. Assuming that

the drag on the half-tubes at the ends of the rows is of the

same intensity as that on the whole tubes in the midst of the nest, then there is the equivalent of 24 tubes.

The sum of the form drags on all the tubes will be

$$24 \times 112,700 = 2,705,000 \text{ dynes.}$$

With a cathetometer reading of 1.17 Cms. the total resistance of the nest was 16.02 Cms. of water = h'' .

The maximum flow area was 175.4 square Cms. = A .

$$\begin{aligned} \text{Therefore total force on the nest} &= g\rho_{\text{water}} h'' A. \\ &= 981 \times 1 \times 16.02 \times 175.4 \\ &= 2,755,000 \text{ dynes.} \end{aligned}$$

$$\text{Therefore ratio } \frac{\text{Form drag}}{\text{Total drag}} = \frac{2,705,000}{2,755,000} = 0.982$$

That is, the form drag is 98.2% of the total resistance and the tangential drag 1.8%.

It is shown in Section 10.3 that with the staggered arrangement the sum of the form drags is only 93% of the total resistance of the nest, thus indicating that the tangential drag is 7%.

While it is probable that these estimates give a reasonable conception of the tangential drag, it must be borne in mind that the differences involved are of the same order as the experimental error. Due to the fluctuations

of pressure on the second and third rows of the parallel arrangement and of the second and all subsequent rows of the staggered arrangement it is impossible to give absolutely definite values to the form drags.

It was originally intended to carry out form drag experiments at five or six sections along the length of every tube in both the parallel and staggered nests. After the first estimation was completed the subject was critically surveyed to see whether the probable result would be sufficiently close to warrant the time spent on the investigation. When it is realised that every single point on the mean value curves on the right hand side of Figure 5.6 B entailed 440 observations and their associated calculations, it will be appreciated that the time involved was considerable. It was thought that doubling or even trebling the time already spent was not likely to yield a more accurate estimate of the tangential drag. The results already obtained appeared to be consistent with other investigators' experimental work on single cylinders.

From the diagram given by Thom⁽¹⁾ for the tangential and form drag for a single cylinder in a wind stream, it was seen that at a Reynolds' number of 35,000 the tangential

(1) Thom. R. & M. No. 1194. 1928. p.183.

drag was an insignificant amount compared with the form drag, certainly less than 1%

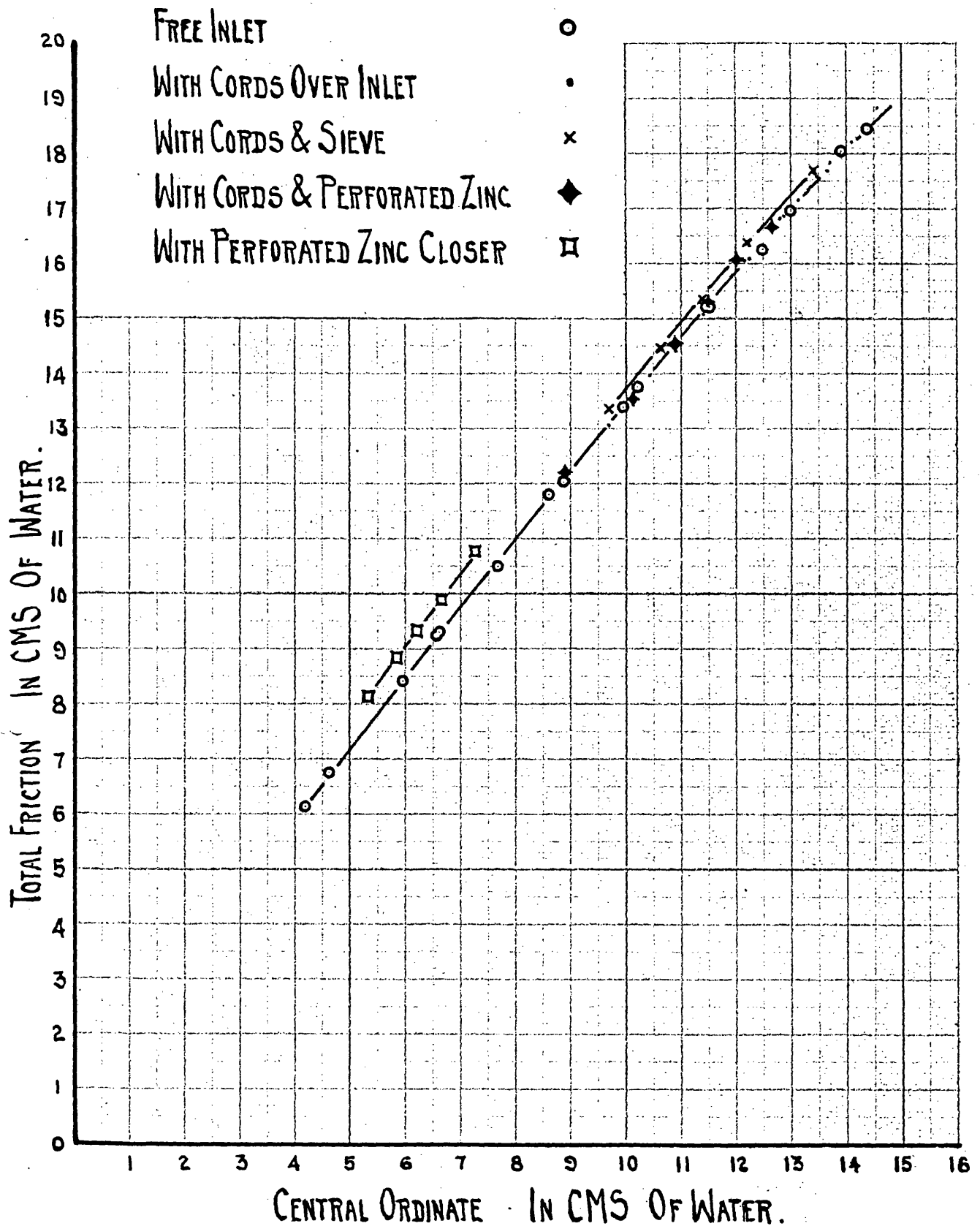
For the form drag experiments on air the value of Reynolds' number based on $V_{N,max.}$, the estimated speed in the gap, is approximately 35,000. This will be the same for the tubes of each of the four rows, but the increase of turbulence of the air as it passes the second and subsequent rows has the effect of lowering the value of the form drag coefficient.⁽¹⁾ It is probable that the increased turbulence has not a similar effect on the tangential drag and thus the ratio of tangential to form drag, although very small on the first row of tubes, may increase somewhat on subsequent rows.

Two other factors confirmed the decision not to spend further time on the endeavour to determine more accurately the tangential drag. Firstly, it was appreciated that the degree of initial turbulence of the air as it entered the apparatus was not constant and that it appreciably affected the form drag of the tubes and the total resistance of the nest. This is discussed in sub-section 5.8. Secondly, the study of the form drag diagrams and the insight which had been obtained of the eddies at the back of the tubes made it quite clear that, even if the tangential drag could be accurately determined, it could not be used in the manner

(1) Fage and Warsap. R. & M. No.1283. 1929.

EFFECT OF INITIAL TURBULENCE IN THE AIR STREAM.

FIG. 5·8.



that was anticipated for the elucidation of the heat transfer. This is further discussed in sub-section 5.9.

5.8 The effect of initial turbulence in the air stream.

When testing the top tube of the first row it was discovered that the half-tube directly above it was vibrating. The half-tube did not fit closely against the top of the box for the whole length. At one end the air was able to enter the half-tube through a narrow opening, thus causing it to vibrate like a reed. The apparatus was dismantled and all the half-tubes securely fixed to the walls.

On re-testing the particular tube it was found that the result of the vibration had been to lower the form drag on the top tube by 3.3% and the total frictional resistance of the nest by 0.75%. When the apparatus was originally constructed and tested on water it was thought that slight traces of impurities or dirt in the water might adhere to the surface of the tubes. This would tend to change the flow pattern and increase the resistance of the nest. This difficulty had been experienced by Eagle and Ferguson⁽¹⁾ in their work on the heat transfer with water passing through brass tubes. The present apparatus was therefore designed so that the tubes could be withdrawn for cleaning.

(1) Eagle and Ferguson. Proc. Roy. Soc. A. Vol.127. 1930. p.540.

In this connection it is interesting to note that with the experiments on water no deposit was found to adhere to the external surface of the tubes, but with the experiments on air a layer of fine dust collected on the tubes. This deposit adhered tenaciously to the surface and the tubes were removed and cleaned by rubbing with a rag moistened with paraffin. Cleaning was necessary after running for 60 hours.

After one of these periodic cleanings and the securing of the half-tubes to the top and bottom walls of the box, a complete set of form drag experiments on the centre tube of the 1st row was repeated. The results of these experiments are plotted in Fig. 5.6 A, and the mean ordinate is 3.1% greater than the mean ordinate obtained from the original experiments performed five months earlier.

When it was first decided to investigate form drag curves, it was found that these could be reproduced on successive days within an experimental error of less than 1%.

The various parts of the apparatus were carefully checked and the method of measuring the constant velocity by means of the manometer tube and cathetometer was examined critically. No fault in the apparatus could be detected and no better method of measuring the air velocity was devised.

It was thought that the variation in form drag might be due to changes in the extent of the initial turbulence in the entering air, and it was therefore decided to investigate this subject.

It was proposed to create artificial turbulence in the stream by suspending a network of cord over the trumpet-shaped mouthpiece at the inlet of the nest, in a manner similar to that used by Relf and Lavender⁽¹⁾ on their investigation of the drag on an airship model.

With such an arrangement the pressure at the first pressure hole in the side of the apparatus could no longer be used for determining the velocity of air flow. The difference of pressure at this point and that of the atmosphere now included the resistance of the net at the inlet. It was decided therefore to use the total resistance of the nest as a measure of the air flow and to plot the relationship between the central ordinate of the form drag diagram against the total resistance of the nest.

It was appreciated that this was not an ideal comparison for the following reasons. If some form of artificial turbulence caused the form drag of the tubes of the 1st row

(1)

Relf and Lavender. R.& M. 597. 1918-19. Vol.1. p.79.

to decrease by 10% and it also had a similar effect on the tubes of all the other rows, then the total form drag of the nest would be lowered by 10%. If, as was indicated in section 5.7, the form drag constitutes 98% of the total resistance, the total resistance will have been lowered by 9.8%. Thus, for this particular form of artificial turbulence, the central ordinate of the form drag curve of the centre tube of the 1st row, and also the total resistance of the nest, would have been lowered by practically the same proportion and on plotting the results it would appear that this form of turbulence had had no effect, whereas in reality it had reduced the form drag on all the tubes by 10%.

It was considered that the effect of artificial turbulence was likely to be appreciably greater on the 1st row, where the air in the initial stream was in steady motion, than on the subsequent rows, after it had been disturbed by its passage over the 1st row.

When discussing the dissipation of eddies, Taylor⁽¹⁾ pointed out that eddies such as those created by a rope netting decay as they pass down-stream: Also, that since this decay arises largely from the action of viscosity, they take a constant time to die down to a given fraction of their

(1) G.I.Taylor. R.& M. 598. 1918-19. Vol. 1. p.73.

initial intensity. From this consideration it might be anticipated that the higher the air speed the less will be the fraction of their original energy that is dissipated before coming in contact with the nest of tubes, and, secondly, the effect of the eddies will be less noticeable at successive points down-stream.

For this reason, and since the investigation on the effect of turbulence was only intended to be qualitative and not quantitative, it was thought that the above method of indicating the results would prove satisfactory.

The relationship was first plotted with free ingress to the air at the inlet of the nest. Variation of the quantity of air passing through the apparatus was obtained by placing a fine mesh sieve over the outlet of the fan. Smaller values of the central ordinate and total friction were obtained by placing a sack on top of the sieve. The results are plotted on Fig. 5.8.

Cords were then placed over the trumpet-shaped mouth-piece at the inlet of the nest. These were spaced 1.27 Cms. apart, the cord being 0.8 Cm. diameter. The results are plotted with dots on the figure. From these it will be seen that while there is a slight indication of a reduction in the values of the central ordinate with the higher total frictions,

there is no perceptible change at the lower values.

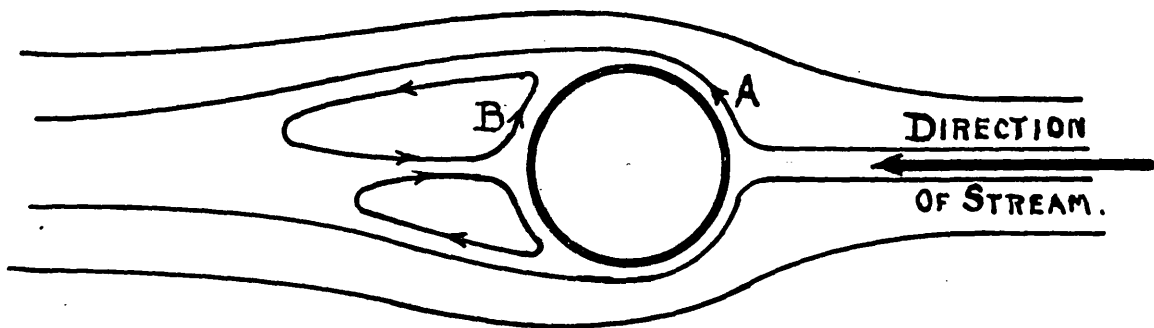
A circular sieve was then placed over the inlet and a series of tests carried out. The results are indicated with crosses on the figure, and it is seen that the points lie consistently on a curve above and practically parallel to the original curve. This reduction of the values of the central ordinates might have been caused by the creation of disturbances in the entering air as was intended or on the other hand the change might have been due to the circular sieve changing the direction of the air as it entered the nest.

In order to make certain which was the real cause of the reduction in the value of the central ordinates the sieve was removed and a piece of perforated zinc was placed on top of the cords. The results are plotted thus ♦ on the figure. While there is a slight indication that the value of the central ordinate has in some cases been reduced, in other cases the points lie on the original curve.

Since the eddies created by the cords or perforated zinc decay as they proceed down-stream, it was decided to increase the degree of turbulence by bringing the cause of the eddies closer to the first row of tubes. With this in view, the cords were removed from the mouthpiece of the nest and a piece of perforated zinc 11.51 Cms. high by 15.24 Cms. long

TANGENTIAL DRAG & HEAT TRANSFER.

FIG. 5.9.



was placed inside the mouthpiece at a distance of 8.25 Cms. in front of the first row of tubes. The results are plotted \bar{M} and show a consistent reduction of the central ordinate of the order of 7.5% of its original value.

5.9 Connection between tangential drag and heat transfer.

White⁽¹⁾ in his paper before the Institution of Chemical Engineers clearly showed the connection between the mechanism of change of momentum in the tangential boundary layer and heat transfer. He points out that in the case of a cylindrical tube the main resistance to a flowing stream was the form drag, whereas it was the tangential drag which was useful in transferring heat.

It was therefore thought that if the total resistance of the nest could be segregated into its constituent parts, viz. the tangential drag and the form drag, it might be possible to establish a relationship between the heat transfer and the tangential drag. Fig. 5.9 shows a cylinder in a fluid stream. At the back of the cylinder will be seen a typical eddy formation. Just as the form drag is the resultant of the horizontal components of the normal pressure at the surface on the right-hand side of the cylinder minus the horizontal components on the left-hand side, so the tangential drag is

(1) C.M.White. Inst. Chem. Eng. Vol.10. 1932. p.66.

the resultant of the horizontal components of the tangential drag at the surface on the right-hand side of the cylinder minus the horizontal components of this drag on the left-hand side: i.e. the horizontal components of A minus the horizontal components of B.

The change of momentum in the boundary layer and therefore the heat transferred is unaffected whether the boundary is straight or curved: and so the heat transfer is proportional to the total tangential drag A and not to the horizontal component of this drag.

Again, the tangential drag at B, as well as that at A, is useful in transferring heat.

It is therefore probable that the heat transfer is proportional to the sum of the tangential drags A and B, while the resultant tangential drag on the tube is the difference of the horizontal components of A and B.

From this it is seen that for the purpose of forecasting the heat transfer it is not sufficient to know the over-all value of the tangential drag in the direction of flow; some insight must also be obtained about the tangential drag of the various portions of the surface of the tubes.

6. EXPERIMENTS IN ORDER TO MAKE THE AIR FLOW VISIBLE

6.1 Design of transparent box

Due to the complexity of the flow with the staggered arrangement of tubes, as discussed in Section 2, and the difficulty in interpreting the curves of transverse and longitudinal velocity distributions for the parallel arrangement of tubes in Sections 3 and 4, it was decided to make serious efforts to render the flow visible.

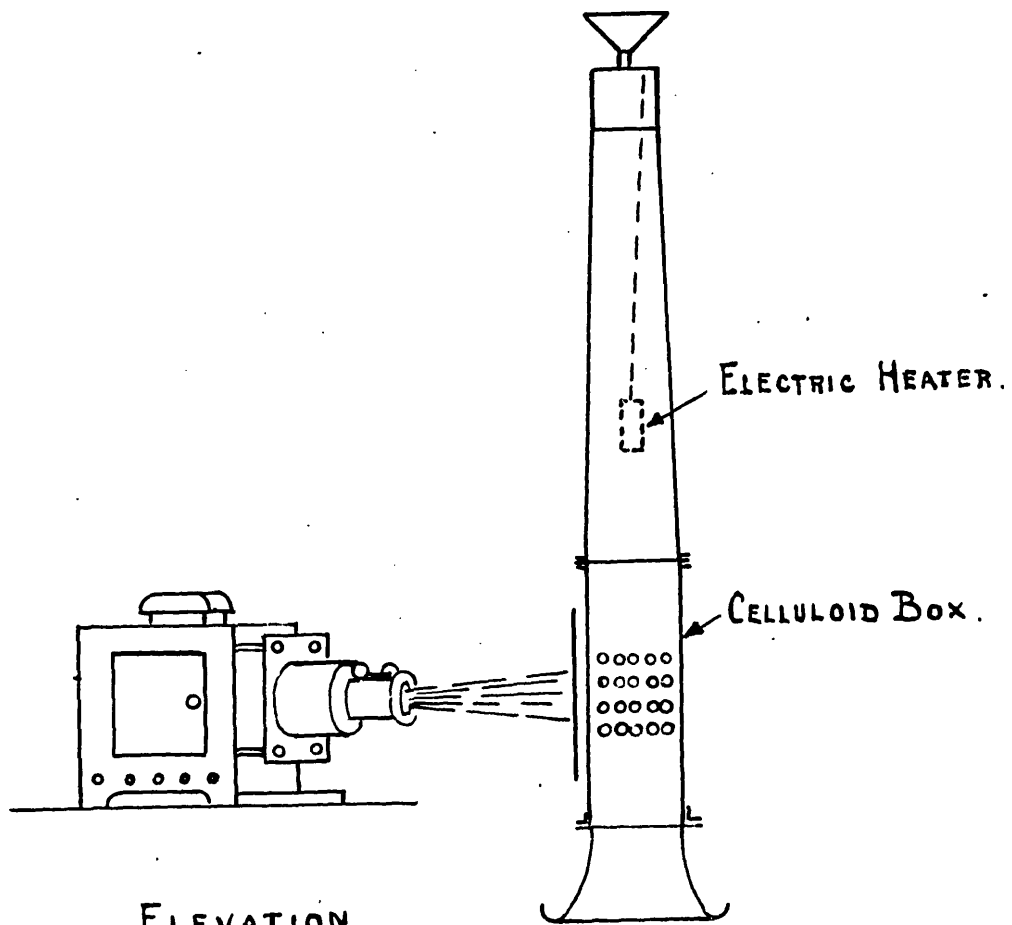
A nest of tubes in parallel arrangement was constructed in a celluloid box. The same 1.27 Cm. diameter brass tubes were used as in the original nest and the vertical and horizontal pitches of the tube centres were the same as before. In this case no half tubes were fitted close to the top and bottom walls.

The celluloid sides of the box, forming the tube plates, were so constructed that they could be easily removed and replaced with other sides drilled for the staggered arrangement of tubes.

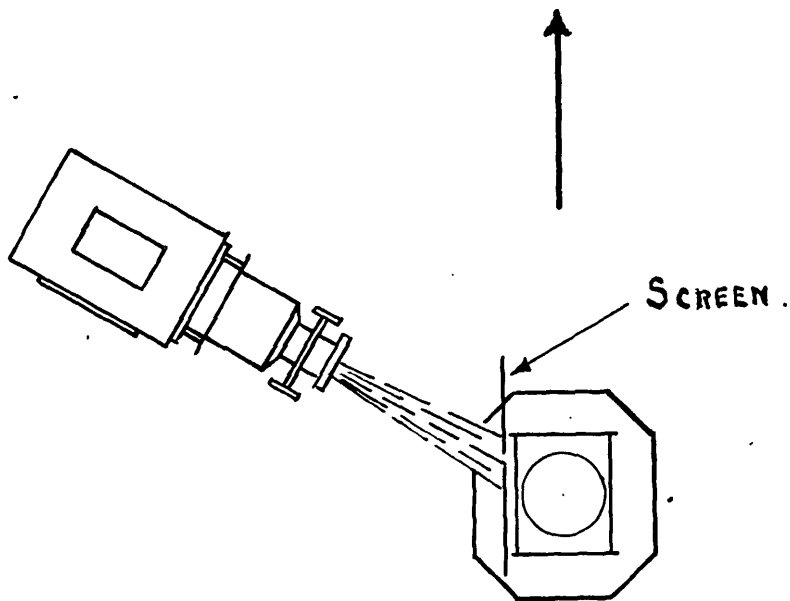
The same converging mouthpiece was fitted to this transparent apparatus.

6.2 Experiments with low air speeds.

The major part of the experiments on form drag curves



ELEVATION.



PLAN.

had been carried out with air speeds of 1370 Cms. per second, in the original stream, and $V_{N,max}$ equal to 4055 Cms.per second. It was therefore obvious that for the first experiments by direct observation the rate of air flow should be greatly reduced.

It was decided not to connect the celluloid box to the induced draught fan, but a steady circulation was induced by fitting a trumpet shaped chimney on top of the box and suspending inside this chimney a small electric heating element. The arrangement is shown in Fig. 6.2. The flow was rendered visible by introducing smoke into the air at the inlet.

Smoke was first produced by the chemical combination of a jet of hydrochloric acid vapour and a jet of ammonia. This appeared to act satisfactorily on a small scale, but when quantities of the smoke were required, difficulty was experienced with the ammonium chloride forming in the jet orifices and choking them. The ammonium chloride was also deposited on the surface of the tubes and in time the shape of the surface over which the air was passing was changed.

This form of investigation might, however, prove extremely useful as a method for the study of the deposition and for the

removal of soot from boiler tubes.

Tobacco smoke was also tried, but this involved considerable effort on the part of the investigator!

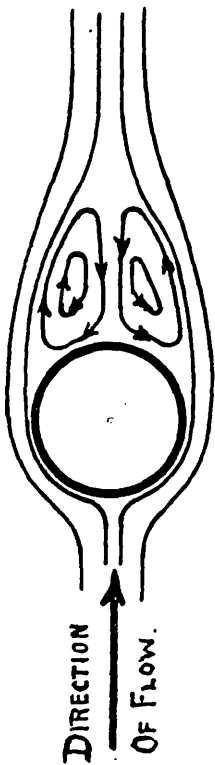
A continuous and effective supply of smoke was eventually derived by burning cotton waste in a closed tin connected to an air reservoir. The pressure in the reservoir was pumped up to 105 to 140 grams per square centimetre, and a steady supply was passed to the tin in which the waste was smouldering. This method appeared to work better at the beginning of an afternoon's experiment than towards the end. The reason for this was that as the cotton waste burned, some water vapour was produced and this condensed on the inner surface of the tube connecting the fire tin to the jet underneath the nest of tubes. This wetted surface acted as a gas washer and washed the particles of smoke out of the products of combustion of the cotton waste.

By the aid of the smoke the shape of the eddies formed with low air velocities could be easily seen. Much more difficulty was experienced when attempts were made to say exactly what had been seen and to draw the flow pattern. Due to the rapid movement of the air in the lanes between the tubes and the varying phases of the eddies between the tubes, considerable uncertainty existed with regard to the

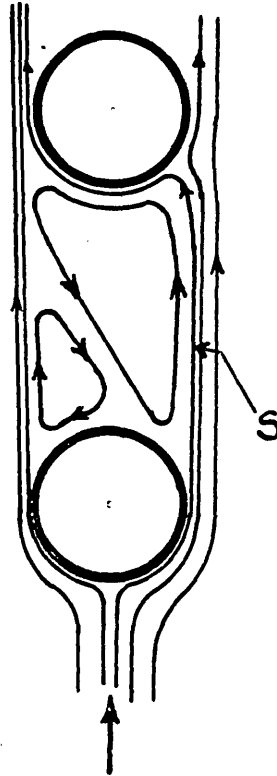
LOW VELOCITY AIR EXPERIMENTS

FIG. 6.2 A-D.

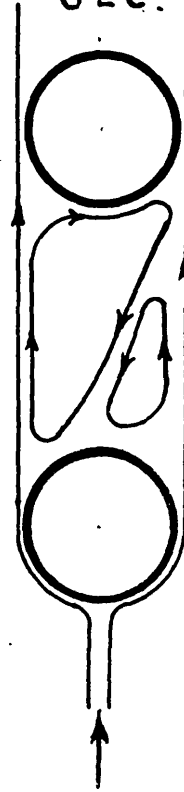
6.2 A.



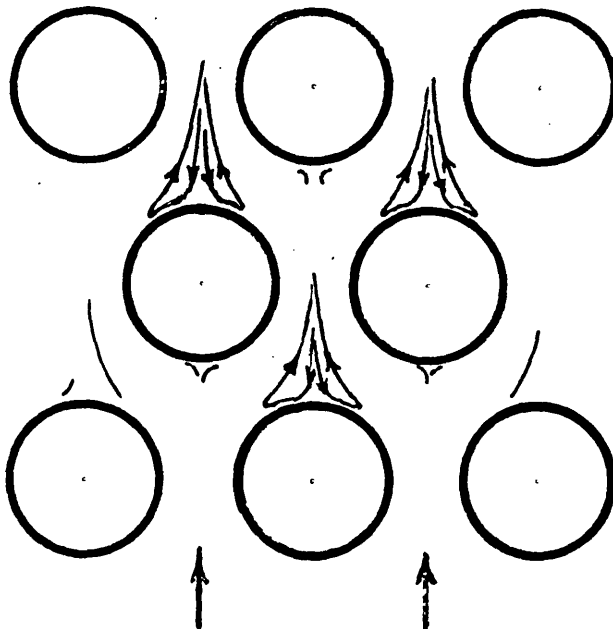
6.2 B.



6.2 C.



6.2 D.



actual path of the flow in the eddies.

Various methods of illuminating the smoke were tried and it was found that for direct vision the most satisfactory method was with a narrow ray of light from a lantern, passing over the tubes at an angle of 30° to 40° as shown in Fig.6.2.

At low air speeds, with a single tube or single row of tubes, two stationary eddies were formed, as seen in Fig. 6.2 A. These were best seen by filling the celluloid box with smoke and then abruptly stopping the smoke supply. The lanes between the tubes were almost instantly cleared from smoke and the two eddies at the back of the tube could be seen distinctly. The leakage of smoke-coloured air from the eddies was so slow that they appeared to persist for periods up to 11 seconds.

With the parallel arrangement and more than one row of tubes, the conditions between the rows appeared to be unstable. First flow pattern "B" would be seen and a moment later flow pattern "C". Occasionally stream lines such as "S" would pass up the right-hand side of the lower tube, appear to come in contact with the under-side of the top tube and flow along its under side and leave on the left-hand side of the top tube.

With the staggered arrangement of tubes the eddies appeared as in Fig. 6.2 D.

Endeavours were made to photograph the eddies, but these were unsuccessful. With exposures under one second duration the light from the lantern was not sufficient to penetrate the smoke and affect the negative, and with longer exposures the movement in the eddies was so great that only blurred images were obtained. For the purpose of these experiments it would appear that a very powerful beam of light and almost instantaneous exposures were required.

6.3 Experiments with high air speed.

Since with low air speeds smoke had failed to give a permanent record of the flow pattern, it was less likely that it would be successful at the high speeds used in the original Pitot tube experiments. Nevertheless the work of Farren⁽¹⁾ had demonstrated that with the dense fumes of titanium-tetrachloride many useful characteristics of air flow could be rendered easily visible. This method might be applicable to the investigation of particular areas in the flow pattern where the flow was practically stagnant. The point of breakaway suggested itself as one suitable for investigation and one which, if it could be definitely obtained, would throw considerable light on the theoretical side of the flow pattern.

The celluloid box with the tubes in parallel arrangement

(1) W.S. Farren, Jour. Roy. Aero. Soc. 1932. Vol. 36, p.451.

was therefore connected to the Sturtevant fan, and the air was drawn over the nest of tubes at approximately $V_0 = 1343$ Cms. per second (corresponding to 1.17 Cm. water gauge).

The centre tube of the first row was replaced with a brass tube of the same diameter in which a hole 0.089 Cm. diameter had to be drilled. A glass rod was dipped into the titanium-tetra-chloride and placed inside the brass tube. This was not successful. Eventually the brass tube was closed at one end and the liquid titanium-tetra-chloride was poured into the tube. Although dense fumes were produced, these did not last in the apparatus more than a small fraction of a second and the flow pattern could not be seen.

The air speed was reduced until it was only one tenth of the standard experimental speed, but the results were no better. When endeavouring to ascertain the point of breakaway the tube was rotated until a small drop of the liquid issued from the hole; the tube was then rotated until the hole and the drop of liquid were at 100° , or approximately the position of breakaway, but the method failed to give useful results.

The causes of failure were:-

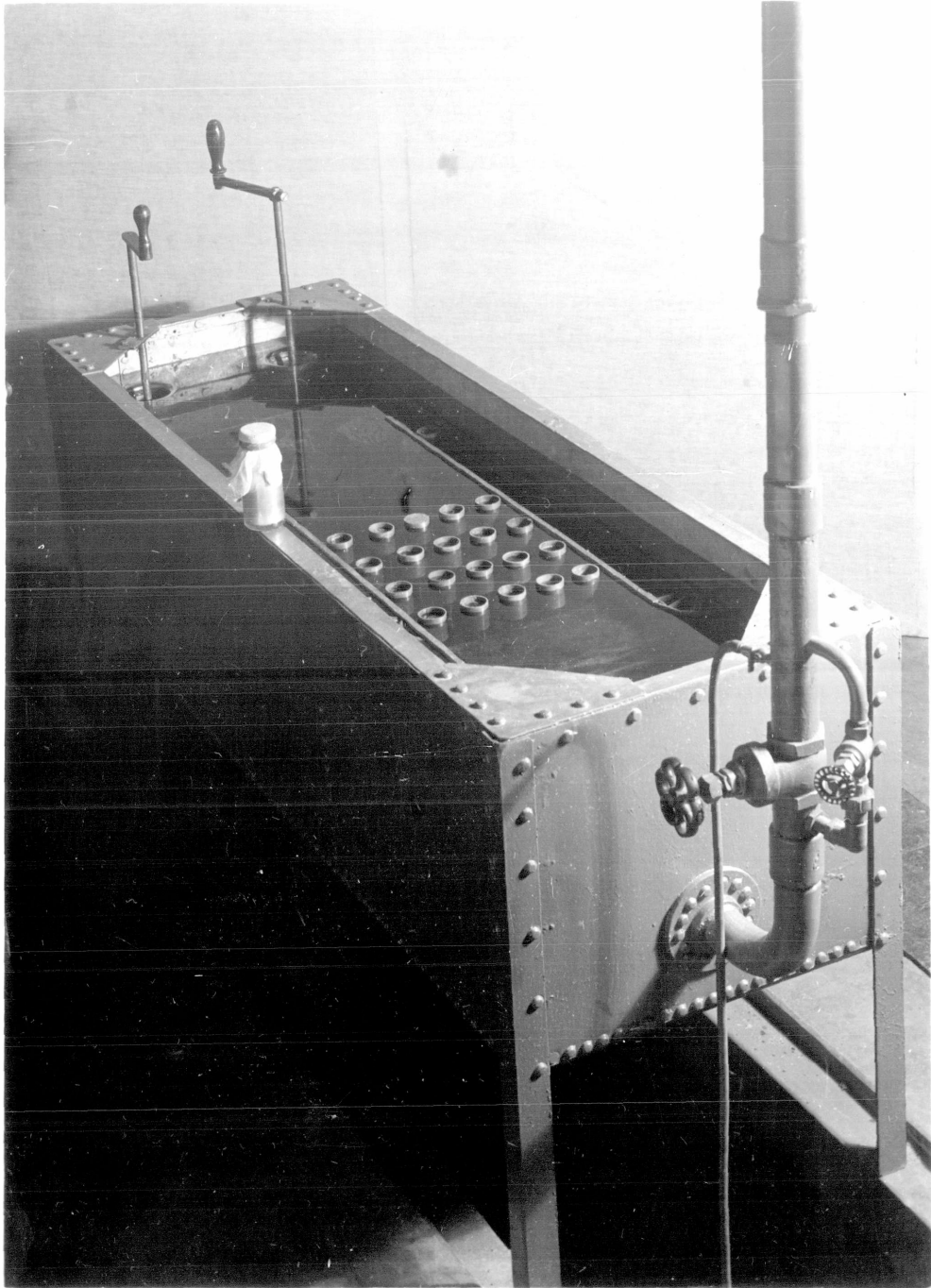
- (1) As the liquid issued from the small hole, it spread over the surface of the tube and made definite location difficult.

- (2) As the titanium-tetra-chloride was emitted, it oxidised, and the oxide was deposited around the small hole. This changed the surface of the tube from that of a true circular cylinder and presumably changed the point of breakaway and the general flow pattern.
- (3) The speed of the air was so great that the smoke did not persist long enough. In Farren's paper, he states that the highest speed at which anything in the nature of turbulent flow can be followed is about 152 Cms. per second, whereas in the present experiments the standard air speed in the original stream was 1343 Cms. per second, and the nominal maximum speed between the tubes approximately three times this figure.

A further attack on the determination of the point of breakaway was made by replacing one of the tubes of the first row with an iron rod of the same diameter. This iron rod was strongly magnetised and the surface covered with fine iron filings. It was anticipated that since the air flow before the point of breakaway was in one direction and that after the point of breakaway in the opposite direction, the iron filings would be slightly inclined in the direction of flow. A strong light on the rod would then show where this inclination of the filings changed and thus indicate the

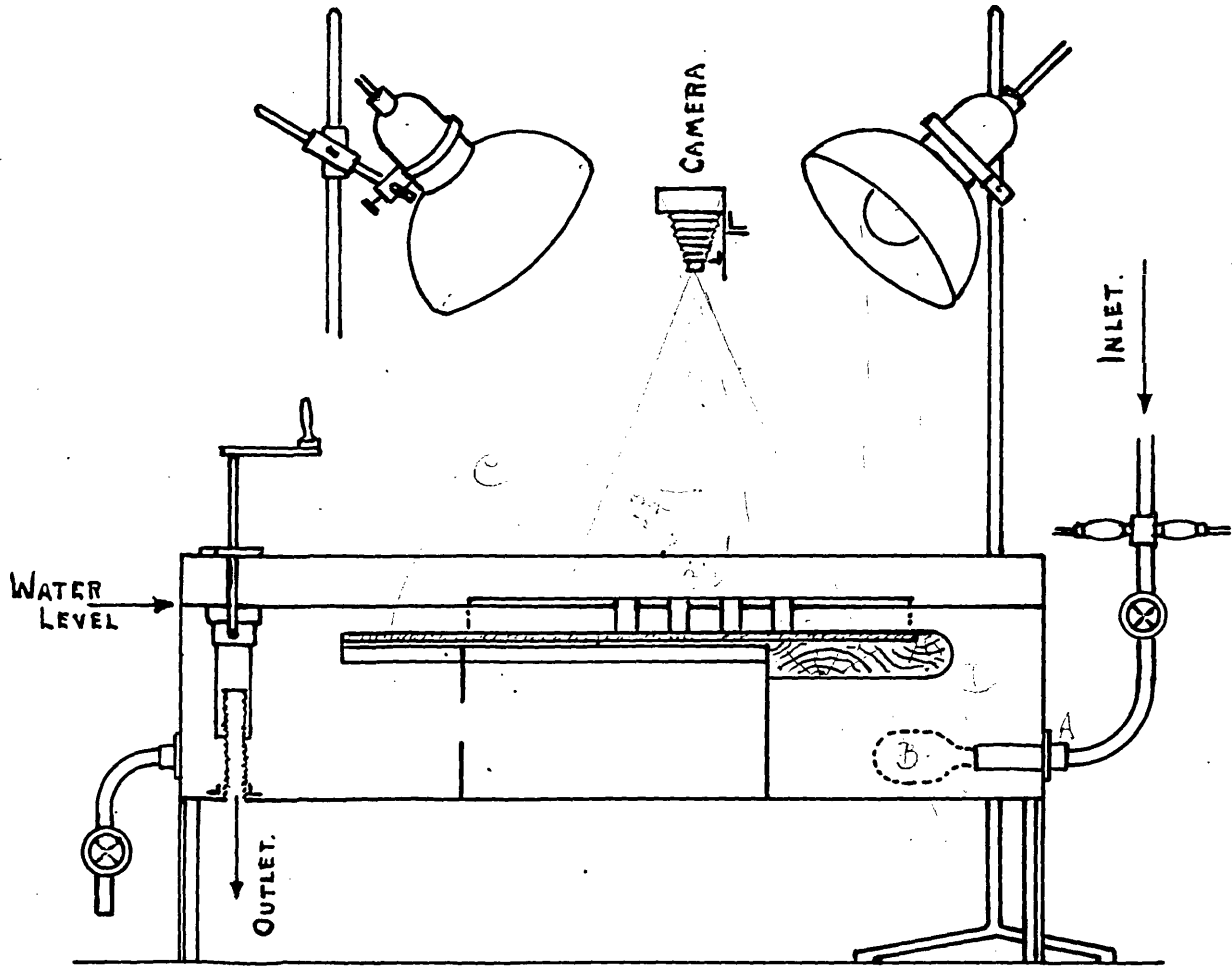
point of breakaway. This was tried but revealed nothing.

It was realised that for the study of the flow pattern the very simplest form of apparatus must be used, even if this necessitated in the first instance the sacrifice of the correct Reynolds' number and the artificial limitation of the problem to two dimensional flow. The next series of experiments was therefore carried out in an Ahlborn tank.



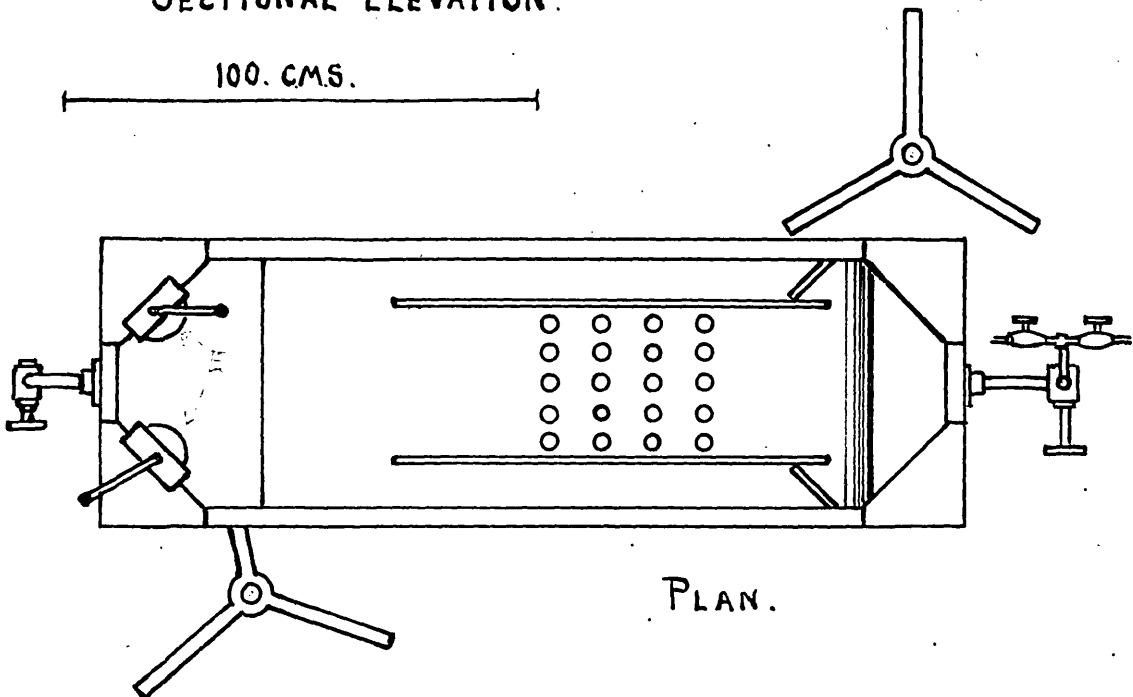
AHLBORN TANK

FIG. 7'1



SECTIONAL ELEVATION.

100. CMS.



PLAN.

7. EXPERIMENTS IN THE AHLBORN TANK. PHOTOGRAPHS
 OF TYPICAL FLOW PATTERNS.

7.1 Description of the tank and method of use.

The tank consists essentially of a wide shallow channel and is called an Ahlborn tank after F. Ahlborn who first carried out such experiments in 1902. The velocity of water through the channel and the depth of the water could be varied at will. The water passes through the channel in steady flow parallel to the sides of the tank.

Fig. 7.1 shows the constructional details.

The tubes in the original nest were represented by cylinders consisting of lengths of copper tubing 4.2 Cms. outside diameter and 8 Cms. long. In most of the experiments the tubes were submerged to within 0.1 or 0.2 Cm. of their height. Single tubes and groups of tubes were placed in the stream and the usual method of investigation was to sprinkle aluminium dust on the surface of the water and to watch or photograph the motion of the particles of aluminium dust as they passed around the tube and indicated the path of the general flow or that of an eddy at the back of the tube.

The surface of the water was illuminated by two 1000 watt filament lamps and the camera was mounted vertically over the

working portion of the tank.

7.2 Investigation to determine the reliability of the results and the range of usefulness of such experiments.

7.21 Indications of general flow pattern. Surface tension ripples restrict range to below, $Re = 2,000$

The bottom of the water channel was first constructed of a large sheet of plate glass, the under-side of which was painted white. With this arrangement the lines of flow could easily be seen with colour bands of potassium permanganate solution.

From these experiments it could be seen that while the flow was undoubtedly three dimensional, the main characteristics could be investigated by considering the motion in planes at right angles to the axes of the tubes.

When the velocity of flow exceed 25.4 Cms. per second surface tension waves are formed on the surface of the water and these prevent the aluminium dust from indicating the general characteristics of flow in the body of the stream.

In the standard arrangement of the nest of tubes the ratio of $V_{N,max}$ to V_0 was approximately 3, with the result that it was impossible to use velocities in the main stream

higher than 8.4 Cms. per second, and in actual practice much lower speeds were employed. With $V_{N,max}$ of 5 Cms. per second, diameter of tube 4.2 Cms. and the water stream at 15°C.,

$$\frac{V_{N,max} \cdot d}{\nu} = \frac{5 \times 4.2}{0.01143} = 1,836.$$
 This should be compared with Reynolds' numbers of 16,000 for the water flow experiments described in Section 1.2 and 32,000 for the air flow in Sections 3, 4 and 5.

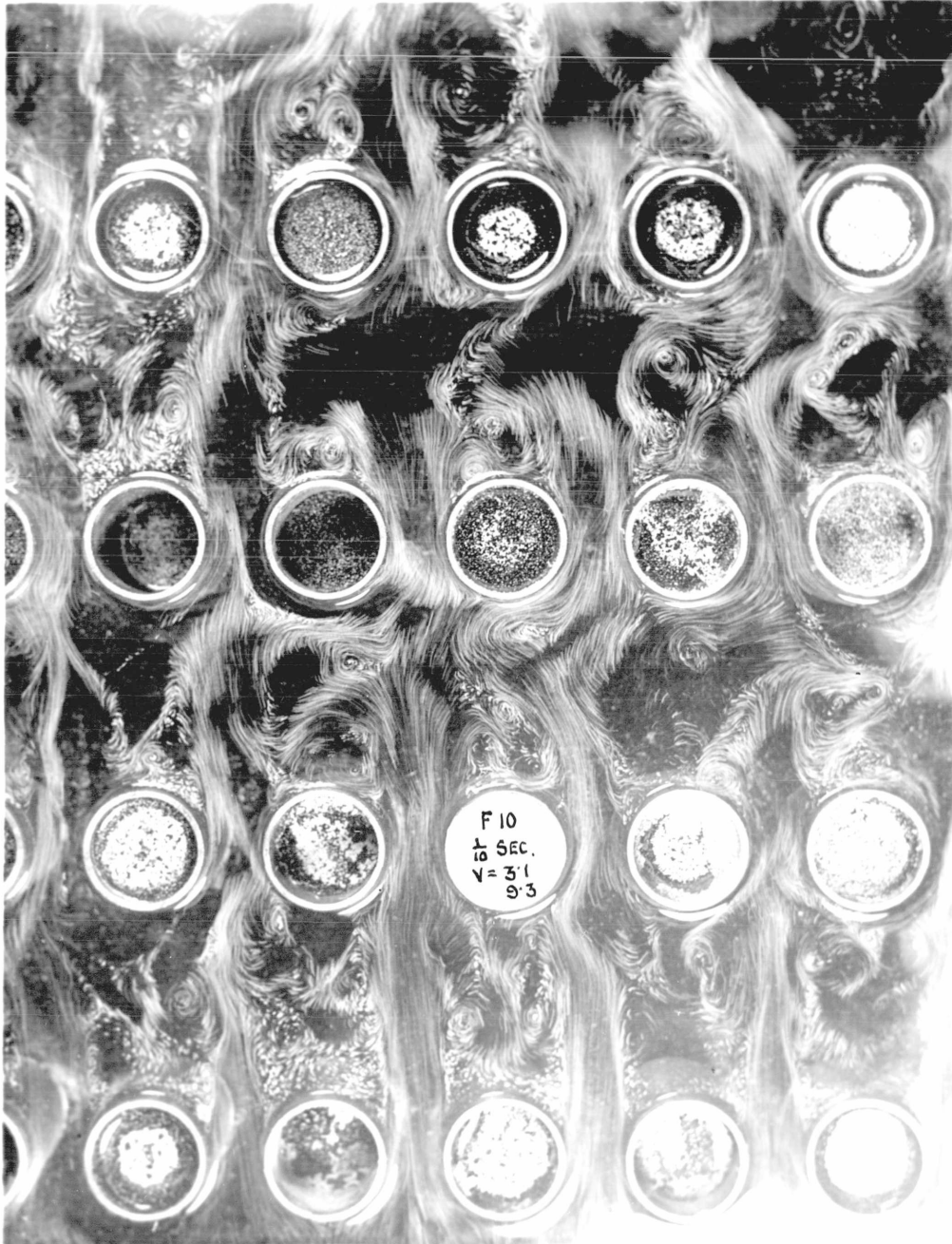
As already pointed out in Section 2.6 the ratio of the length of the cylinders to their diameter is less than 2, and therefore any tendency to three dimension flow would be restricted.

It is necessary to examine critically the conditions of the stream in which the experimental cylinders are immersed. From Fig. 7.1 it will be seen that the working area of the stream is from 30 to 70 Cms. from the inlet, and thus a boundary layer of low velocity water will have formed on the bottom and sides of the tank. Treating the subject as a flat plate in a stream, from an approximation by Blasius the thickness δ of the boundary layer at a distance x from the inlet is given by:-

$$\frac{\delta}{x} = 5.5 \left(\frac{\nu}{Vx} \right)^{\frac{1}{2}}$$

where ν is the kinematic viscosity of the water, which at 15°C = 0.01143 and V is the velocity of the stream outside the boundary layer. If $x = 30$ Cms. and $V = 2$ Cms. per second

FIG. 7'21.



$\xi = 2.75$ Cms. and when $x = 70$, $\xi = 3.48$ Cms.

The cylinders therefore are immersed in a stream 7.8 Cms. high, the top 5 Cms. of which is moving with a uniform velocity of 2 Cms. per second. The velocity in the bottom 2.8 Cms. decreases continuously as the bottom of the tank is approached. While under some conditions the variation of velocity near the bottom may be important, the conditions at the surface of the water are much more likely to affect the indications of the flow pattern. Aluminium has a density three times that of water and when the dust was sprinkled on the surface a portion of it was seen to descend slowly through the stream. When the conditions were favourable and everything working well, it was seen that the particles on the surface were moving in the same direction and at the same speed as those in the midst of the stream. Unfortunately the motion of the particles on the surface was largely influenced by any variation of surface tension. The slightest trace of oil or dust on the surface of the stream would render the path of the surface particles of aluminium quite different from those in the main stream. A small globule of oil coming to the surface of the stream would cause the particles of aluminium dust to disperse quickly from the area. Fig. 7.21, although on the whole not a bad photograph, shows definite indications of oily patches. Even the touching of the water surface with the finger was often

FIG. 7'22A.

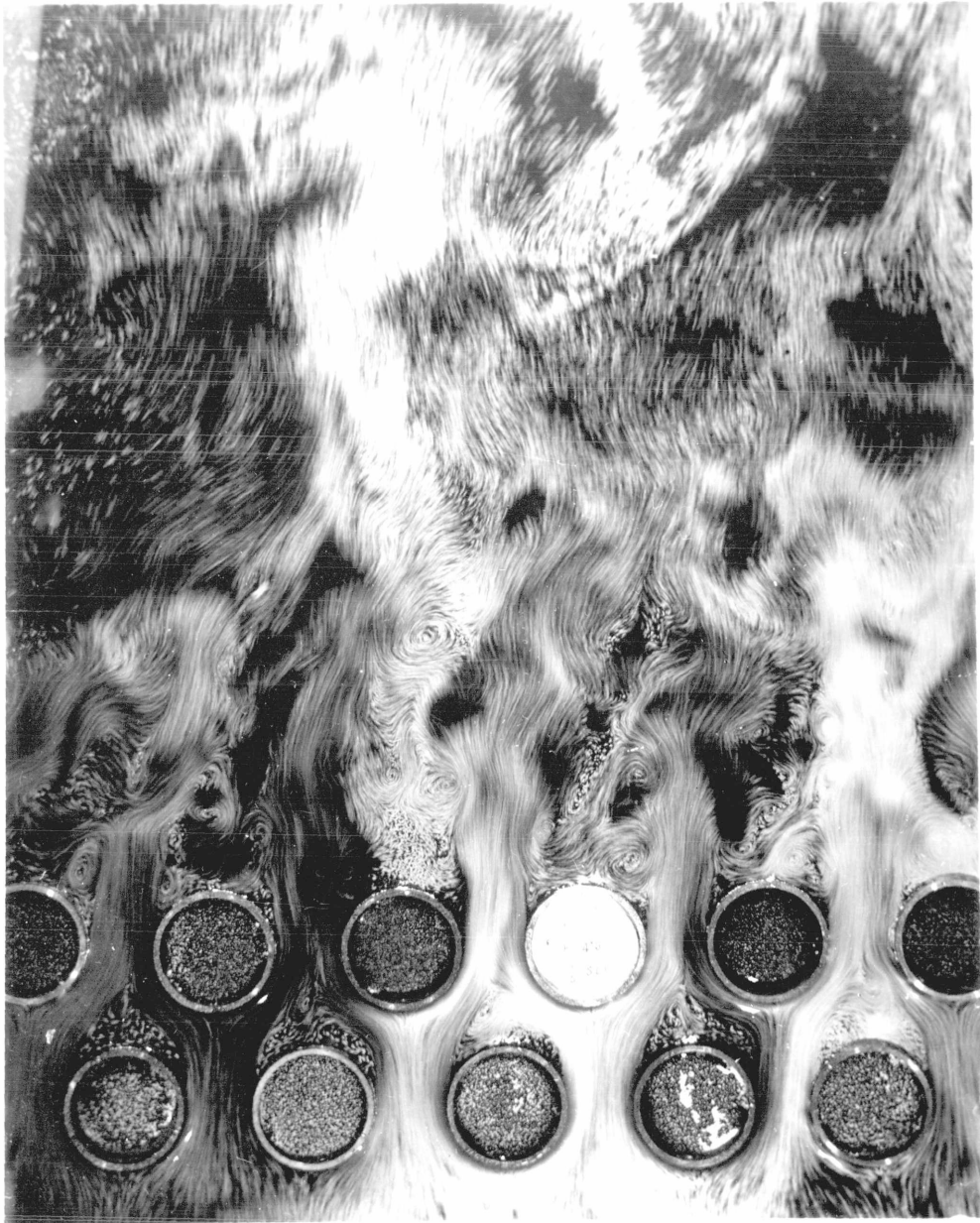


sufficient to cause a change of surface tension and prevent the uniform distribution of dust on the surface. When this difficulty was experienced, it was found that the best way of cleaning the surface was to sprinkle upon it a few flakes of shredded soap or lux.

7.22 Experiments with a single cylinder.

From the work of previous investigators a considerable knowledge was available of the flow around a single cylinder in a uniform stream. Therefore it was decided to carry out a few experiments with such a cylinder in order to confirm that the Ahlborn tank method was suitable to the present enquiry and also to learn to interpret the results. This afforded an opportunity of developing the technique of producing reliable indications of the flow and taking suitable photographs. Fig. 7.22 A shows the flow around a single cylinder with a stream velocity of about 2 Cms. per second. The figures in the centre of the cylinder indicate that the light for the photograph was two 1000 Watt lamps at a distance of 3 feet from the surface of the water. The lense stop was F 12.5 and the exposure 1 second. It was subsequently found that it was unnecessary to vary the intensity of the illumination and so this information is not repeated on the later photographs. However, it was found advisable to vary the speed of the stream and it was decided to mark the

FIG. 7·22 B.



velocity on the photograph. While it was the velocity of the undisturbed stream that was observed, it was realised that when considering groups of tubes the more important velocity was the maximum velocity between the tubes. Since the ratio between these two velocities varied with each particular spacing of tubes, both V_0 and $V_{N,max}$ are marked on the photographs. The velocities were measured in centimetres per second.

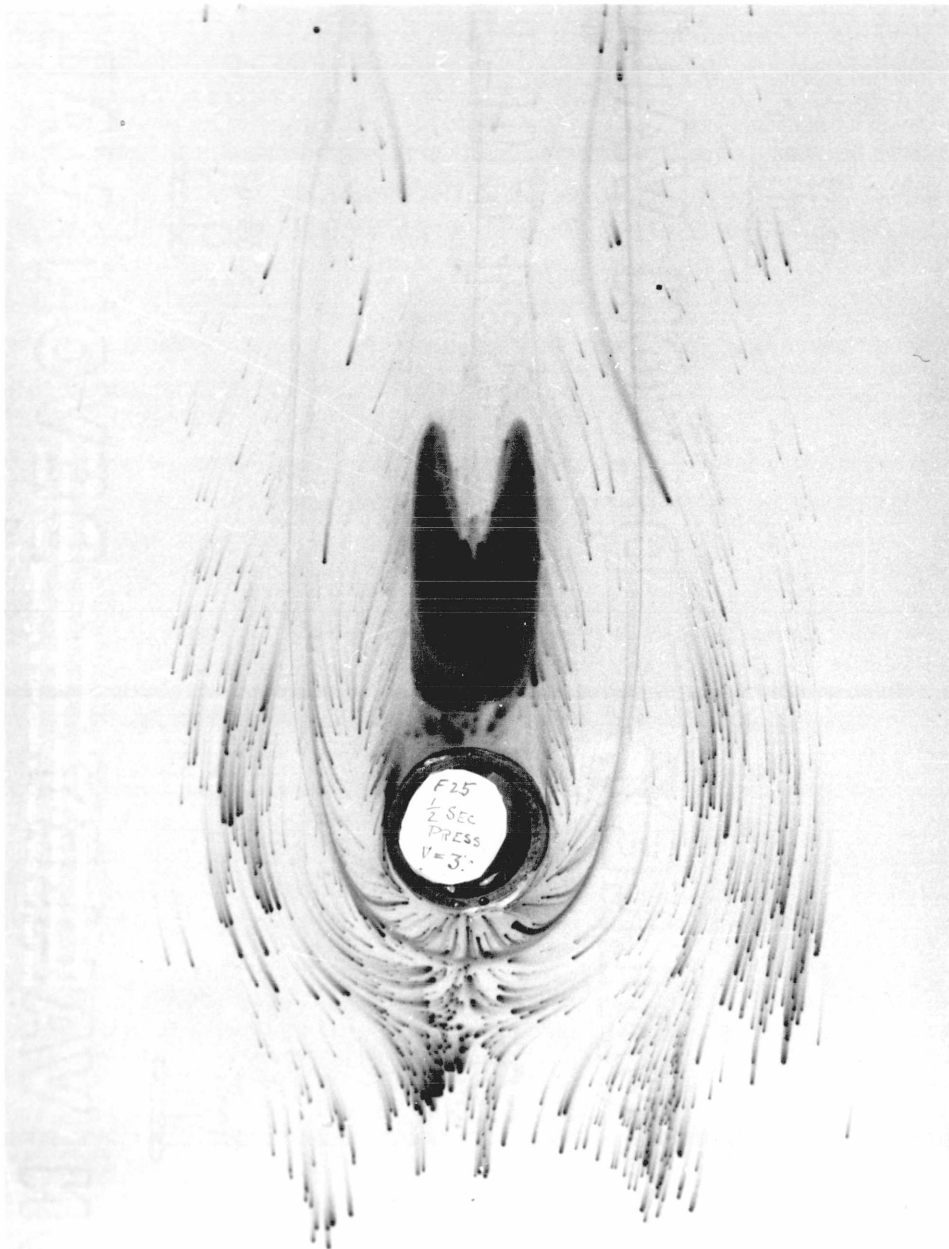
When observing the flow as indicated by the motion of particles of aluminium, the eye instinctively follows an eddy as it proceeds down stream. In this way a study could be made of the motion of the particles in any particular patch of water. When photographs were taken the camera was fixed directly over the group of tubes and the condition was somewhat different. Vortices produced in the patches of water between the two rows of tubes appeared very similar to those observed with the eye. This was due to the motion of such vortices down-stream being very small in the short time of exposure of the photographic plate. With the vortices produced at the back of a single cylinder, or of the last row of tubes, the condition is very different. Shortly after its formation the vortex leaves the back of the tube and travels down-stream with a speed 0.8 of the original undisturbed stream⁽¹⁾.

(1) Fage and Johansen. Phil.Mag. 1928, Vol. 5, p. 417.

FIG. 7'22 C.



FIG. 7'23 A.



If the time of exposure be one second, the particle of aluminium dust has not only whirled round in the vortex, but has also proceeded an appreciable distance down-stream. The path thus indicated in the photograph is the combination of this rotation and translation, and is a series of curves.

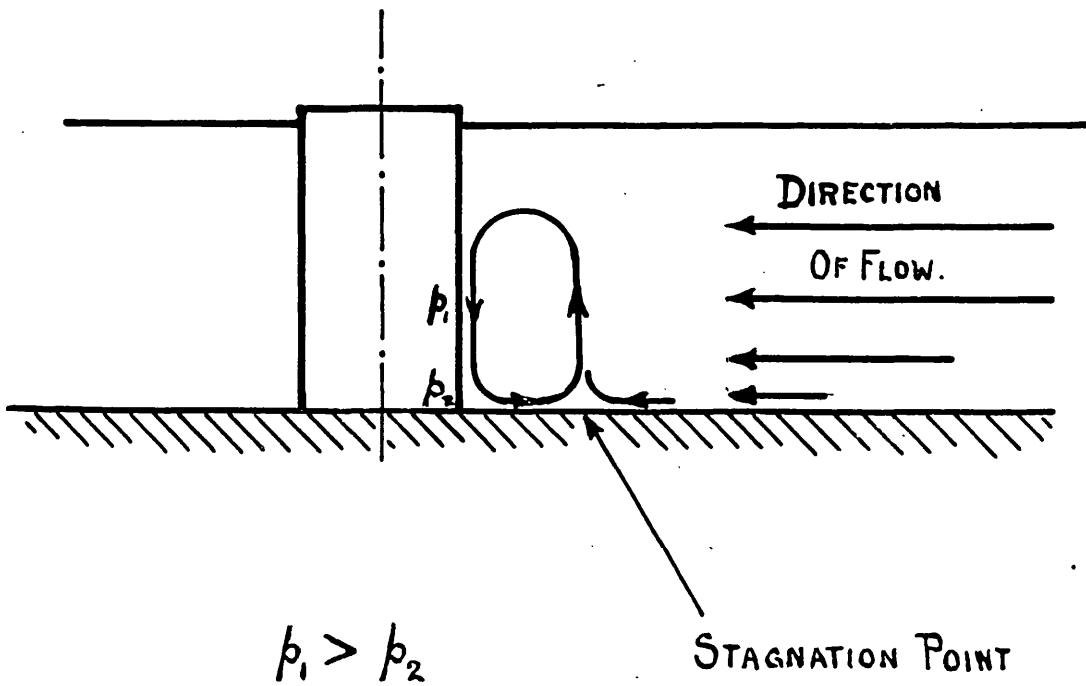
The type of photographs obtained depends to a large extent upon the time of exposure and the amount of aluminium dust on the surface of the water. With a large amount of dust and a long exposure the streaks of light indicating the paths of particles merge into one another and give very good indications of the flow pattern. Such photographs of the eddies at the back of the last row of tubes resemble photographs of burr-walnut. (Fig. 7.22 B) When only a moderate number of particles of aluminium dust are sprinkled on the surface of the water, the photographs appear as a series of curved white streaks. The actual paths of individual particles are lines of finite length and are sufficiently distinct to give a reliable measure of the local velocities (Fig. 7.22 C).

7.23 Flow pattern at bottom of tank.

In Section 7.21 it was stated that the main characteristics of flow could be investigated by considering the motion of particles in planes parallel to the bottom of the tank. One important exception to this conclusion was observed. In

FLOW IN BOUNDARY LAYER

FIG. 7.23B.



the case of a single cylinder it was found that when small crystals of potassium permanganate were dropped on to the bottom on the channel, the colour bands obtained were as seen in Fig. 7.23 A. The colour bands are not indicative of the stream lines of flow around the cylinder. These should be as in Fig. 7.22 A. The colour band from the crystal directly in front of the cylinder is flowing in exactly the opposite direction to the main stream, while the colour band from adjacent crystals indicates motions at right angles to the line of flow. The explanation is that the colour bands indicate the motion not in the main stream but in the boundary layer at the bottom of the tank.

As the bottom of the tank is approached the velocity of the stream is successively reduced. As the velocity is reduced so is the pressure on the front of the cylinder reduced, as was seen in the form drag diagrams in Section 5.4. As a result of this reduction in pressure there is a downward flow on the face of the cylinder from an area of high pressure to that of low pressure. This creates a circulation as shown in Fig. 7.23 B, with a stagnation point $0.75 d$ in front of the cylinder.

The importance of the experiment is that it illustrates the danger of assuming that lines of flow near a boundary are

the same as those in mid-stream. It indicates the futility of trying to ascertain the path of the general flow of water through a centrifugal pump by painting the impeller vanes with special pigment - running the pump for a short time - removing the impeller and assuming that the streaks on the pigment indicate the main flow through the pump.

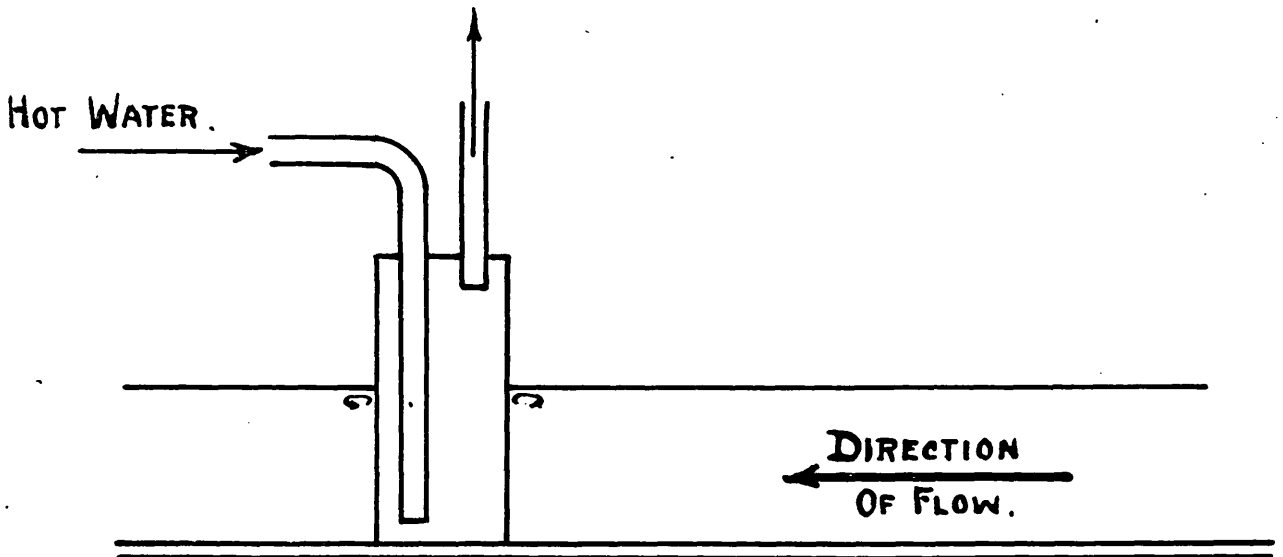
7.24 Surface tension effects cause by temperature differences.

As well as the exceptional case of flow near the bottom of the tank, described in the previous Section, one other interesting exception was observed. In this case it was connected with the flow on the surface of the water and was caused by non-isothermal conditions.

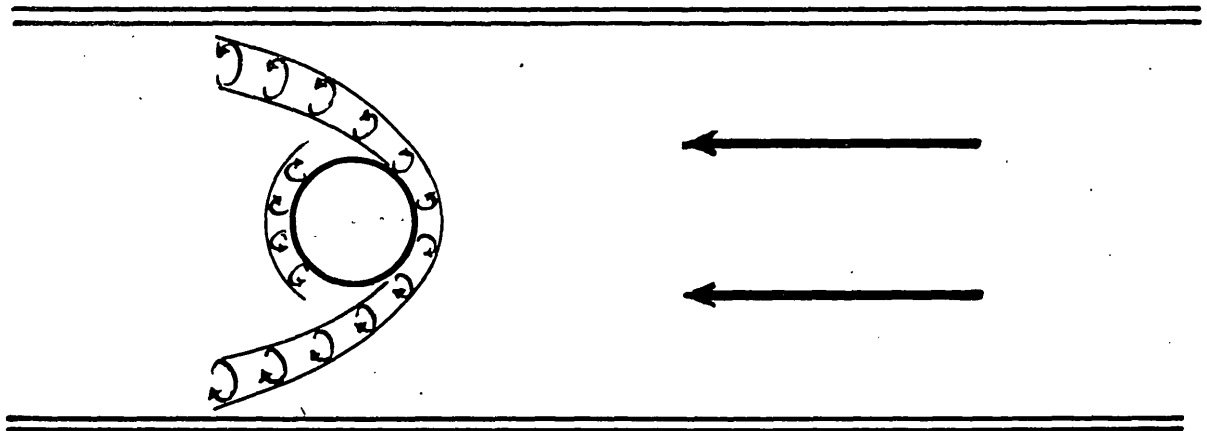
It had been decided to investigate the band of vorticity between the free moving stream and the "dead Water" area at the back of a single cylinder. In the search for a suitable cylinder a large steel nut of cylindrical form was placed in the Ahlborn tank, but difficulty was encountered immediately, due to oil being given off from the screwed thread on the inside of the nut. A solid steel cylinder about 12.7 Cms. diameter was then washed with soap and water and placed in the tank. Trouble was experienced still with oil on the surface of the water and the cylinder was washed in spirit. This did not prove entirely effective, and it was remembered that

SURFACE TENSION EFFECT.

FIG. 7.24.



SECTIONAL ELEVATION.



PLAN.

Tietjens⁽¹⁾ had recommended covering the model with paraffin wax. In order to apply the wax, the steel cylinder was heated sufficiently to melt the wax on the surface.

The wax-covered cylinder was replaced in the water channel before it had cooled completely, and it was observed that the particles of aluminium dust moved radially away from all parts of the circumference of the cylinder at a very high speed. It was realised that if this motion of the fluid away from all parts of the circumference was due to the natural convection caused by the difference in temperature of the fluid and the cylinder, then it would appear that it could not be assumed that the flow pattern in a nest of tubes when transferring heat would be the same as under isothermal conditions. This would be contrary to the conclusions of Drew and Ryan⁽²⁾ and further experiments were carried out in a small water channel.

A closed cylinder was made from a piece of brass tube 3.5 Cms. diameter and 8 Cms. long. This was fitted with an inlet and outlet pipe so that hot water could be circulated through the cylinder as illustrated in Fig. 7.24.

With water in the stream at 11.6°C. and hot water entering the cylinder at 37°C. and leaving at 30°C., the phenomenon

(1) O.G.Tietjens. Applied Hydro and Aeromechanics. 1934. p.270.
Publishers: McGraw Hill Book Co.

(2) T.B.Drew and W.P.Ryan. Amer.Inst. Chem.Eng. 1931.
Vol. 26. p.118.

was investigated, first with aluminium dust, then with a very fine colour band of potassium permanganate solution.

It was found that the effect was entirely confined to the water near the surface and that here a rapid circulation was set up in the form as indicated in the figure. The depth of this circulation could be clearly seen by lowering the colour band until it was level with the under-surface of the circulating water, which was about 0.3 Cm. below the surface of the stream. The potassium permanganate solution was then drawn into the circulation and gave a definite indication of its shape.

By lowering the colour band to a depth greater than 0.3 Cm. it was seen that the flow around the cylinder was similar to that under isothermal conditions, and the general characteristics of flow were as seen in Fig. 7.22 A.

7.3 Flow patterns with various arrangements of groups of tubes.

Fig. 7.3 shows the various arrangements of groups of tubes which were examined in the Ahlborn tank.

Group A is a parallel arrangement with close spacing. In the earlier experiments the group consisted of four rows with five tubes in each row. Fig. 7.3 A shows a photograph of the eddies with this arrangement. It was observed that while there was little similarity in the form of the eddies between

AHLBORN TANK EXPERIMENTS

FIG. 7'3.

ARRANGEMENTS OF VARIOUS NESTS OF TUBES

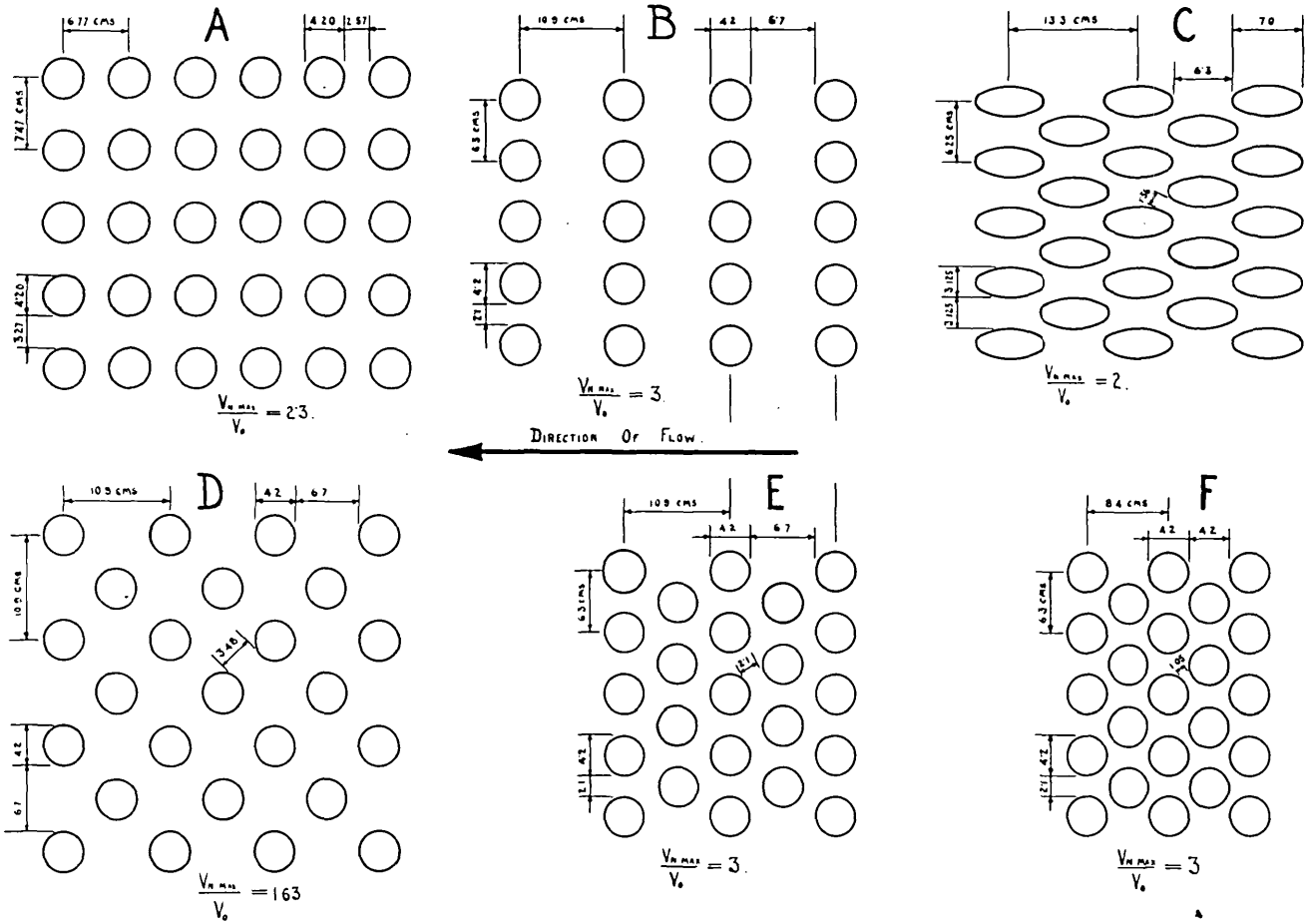


FIG. 7.3A.

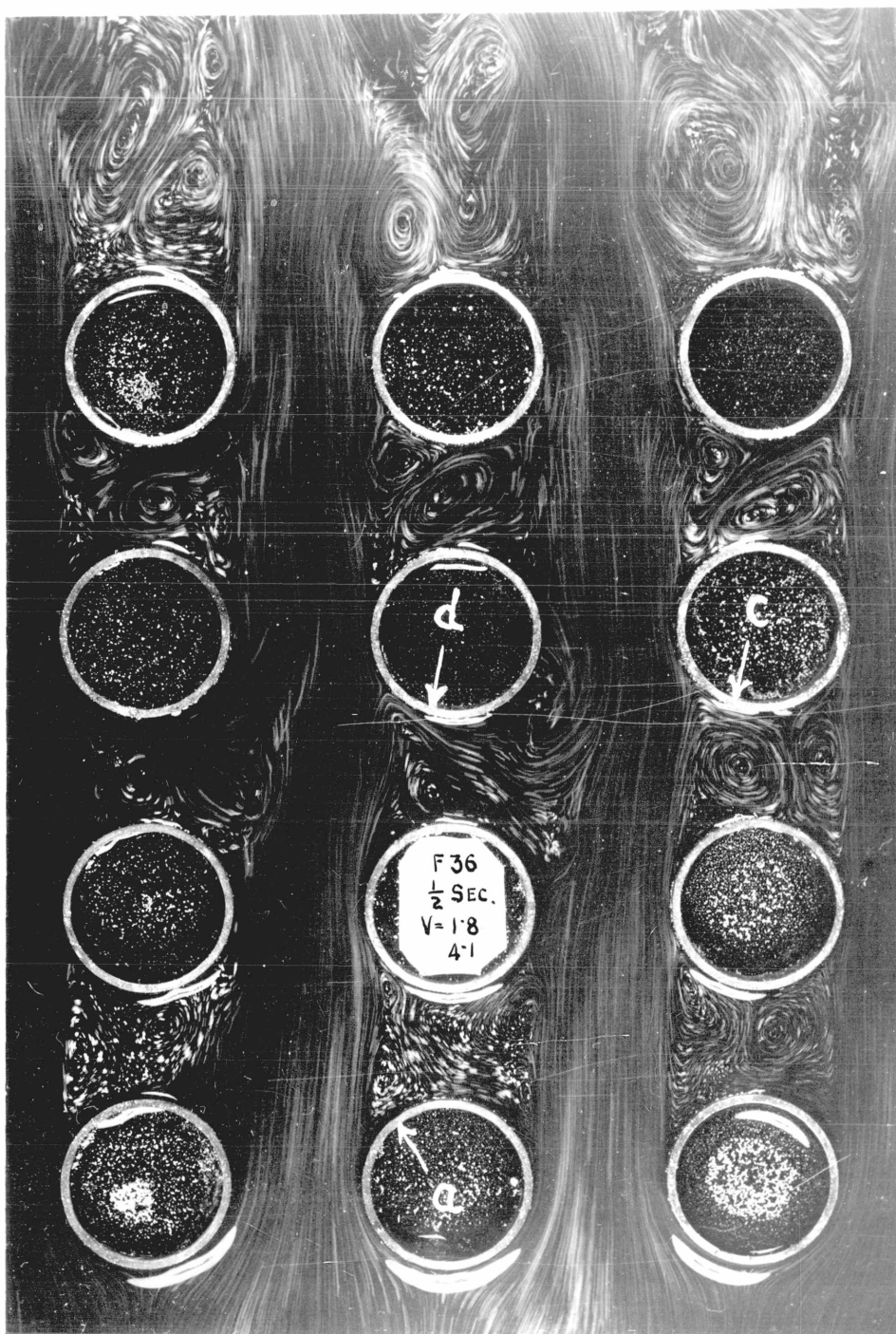


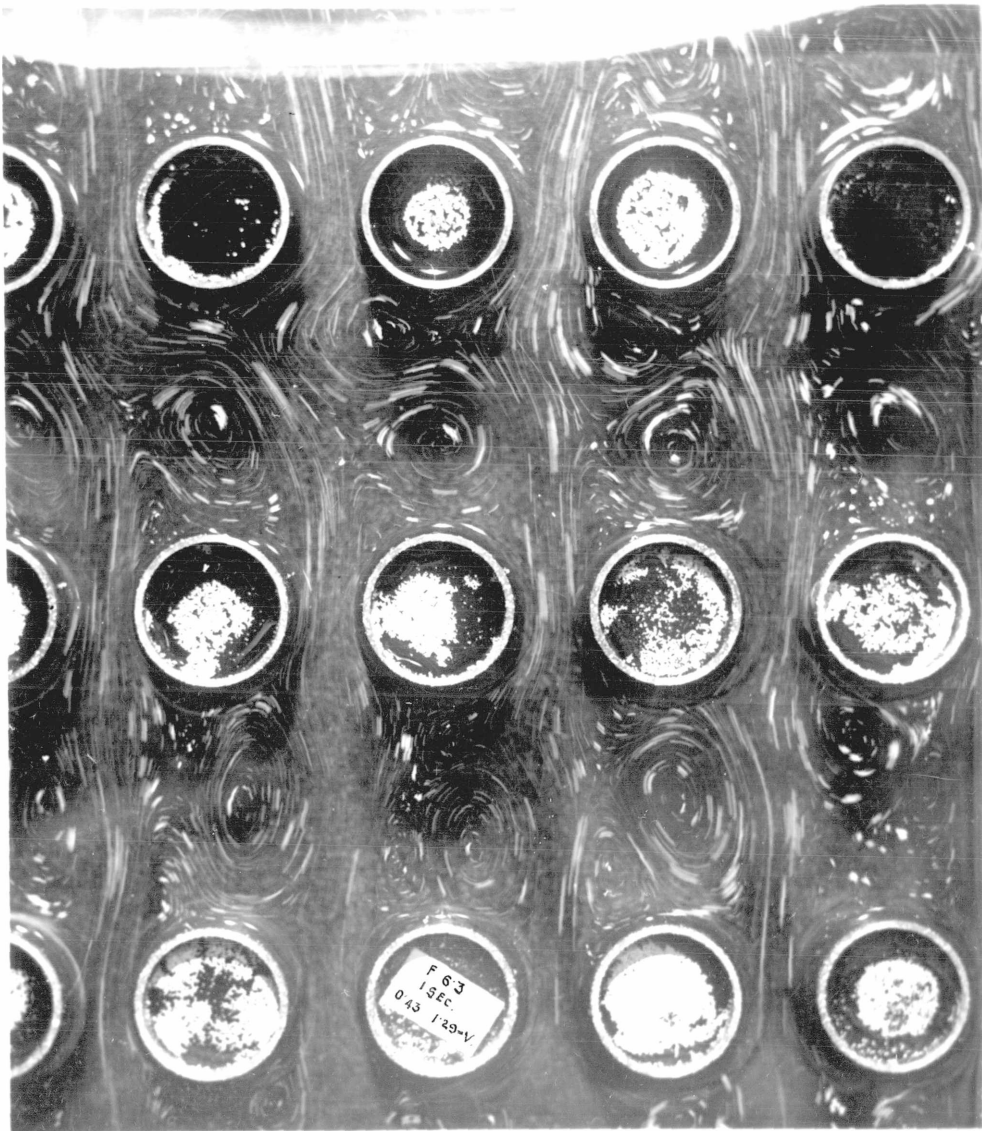
FIG. 7·3 A'.



FIG. 7·3 B.



FIG. 7.3B'



the 1st and 2nd, and 2nd and 3rd rows of tubes, there was definite indication of similarity between the eddies in the areas between the 3rd and 4th rows. It was thought possible that after a certain number of rows a definite flow pattern might be established, and in order to investigate this subject two further rows were added. Fig. 7.3 A' shows the result, but there is even less indication of uniformity of flow pattern.

Group B, in Fig. 7.3, shows the open spacing parallel arrangement, the proportions of which are the same as the nest of tubes used in the Pitot tube and form drag experiments. Fig. 7.3 B is a very good example of the indications of flow by this method. This photograph was taken with a relatively long exposure (1 second) and a liberal sprinkling of aluminium dust.

Fig. 7.3 B' is taken with the same exposure, but with few particles of aluminium dust. While there is little indication of a definite flow pattern in Fig. 7.3 B, Fig. 7.3 B' again shows a similarity of pattern of the eddies between the last two rows of tubes. It would not be difficult to give a cause why a definite flow pattern should or should not exist, and it is possible that under one set of conditions the flow pattern is definite and regular, whereas under another set of conditions the formation of the eddies in time and space produces no

definite periodicity or pattern.

If the stream were to flow at an absolute uniform velocity and the path of each particle in the stream was parallel to the path of every other particle, this would constitute an ideal stream. Simple experiments with potassium permanganate colour bands showed that such a stream did not exist. While the general direction of flow was uniform, the paths of individual stream lines were not parallel always.

If the nest were to consist of tubes of exactly the same diameter and of exactly the same surface roughness, and the pitching of the tubes in each row and the distance between consecutive rows were absolutely correct, this would constitute an ideal nest of tubes. If the ideal fluid stream were to pass over the ideal nest of tubes there is every probability that a definite flow pattern would be established and maintained.

Under such conditions the periodicity of the formation of eddies between the first and second rows would affect the periodicity of the flow pattern between the second and third rows, making the definite period of cyclic changes in this area either the same period or some multiple of the cyclic period of the eddies shed from the first row of tubes. The periodicity of the flow pattern between the 2nd and 3rd rows would affect that in the space between the 3rd and 4th rows,

and so on with each successive row.

In the actual experiment the stream is neither an ideal stream, nor is the nest an ideal nest of tubes. The particles of water in the local stream impinge on one of the tubes at a slightly different angle or with a slightly different velocity from the local stream on the adjoining tube. This causes the point of breakaway on the first tube to be slightly different from that on the second tube, and a vortex commences to build up behind the first tube a fraction of a second before a similar vortex is formed behind the second tube. The flow pattern is thus interrupted. The existence of the vortex behind the first tube creates a set of pressure and velocity conditions, the influence of which is transmitted through the main stream to the area at the back of the second tube. The vortex at the back of the second tube does not develop under the same environmental conditions as the first one.

It will be realised that in time this mutual interference will so distort the flow that it will be impossible to say that any regular pattern exists. The eddies at the back of any one tube are evolved, developed and shed at periods which are entirely dependent upon the local conditions under which the eddy is born, and these will vary from tube to tube and from moment to moment.

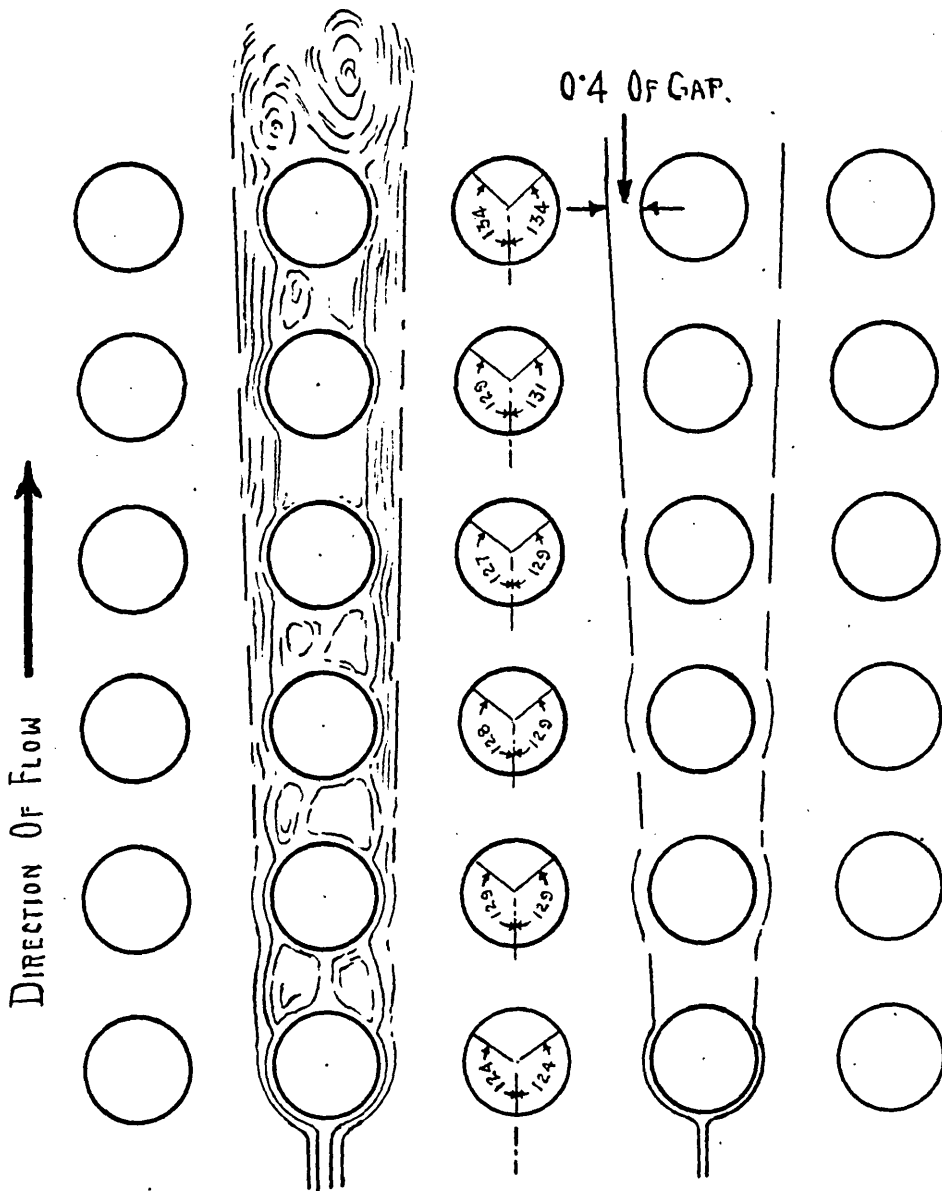
AHLBORN TANK EXPERIMENTS

INVESTIGATION OF POINTS OF

BREAKAWAY USING LATEX AS INDICATOR

FIG. 7.3A"

$$\frac{V_{N.MAX.} \cdot d}{\nu} = 286$$



Taking this into consideration, it is a matter for comment that Figs. 7.3 A and 7.3 B' give evidence of a regular flow pattern with regard to the central three tubes. It is not surprising that the flow pattern behind the two outer tubes is not the same as that behind the central tubes, since the outer surface of these areas is bounded by a straight wall.

Although the aluminium dust had given good indication of the flow, and yielded some very good photographs, other indicators were tried. Fresh cow's milk and also solutions of condensed milk were used, but there seemed to be considerably denser than water and the indicator soon sank to the bottom of the channel. Tincture of benzoin in solution in water gave a milky indicator which is lighter than water and tended to rise to the surface.

A mixture of this solution with milk or condensed milk was made so that it had the same density as water and this acted very well and did not have any tendency to rise or sink. With this indicator any particular area or the general flow at any particular depth could be examined.

Although the introduction of latex into the dead water region at the back of the tubes cause a momentary disturbance and surface tension effect, this soon passed away and the latex provided a very useful indicator. The best method

of introducing the indicator was by means of a pipette. The general lines of flow could be clearly seen and the indication persisted for several minutes. Individual cylinders were removed from the stream and a wide white band of latex was painted on their surfaces. The cylinders were immediately replaced in the stream. By this method the point of breakaway of the stream from the various cylinders could be determined. Figure 7.3A'' shows the general appearance of flow with this indicator and the points of breakaway. $V_{N,max}$ in this case was only 0.78 Cm. per second, whereas in most of the experiments with aluminium dust the velocity was four times this figure.

From the observations made with the aluminium dust and other indicators it was seen that in the case of a single row of tubes eddies are formed at the back of each tube. The eddies are periodic in character, leaving the tubes first on the right and then on the left, and passing down stream similar to those shed from a single cylinder. They are somewhat smaller in comparison with the diameter of the cylinder and more irregular with regard to periodicity.

When the nest consists of more than one row of tubes arranged in parallel formation, for an appreciable length of time the main stream appears to pass straight down through the gaps, presumably with little loss of energy on the centre

FIG. 7.3C.



of the stream. Such flow does not continue indefinitely. Caused by the dissipation of some particular eddy, the main stream appears to flick over into the space which had been occupied previously by the eddy and to push what remains of the eddy into the stream of an adjacent channel. Meanwhile some of the new high energy fluid is combining with the dead water at the back of the tube and together with the new boundary layer fluid forms another eddy. This eddy may remain for sufficient time to complete several revolutions during which period it appears to receive energy continuously from the main stream and simultaneously to lose energy by surface friction, mainly on the upstream face of the second row of tubes, although partly on the downstream face of the first row.

This process is repeated in a progressively greater degree between the succeeding rows of tubes.

Group C Figure 7.3 shows a staggered arrangement of elliptical tubes. These tubes were arranged so that the diagonal distance between two tubes was half the distance between adjacent tubes in a row. With this particular spacing the velocity of the main stream is practically constant. Figure 7.3C shows the resultant flow. The first impression of this photograph is the notable absence of eddies.

FIG. 7.3 C'

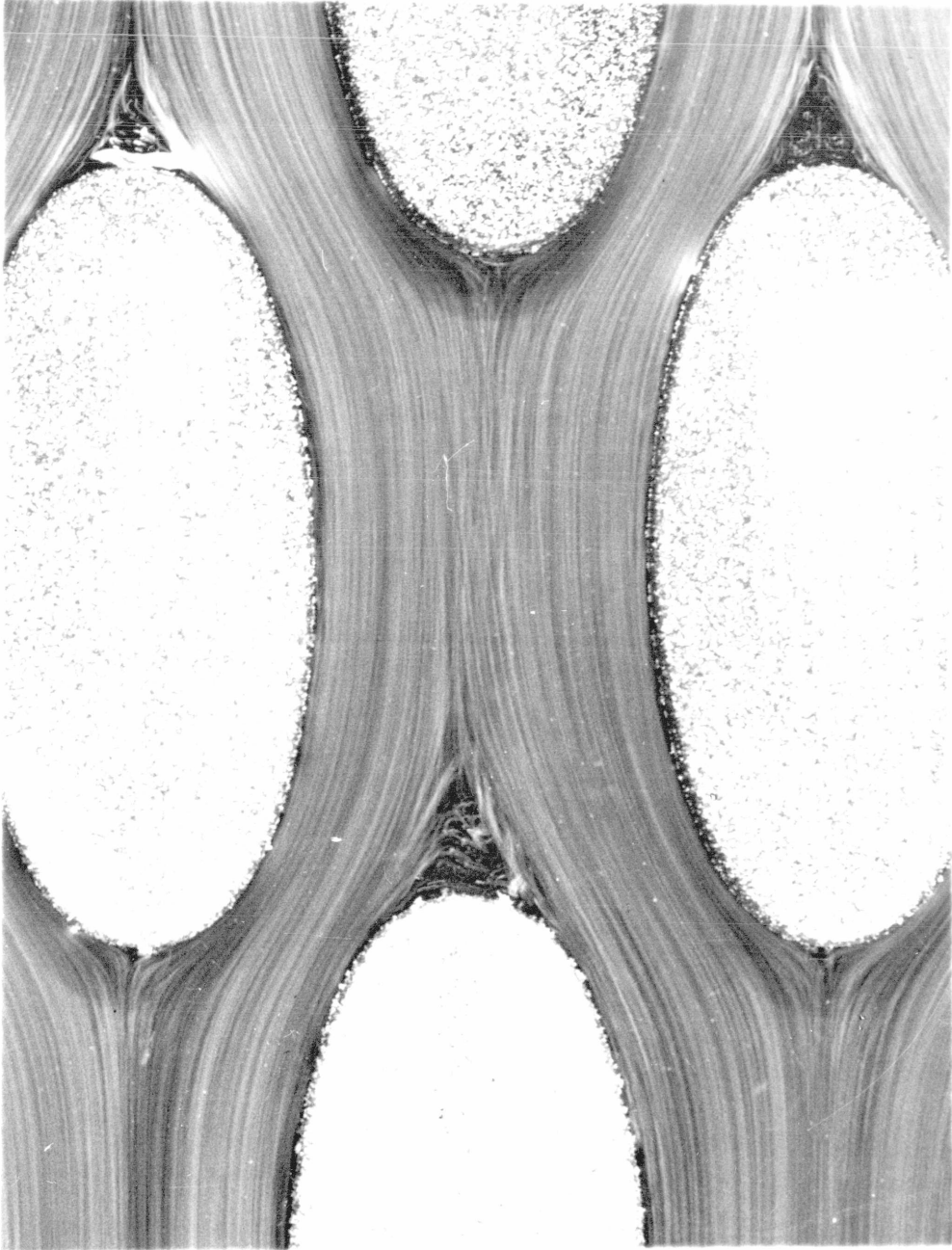
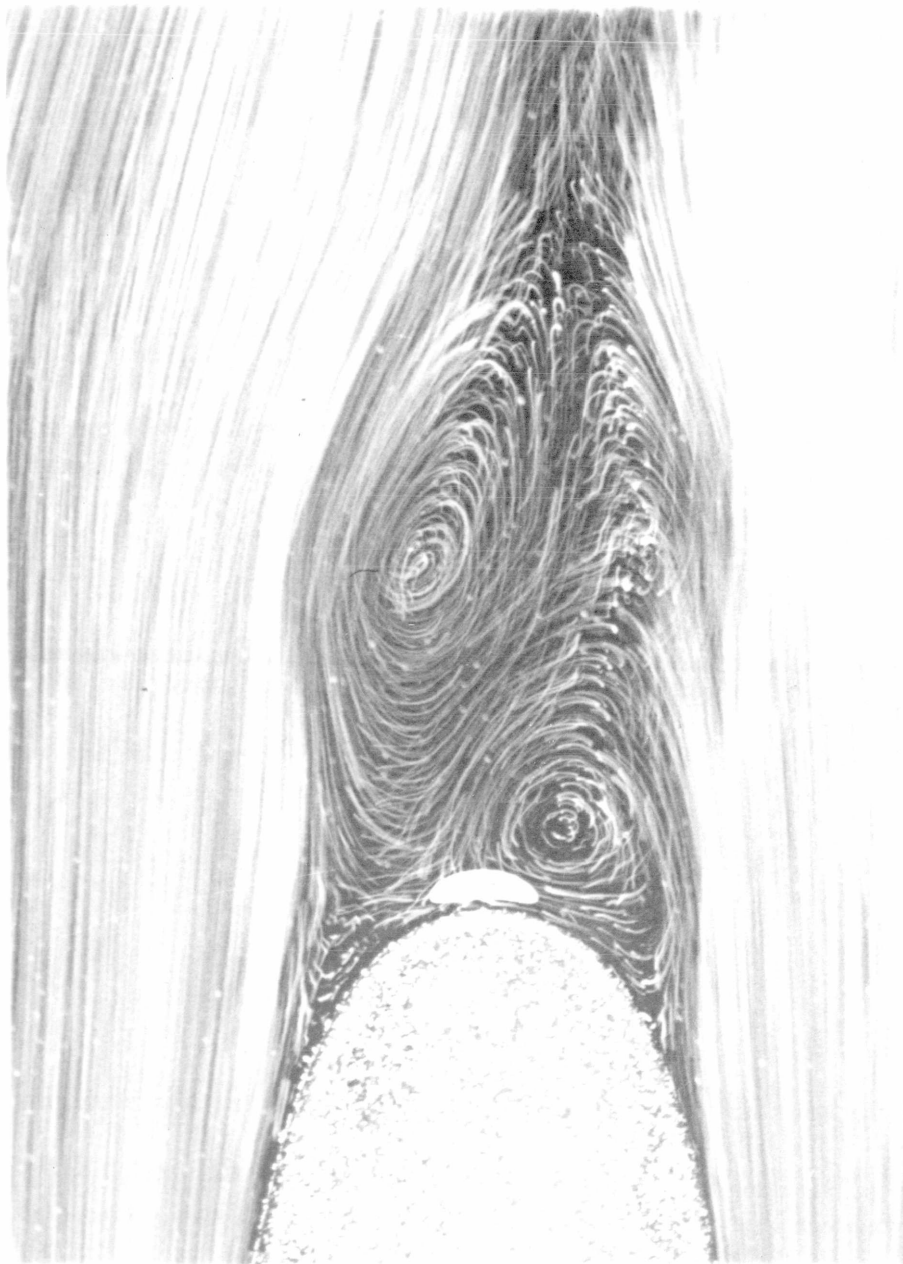


FIG. 7.3C."



From a closer study of the figure it will be seen that there are small eddies at the rear of each tube: these are seen in the enlargement, Figure 7.3C'. Also large eddies form behind each of the tubes of the last row; one of these is shown in Figure 7.3C". It is interesting to note that with the centre tubes of the group the eddies are extremely small, but behind the side tubes where the velocity is not constant, eddies of appreciable size have developed. The main stream passes round the tubes in a manner which conforms to the shape of the tubes. There is less loss of energy in the creation of eddies and it would be expected that the form drag on these tubes would be appreciably less than with groups A or B.

There are many practical considerations which preclude the use of elliptical tubes in heat exchangers and efforts have been made to approximate to the smooth flowing streamline conditions of group C, by arranging cylindrical tubes in staggered arrangement. Groups D, E and F (Figure 7.3) have been investigated. Group D is an open spacing with the diagonal distance between the tubes slightly greater than half the distance between adjoining tubes in any one row. Figure 7.3D is a photograph of the flow. Figure 7.3D' is another photograph with the same spacing. In this case lycopodium powder was sprinkled on the surface of the water

FIG. 7.3 D.



FIG. 7.3D'

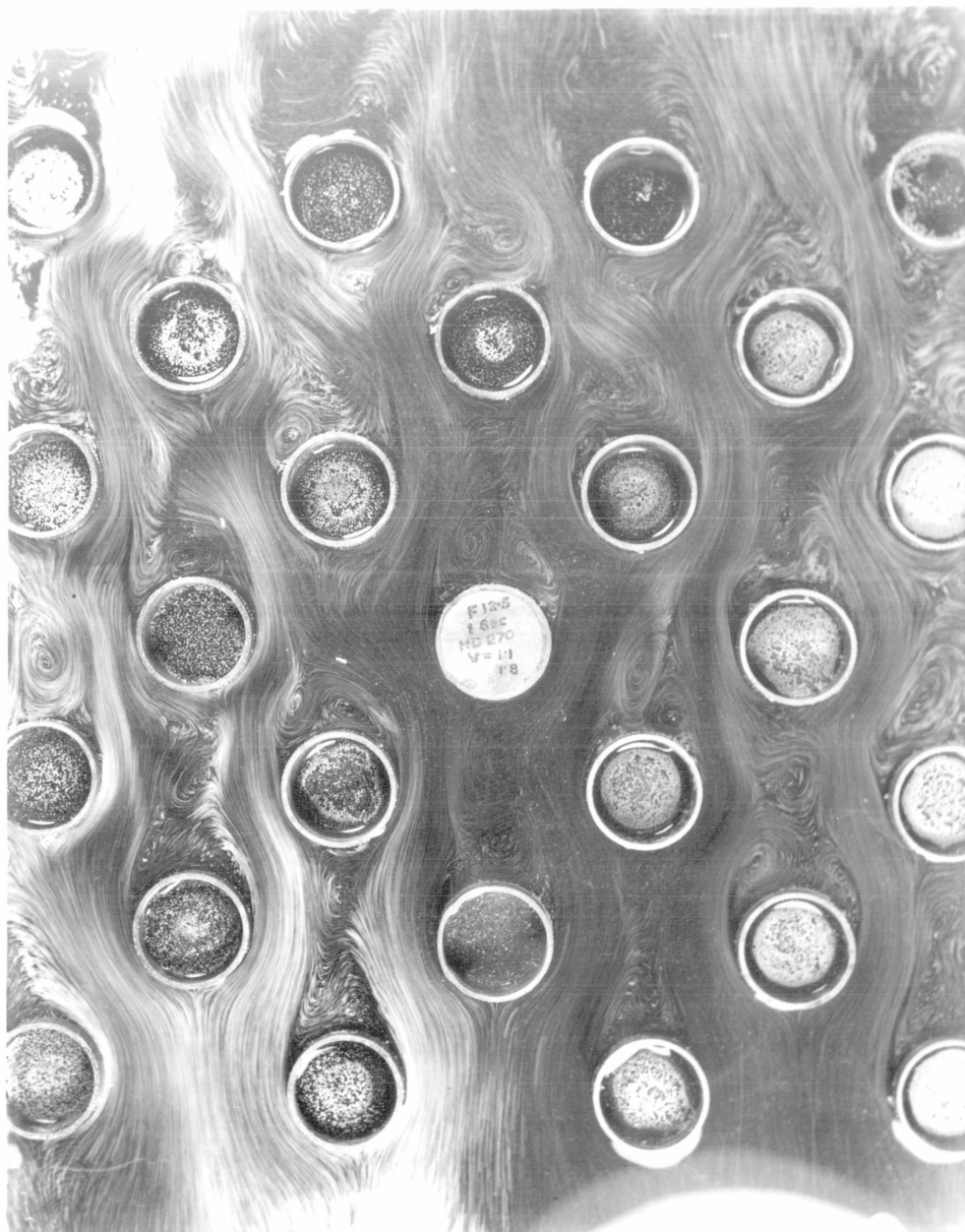
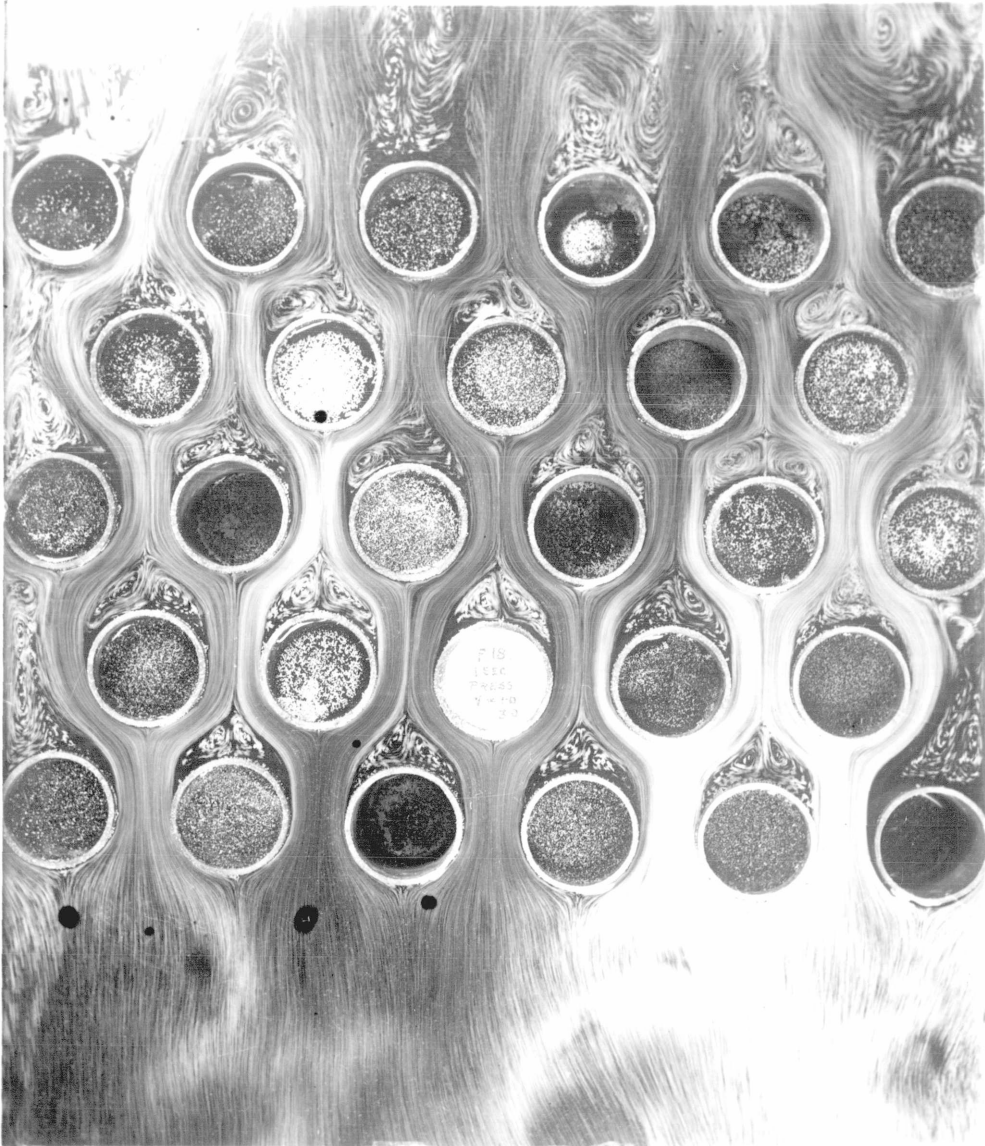


FIG. 7'3D".



FIG. 7'3E.



flowing between the right hand side tubes while aluminium dust was used on the left hand side. The lycopodium powder gave finer lines but the contrasts were not so distinct. The impression obtained was that this would prove a useful indicator for the examination of small areas where the camera was relatively close to the particular area, but was not as good as the aluminium dust for the investigation of the general flow pattern. With this spacing the eddies that are formed at the backs of the tubes pass down the main stream as complete eddies with less disintegration than in the cases of the parallel arrangement. This causes greater distortion of the main stream.

Figure 7.3D" shows an enlargement of one of the eddies as indicated with lycopodium powder. It is an excellent example of the theoretical Karman street.

Group E is the original staggered arrangement of the nest of tubes. It was with this arrangement that the asymmetrical difficulties were encountered when testing the first nest on water flow as described in Section 2. It was by removing the tubes of alternate rows of this staggered arrangement that the parallel arrangement Group B, Figure 7.3 was obtained.

Figure 7.3E shows the conditions of flow in this group.

FIG. 7'3F.



FIG. 7'4A.

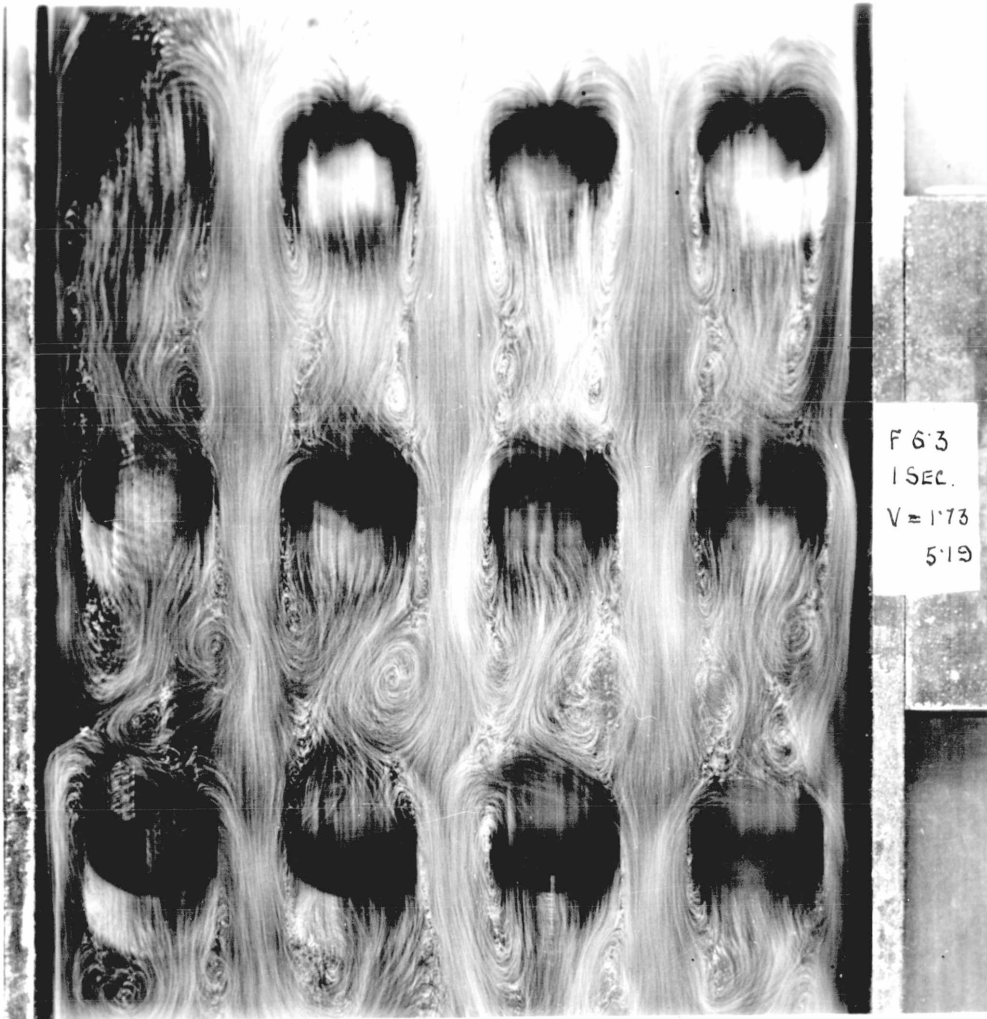
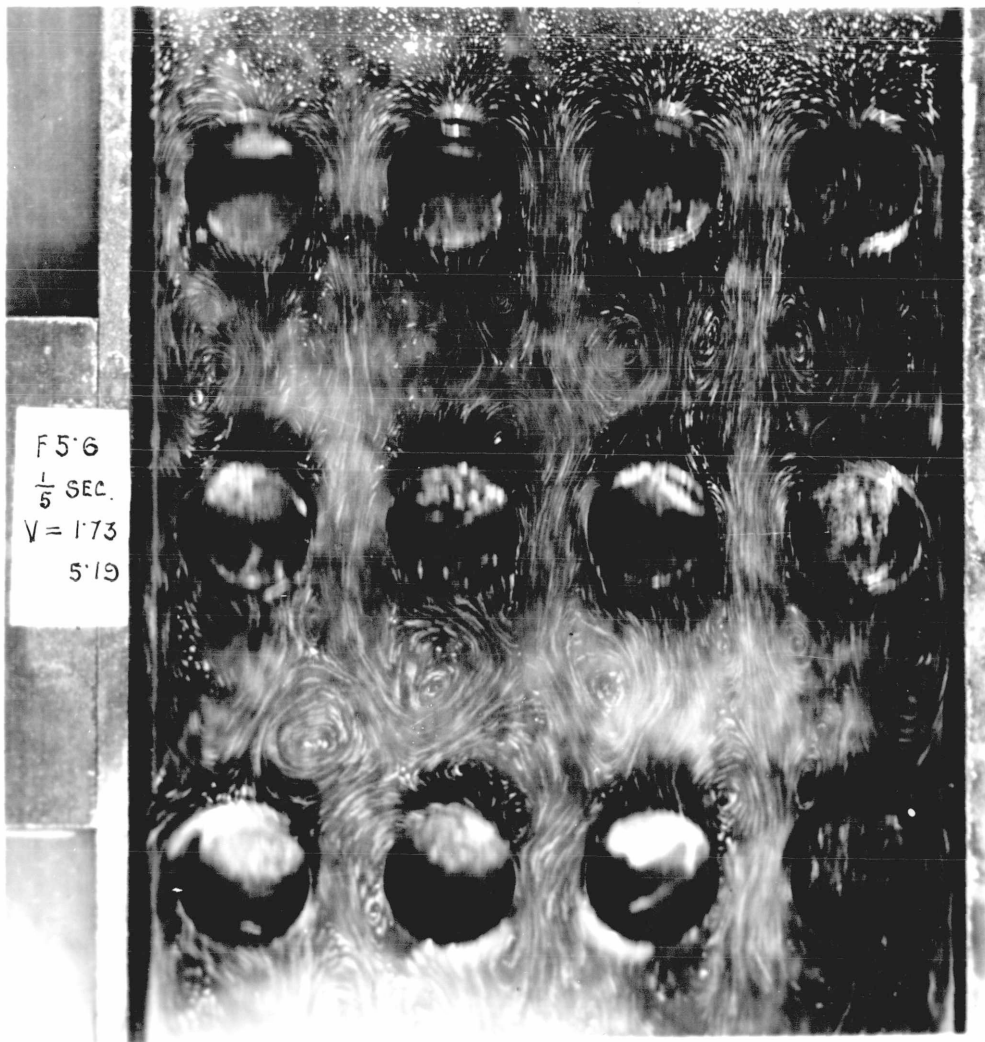


FIG. 7'4B.



It will be seen that since the diagonal distance between the tubes is equal to the distance between adjoining tubes of any row, and only half the quantity of water has to flow down the diagonal gaps, there is left an appreciable area at the back of each tube in which eddies can form.

Group F was an effort to overcome this condition by making the diagonal distance between the tubes half the transverse distance and thus keep the area at right angles to the flow approximately constant. From Figure 7.3F it will be seen that the eddy area is now reduced to a small triangle at the back of each tube.

7.4 Flow pattern as seen by observer moving relative to nest.

It was realised that all the previous photographs had been taken with a flowing stream and the camera fixed relative to the tubes. The impression obtained from these photographs was not the same as that obtained by visual observation. With direct vision the eye could follow an eddy as it left the back of a tube and floated downstream. This would appear as a rotating eddy, but a photograph with a stationary camera of this phenomenon would show a series of superimposed waves.

Two photographs, Figures 7.4A and B, were taken with the camera fixed and the nest of tubes was moved through the stationary water. The spacing of the group was similar to

Group B, Figure 7.3, but there were only three rows of four tubes each. The tubes were fixed to a brass sheet and all painted black in order to show up the motion of the aluminium particles on the surface of the water.

The osprey-like effect on the front of the first row of tubes is simply the effect of the relative motion of the tubes and the water. It is interesting to compare the photographs with the results of the motion of a sphere through a solution of glycerine as obtained by Williams.⁽¹⁾ In his experiments Williams rendered the flow visible by suspending tiny flakes of aluminium powder in the glycerine solution and illuminating the field of vision with a powerful beam of light. The same feather-like appearance at the head of the sphere was obtained.

In Figure 7.4A the early stages of the eddies in the bands of vorticity which are shed from the two sides of the cylinders can be clearly seen. Under normal conditions these eddies develop until they fill the whole of the space behind the cylinders, but it has been suggested by Relf and Simmons⁽²⁾ that at a Reynolds' number of 10^5 this changes to a dead water region which is fringed by small eddies.

(1) W.E.Williams. Phil.Mag. 1915. Vol. 29, p.526.

(2) E.F.Relf and L.F.G.Simmons. Phil. Mag. 1925. Vol.49, p.509.

FIG. 7'5.



It was thought that some further insight into the mechanism of the generation of eddies might be obtained by studying the velocity distribution in an eddy and the relative velocity of eddies between successive rows of tubes.

7.5 Analysis of individual eddies.

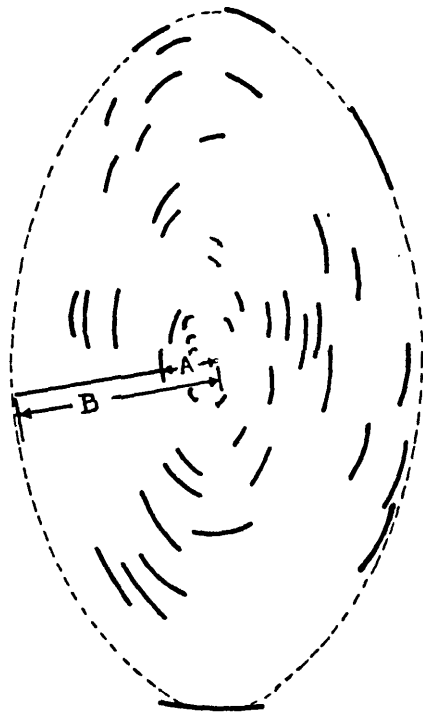
In a free vortex the velocity at any point is inversely proportional to the distance of that point from the centre of the vortex. From a casual observation of any of the "fine line" photographs it was seen that the velocity distribution in the eddies in groups of tubes did not conform to this law. Efforts were therefore made to analyse some of the individual eddies.

Figure 7.5 is an enlargement of a portion of Figure 7.3B' between the second and third rows of tubes. Both the large eddy A and the smaller eddy B were analysed. These are shown in Figures 7.5A and 7.5B. Separate enlargements of these eddies were made and pieces of cellophane were placed over the photographs. The paths of the various particles of aluminium dust were traced with indian ink on to the cellophane and these were transferred to tracing paper. The centre of the eddy was then determined and an ellipse was described around the eddy. A line was drawn from the centre of the eddy through the centre of the path of the particle to the circumference of the ellipse. The distance from the centre of the eddy

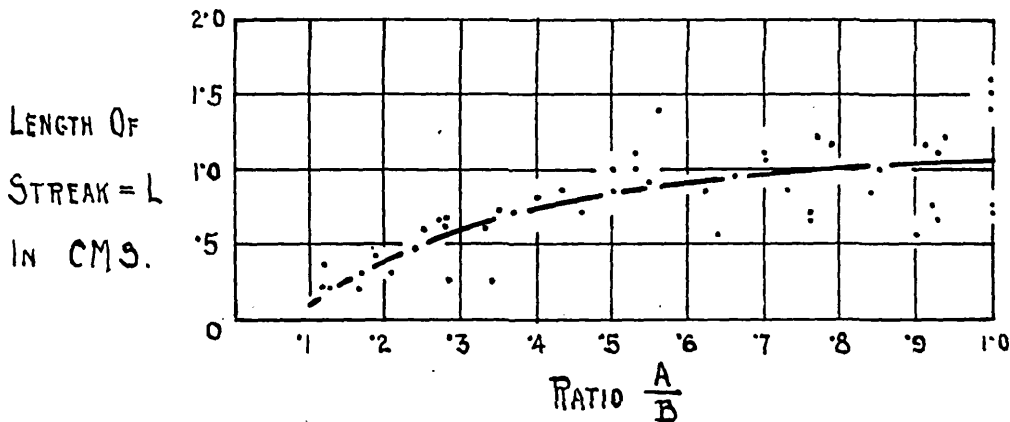
VELOCITY DISTRIBUTION IN EDDY "A" FROM FIG. 7.3B' FIG. 7.5A.

EXPOSURE 1 SECOND V_0 0.43 CM/SEC. $V_{N.MAX.} = 1.29$ CMS/SEC.

SCALE 1.64 FULL SIZE \therefore VELOCITY = $\frac{L}{1.64}$ IN CMS/SEC.



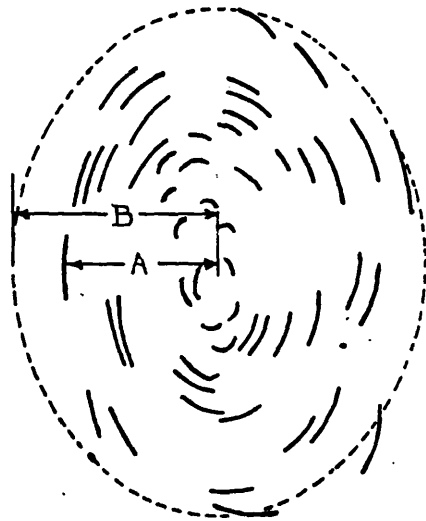
DIRECTION OF
MAIN STREAM



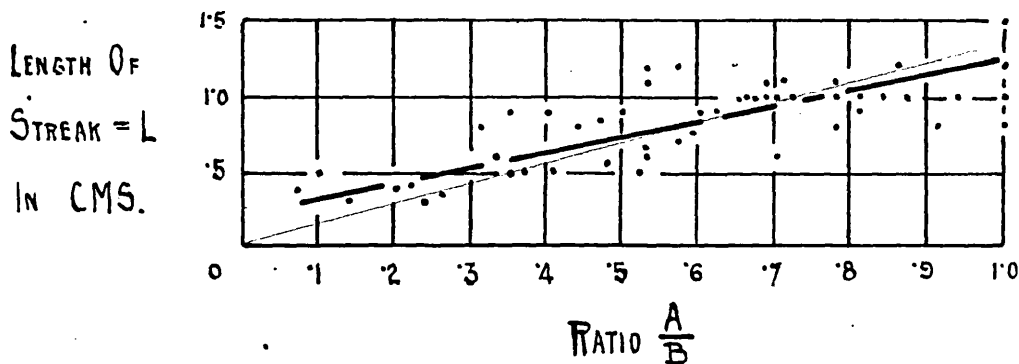
VELOCITY DISTRIBUTION IN EDDY "B" FROM FIG. 7.3B' FIG. 7.5B.

EXPOSURE 1 SECOND $V_0 = 0.43 \text{ CM/SEC.}$ $V_{N.MAX.} = 1.29 \text{ CM/SEC.}$

SCALE 1.64 FULL SIZE $\therefore \text{VELOCITY} = \frac{L}{1.64} \text{ IN CM/SEC.}$



DIRECTION OF
MAIN STREAM



along this line to the path of the particle is denoted by A and the distance from the centre to the circumference by B. The velocity of the particle was measured directly from the photograph and this length was plotted against the ratio A/B.

Tables 7.5A and B give the data from which the corresponding curves are plotted. In each case the points are scattered over a fairly wide band, but it has been possible to draw an approximate mean line. From these two lines (Figures 7.5A and B) it is seen that the velocity increases from the centre to the periphery of the eddy, but the two curves do not appear to indicate the same relation of velocity with distance from the centre. The results are in general agreement with the conclusions of Williams⁽¹⁾, who states that "In the eddies the central part of the liquid moves more or less as a solid body, the velocity diminishing towards the centre of the eddy where there is always a point of zero velocity."

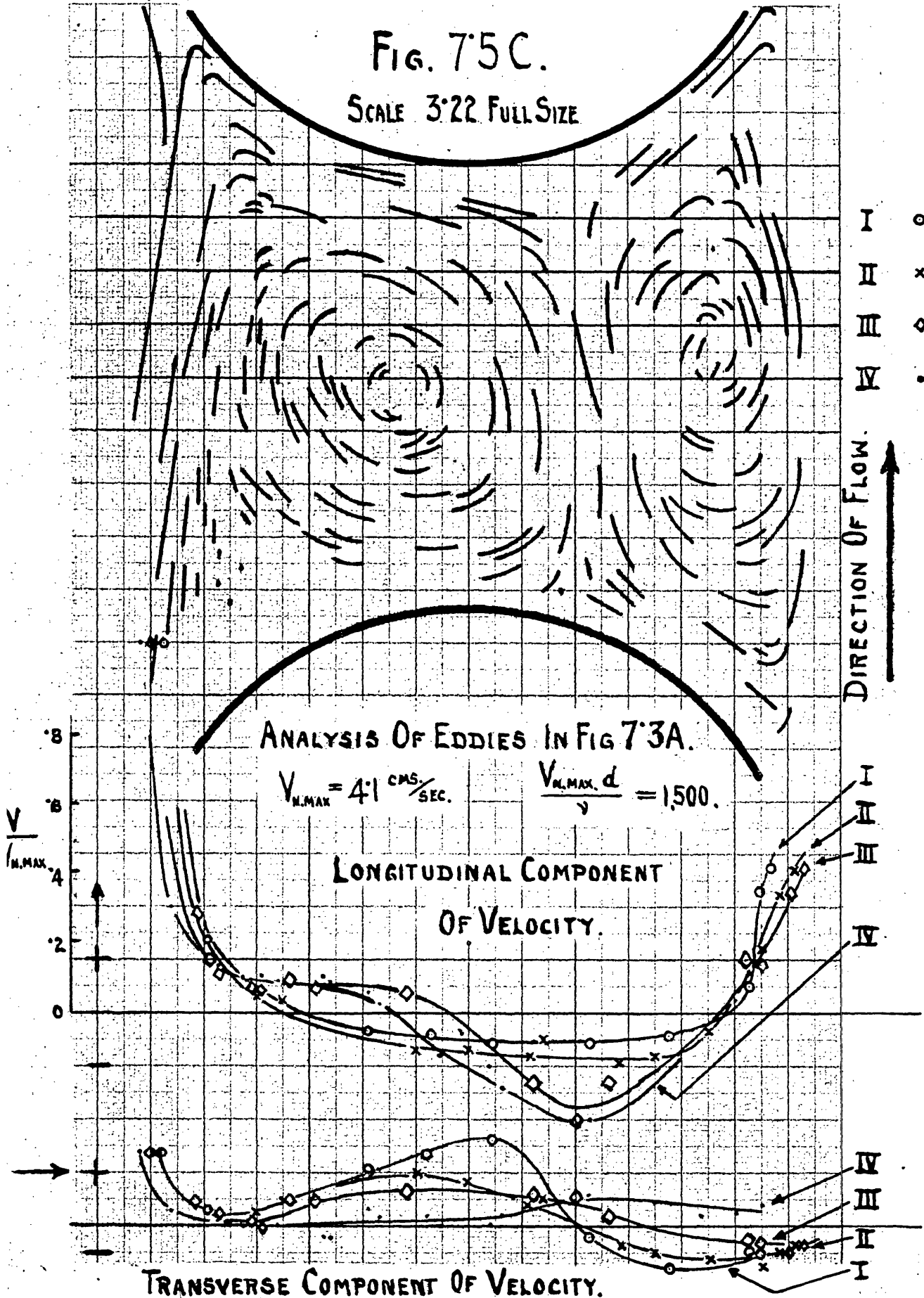
Following the method used by Nisi and Porter⁽²⁾ for the analysis of eddies behind spheres and cylinders at low Reynolds' numbers, the longitudinal and transverse components

(1) W.E. Williams. Phil. Mag., 1915. Vol. 29, p. 526.

(2) Nisi and Porter. Phil. Mag., 1923. Vol. 46, p. 754.

FIG. 75C.

SCALE 3:22 FULL SIZE



of the streaks of aluminium dust were plotted separately.

Figure 7.5C shows the eddies between tubes in the second and third row of Figure 7.3A. The longitudinal and transverse components of the streaks crossing lines I, II, III and IV are shown below. Bearing in mind that in Nisi and Porter's experiments on the isolated cylinder the Reynolds' number was 11.6 and the eddies at the back of the cylinder were stationary and symmetrical, whereas in the present experiments $\frac{V_N \cdot \max d}{\nu}$ was 1,500 and the eddies were asymmetrical, the curves are of very similar form to those of Nisi and Porter.

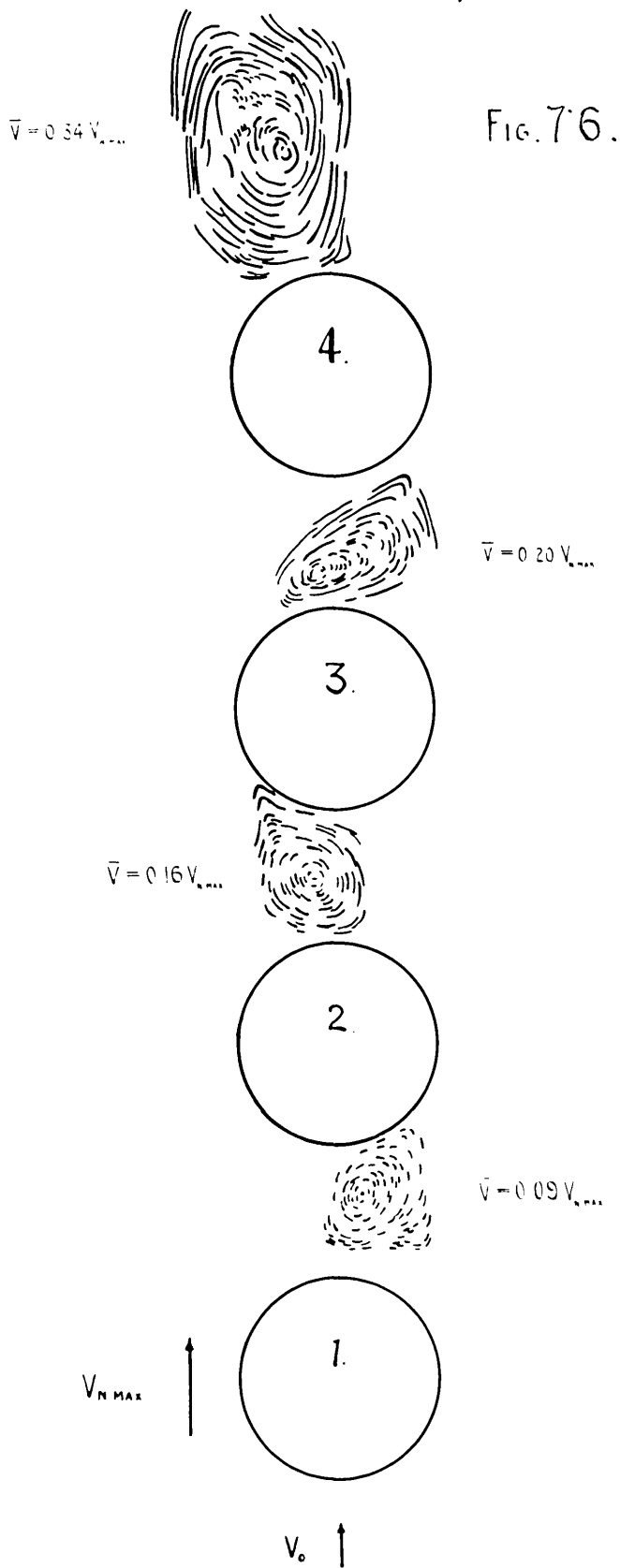
7.6 Determination of the velocity in eddies between successive rows of tubes.

From inspections of numerous photographs the opinion was formed that in general it could be said that the velocity of the eddies at the back of the first row of tubes was not as great as that in the eddies between the second and third rows of tubes. In many photographs there was a successive increase of the velocity in the larger eddy from the first to the last row of tubes. This was most marked in the parallel arrangements, but was also noticed to a lesser degree with the staggered arrangements with open spacing.

It was appreciated that the velocity in any eddy depended upon the length of time the eddy had been in existence and so the analysis of any series of eddies would depend upon the

VELOCITY IN EDDIES BETWEEN SUCCESSIVE ROWS OF TUBES

$$\frac{V_{max} d}{\nu} = 1,500$$



particular instant when the photographic exposure was made. Some idea of the relative increase in velocity in the eddies might be obtained by selecting a typical series of eddies and obtaining the average velocity in each.

For the purpose, Figure 7.3A was again used and the velocities of the streaks in the major eddies are reproduced in Figure 7.6. The length of the arrow below the first tube indicates the initial velocity of the stream and the arrow on the left $V_{N,max} = 4.115$ Cms, per second.

The average velocity in the eddy at the back of the first tube $V_1 = 0.374$ Cm. per second:

$$\frac{V_1}{V_{N,max}} = \frac{0.374}{4.115} = 0.091$$

Average velocity in eddy between tubes No. 2 and No. 3

$V_2 = 0.674$ Cm. per second:

$$\frac{V_2}{V_{N,max}} = \frac{0.674}{4.115} = 0.164$$

Average velocity in eddy between tubes No. 3 and No. 4

$V_3 = 0.825$ Cm. per second:

$$\frac{V_3}{V_{N,max}} = \frac{0.825}{4.115} = 0.200$$

Average velocity in eddy behind No. 4 tube

$$V_4 = 1.404 \text{ Cms. per second:}$$

$$\frac{V_4}{V_{N.\max}} = \frac{1.404}{4.115} = 0.341$$

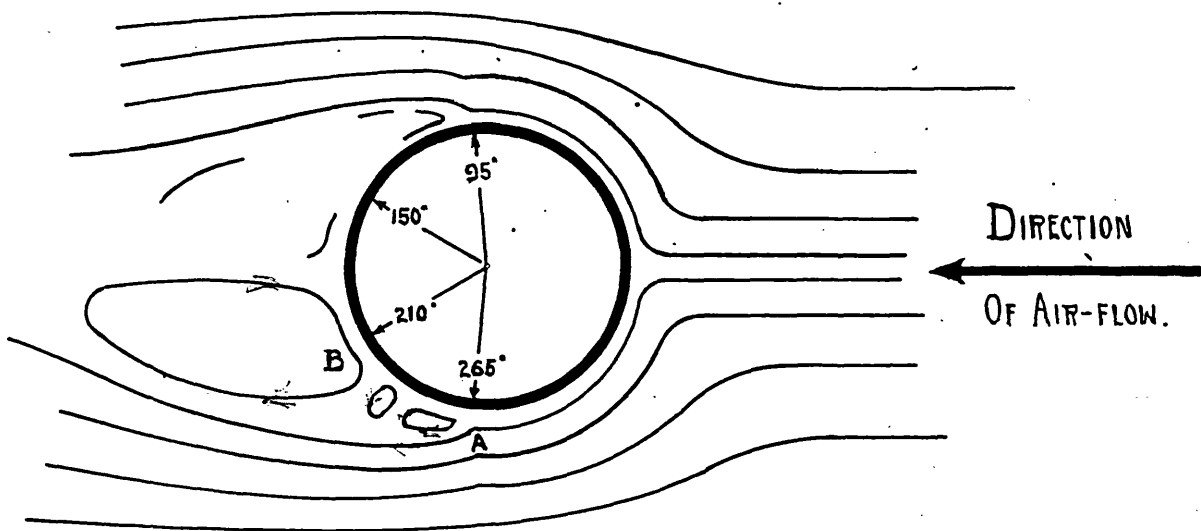
While the above figures give an idea of the relative eddy velocities, they should be considered as typical and it must be remembered that these figures will change from instant to instant.

7.7 Diffusion from the surface of a cylinder.

In section 5.7 it has been shown that the tangential drag or skin friction contributes only a small amount to the resultant total pressure loss through the nest. It has been possible in Section 8.84 to compute the skin friction on the upstream faces of the tubes, basing the calculation on the form drag curves. The value so determined is in excess of the total effective skin friction, thus showing that skin friction in the opposite direction exists at the rear of the tubes. The measurements of total drag and form drag are not sufficiently precise to enable estimation of the rear portion of the skin friction. Nor are the variations in pressure as indicated on the rear half of the form drag diagrams sufficiently large to permit of satisfactory calculation on the lines adopted for the upstream face.

EDDY MOTION AT THE REAR OF THE TUBES.

FIG. 7-7A.

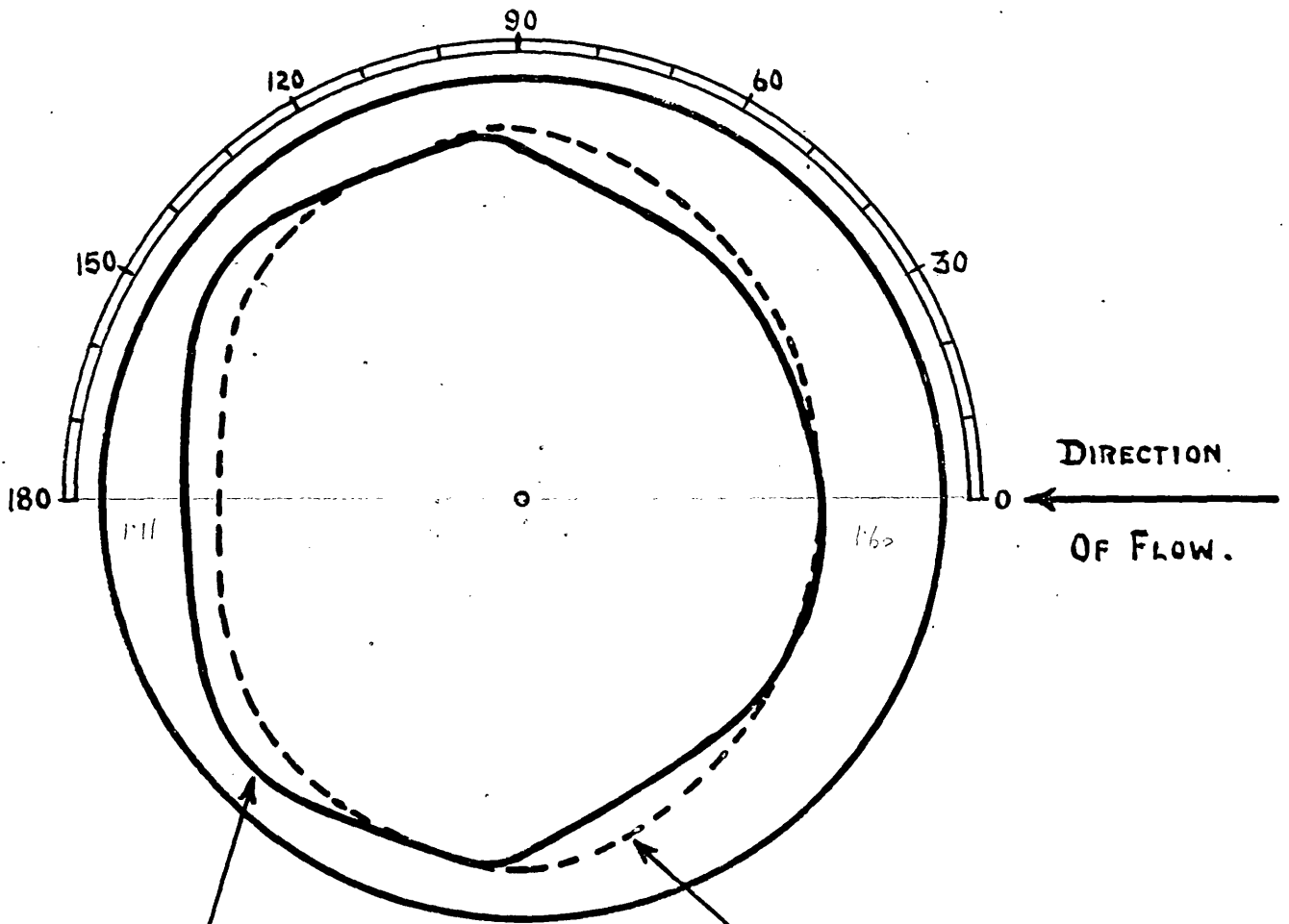


The type of motion at the rear has been demonstrated by the Ahlborn method. The velocities involved are not sufficient to cause large pressure differences. Nevertheless their influence on the form drag curves is noticeable in Figures 5.2E and 5.4B. This is particularly noticeable on the last row (Figure 5.2E) where the eddy speeds are greater than on the forward rows. The two points of relatively low pressure at angles of 150° and 120° ^{210°} seem consistent with the view that at these points the outer filaments of the eddy move in paths convex towards the eddy centre, as shown in Figure 7.7A. It should be noted that this conception suggests the existence of two distinct points of breakaway. These points may be separated by as much as 40° or 50° , the intervening space being occupied by a pair of much smaller and elongated eddies or by a triangle of relatively stationary fluid. The skin friction in this region must be very small. An interesting sidelight was thrown on this subject by a diffusion experiment in which a stick of shaving soap was used as an isolated cylinder in a stream of water.

The mechanism of the diffusion of a soluble substance in a moving stream is the same as that of heat transfer, and Reynolds' analogy with respect to the corresponding nature of skin friction and heat transfer applies also to diffusion. It should therefore be expected that the amount of soap

DIFFUSION & HEAT TRANSFER

FIG. 7.7B.



SHAVING SOAP

$$\frac{Vd}{\nu} = 2,800.$$

HEAT TRANSFER

PALTZ & STARR

$$\frac{Vd}{\nu} = 39,600.$$

dissolved from the various parts of the shaving stick should give a fair qualitative indication of the magnitude both of skin friction and heat transfer. The full line in Figure 7.7B gives the cross section of the shaving stick after this had been exposed for 39 minutes in a stream of water at 15°C . and 11.1 Cms. per second.

It will be seen that the greatest effect occurred at the upstream generator, reducing gradually to a first minimum at 95° . At this point breakaway no doubt occurred. From 95° to 140° there was considerably less effect. This corresponds to the region AB in Figure 7.7A. From 140° onwards the effect increases again, becoming a maximum at 180° . There are two main stagnation points, one at 0° and the other at 180° , both with high skin friction and high heat transfer, and two main points of breakaway at 95° and 265° and two secondary points of breakaway at 140° and 220° . The points of breakaway are associated with minimum skin friction and minimum heat transfer. The skin friction changes in sign and even though the instantaneous zero point fluctuates, nevertheless the time average does exhibit a zero value. The heat transfer and diffusion are always positive in sign and in the case of a fluctuating point of breakaway give a minimum and not a zero value. This is an example of a deviation from the conditions necessary for a complete

analogy between skin friction and heat transfer or diffusion.

The result of the soap experiment is compared with the actual heat transfer measurements by Paltz and Starr⁽¹⁾, whose results are shown by the dotted line in Figure 7.7B. The shape of the curve is very similar, particularly when it is remembered that the heat transfer experiment was at a Reynolds' number of 39,600, whereas the shaving soap experiment was at $Re = 2,800$ and Lohrisch⁽²⁾ by ammonia diffusion experiments had shown that the diffusion at the rear of a cylinder increased more rapidly than that at the front with increasing Reynolds' number. It was appreciated that in these experiments the dissolving surface of the shaving stick did not remain a true circular cylinder, whereas in the case of heat transfer the metal tubes would retain their original form. The result was sufficiently good to suggest that this method could be used for indicating the relative heat transfer of a particular tube in various positions in a nest of tubes. The method could also be used for the investigation of heat transfer from bodies where it is known that the flow is of a three dimensional character and where the Ahlborn tank could not be used to indicate the flow pattern. It might be of particular use

(1) Vide Drew and Ryan. Amer. Inst. Chem. Eng. 1931. Vol.26, p.118.

(2) W.Lohrisch. Forschungsarbeiten. No. 322, p.46.

EFFECT OF TUBE SPACING ON EDDY FORMATION FIG. 7.8.

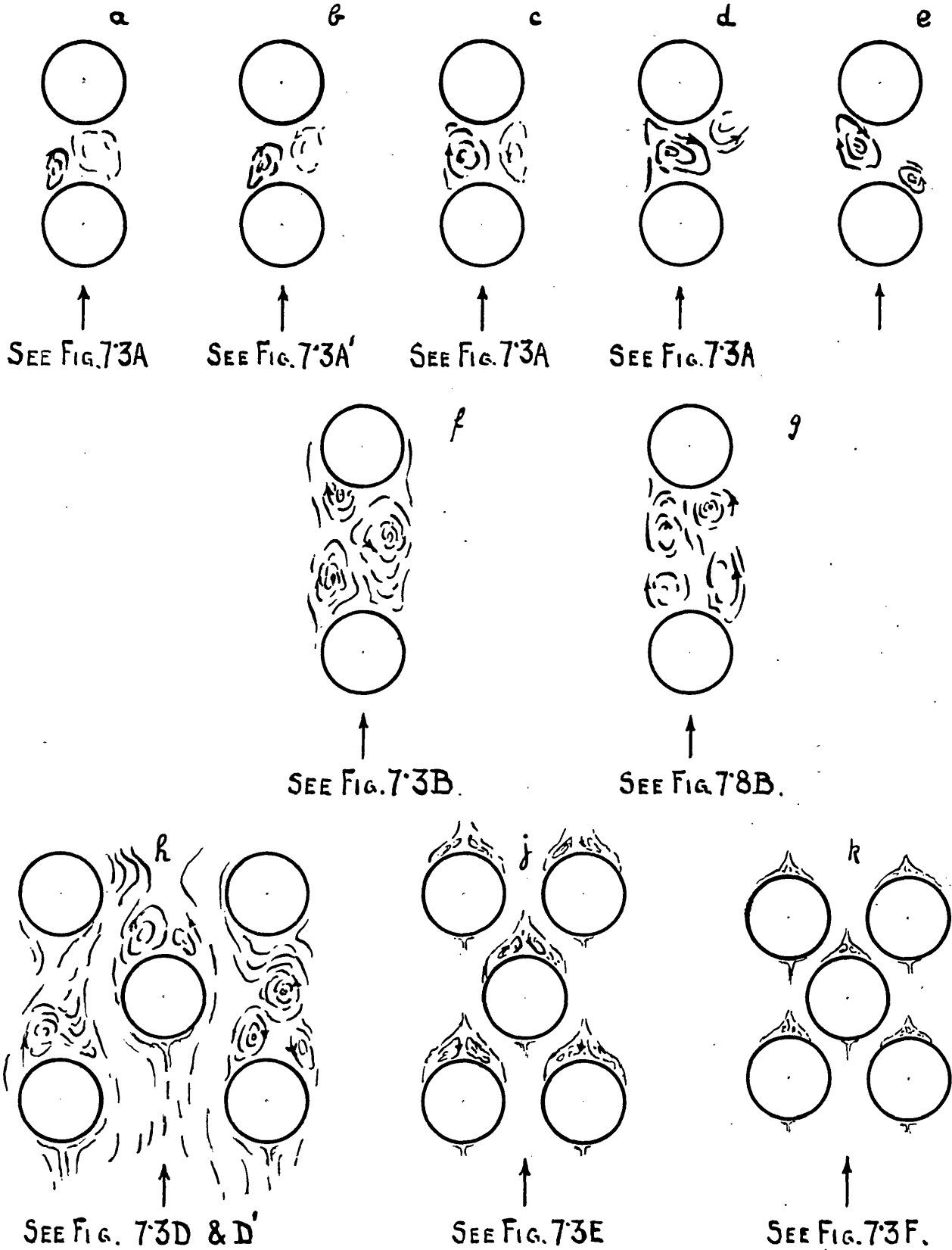


FIG. 7·8B.

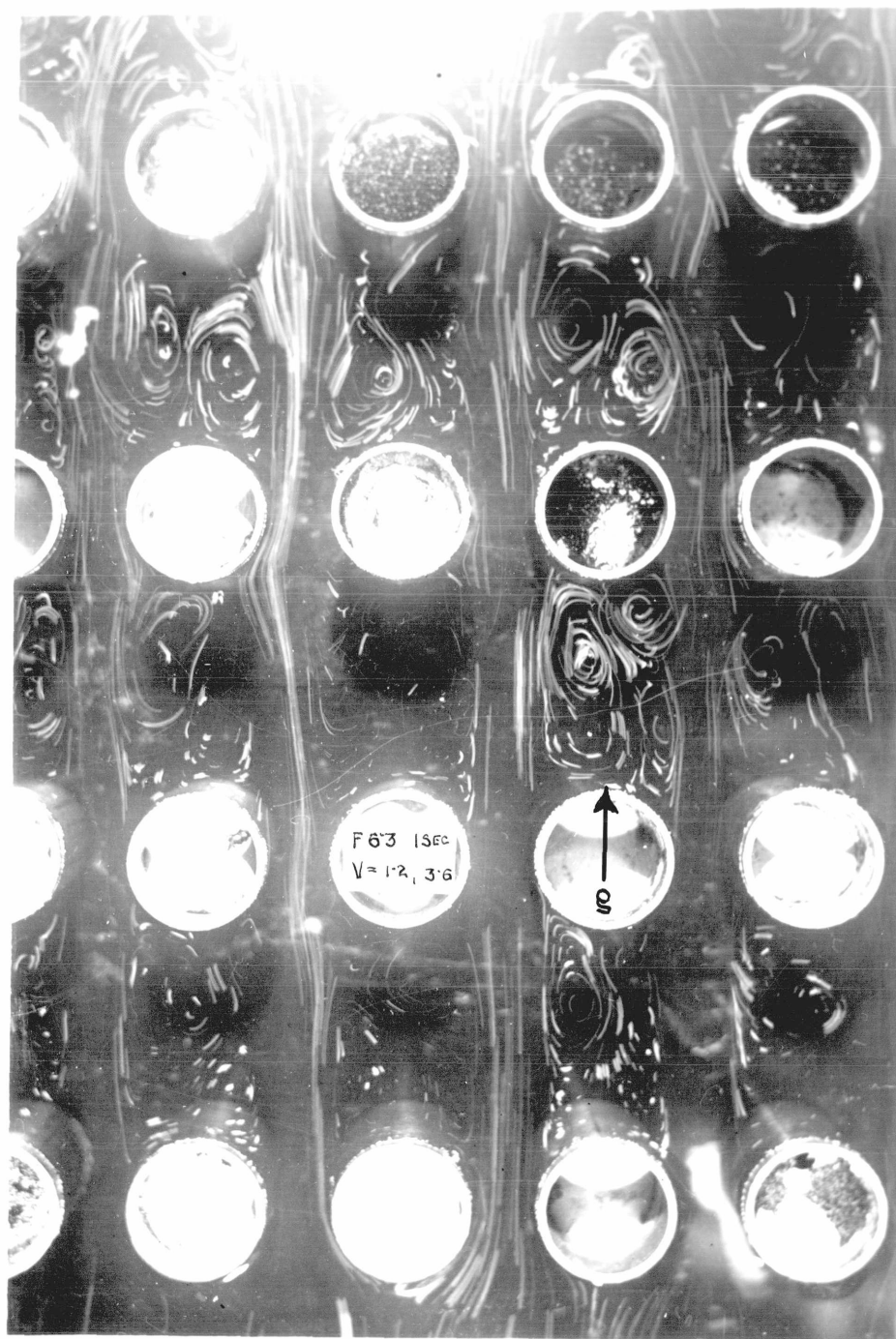


FIG. 7·8A.



in investigation of the relative heat transfer from various portions of the surface of gilled tubes, either individually or in nests.

7.8 General conclusions of the effect of longitudinal and transverse spacing on the flow pattern.

From the various experiments in the Ahlborn tank several general impressions were obtained with regard to the formation of eddies and the general flow pattern.

Whether eddies are formed or not depends mainly upon the shape and spacing of the tubes. If there are no abrupt changes of direction of the stream and the cross-sectional flow area remains constant, few eddies will be formed and these will occupy very small areas. If, on the other hand, the cross-sectional area increases abruptly, the the reverse pressure gradients exceed that value at which reverse flow occurs at the wall and separation is inevitable. Eddies are formed and their size is governed by the space available.

After separation or breakaway the main stream does not change much in size and if the walls curve away then the conditions are ideal for the formation of a pocket of dead water. The main stream passing beside such dead water entrains some of it and so loses energy while generating a swirl within the dead water. The first stage is the

generation of small eddies adjacent to the main stream.

These eddies increase in size and tends to move slowly down-stream. (See Figure 7.8b and 7.3A' eddy marked "b".) This process is continued as in Figure 7.8 c and d. The velocity of rotation of an eddy appears to increase to a maximum and then decrease as the amount of fluid incorporated in the eddy increases. In some cases an eddy becomes so large that it forces the preceding eddy on the opposite side out into the stream, as is illustrated in "d", Figure 7.8, but more usually it seemed as if the velocity died down and a moment or two later the same fluid was used in the formation of another eddy. Eventually this fluid finds its way into the main stream. This is evidenced by the somewhat slow dispersal of aluminium dust from the dead water region when further aluminium dust is not sprinkled on the oncoming stream.

It was noticeable that the fluid behind the first row of tubes changed more slowly than that behind the second and subsequent rows.

As the first eddy dies down a new eddy is formed at the other side of the tube, as in Figure "e". This passes through a similar life history. With reasonably close transverse pitching the eddies appear to be dissipated and not to pass down the stream as individual eddies.

The number of eddies present at any one time depends upon the length to breadth ratio of the dead water region, i.e. upon the longitudinal spacing. With grouping A, Figure 7.3, the length/breadth ratio is 0.6 and more than two eddies are rarely present. With the grouping B, Figure 7.3, the length/breadth ratio is 1.6 and as will be seen in Figs. 7.8 f and 7.3B, there are usually three large eddies present. A group of four distinct eddies is evident in Fig. 7.8B and these are redrawn in 7.8 g but this appears to be the maximum number under these conditions with this spacing.

Alteration to the transverse spacing affects the ratio of $\frac{VN_{.max}}{V_o}$, and since all eddy formation is determined by the velocity in the gaps, it is thereby affected by the transverse pitch.

An open transverse spacing as well as reducing the gap velocity gives a wider main stream and it is easier for eddies to be pushed out from the dead water region into this stream. This is most marked in the staggered arrangements, Groups D, E and F, Figure 7.3. With D, the most open spacing, eddies are seen floating down the stream and as many as three individual eddies can be seen at the back of one tube (See Figure 7.3D' and D"). This is illustrated in Figure 7.8 h.

With the closer spacing, 7.3 Group E, two distinct eddies are formed and the associated dead water area has a well defined shape. The proportion of the total time in which eddies are being dissipated into the stream or passed down the stream is small compared with that in the open spacing 7.8 h.

With the closest spacing of staggered tubes (Figure 7.3, Group F) only a small triangular area of dead water is seen. Little energy is spent in the formation and dissipation of eddies. The main stream and boundary layer occupy practically the whole of the flow area. This is illustrated in 7.8 k.

From a comparison of Figures 7.8 "h", "j" and "k" it will be seen that any efforts to streamline tubes in a nest must take into consideration the longitudinal and transverse spacing as well as the diameter of the tube and the velocity of the stream.

7.9 The formation and dissipation of eddies.

7.91 Formation of eddies.

There is little doubt that the cause of the formation of eddies in a nest of tubes is the same as that at the rear of a single cylinder in a wind stream. Due to the loss of energy within the boundary layer the stream cannot follow round the rear half of the tubes but separates from their walls in the

vicinity of 90° , passing down stream on either side of a dead water region at the rear of the tube. Two bands of high vorticity originating in the boundary layer separate the freely moving stream from a region of low pressure dead water at the back of the tubes. At some distance behind the tubes these vortex sheets break up into discrete cylindrical vortices of opposite direction of rotation.

In the case of a single cylinder⁽¹⁾ the two vortex sheets break up with uniform frequency and the two trails of discrete vortices arrange themselves alternately in a Karman street.

It will be seen that while the fundamental cause of generation of the eddies in a nest is the same as that in the case of a single cylinder, the effect of adjacent tubes on one another and of the successive rows of tubes is to distort the regular flow pattern and to interfere with the natural periodicity of the shedding of the vortices.

7.92 Dissipation of eddies.

Taylor⁽²⁾ has pointed out that "the two main causes of dissipation of eddies are (a) the action of viscosity between

(1) Fage and Johansen. Phil. Mag. 1928. Vol. 5, p. 417

(2) G.I. Taylor. R & M. 589. 1918-19. Vol. 1, p. 73.

rings of fluid rotating with different angular velocities and (b) forces due to dynamical causes which tend to reduce the tangential velocity of the fluid in the eddy. A possible cause of this kind would be a flow inwards from the ends of the eddy towards the middle down the axis of the eddy. This flow would allow the radius of the rotating part to increase, and at the same time the velocity would necessarily decrease in order to keep the angular momentum constant. The action, in fact, would be the opposite of that in a sink, e.g. the waste hole in a bath where the taking away of fluid from the middle decreases the radii of the rotating rings of fluid and consequently increases their angular velocity".

The theoretical aspect of the decay of eddies due to cause (a), the action of viscosity, has been worked out by Taylor. This work was extended by Webb⁽¹⁾ to cover the effect of both causes (a) and (b). While these causes are sufficient to explain the dissipation of eddies in the centre of a body of fluid, in the case of nests of tubes there is the additional friction between the tube surfaces and periphery of the eddy.

With close spacing, the majority of the eddies decay in the dead water region as mentioned in Section 7.8. With open spacing the eddies are carried into the main stream and are dissipated in the general wake of the nest.

(1) H.A.Webb. R. & M. 609. 1919.

Whenever a turbulent stream passes through a constriction the effect of the convergence is to damp out the initial velocity fluctuations. The result of this damping effect is not equal in the longitudinal and transverse direction. Simmons, Fage and Townend⁽¹⁾ investigated this effect in a pipe whose convergence was practically the same as that between the transverse pitch and the gap in the present nest. They discovered that the effect of convergence was to reduce longitudinal velocity fluctuations to about one-fifth of their initial value, but the reduction in transverse fluctuations was not so great. In any nest of tubes this damping effect will be largely influenced by the transverse pitch to gap ratio. The longitudinal damping being greater than the lateral damping, offers an explanation of the readiness of the stream to "flick over" into the dead water regions.

(1) The staff of the Aerodynamical Dept. of the N.P.L.

FLOW IN NESTS

OF

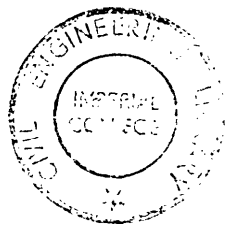
TUBES.

VOL. II.

R. Pendennis Wallis, M.Sc.,

King's College,

London.



October 1937.

8. EXPERIMENTS WITH THE ELECTRIC TRAY

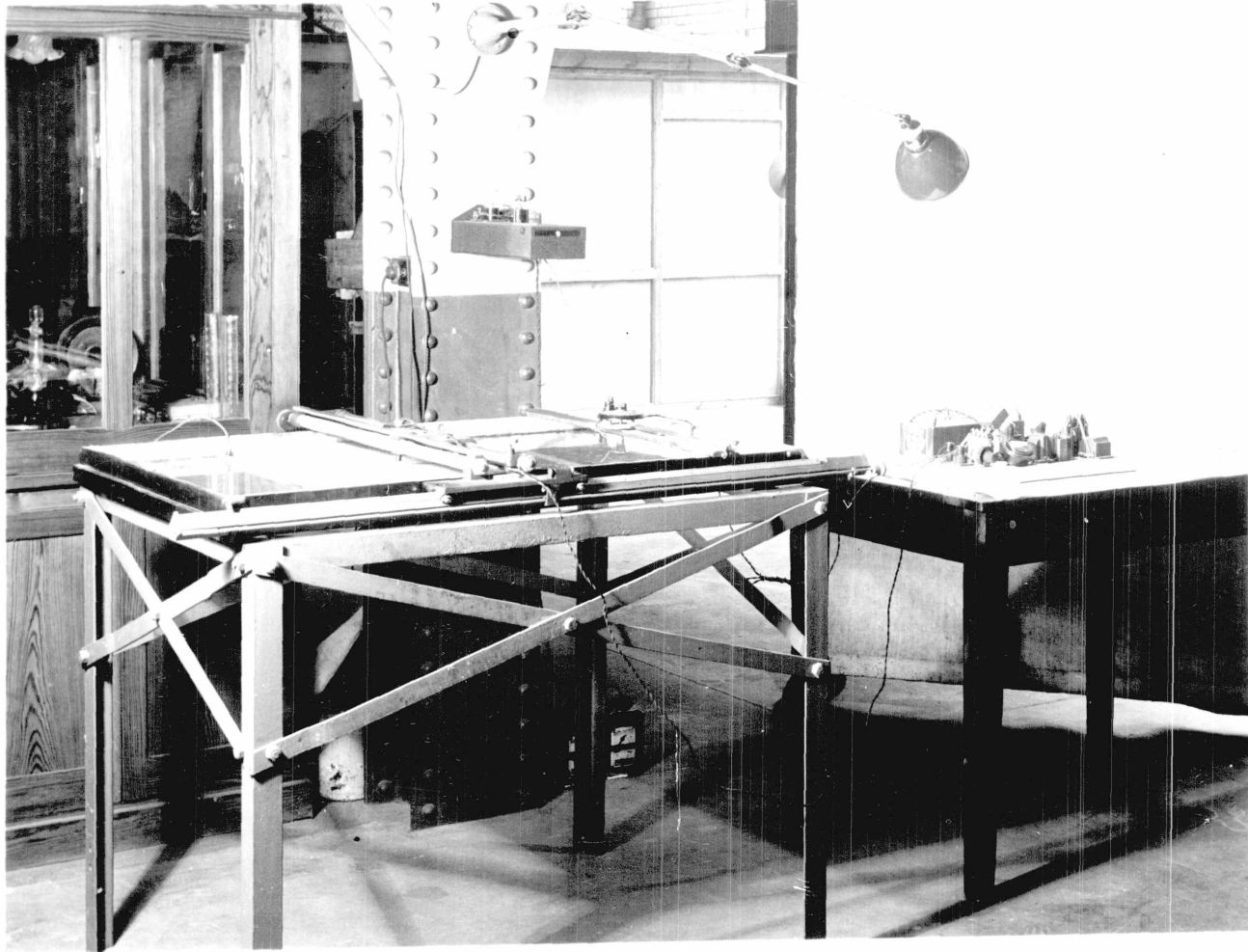
8.1 Analogy between frictionless fluid flow and electric flow

Mathematical solutions of fluid motion past fixed boundaries can be obtained but in the main they involve tedious and difficult computations. An alternative method for determining flow patterns was used by Relf⁽¹⁾ who showed that simple electrical measurements on a suitable model could provide the information normally obtained by analytical treatment.

The equations of motion of a frictionless fluid are analogous to those of electric flow in a conducting medium. In this analogy lines of electric flow correspond to stream lines; lines of constant electric potential correspond to velocity potential lines in the fluid case; current density corresponds to velocity, provided that boundary conditions are satisfied. The analogy requires that solid surfaces in the fluid case shall be represented by surfaces of infinite electrical resistance, i.e. by perfect insulators.

Such experiments, were carried out to determine the velocity distribution for a row of cylinders of similar spacing to that used in the nest of tubes.

(1) E.F.Relf, R & M, 905, 1924.



8.2 Description of apparatus.

Figure 8.2 shows the electrical model. The tubes were represented by discs of paraffin wax 25.4 Cms. diameter. These were placed in a shallow level glass tray 122 Cms. long by 76.2 Cms wide. The tray was filled to an approximate depth of 1.5 Cms. with acidulated copper sulphate solution to act as conductor. The current was supplied to the ends of the tray through copper strips extending the full width of the tray.

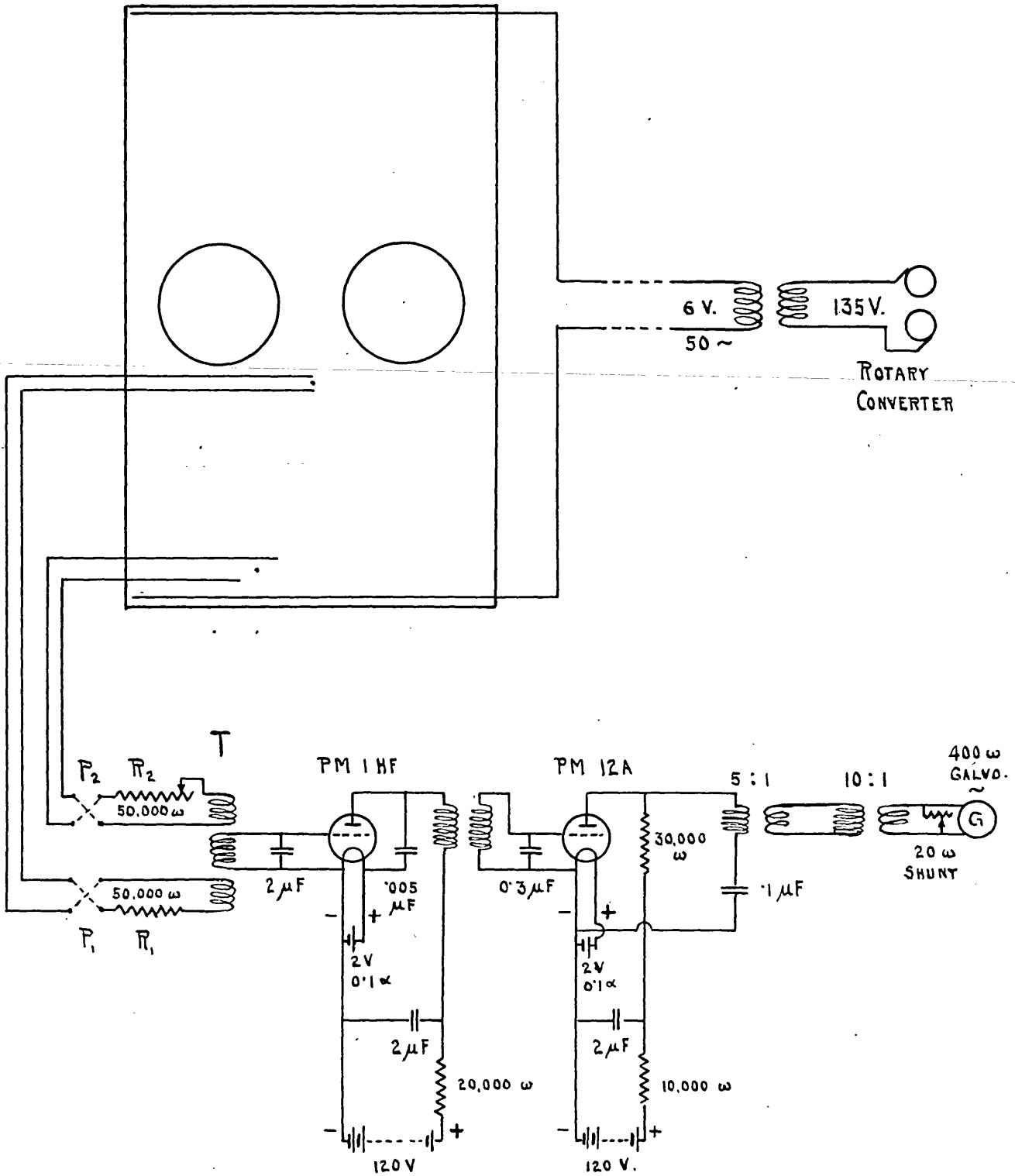
With such an arrangement the current density at any point in the electrolyte is proportional to the velocity of an inviscid fluid flowing through a similar row of tubes. The current density cannot be measured directly and so use is made of the fact that current density is proportional to electrical potential gradient. This potential gradient was measured by inserting a pair of vertical parallel copper pins at any desired point in the electrolyte. In order to approximate to values at a point the spacing between the pins was made small (approximately 0.6 Cm.).

The pins could be rotated about a vertical axis so permitting them to be orientated into the stream lines.

To avoid polarisation effects alternating current (50 cycles per second) was used. Voltages from 2 to 135 were

ELECTRIC TRAY CIRCUIT

FIG. 8·2 A.



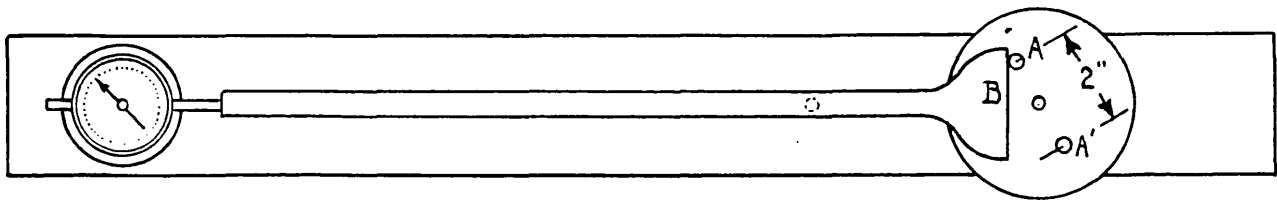
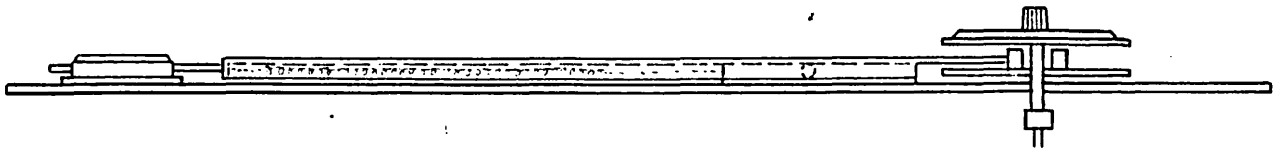
tried but finally 6 volts was selected as the best compromise between the requirements of a simple measuring circuit on the one hand and avoidance of stray capacity currents on the other. The search pin was supported on graduated slides giving two motions at right angles and enabling direct readings to be taken of rectangular co-ordinates.

The potential differences to be measured were small, being of the order of 0.025 volts A.C. It was important that the resistance of the measuring circuit should be very high in order to avoid the abstraction of appreciable currents from the field. It was decided that anything less than 50,000 ohms in series with the pins would distort the field to a measurable degree. With this resistance the currents to be measured were of the order of 0.5 micro-amperes and in order to obtain 1% accuracy it was necessary to be able to detect 0.005 micro-ampere. It was desirable that readings of potential differences should be given directly and that the method should be speedy in use.

The circuit shown in figure 8.2 A was developed to meet these requirements. It is essentially a null method in which the potential picked up by the search pins is balanced against that picked up by a second pair of pins placed in the electrolyte at a point where the field was known.

MECHANISM FOR READING DIRECTLY THE SINE OF
THE ANGLE OF ROTATION

FIG 8.2B.



Balance was obtained by rotating the second pair of pins about a vertical axis, the potential so obtained being directly proportional to the sine of the angle of rotation. In this way polarisation effects, contact potentials and other unknown quantities were presumably nullified.

Direct reading of the sine of the angle of rotation was obtained by the simple mechanical device shown in fig. 8.2 B. The cylindrical pin A or A' bears against the straight edge B which transmits the motion to an Ames dial indicator. This gave a direct reading of the sine of the angle from 0° to 90° in readings of 0° to 1000, thus permitting an 1% accuracy in indication at angles as small as $\text{sine}^{-1} 0.1$.

In use these pins were rotated until balance was obtained as shown by a vibration galvanometer. The basis of connection between the pins and the galvanometer was the transformer T. This had two symmetrically arranged equal primaries wound on metal bobbins for electro-static shielding. The secondary was coupled to the galvanometer via a two valve amplifier. The valves shown on the amplifier circuit were found satisfactory but were mainly decided by the equipment immediately available. Actually it was unstable and damping was introduced by connecting the grids to the negative side of the filaments without additional grid bias.

The amplification with this arrangement was sufficiently great to permit shunting of the galvanometer and the obtaining of almost instantaneous readings.

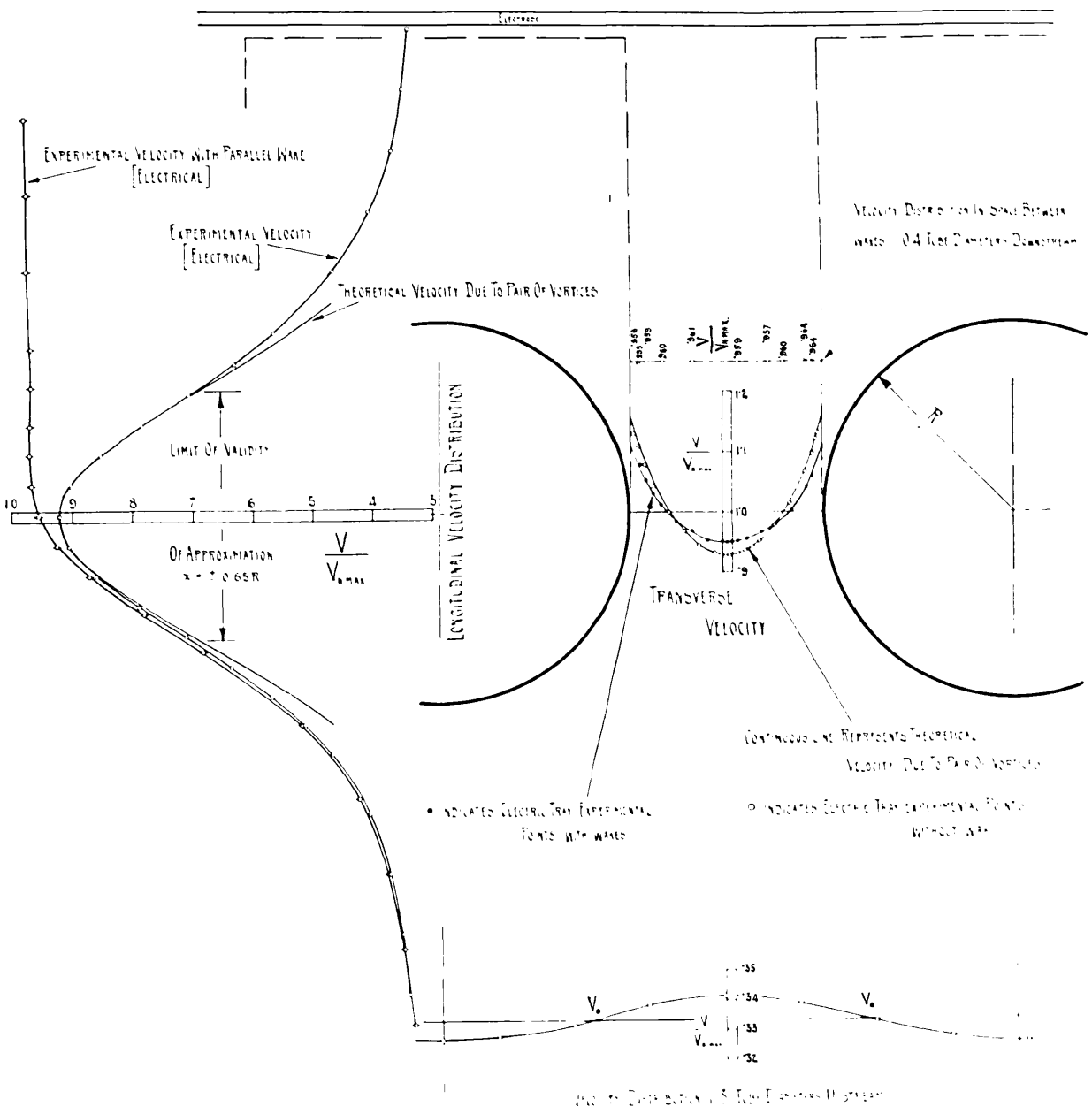
Normally two readings were taken these being obtained by reversing plug connections at P_1 . This reversal eliminated any zero error on the sine indicator and to some extent also errors due to stray capacity currents.

Reversal of P_2 provided another pair of readings eliminating other minor stray currents, though in general a single reversal was sufficient.

At first some difficulty was experienced due to differences of phase in the two circuits. Unless these were exactly coincident there was no position of equilibrium and the galvanometer merely dropped to an indifinite minimum vibration instead of becoming stationary. This difficulty arose from three causes :-

- (1) out of phase direct electro-magnetic pick up by the amplifier. This was eliminated by disconnecting the amplifier from the tray and orientating it until it was so placed in the stray electro-magnetic field that the galvanometer came to rest.
- (2) electro-static pick up in the amplifier. This was eliminated by reducing the E.M.F. across the tank to 6 volts and transforming from the original higher voltage at a distance from the apparatus.

ELECTRIC TRAY DETERMINATION OF THE LONGITUDINAL AND TRANSVERSE VELOCITY DISTRIBUTION IN THE GAP BETWEEN A PAIR OF CYLINDERS. FIG. 8'3.



- (3) differences in the resistance of the circuits of the two pins. This was eliminated by slight variation in R_2 .

8.3 Verification of the method.

In order to verify that the readings obtained from the tray were consistent with theory, velocity distributions were taken in the gap between two cylinders. For this particular case it is possible to deduce a simple mathematical approximation.

The distributions obtained from the electrical tray are shown by the test points in figure 8.3 whereas the distributions given by the theory (see appendix No.3) are indicated by the continuous line.

It will be seen that both across the gap and longitudinally along the centre line of the gap the agreement between the theory and experimental points is excellent.

In the case of the longitudinal distribution the theory and tray measurements cease to agree after a distance of $0.65 R$ up and down stream. This is to be expected as the approximations of the theory are such that the theory can only be expected to hold in the vicinity of the maximum constriction.

Both in the gap and in the main stream the electric

tray velocity distributions (and not the theory) represent the true inviscid flow.

8.4 Velocity distribution across the tray at a distance of 1.3 tube diameters upstream.

A traverse across the relatively undisturbed stream was made primarily to check the electrical method by using it at a section where the velocity was much lower than that in the gap.

The resulting distribution is plotted to an enlarged scale at the bottom of figure 8.3. It is interesting to note what little effect the row of tubes has at a distance of only 1.34 diameters upstream. The velocity on the centre line is certainly greater than the mean but only by $2\frac{1}{2}\%$.

The electrical measurements are checked by integrating across this upstream section to obtain the total flow. This should be equal to the value obtained by integration across the gap. Actually a discrepancy of the order of 6% was found but this was traced to leakage under the paraffin wax models of the tubes. This was overcome by skimming the base of the cylinders with a pointed tool thus making a series of fine serrations which were smeared with a trace of vaseline. The wax models were then replaced in the tank and loaded with three pound weights. After a couple of days the cylinders

had bedded themselves on to the glass bottom and the above error was reduced to 0.9%

This residual error could not be further reduced. In fact at a subsequent attempt errors as great as 2% were observed. When such errors were found they could as a rule be allowed for by applying a suitable correction factor. It may be said therefore, that within a restricted locality such as the gap, the tray gives measurements which may be read to 1 part in 1000 and which appear to be accurate within $\frac{1}{2}\%$. On the other hand when comparing velocities in different parts of the tray errors up to 2% may be anticipated, particularly when velocities of different magnitude are being compared.

When using the electrical analogy it is often convenient to express all velocities as multiples of the velocity at some clearly defined point. As an illustration of this the undisturbed velocity far upstream of the row of tubes is a convenient unit and in the present case might quite well have been used in place of $V_{N,max}$. There is difficulty however since the tray must necessarily be restricted in length and so the influence of the model may extend almost, if not quite, to the end of the tray. By making use of the velocity distribution curve at the bottom of figure 8.3 it is possible to locate one or more

points at which the velocity is precisely equal to the integrated mean. Two such points are marked V_0 in the diagram. During any experiment the search pins should be returned repeatedly to one or other of these points for checking purposes. The reading obtained here, provides the scale of velocities.

8.5 Representation of fluid with friction.

From the previous longitudinal results it is seen that the velocity distribution is symmetrical up and down stream of the gap. That is to say the pressure is lowest in the gap and again rises rapidly down stream. With a viscous fluid this does not take place owing to the presence of the boundary layer. This, in the presence of a reverse pressure gradient rapidly swells out and permits the main stream to separate from the tube surface.

The main stream actually proceeds down stream with approximately constant velocity, i.e. approximately constant width, the space behind the cylinders being occupied with turbulent dead water.

In an attempt to represent this state of affairs parallel sided wax models were placed in the dead water regions as indicated by the dotted lines in figure 8.3.

The curve to the extreme left of figure 8.3 was then obtained. Upstream it is practically indistinguishable from that obtained without the wakes. In fact their influence only becomes appreciable at a distance $1/5$ of the gap upstream. In the gap itself the centre line velocity is increased by some 3%. Further down the stream however the difference naturally becomes very marked, the velocity rising to a maximum. This it attains at a distance of approximately $1/3$ of the gap down stream.

It must be remarked that these electrical tray measurements represent essentially the motion of an inviscid fluid although the major influence of viscosity has been included by the addition of the wakes. Actually a viscous fluid will deviate from these results, partly because of turbulent intermixing between the stream and the wake is ignored and partly because the boundary layer has not been represented.

Turbulence at the edge of the wake could no doubt be represented by a combination of a diverging channel and controlled leakage but the numbers of such combinations are infinite.

With regard to the boundary layer this represents

less difficulty. The work of Blasius⁽¹⁾ and others has shown that the thickness of the boundary layer remains approximately constant when pressure gradients are of the nature found in this problem. As an approximation the effect of viscosity in the boundary layer can be represented by an increase in diameter of the tube, i.e. it is equivalent to a decrease in the gap. It could be represented by moving the cylinders closer to one another in order to reduce the gap.

The magnitude of this movement may be determined by the Blasius method but for this purpose the variation of velocity around the tube wall must be known. But before discussing this it is convenient to consider the effect of the wakes on the transverse distribution in the gap. As seen in figure 8.3 this becomes flattened in the centre as shown by the curve with black dots. That is to say when the wakes are present the difference in the velocity at the centre and at the sides of the gap is less since on the whole the stream lines have less curvature and so the high pressure in the centre of the gap is less pronounced.

It will be noticed that the curves intersect at points approximately a quarter of the gap on each side of the centre

(1) For English summary see L.Howarth, R & M, 1632. 1934.

line. The location of these points cannot vary much and they therefore provide convenient points of reference. For the particular geometrical arrangement of the nest the velocity at these points of intersection is 0.98 of the mean velocity in the gap $V_{N,max}$.

With the wakes the velocity variations in the gap are only about $\frac{2}{3}rd$ of the magnitude of the variations without wakes.

8.6 Velocity at the tube surface.

With the wakes present the velocity distribution at the surface of the tube is given in table 8.6 and plotted with crosses on fig. 5.2F. Except at 90° the electrical measurements are in almost exact agreement with the observed air pressures after these have been corrected for the size of the pressure hole.

This agreement is surprising for it indicates that the presence of the boundary layer, which is ignored in the electrical model, has but little effect upon the pressures at the wall.

At first sight it would be thought that the space occupied by the boundary layer would so decrease the effective flow area that the velocities in the gap would be increased

sufficiently to lower the pressure throughout the gap. Fig. 8.3 shows however that there is a very steep velocity gradient close to the wall, i.e. just in the neighbourhood occupied by the boundary layer. A decrease in pressure in the centre of the gap can therefore be more than compensated by absence of the steep pressure gradient near the wall.

8.7 Estimation of the effective thickness of the boundary layer⁽¹⁾

According to the electrical method the velocity at the centre of the gap is $0.950 V_{N,max}$. On the other hand the mean of the air measurements as calculated from figures 4.2 and 4.3 B show that the velocity was actually $\frac{0.975}{0.983} V_{N,max}$.

Assuming for a first approximation that the shape of the pressure distribution curve is unaffected by the presence of the boundary layer, then the effective thickness of the two boundary layers $2\delta^*$ is $0.026 G$. However it must be borne in mind that this quantity is the result of the subtraction of two nearly equal quantities and that if the original pressure difference had been 1% less the thickness of $2\delta^*$ would be reduced to $0.021 G$.

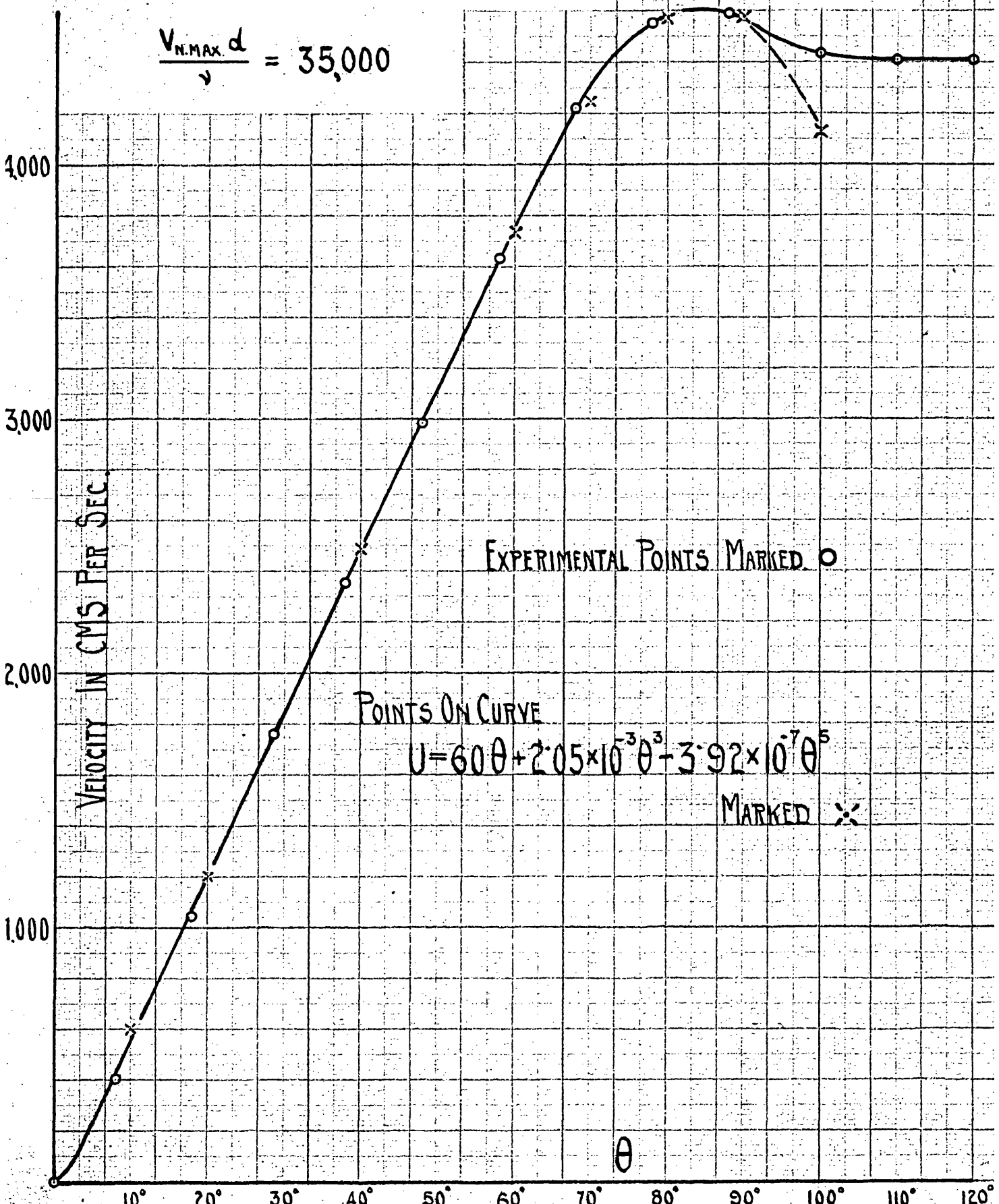
It is interesting to observe that when this dimension

(1) See appendix No.4.

VELOCITY AT THE SURFACE OF CENTRE TUBE 1ST ROW.

FIG. 8.7.

$$\frac{V_{N.MAX} d}{\nu} = 35,000$$



for the boundary layer is subtracted from the outer edges of the velocity distribution given in figure 8.3 the velocity at that point is 0.975 of its previous maximum. Therefore when the velocities are scaled up to compensate for a reduction in gap area, the pressure on the tube wall remains sensibly unchanged. Therefore it is impossible to estimate the thickness of the boundary layer from the wall pressure at 90°.

The Blasius theoretical method for determination of the boundary layer utilises the variation of pressure from point to point along the wall. In essence these pressures are expressed as velocities using a power series thus:-

$$U = u_1x + u_3x^3 + u_5x^5 + \dots$$

where U is the velocity immediately outside the boundary layer at a distance x from the upstream generator.

u_1 , u_3 and u_5 are coefficients so selected that the velocity U is a good approximation to the true value.

In the present experiments the variation of the velocity with θ is readily obtained from form drag diagrams.

A typical example for one of the first row tubes is given in figure 8.7. This diagram has been corrected for the size of the pressure hole by moving all the velocity readings from 0° to 90° upstream by 2°.

Cathetometer reading 1.179 Cms. 13°C 29.46"Hg $\nu =$
0.145 c.g.s. units

| Angle | Pressure "h" in Cms. of water | \sqrt{h} | Velocity Cms. per sec. $= 1272 \sqrt{h}$. |
|-------|----------------------------------|------------|---|
| 0 | 0 | 0 | 0 |
| 10 | 0.1 | 0.0316 | 402.5 |
| 20 | 0.67 | 0.819 | 1042 |
| 30 | 1.91 | 1.382 | 1759 |
| 40 | 3.48 | 1.865 | 2373 |
| 50 | 5.50 | 2.345 | 2984 |
| 60 | 8.15 | 2.855 | 3632 |
| 70 | 10.99 | 3.315 | 4220 |
| 80 | 12.80 | 3.578 | 4553 |
| 90 | 13.00 | 3.605 | 4589 |
| 100 | 12.15 | 3.486 | 4437 |
| 110 | 12.00 | 3.465 | 4405 |
| 120 | 12.00 | 3.465 | 4405 |

These are plotted in Fig. 8.7 from which it is seen that the velocities calculated from the pressure distribution are well represented by the equation

$$U = 6.0 \times 10 \theta + 2.05 \times 10^{-3} \theta^3 - 3.92 \times 10^{-7} \theta^5$$

The relative importance of the three terms is seen from the following table:-

| | $\theta = 20^\circ$ | 40° | 60° | 70° | 80° | 90° | 100° |
|-----------|---------------------|------|-------|-------|--------|--------|--------|
| 1st Term | 1200 | 2400 | 3600 | 4200 | 4800 | 5400 | 6000 |
| 2nd " | 16.4 | 131 | 443 | 703 | 1050 | 1495 | 2050 |
| 1st + 2nd | 1216.4 | 2531 | 4043 | 4903 | 5850 | 6895 | 8050 |
| 3rd Term | - 1.25 | - 40 | - 305 | - 659 | - 1284 | - 2315 | - 3920 |
| U | 1215.15 | 2491 | 3738 | 4244 | 4566 | 4580 | 4130 |

With these values the stream function ψ and the velocity distribution in the boundary layer can each be expressed in terms of four functions which have been calculated by Howarth. These are tabulated for different values of a quantity proportional to the distance "y" from the tube wall.

$$\psi = f_1 u_1 x \left(\frac{y}{u_1}\right)^{\frac{1}{2}} + 4f_3 u_3 x^3 \left(\frac{y}{u_1}\right)^{\frac{1}{2}} + 6u_5 x^5 \left(\frac{y}{u_1}\right)^{\frac{1}{2}} \left(g_5 + \frac{u_3}{u_5} \cdot \frac{u_3}{u_1} \cdot h_5\right)$$

In representing the velocity distribution in figure 8.7 and in the above table the angle θ has been used instead of the distance "x" from the upstream generator. The above equation may therefore be replaced by:-

$$\psi = f_1 u_1' \theta \left(\frac{y}{u_1}\right)^{\frac{1}{2}} + 4f_3 u_3' \theta^3 \left(\frac{y}{u_1}\right)^{\frac{1}{2}} + 6u_5' \theta^5 \left(\frac{y}{u_1}\right)^{\frac{1}{2}} \left(g_5 + \frac{u_3'}{u_5'} \cdot \frac{u_3'}{u_1'} \cdot h_5\right)$$

$$\text{where } u_1' \theta = u_1 x \quad \text{and } u_3' \theta^3 = u_3 x^3 \quad \text{etc.}$$

For example inserting appropriate values from the table for

$$\theta = 90^\circ \text{ and assuming "y" such that } \left(\frac{y}{u_1}\right)^{\frac{1}{2}} = \frac{y}{3.1}$$

$$\begin{aligned} \psi &= 2.4523 \times 5400 \frac{y}{3.1} + 4 \times 0.802 \times 1495 \frac{y}{3.1} \\ &\quad - 6 \times 2315 \left[.58 - \frac{1495 \cdot 1495}{2315 \cdot 5400} \times (-.05) \right] \frac{y}{3.1} \\ &= 13,250 \frac{y}{3.1} + 4,796 \frac{y}{3.1} - 13,890 \frac{y}{3.1} \left[.58 + .008945 \right] \\ &= (13,250 + 4,796 - 8,180) \frac{y}{3.1} \\ &= 9,866 \frac{y}{3.1} \end{aligned}$$

$$\text{When } \theta = 90^\circ \quad x = \frac{\pi d}{4} = .7854 \times 1.27 = 0.997 \text{ Cm. say } 1 \text{ Cm.}$$

$$\frac{y}{x^{\frac{1}{2}}} = 3.1 \times \left(\frac{v}{u_1 x}\right)^{\frac{1}{2}} = 3.1 \left(\frac{0.1452}{5400}\right)^{\frac{1}{2}} = 3.1 \left(\frac{1}{37,200}\right)^{\frac{1}{2}} = 3.1 \times \frac{1}{192.8}$$

$$\frac{y}{1} = 3.1 \times \frac{1}{192.8}$$

$$\text{Therefore } y = 0.01608 \text{ Cm.}$$

The effective thickness of the boundary layer is conveniently defined by the distance the boundary layer causes the stream lines to be shifted away from the tube surface.

Let δ^* be this distance.

$$\delta^* = \int_0^y \left(1 - \frac{u}{U}\right) dy \quad \text{where } y \text{ is sufficiently great to include the whole of the boundary layer.}$$

In terms of the stream function this definition becomes

$$\delta^* = y - \frac{\psi}{U}$$

$$\frac{\delta^*}{y} = 1 - \frac{\psi}{Uy}$$

$$\text{Since } \psi = 9,866 \frac{y}{3.1} \quad \text{and } U = 4580$$

$$\frac{\delta^*}{y} = 1 - 0.695 = 0.305$$

Therefore δ^* = $0.305 \times 0.01608 = 0.004905$ Cm.
and $2\delta^*$ = 0.00981 Cm.

$$\frac{2\delta^*}{G} = \frac{0.00981}{.648} = 0.01513$$

This value is based on sounder premises than that calculated from the centre line pressure which gave $2\delta^* = 0.026$ G

It is necessary to prove that y has been taken sufficiently large to include the whole of the boundary layer. This was done by making

$$\left(\frac{v}{u_1}\right)^{\frac{1}{2}} = \frac{y}{2.4}$$

when $\frac{\delta^*}{y} = 0.3855$ and $2\delta^* = 0.00958$ Cm.

which agrees with the previous value within the limits of accuracy of Howarth's tables. Further confirmation on this point is given in the next sub-section when the distribution of the velocity in the boundary layer is considered.

8.8 Distribution of velocity in the boundary layer and its tangential drag.

8.81 Velocity distribution in boundary layer in gap of nest of tubes.

By converting Blasius's equation for the velocity in the boundary layer

VELOCITY DISTRIBUTION IN THE BOUNDARY LAYER

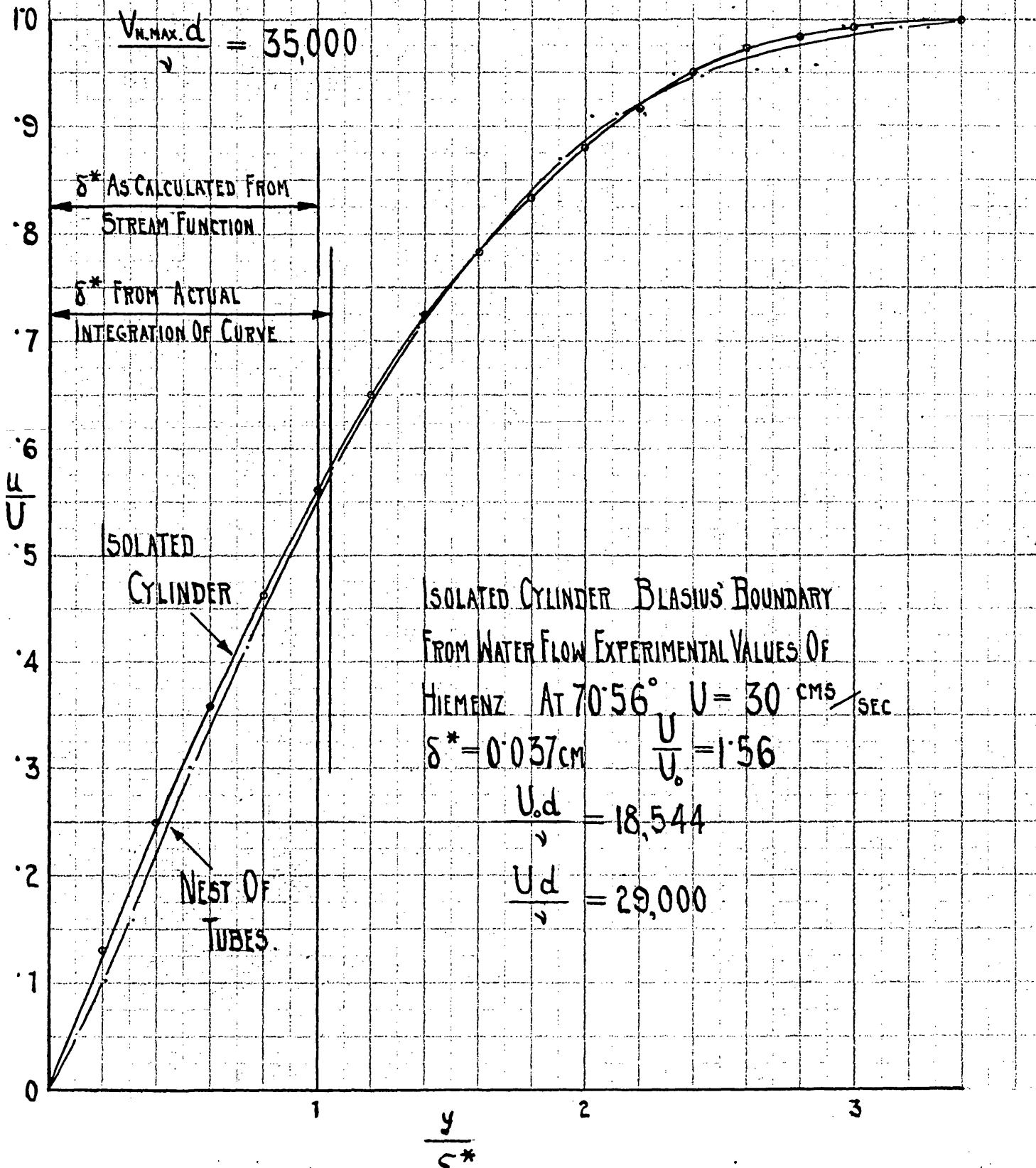
FIG. 8.81.

IN GAP OF 1ST ROW OF TUBES I.E. AT 90°

$U = 4580 \text{ CMS/SEC}$

$\delta^* = 0.004905 \text{ CMS.}$

$\frac{V_{H,MAX}.d}{\nu} = 35,000$



δ* AS CALCULATED FROM
STREAM FUNCTION

δ* FROM ACTUAL
INTEGRATION OF CURVE

ISOLATED
CYLINDER

NEST OF
TUBES

ISOLATED CYLINDER BLASIUS' BOUNDARY
FROM WATER FLOW EXPERIMENTAL VALUES OF
HIEMENZ AT 70.56° $U = 30 \text{ CMS/SEC}$
 $\delta^* = 0.037 \text{ cm}$ $\frac{U}{U_0} = 1.56$
 $\frac{U_0.d}{\nu} = 18,544$
 $\frac{U.d}{\nu} = 29,000$

$$\begin{aligned}
u = & u_1 f_1' x + 4u_3' f_3' x^3 + 6(u_5 g_5' + \frac{u_3^2}{u_1} h_5') x^5 \\
& + 8(u_7 g_7' + \frac{u_3 u_5}{u_1} h_7' + \frac{u_3^3}{u_1^2} k_7') x^7 \\
& + 10(u_9 g_9' + \frac{u_3 u_7}{u_1} h_9' + \frac{u_5^2}{u_1} k_9' + \frac{u_3^2 u_5}{u_1^2} j_9' + \frac{u_3^4}{u_1^3} q_9') x^9 + \dots
\end{aligned}$$

into the form using the angle θ from the upstream generator and assuming that all terms higher than x^5 can be ignored we have

$$u = u_1' \theta f_1' + 4u_3' \theta^3 f_3' + 6u_5' \theta^5 (g_5' + \frac{u_3}{u_5} \cdot \frac{u_3}{u_1} \cdot h_5')$$

By using various values of $y(\frac{u_1}{y})^{\frac{1}{2}}$ and obtaining the appropriate values for the coefficients f_1' , f_3' , g_5' and h_5' from Howarth's tables, the velocity at any distance y from the tube surface can be calculated. In this way the velocity distribution in the boundary layer at 90° was obtained and is shown in figure 8.81.

8.82 Comparison with the velocity distribution for an isolated cylinder.

The ratio $\frac{\text{gap width}}{\text{transverse pitch}}$ appreciably modifies the boundary layer and its influence can be studied by a comparison with the boundary layer of an isolated cylinder

in a wind tunnel. In the present nest the

$$\frac{\text{gap width}}{\text{transverse pitch}} = \frac{1}{2.96} \text{ and this represents a fairly}$$

extreme case of close spacing. The other extreme is represented by a completely isolated tube. Howarth has worked out the boundary layer for the latter case for a Reynolds' number of 18,544 reckoned on the free stream velocity. Using his figures the Reynolds' number becomes 29,000 when based on the maximum velocity. From the experimental pressure distribution by Hiemenz, Howarth represents the velocity around the cylinder by the equation.

$$U = 7.151x - 0.04497x^3 - 0.00033x^5$$

At 90° the boundary layer of the isolated cylinder has already broken away and a comparison between the two cases is more fairly made at or near the point of minimum pressure. From figure 8.7 it will be seen that in the nest at 90° the velocity has passed its maximum by a few degrees. In Howarth's case the minimum pressure occurs at 68° and in his figure 5 he gives the boundary layer for the isolated cylinder at 70.56°. Therefore it is appropriate to compare the velocity distribution at this point and Howarth's figure 5 has also been reproduced on figure 8.81.

The corresponding importance of the three terms u_1x ,

u_3x^3 , and u_5x^5 is shown below.

Table 8.82

| | Nest at 90° | Isolated cylinder at 70.56° |
|----------|-------------|-----------------------------|
| u_1x | + 1.179 | + 1.401 |
| u_3x^3 | + .326 | - .317 |
| u_5x^5 | - .505 | - .084 |
| | 1.000 | 1.000 |

The velocity of water flow at 70.56° was 30.0 Cms. per second. Therefore the Reynolds' number based on this velocity = $18,544 \times \frac{30.0}{19.2} \approx 29,000$. Since the geometrical configuration of the boundary layer is controlled by $Re^{\frac{1}{2}}$, we can adjust from one Reynolds' number to another by multiplying ratios such as $\frac{\delta^*}{x}$ or $\frac{\delta^*}{d}$ (for a given angle) by $(\frac{Re.1}{Re.2})^{\frac{1}{2}}$ an increase in Reynolds' number causing a decrease in the thickness of the boundary layer.

Therefore to adjust Howarth's boundary layer to that of the nest so far as Reynolds' numbers are concerned we multiply by $(\frac{29,000}{35,000})^{\frac{1}{2}} \approx 0.91$, Howarth's $\frac{\delta^*}{d}$ was 0.0038 which when multiplied by 0.91 becomes 0.003457. In comparison with this the nest value is computed to be 0.003862.

So it is seen that the two quite different pressure distributions represented in table 8.82 both lead to

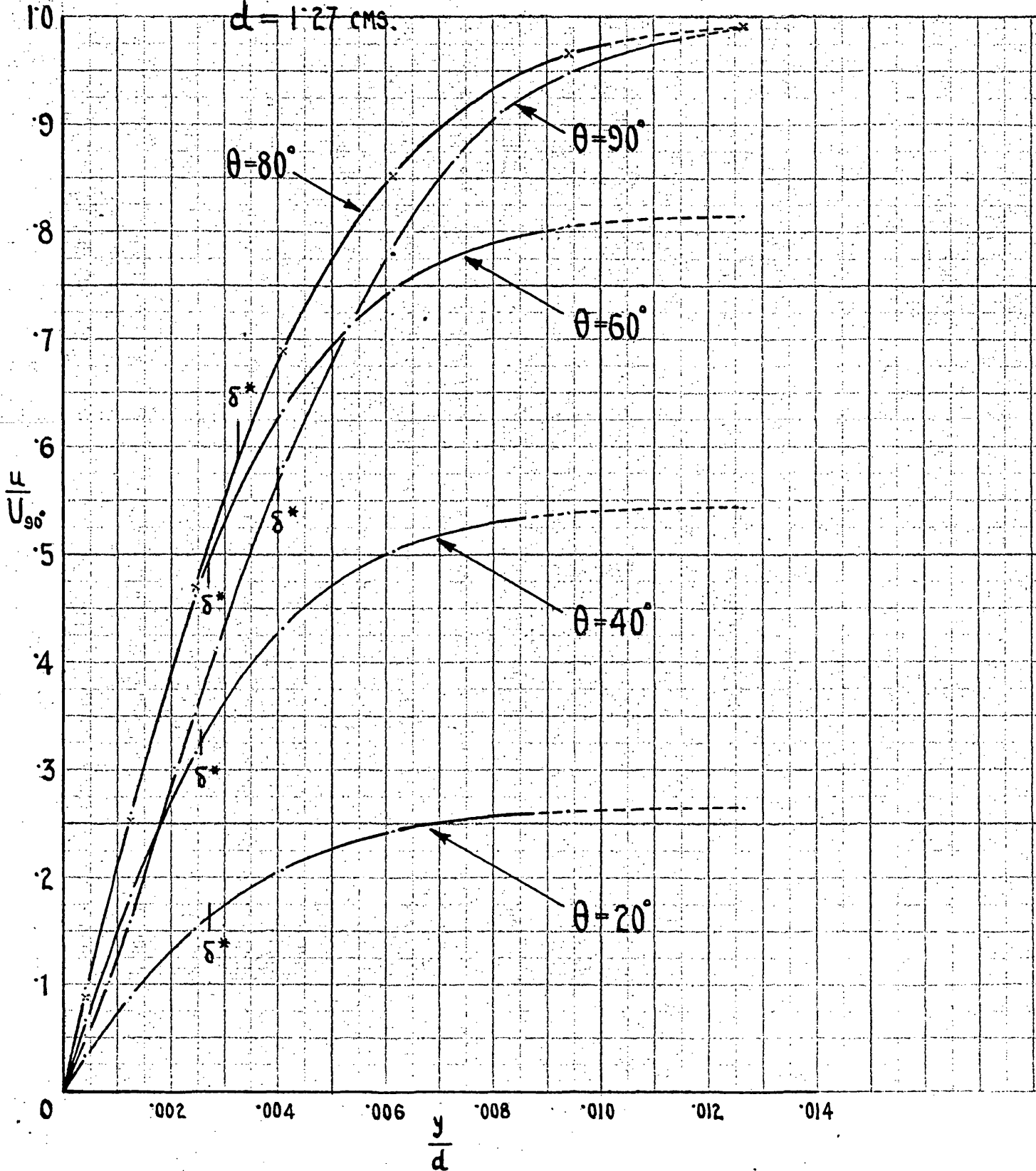
VELOCITY DISTRIBUTION IN THE BOUNDARY LAYER.

FIG. 8·83.

$$\frac{V_{N.MAX.} d}{\nu} = 35000$$

$$U_{90} = 4580 \text{ CM/SEC.}$$

$d = 1.27 \text{ CMS.}$



approximately the same effective boundary layer thickness when the comparison is made for equal maximum velocities. In other words, in such boundary layers the most important variable in determining δ^* is the value of the maximum velocity rather than the manner with which the velocity is varying with x .

With regard to the velocity distribution within the boundary layer it might have been expected that this would be more affected by the relative importance of the three terms in table 8.82. Nevertheless its general appearance is almost identical as is shown in figure 8.81. Despite the very different set of values in table 8.82 both relate to conditions a few degrees past the point of minimum pressure and some ten degrees before breakaway.

8.83 Variation of thickness of the boundary layer.

Using Blasius' method as described in section 8.81, the velocity distributions in the boundary layer at 20° , 40° , 60° , 80° and 90° were calculated and these are shown in fig. 8.83.

In all cases the velocity in the boundary layer asymptotically approaches that in the main stream. In order to estimate the thickness of the boundary layer it is therefore necessary to premise some arbitrary small difference in velocity which can be considered negligible. For example

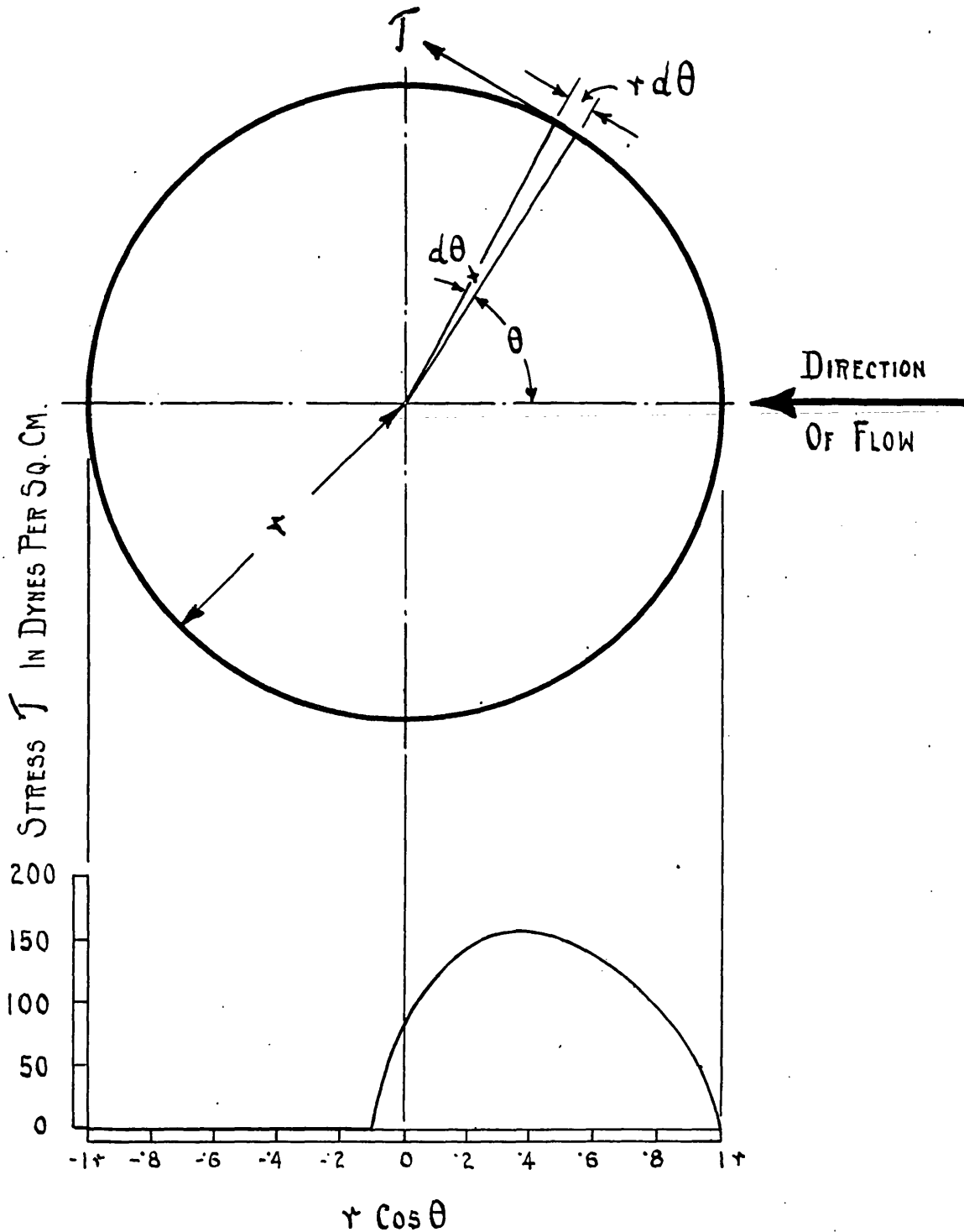
the boundary layer may be regarded as terminating when the velocity in the layer is 2% less than that in the main stream just outside the layer. The velocities in the main stream are obtained from the table in section 8.7 and the velocity distribution curves in figure 8.83 are drawn with a continuous line until 98% of this velocity is reached. The remaining 2% of the velocity is shown with a dotted line.

By noting the values of y or $\frac{y}{d}$ at the commencement of the dotted curves some idea of the variation in thickness of the boundary layer can be obtained. At 20° it is $0.0088 d$ and its thickness remains constant at this value from 20° to 60° . From 60° onwards it opens out at an increasing rate being $0.0102 d$ at 80° and $0.0115 d$ at 90° . This gives an indication of the approach of that extremely rapid thickening associated with breakaway which in the present case occurs at 95 or 100° .

The effective thickness of the boundary layer δ^* has also been indicated on figure 8.83. This shows the same characteristics remaining sensibly constant over the major portion of the upstream periphery of the tube. In fact this constancy in thickness may be regarded as a general characteristic of boundary layers in almost all flow problems in which the main stream is flowing from a point of high pressure to one of lower pressure. It is in fact the result

TANGENTIAL DRAG UP TO POINT OF BREAKAWAY ON
 FIRST ROW OF TUBES

FIG. 8·84.



of the velocity increasing approximately in direct proportion to the distance travelled and reflects the importance of the first term in the power series.

$$u = u_1x + u_3x^3 + u_5x^5 + \dots$$

8.84 Total drag up to point of breakaway.

The tangential drag on the first row of tubes up to the point of breakaway can be calculated from the data in figure 8.83.

$$\tau = \mu \frac{du}{dy} \quad \text{when } y \text{ approaches zero}$$

where τ = tangential drag per unit area

μ = the coefficient of viscosity

$$= 1.757 \times 10^{-4} \text{ grams.Cms}^{-1}.\text{sec}^{-1}.$$

From the data upon which figure 8.83 was plotted the following table was obtained.

| Angle | $\frac{du}{dy}$ | τ in dynes per sq.cm. |
|-------|-------------------------|-------------------------------|
| 20° | 28.18 x 10 ⁴ | 49.5 |
| 40° | 58.1 x 10 ⁴ | 102.1 |
| 60° | 85.0 x 10 ⁴ | 149.2 |
| 80° | 78.2 x 10 ⁴ | 137.5 |
| 90° | 45.75 x 10 ⁴ | 80.4 |
| 96° | 0 | 0 |

From figure 8.84 it is seen that if τ is the tangential stress acting over a small arc $r d\theta$, then the tangential force per unit length of tube is $\tau r d\theta$.

These forces act in various directions and it is convenient to integrate their components in the direction of flow.

This resulting force in the direction of flow (per unit length of tube) is

$$\int_0^{180} \tau r d\theta \sin\theta$$

$$\text{Now } r \sin\theta d\theta = -d(r \cos\theta)$$

$$\text{Therefore } \int_0^{180} \tau r d\theta \sin\theta = - \int_{+r}^{-r} \tau d(r \cos\theta)$$

This integration is performed by plotting the stress τ as ordinate on a base of $r \cos\theta$.

The area A of this diagram is $124 r$

This area gives the force per unit length of tube, in the direction of flow, for one boundary layer.

Therefore force on the two boundary layers = $2 \times 124 r$

It is convenient to express this force as a stress per unit area of tube diameter.

Thus average tangential stress $\bar{\tau}$ per sq.cm. of the tube diameter in the direction of flow is 124 dynes. In order to compare this with the form drag coefficients it is expressed in the dimensionless form $\frac{\bar{\tau}}{\rho V_{N,max}^2} =$

$$\frac{124}{1.179 \times 8.76 \times 981} = 0.012$$

comparing this with the form drag coefficients it is

$$\frac{.012}{.435} = 2.8\% \text{ of the form drag of the first row}$$

$$\frac{.012}{.253} = 4.7\% \text{ of the form drag of the second row}$$

$$\frac{.012}{.305} = 3.9\% \text{ of the total resistance coefficient of the nest.}$$

When it is remembered that the unknown tangential resistance on the rear of the tubes acts in the upstream direction, the above values are consistent with the observed difference between the total resistance and the sum of the form drag diagrams. As shown in section 5.7 the sum of the form drag coefficients was 98.2% of the total resistance, thus leaving 1.8% to be accounted for by tangential resistance.

In viscous boundary layer phenomena stresses are proportional to $V^{1.5}$ where the other factors are constant. At the rear of the tubes the velocities appear to be of the order $0.4 V_{N,max}$ so the estimated tangential stresses will

be of the order 0.25 of those on the upstream faces of the tubes. On this basis the tangential drags at the rear would be approximately $0.25 \times 3.9 = 1.0\%$ of the total resistance of the nest. This gives the estimated net tangential drag of the nest as $3.9 - 1.0 = 2.9\%$. Therefore the form drag should constitute 97.1% of the total resistance whereas the observed value was 98.2% ^{97.3}

8.9 Summary of results of the electric tray.

Summarising the preceding paragraphs it may be said that the electric tray method can give pressure distributions similar to those found in a fluid where viscosity is not negligible but to obtain these results the dead water regions must be suitably represented.

The dead water regions can in fact be predicted analytically with the aid of the electric tray. Breakaway occurs when a boundary layer is present and the main stream is decelerating at a sufficiently rapid rate to reverse the direction of motion within the boundary layer. Howarth summarises the methods available for predicting these conditions. For example according to the Kármán-Pohlhausen method breakaway occurs as soon as the deceleration exceeds the value given by

$$\frac{U' \delta^2}{\nu} = -12 \quad (1) \quad \text{where } U' = \frac{dU}{dx}$$

If therefore an experiment is made with the electric tray without any wakes in position sufficient data will be obtained to compute the boundary layer and to determine the point at which breakaway occurs. Wakes can then be introduced and the velocity and pressure distributions redetermined. The first wakes could if necessary be subsequently modified in the light of the new pressure distributions. So by a series of successive approximations it is possible to outline completely the flow pattern in a practical two dimensional problem.

(1) The present experiments appear to require a numerical value less than 12, see section 9.4.

9. INTERPRETATION OF RESULTS AND EXPOSITION
OF FLOW PATTERN OF PARALLEL ARRANGEMENT.

9.1 Analysis of form drag diagrams for first row of tubes.

Figure 5.2F shows a typical curve of pressure distribution at the surface of a tube in the first row. From this it will be seen that the pressure is atmospheric when the pressure hole is facing directly upstream. In such a position the pressure measuring hole faces the direction of motion and so records the total energy of the stream. The agreement with the atmospheric line may be regarded either as indicating, that no loss of energy has occurred in the upstream part of the casing or alternatively, that the pressure measuring device was functioning satisfactorily. The velocity increases as the cross-sectional area decreases towards the centre of the gap. Further the distribution of velocity across the gap is such as to give the greatest velocity near the tube since the surface of this is convex. The pressure is therefore seen to decrease continuously and by an amount greater than that due to the reduction in cross-sectional area. The minimum pressure occurs slightly before the 90° .

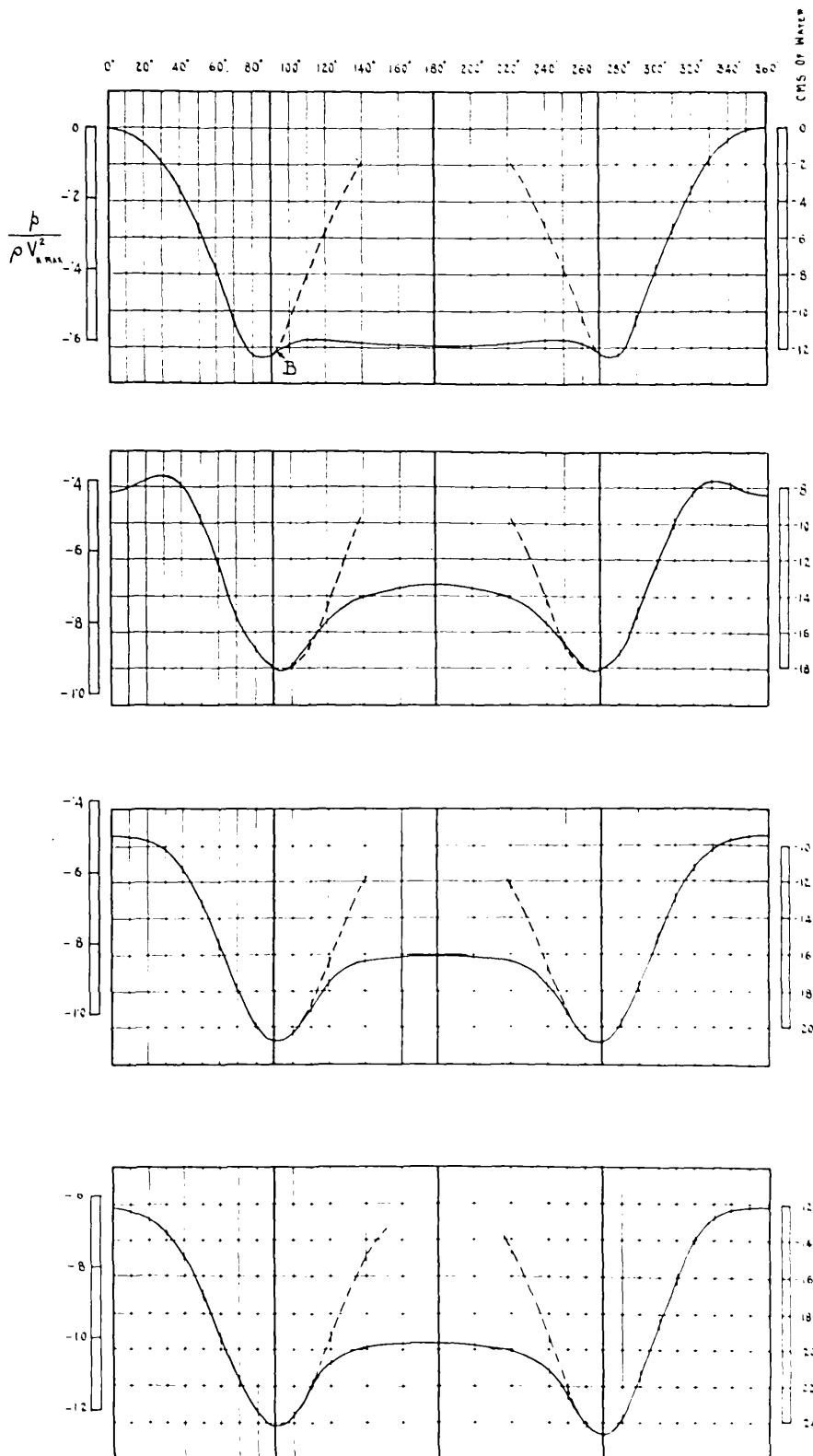
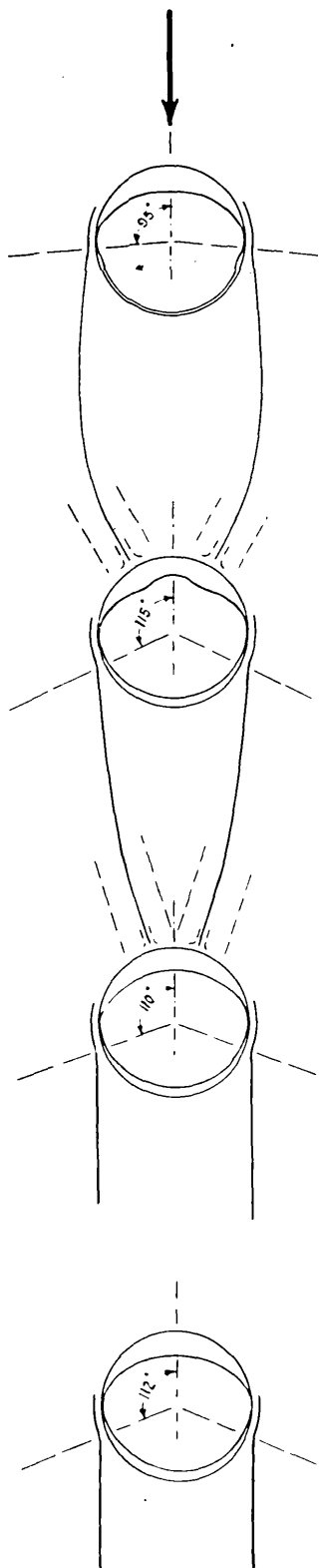
From 90° to 110° there is rise in pressure and at, or about 110° the flow ceases to follow the surface of the tube.

EFFECT OF POINT OF BREAKAWAY ON FORM DRAG DIAGRAMS.

FIG. 9-1.

PARALLEL ARRANGEMENT

$$\frac{V_{N,MAX} d}{\nu} = 35,000$$



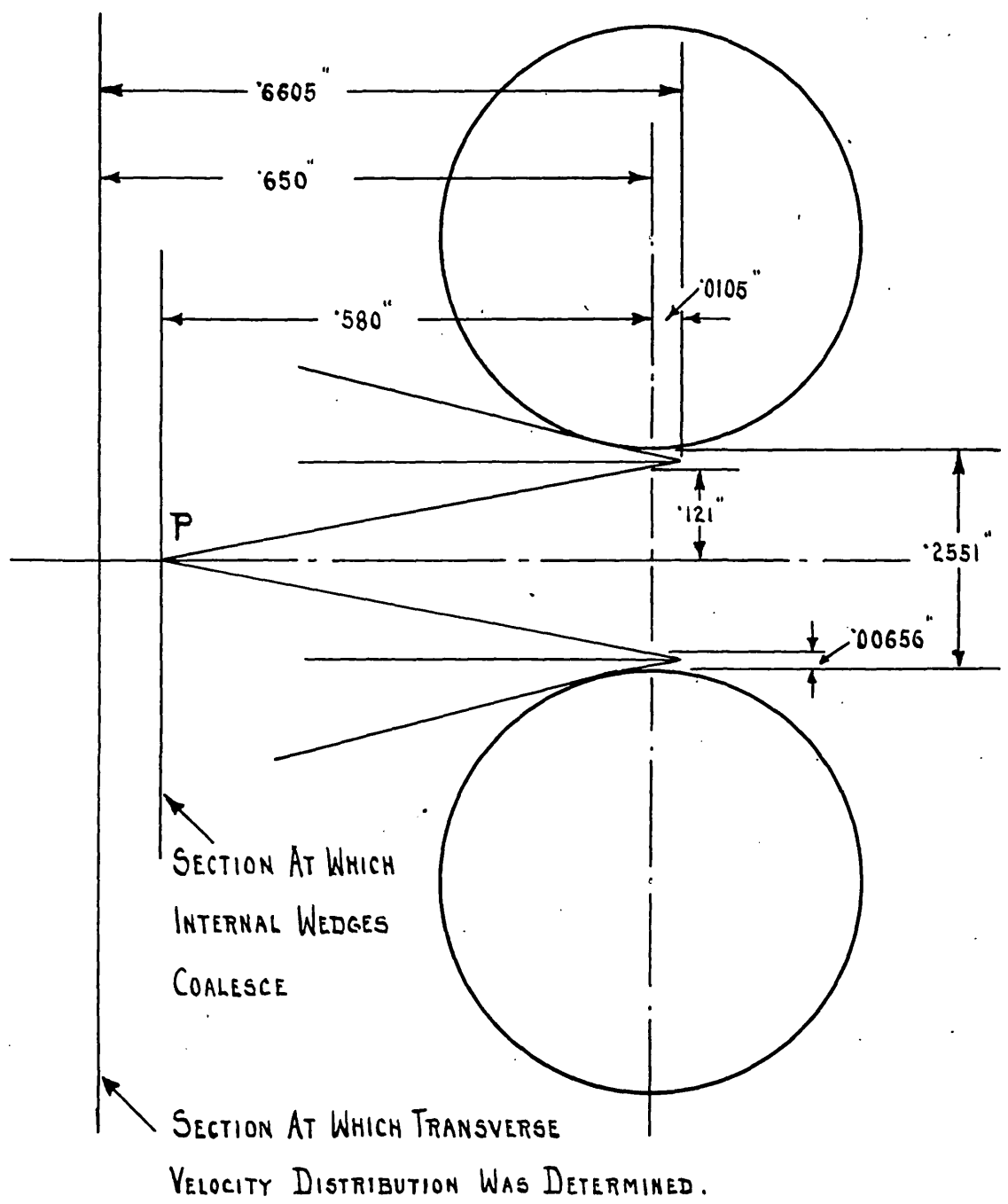
This is more clearly seen by reference to figure 9.1. If the fluid expanded in the same way as it contracted it would follow the dotted curve. It will be seen that at the point B the pressure shows a marked deviation from this hypothetical expansion and it can be concluded that this indicates roughly the point of breakaway and from 110° onward the main stream has separated from the tube surface.

From 110° to 180° the pressure remains sensibly constant although in most cases there is a further slight fall. Over this range the tube is in contact with the "dead water", i.e. a region in which the total energy is considerably less than that of the original fluid.

The pressure variations across the rear of the tube are so small that it cannot be said that they give definite indications of the type of motion in the "dead water" region.

In figure 5.4B there is the suspicion of a lower pressure at 150° and 210° . This is more clearly seen in the form drag diagrams of the last row of tubes: figures 2.6A and 5.2E. It is still more definitely indicated in the water flow experiments with staggered arrangement of tubes as illustrated in figures 2.2A and B.

DISPERSION OF THE STREAM AFTER PASSING
 THROUGH THE 1ST GAP FIG. 9.2A.



These two points are either secondary stagnation points as suggested in section 7.7 or it is possible that the point of breakaway oscillates between the limits of 110° and 150° thus creating a stagnation point at 150° .

9.2 The dispersion of the stream after passing through the gap.

As previously outlined the main characteristics of the flow pattern upstream of the first gap are, on the one hand, an inviscid flow occupying most of the space, and, on the other, a thin boundary layer close to the tube surface where the motion is retarded by viscosity. The main picture consists of a free flowing stream together with a very restricted area in which frictional effects are confined.

Downstream of the gap there exists a very different state. In the first place, the main stream separates from the wall leaving a dead water region between it and the wall. The surfaces of discontinuity between the stream and the dead water region are unstable and break up into a series of eddies which lead to considerable mixing between the stream and the adjacent dead water. The zones within which the mixing occurs spread out rapidly and are of an altogether larger magnitude than the somewhat analogous

upstream boundary layer.

Tollmien⁽¹⁾ has applied Prandtl's momentum transport theory to such mixing zones and he deduces the velocity distributions within them both longitudinally and transversely.

The case considered by Tollmien is for a jet issuing into a still fluid of unlimited extent. His results while giving the forms of the velocity distributions require the addition of an empirical coefficient before they can be used to predict numerical results.

From Prandtl's statement that the shear stress = $\rho \ell^2 \left(\frac{du}{dy}\right)^2$ where ℓ is Prandtl's "mischungsweg", Tollmien deduces that as seen in figure 9.2A, the mixing zone spreads out downstream in direct proportion to the distance from the origin O. Further he finds that the stream line which passes through the origin remains straight and is inclined outwards at a very small angle. The mixing zone is wedge-shaped but is not symmetrical about the axis of x. The divergence of the inner portion being half that of the outer portion.

The numerical value of these angles involves one experimental coefficient which, according to wind tunnel

(1) Tollmien W. z.fur angewandte Math.u.Mech. Vol.6 p.468 - 1926.

measurements at Gottingen, is $\frac{\ell}{x} = 0.0174$ where x is the distance downstream from the origin where mixing begins. Based on this value the breadths of the inner and outer zones are $0.085x$ and $0.170x$ respectively; while the stream line through the origin is inclined at an angle of 0.92° outwards towards the dead water region.

With regard to the value of the coefficient $\frac{\ell}{x}$ this in the present case is most readily determined from the location of the point P figure 9.2A where the mixing zone originating on one side of the stream meets that originating on the other side. The point P is clearly defined from the longitudinal total energy distribution figure 4.2 and is $2.27G$ downstream from the gap.

The origin for the mixing zone is somewhat indefinite since a boundary layer already exists at the gap. There will not be much error however if the mixing zone in the gap be assumed to be already as wide as the boundary layer at that point, viz. $0.0257 G$. The internal wedge angle is therefore $\tan^{-1} \frac{.4743G}{2.27G} = \tan^{-1} .209 = 11^\circ 48'$. Tollmien deduces that the tangent of this internal wedge angle is $\sqrt[3]{2C^2}$. (The external wedge angle is twice the internal angle and the total is approximately $3\sqrt[3]{2C^2}$)

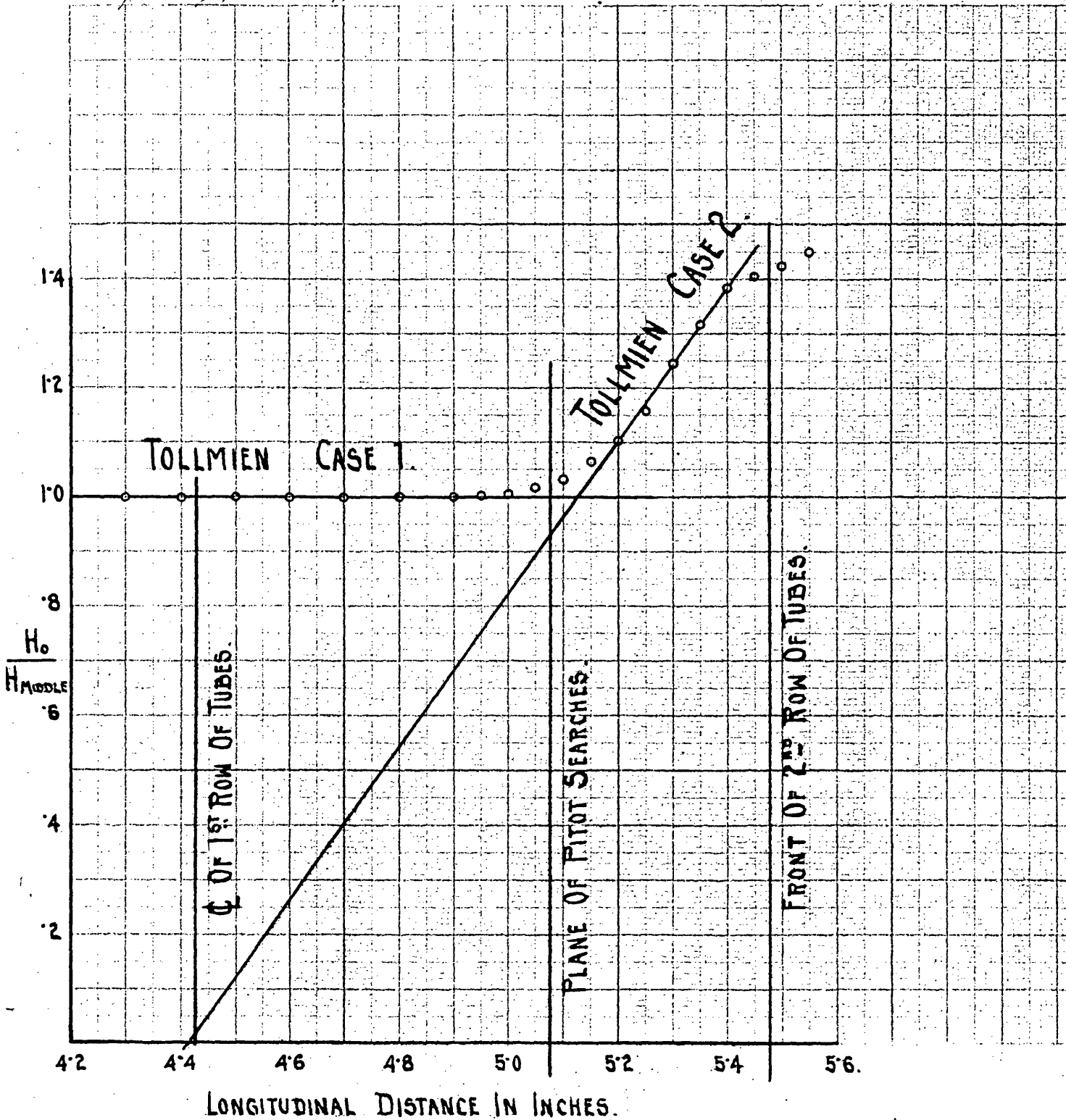
DISPERSION OF THE STREAM COMPARED WITH THE WORK OF TOLLMIEIN

FIG. 9'2 B.

Effective gap = 0.25" approx

Slope $\frac{\partial H_{11}/\partial h}{10} = \frac{1.4}{1/25} = 0.35$

cf. Gayed $\frac{\partial H_{11}}{\partial h} = 0.253$



Writing $\sqrt[3]{2C^2} = .209$, $2C^2 = .00913$ and $C = 0.0681$.
 In comparison with this Tollmien, from measurements at the edge of an open jet wind tunnel, found $C = 0.0174$.

The coefficient "C" defines the "mischungsweg" " ℓ " in terms of the distance "x" from the origin thus:- $\ell = Cx$.
 So in comparison with Tollmien's results the mixing length in the nest is approximately four times as great, due no doubt to the large disturbances already existing in the dead water region at the rear of the tubes.

In figure 9.2B the ratio of the total energy in the original stream divided by the total energy along the centre line of the gap has been plotted. From this it is seen that the transverse velocity distribution shown in figure 3.1C was taken at a section where the flow is just changing from Tollmien's first case of a homogeneous air stream issuing into air at rest to that of his second case of a spreading stream issuing from a narrow slit. Actually the present problem approximates far more closely to the first one since it is only at the centre of the jet that interference from the two sides of the jet can have taken place. Tollmien's second case is in fact developed on the basis of an infinitely small jet or alternatively for infinitely great distances from a slit of finite dimensions. For this reason the second case can hardly be expected to apply.

The transverse velocity distribution at the section midway between the first and second rows of tubes has therefore been compared with Tollmien's case 1. Using the above value for the coefficient "C" the velocities are given in table 9.2 and shown in the right hand bottom corner of figure 3.1C. The full line shows Tollmien's velocity distribution and the test points give the observed velocities after correction for Pitot tube shift.

It will be seen that over the inner part of the jet there is very satisfactory agreement except near the centre line where the observed velocities are low in comparison with the theory. Here a difference is to be expected because the two mixing zones have already coalesced and the central filaments are subjected to the effects of mixing from both sides. The slight lack of symmetry noticeable in this figure is without significance and represents a displacement of only 0.02 Cm.

Towards the outer edges of the jet there is naturally a considerable discrepancy between the Tollmien curve and the experimental points. This is due to the fact that the theory is based on the assumption that the jet issues into a quiescent fluid of unlimited extent. The negative velocities and the turbulence in the dead water region have no counterpart in the theory.

9.3 Comparison of the shape of the form drag diagrams of the first and subsequent rows of tubes.

Again considering figure 5.2F there is a marked difference in the distribution of pressure on the front of the second row of tubes, i.e. the rear boundary of the first dead water region. In taking the records of this distribution of pressure the manometer fluctuated by as much as $0.05 \rho V_{N.\max}^2$ and this despite considerable damping.

Figure 5.2C shows a typical form drag diagram. The two curves on the diagram indicate the magnitude of the pressure variations which appeared to have no definite periodicity. The fluctuations in pressure were approximately five times as great as those observed on the front of tubes of the third row, e.g. figure 5.2D. and ten times as great as the majority of the pressure readings.

Apart from this, there is a very noticeable region of reduced pressure in the vicinity 0° . All other rows are consistent in showing a maximum pressure in this region whereas on the second row the maximum pressures occur at 30° and 330° .

The experiments in the Ahlborn tank showed clearly how such a pressure distribution could arise. Figure 7.3B shows the main stream curving round towards the cylinder to

form an eddy and at the same time giving rise to a stagnation point at 40° in this particular instance.

In some cases this type of flow pattern is occurring simultaneously at both sides of a dead water region but more usually the stagnation point would occur first on one side and then on the other at irregular time intervals. This process explains both the observed instability of the pressure readings and the presence of two maxima at 30° and 330° . The aluminium dust experiments while thus explaining the shape of the form drag curve for the second row of tubes, raise a serious difficulty, since all the photographs obtained consistently show that these motions, while noticeable in the first dead water region, are progressively more marked in the second and subsequent regions, whereas the form drag curves for the third and fourth rows do not give the same indications or if they do, only a lesser degree.

It is probable that the more rapid movements of the stream found in subsequent rows lead to rapid movement of the stagnation points over the whole of the front of the tube and not over limited arcs from 20° to 40° and 320° and 340° .

This is associated with a later breakaway of the boundary layer and accordingly the main streams tend to diverge

away from the gaps and converge on to the centre line of the tube. This is illustrated on figure 9.1.

The large differences in the shape of the form drag curves for the first and second rows and the accompanying differences in energy dissipation is further explained by the fact that the stream as it approaches the first row of tubes is in a relatively undisturbed state. Under these conditions wind tunnel tests of isolated cylinders show that the boundary layer maintains a stream line formation up to approximately 90° at which point separation occurs and consequently there can be little rise in pressure further round the cylinder.

Fage⁽¹⁾ has shown that at a sufficiently high Reynolds' number (200,000) the disturbances present in most artificial wind streams are sufficiently great to cause the motion in the boundary layer to become turbulent before the point of breakaway. This renders it possible for the boundary layer to receive new energy from the main stream and so enable it to flow round the cylinder considerably beyond 90° . In this way the pressure at the rear of the cylinder is much greater and the drag coefficient falls from 0.6 to 0.2.

(1) Fage R. & M. 1179, 1929.

Fage and Warsap⁽¹⁾, by placing slight irregularities on the surface of the cylinder, were able to produce this effect at Reynolds' numbers as low as 70,000.

In the present experiments the Reynolds' number based on $V_{N.max}$ is 35,000 and the above effect could not be expected in connection with the first row of tubes.

The passage of the air over the first row creates an extremely high degree of turbulence in the stream, with the result that subsequent rows exhibit phenomena normally associated with higher Reynolds' numbers.

In support of the view that variation in the initial disturbances in the stream from row to row could have such a marked effect, it is enlightening to consider the results of sub-section 5.8. In these experiments a piece of perforated zinc placed at the inlet of the nest caused a reduction in form drag on the first row of tubes of 7.5%.

9.4 Pressure recovery after the constrictions and the point of breakaway.

From figures 5.2F and 9.1 it is seen that the pressure recovery at the rear of the first tube is $0.05 \rho V_{N.max}^2$.

(1) Fage, A. and Warsap, J.H. R.& M. 1283 - 1929.

This recovery is greatly increased in all subsequent rows, becoming approximately $0.40 \rho V^2_{N.\max}$ in the later rows of tubes.

This recovery is undoubtedly associated with the point of breakaway of the main stream from the tube surfaces, and a calculation was made of the theoretical position of breakaway assuming that the whole of the pressure recovery at the rear of each tube was due to the deceleration of the main streams after passing the point of maximum constriction⁽¹⁾. These are given in the third column of the table below.

| After | Recovery as % of $\rho V^2_{N.\max}$ | Position of Breakaway | | | |
|-----------|--|---|--------------|---------------------------------|--------------------------|
| | | as computed from pressure recovery. | From Fig.9.1 | | From soot deposit. |
| | | | Point B | Point of Contra- flexure. | |
| 1st Row | 5.28 | $98\frac{1}{2}^\circ$ | 92° | 95° | 100° |
| 2nd " (a) | 47.65 | 122 | 117 | 110 | 122 |
| 2nd " (b) | 43.00 | $119\frac{1}{2}$ | | | |
| 3rd " | 41.93 | 119 | 109 | 114 | (117) |
| 4th " | 38.00 | 117 | 112 | 118 | (111) |

With regard to the second row the pressure recovery can be expressed as a proportion of the pressure on the face of the tube at 0° or as a proportion of the maximum pressure which occurs at 30° . These are recorded as (a) and (b) in the above tables.

(1) See appendix No.5.

It is interesting to compare the above estimation of the points of breakaway with the indications of these important points as ascertained from other parts of the work. In figure 9.1 a crude estimate may be made from the point of separation of the full line pressure curve and the dotted hypothetical expansion curve as suggested in sub-section 9.1. These are shown in column 4 of the above table. The points of contraflexure of the pressure curves in figure 9.1 may give even a better indication of the points of breakaway and these have been given in column 5.

The deposition of dust and soot as described in section 12 gave additional evidence of the point of breakaway. The indications from this source are included in the last column, the figures in brackets are the result of only one observation and are therefore not as reliable as the remainder of the data.

It is interesting to note that these values for the point of breakaway do not entirely comply with the Karman-Pohlhausen expression

$$\frac{dU}{dx} \cdot \frac{\delta^2}{v} \longrightarrow - 12$$

According to the above table breakaway on the first row occurs between 92° and 100°. The corresponding values of

δ were computed by the Blasius method up to 90° and subsequently extended by steps of 2 degrees using the Karman-Pohlhausen method (Howarth's equation 3.23). The values of $\frac{dU}{dx}$ were obtained from figure 8.7 and the results are shown below:

| Angle | $\frac{dU}{dx}$ | δ | $\frac{dU}{dx} \cdot \frac{\delta^2}{\nu}$ |
|-------|-------------------------|------------|--|
| 92 | - 870sec. ⁻¹ | 0.0173 Cm. | - 1.8 |
| 95 | -1200 | 0.0186 | - 2.86 |
| 100 | - 950 | 0.0212 | - 2.95 |

The maximum value in the last column is of the order - 3 instead of the - 12 deduced by Pohlhausen. Some discrepancy would not be surprising since the velocity gradients were obtained by differentiation of an experimental curve with points at 10° intervals. It is difficult however to think that this cause alone is sufficient to explain the discrepancy. It could be explained on the assumption that the value of δ at 90° given by the Blasius method was erroneously small but again there appear to be no grounds for believing this. In which case one is forced to conclude that the experimental points, representing as they do the time average, yield values for $\frac{dU}{dx}$ which are markedly less than the instantaneous values.

9.5 Form drag diagrams in their relation to one another

9.51 Distribution of kinetic energy throughout the nest.

When considering the form drag diagrams in their correct relation to one another, i.e. when plotted to a common pressure

datum, as in figure 5.2F, the most striking feature is that the highest pressure on the second, third and fourth rows exceeds the minimum pressure on the first row. And further, so far as the second and third rows are concerned, the maximum pressure exceeds very considerably that on the rear of the first row.

This demonstrates clearly that a considerable proportion of the kinetic energy existing at the first constriction passes through subsequent constrictions.

It is seen that the pressure and therefore the total energy at the front of the second and subsequent rows of tubes exceeds appreciably the pressure energy in the preceding dead water region. It is clear, therefore, that the major portion of the stream flows with but little reduction in velocity.

9.52 Estimation of the velocity in the eddies at the rear of the tubes.

There is also an unexpectedly large difference of pressure between the back of one row and the front of the subsequent row. The magnitude of this is seen to be of the order of $0.2 \rho V_{N.\max}^2$ corresponding to a velocity of the order of $0.45 V_{N.\max}$.

Except on the line of symmetry, where the average shear force is zero, this figure cannot be accepted as the

actual velocity within the eddy, since part of the forces due to these pressures is balanced by the shear forces in the fluid. Nevertheless $0.45 V_{N,max}$ must give a good indication of the velocities which exist in the eddy region.

In comparison the Ahlborn tank experiments section 7.6, carried out at the lower Reynolds' number of 1,500 indicated space average eddy velocities at a particular instant of from $0.1 V_{N,max}$ to $0.34 V_{N,max}$. It should be remembered that ⁱⁿ ~~the~~ Ahlborn experiments the length-breadth ratio of the tubes was much shorter than in the nest, therefore the end damping effect would be much greater.

Again the Pitot tube search carried out behind the first row of tubes and restricted to one particular plane (see figure 3.1C) gave a maximum velocity in the upstream direction of approximately $0.38 V_{N,max}$:

It is probable that the form drag pressure measurements give the best indication and that the time average of the maximum upstream velocity within the eddies is not far from $0.45 V_{N,max}$.

9.53 Recovery of pressure after passing the last row of tubes.

Figure 5.2F shows a remarkably high pressure recovery subsequent to the last row of tubes. The pressure at the

outlet of the nest is $0.36 \rho v_{N,max}^2$ greater than the minimum pressure at the last constriction: the pressure downstream of the nest does not differ materially from that at the rear of the third row and is $0.13 \rho v_{N,max}^2$ greater than that at the rear of the last row. That is to say the loss of energy after the jet issues from the last constriction is only about 30% of its initial kinetic energy.

The figure is worthy of note when it is remembered that a loss of 15% is quite normal in well designed turbine draught tubes and Venturi meters.

9.6 Dissipation of energy in the dead water region.

The rate at which energy is being dissipated in the dead water regions can be assessed by considering the rate at which energy passes through any successive pairs of gaps.

With regard to the first row the kinetic energy per unit volume is approximately $\frac{1}{2} \rho v_{N,max}^2$. The precise value is somewhat in excess of this since the velocity is not uniform across the gap, but this effect does not exceed 1 or 2% and is neglected.

Since the mean velocity through the second gap is equal to that in the first gap and the velocity distribution is not greatly dissimilar the kinetic energy may be regarded

as passing away through the second gap at precisely the same rate at which it flows in through the first gap. The pressure however differs considerably in the two gaps and from figure 4.2 it is seen to be $0.1673 \rho V_{N.\max}^2$. The volume flowing per unit time is $V_{N.\max} \times G$ where G = width of gap, whereas the volume of the dead water region is $(p_e \times d) - \frac{\pi d^2}{4}$ where " p_e " is the longitudinal pitch and " d " the diameter of the tubes. Thus the rate at which energy is being dissipated per unit volume of dead water region is:

$$\frac{0.1673 \rho V_{N.\max}^2 \times V_{N.\max} \times G}{p_e d - \frac{\pi d^2}{4}}$$

with the open parallel spacing used $G = 0.648 \text{ Cm.} = 0.5105d$
 in experiment figure 4.2 $p_e = 3.300 \text{ Cms.} = 2.600 d$

Therefore energy dissipated
 per c.c. of dead water region = $0.0470 \frac{\rho V_{N.\max}^3}{d}$ Cm. dynes
 per sec.

In succeeding dead water regions the rate of dissipation is found to be somewhat greater although of the same order viz. $0.0627 \frac{\rho V_{N.\max}^3}{d}$ and $0.0551 \frac{\rho V_{N.\max}^3}{d}$ Cm. dynes per sec.

With regard to the last row it is impossible to give a comparative figure for the reason that the dead water region is indefinite in area and extends far down the stream.

The figures given above include in each case the losses of the boundary layer of the downstream half of the tube and to this extent they are over-estimates but the tangential losses are small and do not materially effect the figures given.

From another point of view also, the figures are over-estimates for they are based on the assumption that the energy is being dissipated in the dead water region alone and not in the main stream itself. In actual fact a considerable dissipation occurs in the main stream, i.e. in fluid which has not actually passed into the dead water region and subsequently returned to the main stream.

The fact remains that it is the motions within the dead water region which cause the major portion of the loss and thus it is not unreasonable to state this loss in terms of the volume of the dead water.

With regard to variation of dissipation from row to row it is very noticeable that the first and second rows differ materially from the third: the first row showing 14.5% less and the second row 14.0% greater than the third row.

As far as the first dead water region is concerned this difference cannot be regarded as due to errors in

SHEAR STRESSES ON DEAD WATER REGIONS.

FIG. 9.7.

PARALLEL ARRANGEMENT

$$\frac{V_{n, \max} d}{\nu} = 35,000.$$

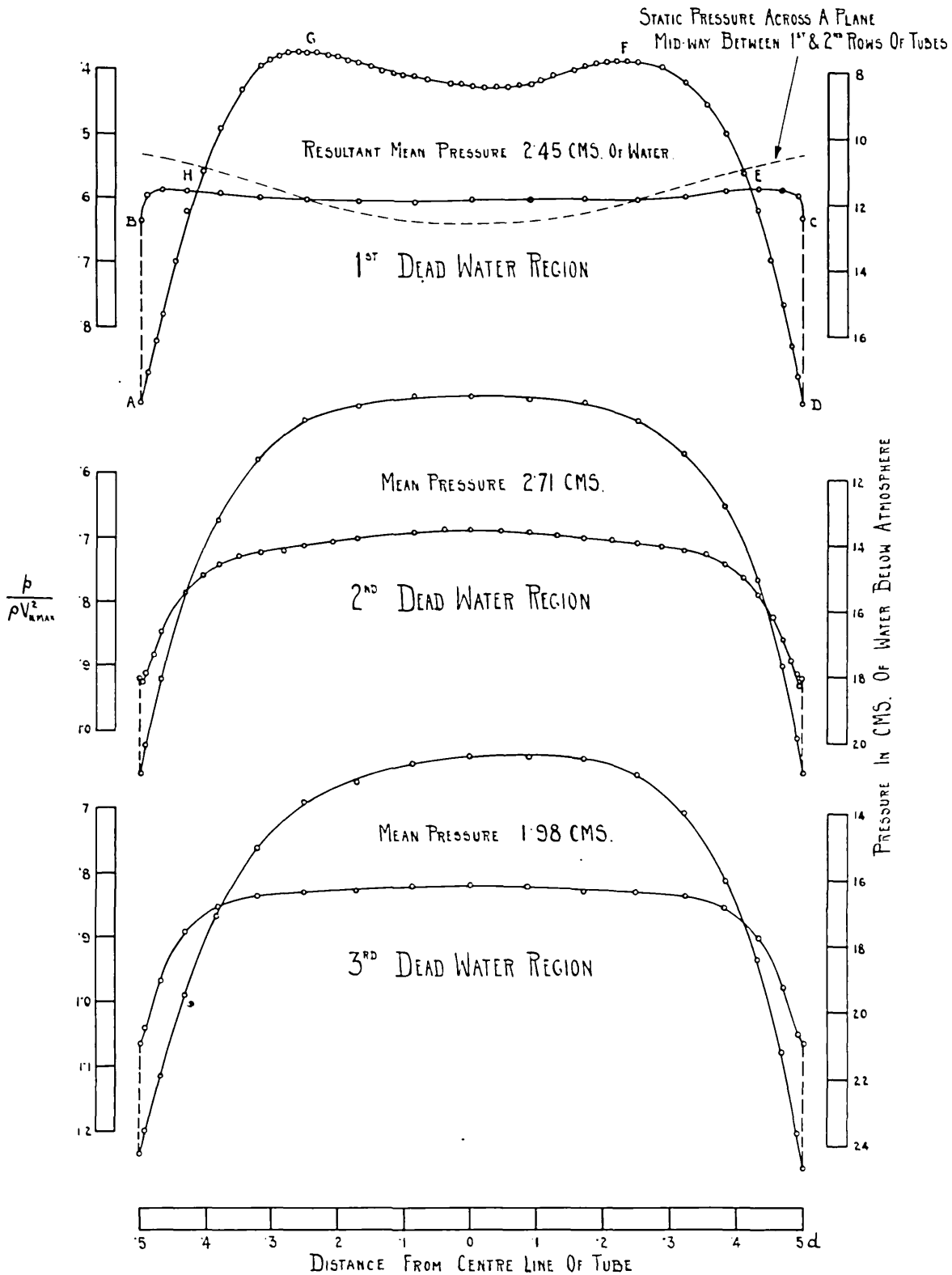


figure 4.2 since there is ample evidence to be found in the form drag diagrams showing that the motion following the first row is characteristically different from that of later rows.

9.7 Shear stresses on dead water region.

The dead water region has the form of a parallelogram bounded at the ends by the downstream and upstream cylindrical faces of the adjacent tubes: Figure 9.7 is obtained from figure 5.2F and shows the pressures on the dead water regions. The total forces acting on this region are obtained by integrating the area A B C D E F G H A. The resulting force is balanced by shear stress existing on the two parallel sides A B and D C.

The numerical values of the forces on the several dead water regions are expressed most conveniently as shear forces \bar{T}_{dw} . These again are reduced to pure numbers by comparing them with $\rho V^2_{N,max}$ thus forming dimensionless numbers $\frac{\bar{T}_{dw}}{\rho V^2_{N,max}}$.

The values obtained for the three dead water regions are given in the table.

| Dead water region No. | τ_{dw} dynes per sq. cm. | $\frac{\tau_{dw}}{\rho V_{N,max}^2}$ calculated from figure 9.7 | $\frac{\tau_{dw}}{\rho V_{N,max}^2}$ Estimated from the work of Fage |
|--------------------------|-------------------------------------|---|--|
| 1 | 462.5 | 0.024 | 0.02 |
| 2 | 511.5 | 0.027 | |
| 3 | 373.6 | 0.019 | |

It is interesting to compare these with the work of Fage⁽¹⁾ on the microscopic examination of specks of dust in water flowing through a smooth pipe. He found a relation between shear stress and variation from mean velocity caused by the turbulence of the order of

$$v' = 6.8 V_{\bar{x}} \text{ where } V_{\bar{x}} \text{ is defined as } \sqrt{\frac{\tau_{dw}}{\rho}}$$

In the present experiments figure 3.1C shows that the mean velocity on the planes A B and D C is of the order of 3000 Cms. per sec., i.e. 0.75 $V_{N,max}$.

No information is available as to the maximum instantaneous velocity on these planes but a fair estimate can be made of the minimum value. The photograph 7.3 B shows that the longitudinal velocity component certainly drops to zero and probably attains negative values of perhaps 0.2 $V_{N,max}$. Thus there are grounds for thinking

(1) Fage, A. Phil.Mag. Vol.21, p.80. 1936.

that the turbulence component is of the order of $0.95 V_{N.\max}$ or 1.27 of the mean velocity in this plane.

Thus according to Fage's relation

$$v' = 6.8 V_{\bar{x}} = 0.95 V_{N.\max}$$

Therefore $V_{\bar{x}} = 0.14 V_{N.\max}$

$$\text{and } \sqrt{\frac{\bar{\tau} dw}{\rho V_{N.\max}^2}} = 0.14$$

$$\text{Therefore } \frac{\bar{\tau} dw}{\rho V_{N.\max}^2} = 0.02$$

It is extremely interesting to find that this application of Fage's work in smooth pipes does predict the shear stress in a complicated arrangement such as a nest of tubes.

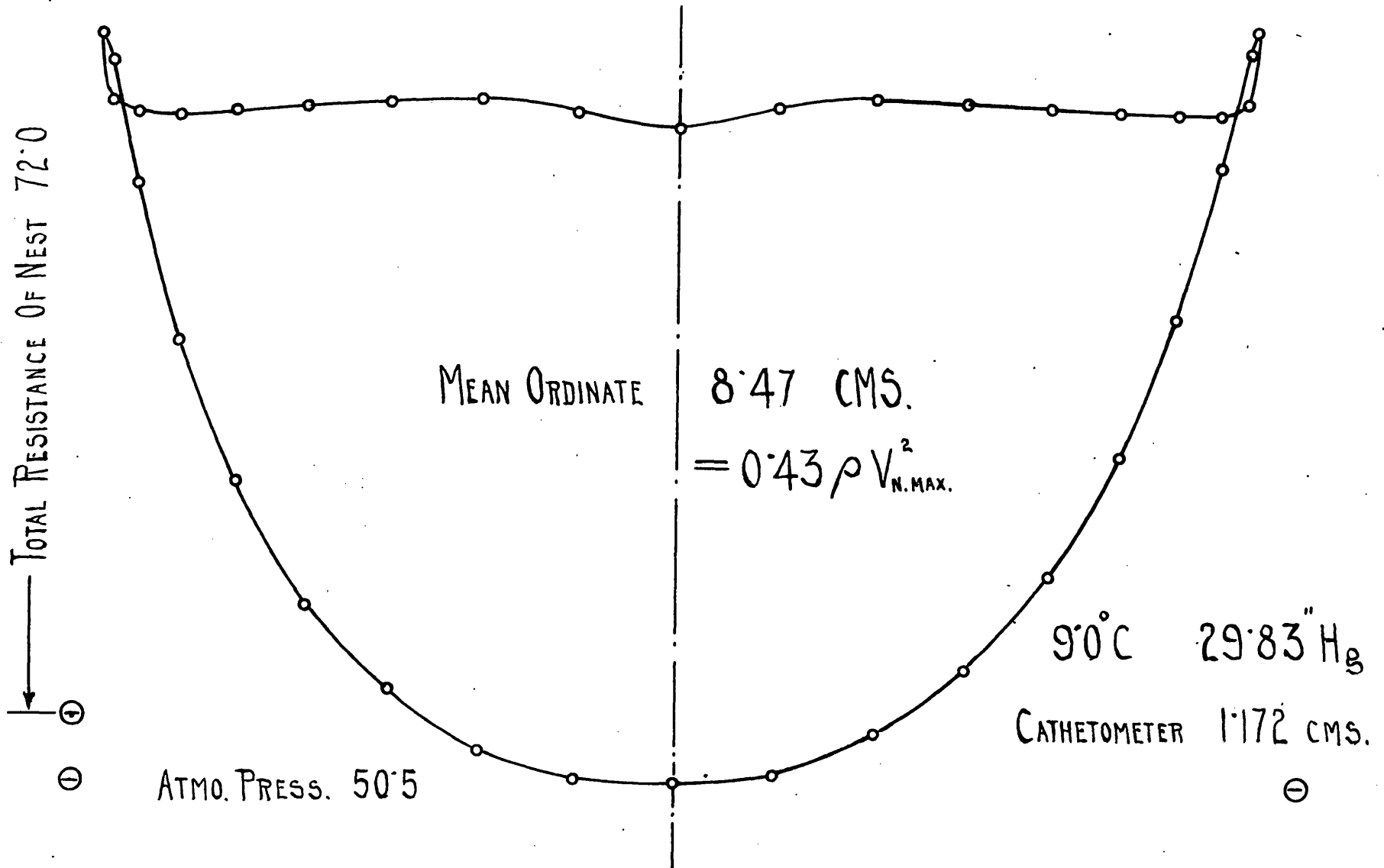
FORM DRAG WITH CONSTANT AIR VELOCITY

FIG. 10.1A.

STAGGERED ARRANGEMENT

1ST ROW CENTRE TUBE

1/2" FROM BACK WALL.



FORM DRAG WITH CONSTANT AIR VELOCITY.

FIG. 10'B.

STAGGERED ARRANGEMENT.

2ND ROW NEXT ABOVE &

1 1/2" FROM BACK WALL.

TOTAL RESISTANCE OF NEST 72.2

⊖

ATM. PRES. 50.45.

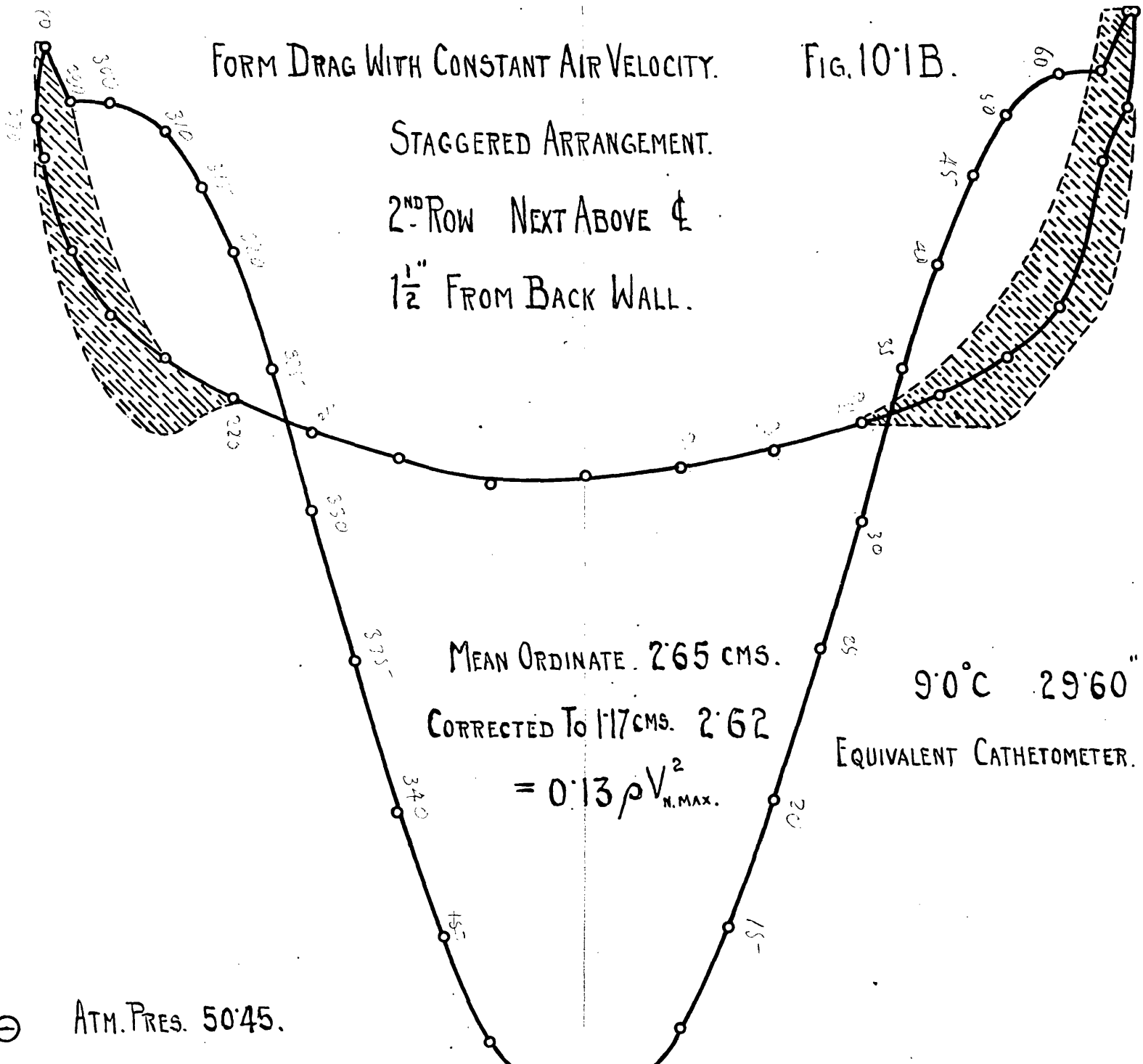
MEAN ORDINATE. 2.65 CMS.

CORRECTED TO 1.17 CMS. 2.62

$$= 0.13 \rho V_{N.MAX.}^2$$

9.0°C 29.60" Hg.

EQUIVALENT CATHETOMETER. 1.183 CMS.



FORM DRAG WITH CONSTANT AIR VELOCITY

FIG. 10'1 C.

STAGGERED ARRANGEMENT.

3RD ROW

CENTRE TUBE

1/2" FROM BACK WALL

TOTAL RESISTANCE OF NEST 68.17

ATM. PRES. 46.3

MEAN ORDINATE 3.34 CMS.

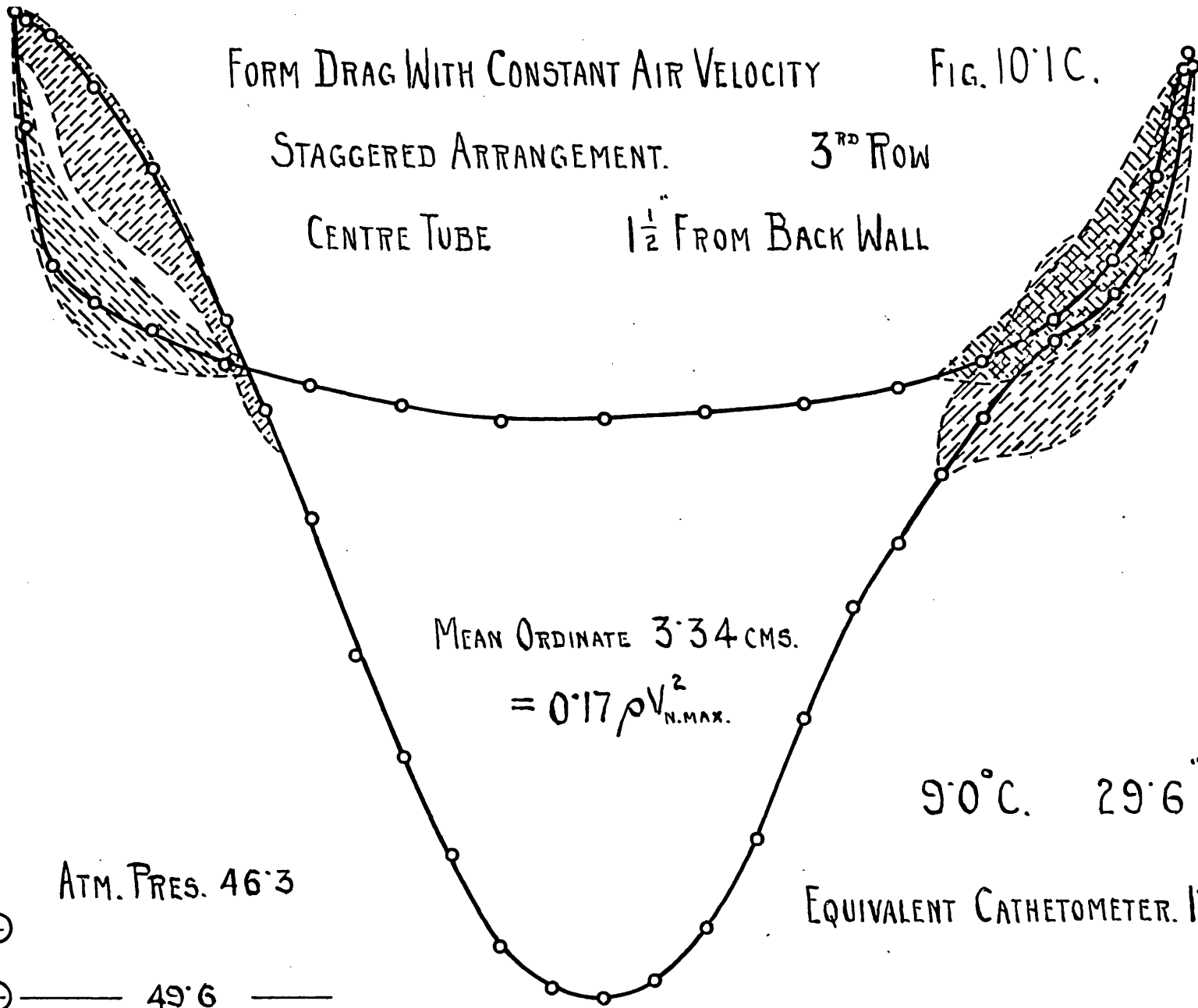
$$= 0.17 \rho V_{N.MAX.}^2$$

9.0°C. 29.6 Hg.

EQUIVALENT CATHETOMETER. 1.172 CMS.



49.6



FORM DRAG WITH CONSTANT AIR VELOCITY.

FIG. 10'1 D.

STAGGERED ARRANGEMENT.

4TH ROW.

TUBE NEXT ABOVE ϕ

$\frac{1}{2}$ " FROM BACK WALL

TOTAL RESISTANCE OF NEST

MEAN ORDINATE 3.87 CMS.

CORRECTED TO 1.17 CMS. 3.93.

$$= 0.20 \rho V_{N.MAX.}^2$$

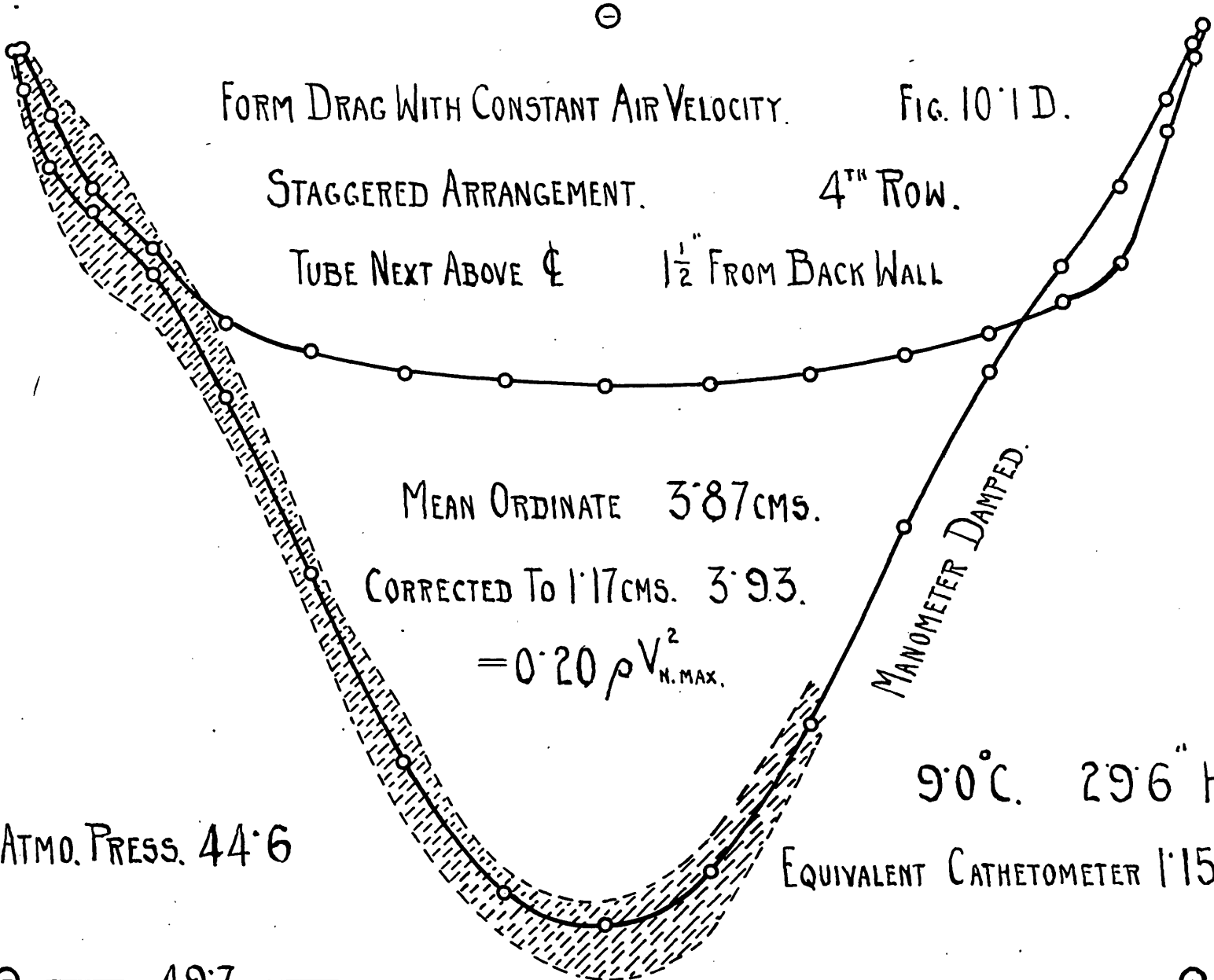
MANOMETER DAMPED.

ATMO. PRESS. 44.6

9.0°C. 29.6" Hg.

EQUIVALENT CATHETOMETER 1.15 CMS.

— 49.7 —



FORM DRAG WITH CONSTANT AIR VELOCITY.

FIG. 10-1 E.

STAGGERED ARRANGEMENT

5TH ROW

CENTRE TUBE

1 1/2" FROM BACK WALL.

TOTAL RESISTANCE OF NEST.

MEAN ORDINATE 3.70 CMS.

CORRECTED TO 1.17 CMS 3.76 CMS.

$$= 0.19 \rho V_{N.MAX.}^2$$

9.5°C 29.60" Hg.

ATMO. PRESS. 41.8

EQUIVALENT CATHETOMETER 1.15 CMS.

50°0

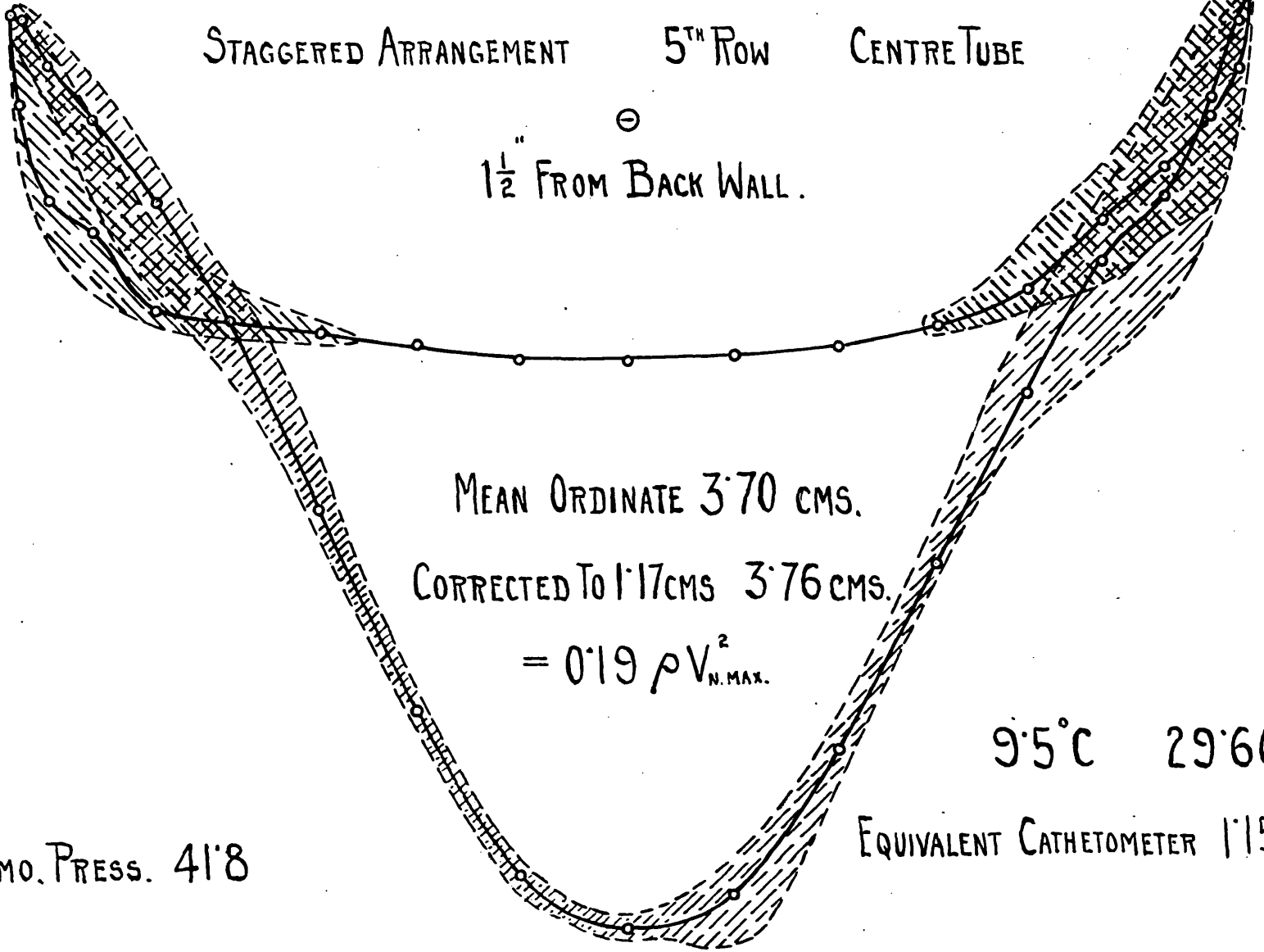
○

○

○

○

○



FORM DRAG WITH CONSTANT AIR VELOCITY.

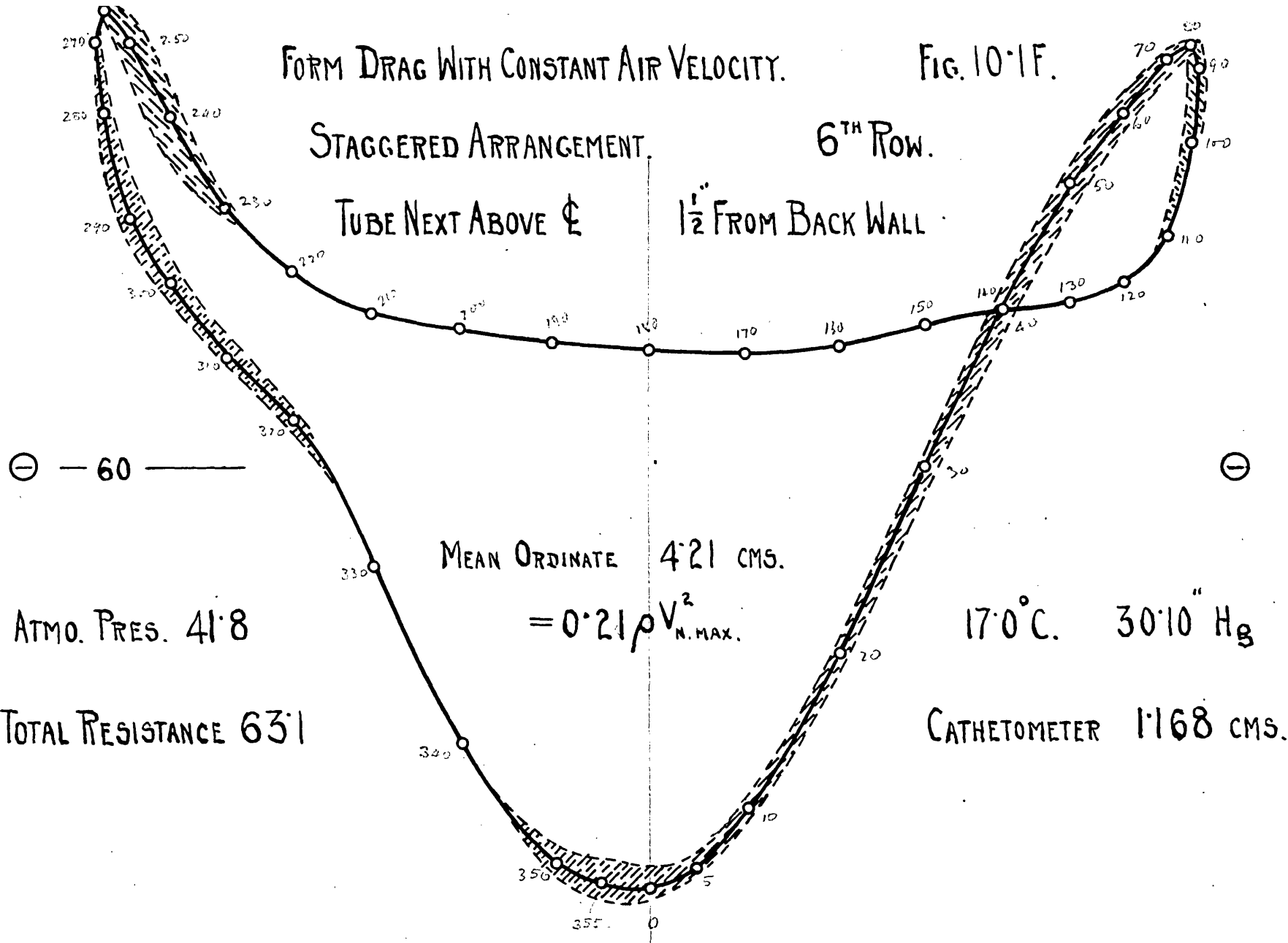
FIG. 10-1F.

STAGGERED ARRANGEMENT.

6TH ROW.

TUBE NEXT ABOVE ϕ

1/2" FROM BACK WALL



FORM DRAG WITH CONSTANT AIR VELOCITY.

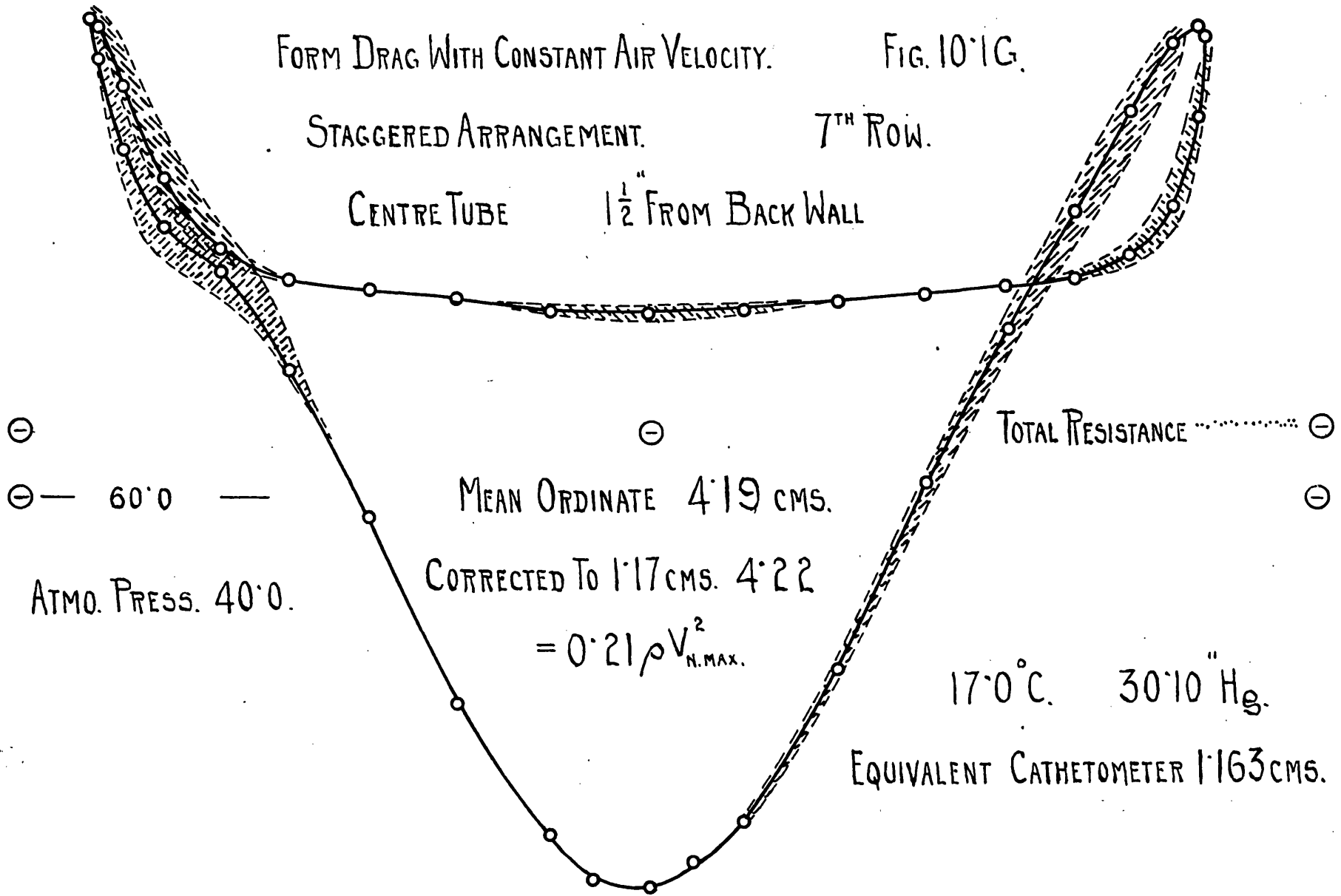
FIG. 10'1G.

STAGGERED ARRANGEMENT.

7TH ROW.

CENTRE TUBE

1/2" FROM BACK WALL



10. INTERPRETATION OF THE RESULTS OF THE
STAGGERED ARRANGEMENT AND COMPARISON
OF THE TWO ARRANGEMENTS.

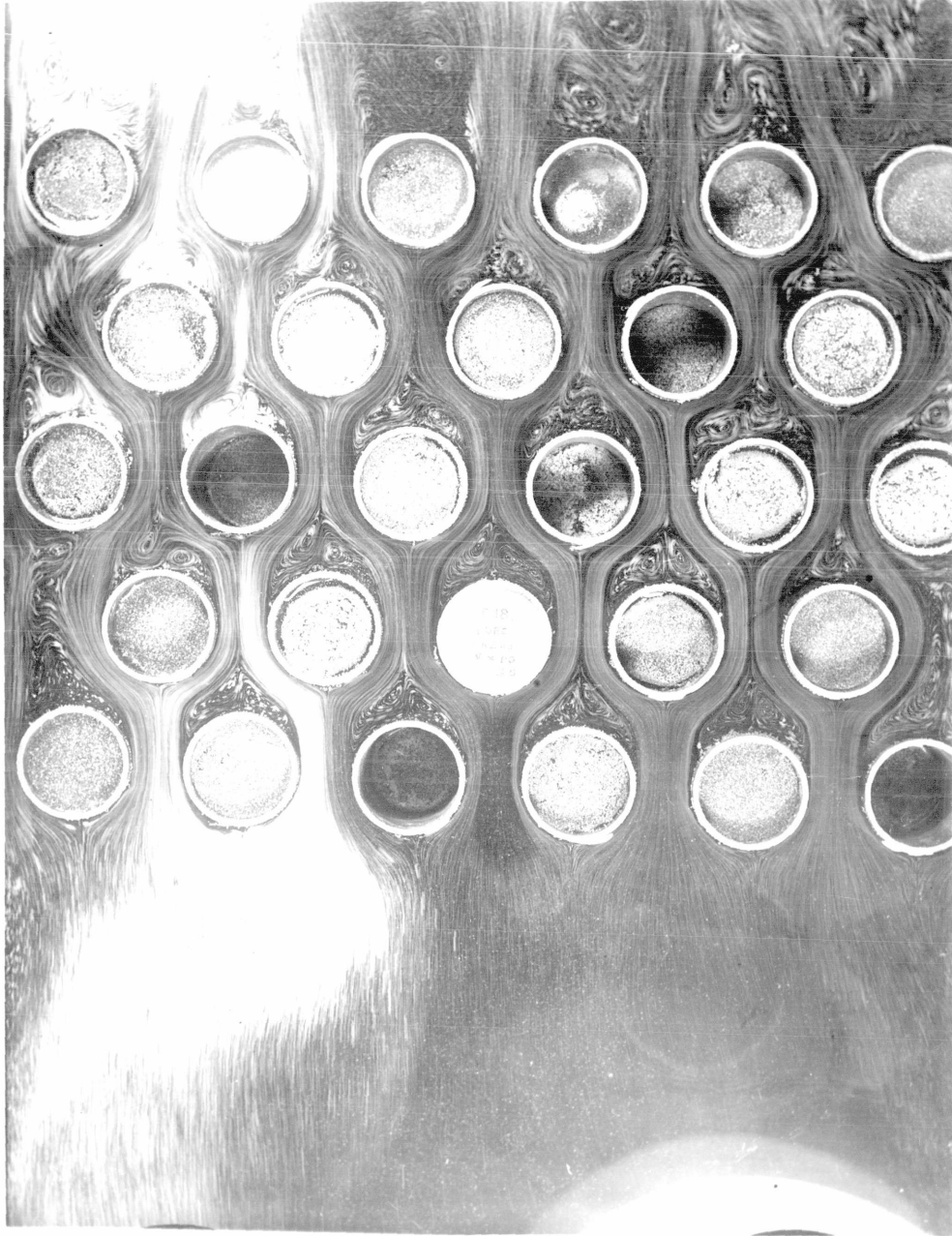
10.1 Comparison of form drag diagrams.

The outstanding feature of the staggered arrangement is again the anomalous behaviour of the first and second rows. The form drag diagrams figures 5.2G and 10.1 A and B show this most clearly.

The diagram for the first row has an area of approximately twice that of subsequent rows. The cause of this is twofold. On the upstream face of the first row the pressure distribution is almost identical with that found in the parallel arrangement whereas in the second and subsequent rows the presence of the two adjacent tubes of the previous row causes much lower pressure in the region from 10° to 70° . The breakaway at the rear of the first tube appears to be a shade later than in the parallel arrangement. But the difference is so small that it only shows what little influence the location of the later tubes has upon this important phenomenon.

The second row is anomalous in the lowness of the pressure at 90° , which taking 0° as datum, is nearly 50% lower than the first row or 25% lower than subsequent rows.

FIG. 10'1.



The cause of this appears to be due to the relatively large form drag of the first row. This must be associated with a wake of low energy. The stream as it passes the constriction of the second row contains a central core of fluid moving at low velocity, thus reducing the effective width of the gap and increasing the speed of the two parts of the main stream adjacent to the second tube. This is seen clearly in figure 10.1. The magnitude of the effect is obviously linked closely with the magnitude of form drag since the latter only exists by virtue of the shedding of vorticity. Unless the dead water region is losing low energy fluid the pressure there, will build up until eventually the pressure on the rear of the tube is equal to that on its upstream face, with consequent disappearance of form drag. In the nest of tubes one visualises each tube as shedding a stream of low energy fluid - large in the case of the first tube - small for the second tube and normal for the rest.

Incidental to the low pressure at and before 90° , the diagram exhibits two large negative loops which reduce greatly the total drag on the second row. Pressure recovery at the rear of this tube is good, being about 43% of the drop from 0° to 90° , a result numerically similar to that for the parallel arrangement.

Since the pressure at 0° is atmospheric there can be no doubt that this tube is fed with undisturbed fluid and yet its breakaway characteristics are those of a tube in a highly degraded stream. This is interesting for it shows that breakaway is controlled not so much by energy variations but rather by pressure fluctuations and that even when these originate at a considerable distance from the surface of the tube, they are still effective.

Of the remaining tubes, the fourth to seventh rows appear to be almost identical, indicating that after the first three rows the flow conditions attain a relatively constant state. The geometrical arrangement on the downstream side of the last row, of course, differs materially and some influence of this might have been expected but from the diagrams it is seen that the actual differences are very small.

The third row shows some influence of the abnormal first and second rows. Together these have a resistance well above the average and it is not surprising to find that the drag on the third row is correspondingly low.

In figures 10.1 B to G the extent of the pressure fluctuations has been marked on the various diagrams.

10.2 Loss of energy throughout the nest.

From figure 5.2G it is seen that the general pressure gradient through the nest as represented by the progressive downward displacement of individual form drag diagrams is relatively small compared with the pressure difference which exists in one diagram. For example, the pressure at 0° on the sixth row is actually greater than that at 180° on the first row. That is to say the average total energy in the region of the sixth row is still in excess of that in the dead water region at the rear of the first row. In short only about one sixth of the fluid passing is effectively degraded by each row.

10.3 Estimation of the tangential drag for the staggered nest

A perusal of figures 10.1B to G shows the considerable fluctuation of pressure which takes place at the sides of all the tubes except those of the first row. With such pressure fluctuations it is difficult to arrive at the true time mean average which is the determining factor in the form drag. Nevertheless it was considered advisable to make an estimation of the ratio of the sum of the form drags, to the total resistance of the nest.

From figure 5.2G it is seen that the uncorrected mean ordinate of the form drags are as follow:

| | | |
|---------|--------------|--------------------|
| 1st Row | 0.431 | $\rho V^2_{N.max}$ |
| 2nd " | 0.133 | " |
| 3rd " | 0.170 | " |
| 4th " | 0.200 | " |
| 5th " | 0.191 | " |
| 6th " | 0.215 | " |
| 7th " | <u>0.215</u> | " |
| | 1.555 | |

Therefore average mean ordinate = $0.2225 \rho V^2_{N.max}$.

From section 5.2 it is known that correction necessary to compensate for the size of the pressure hole is a reduction of the mean ordinate by 8.93%. Thus the corrected drag coefficient = $0.225 - 0.0199 = 0.2026$.

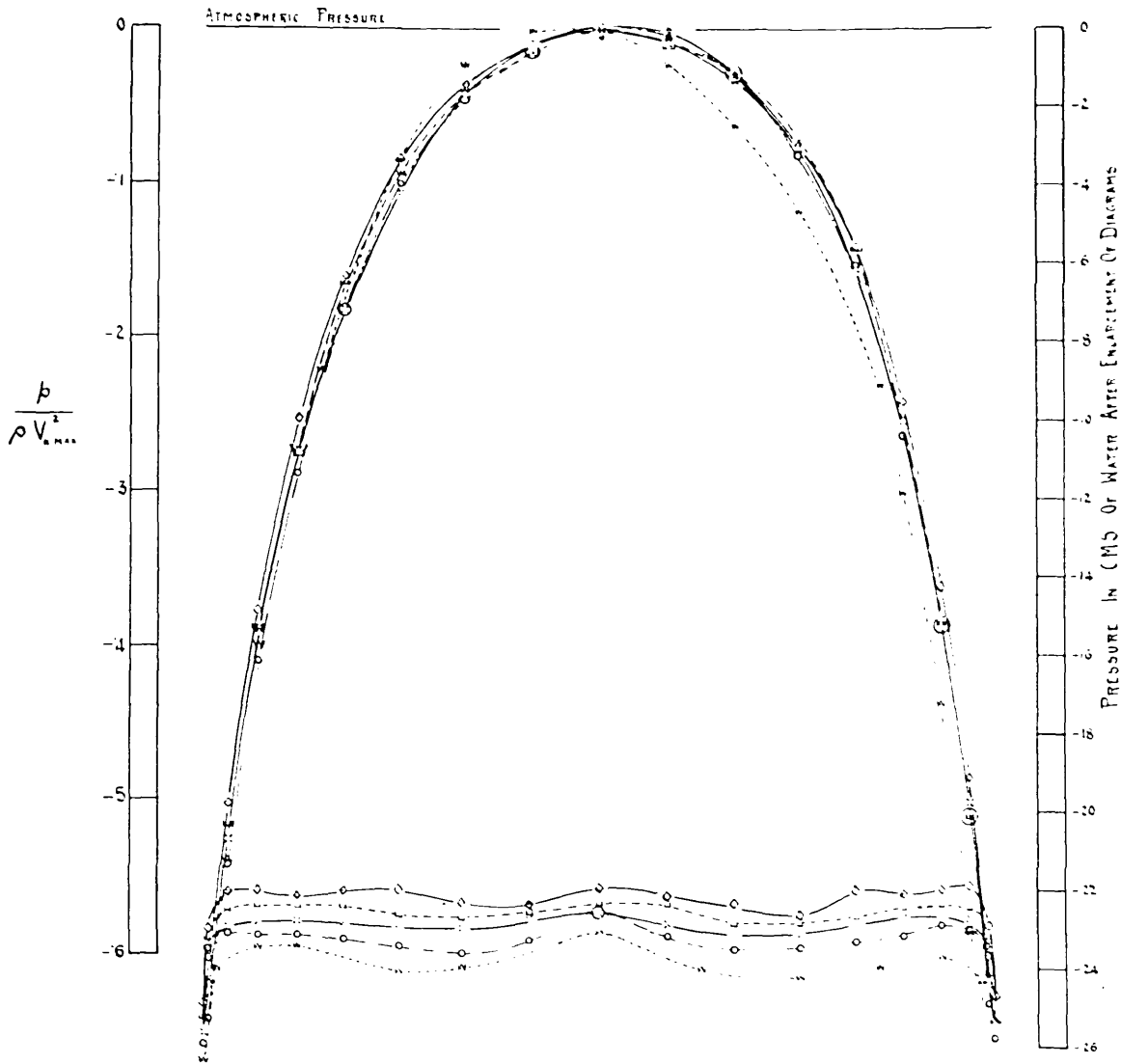
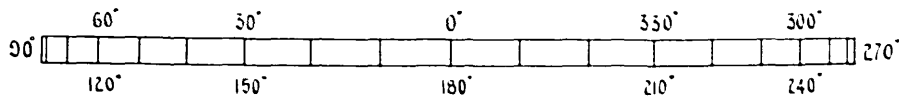
The Reynolds' number at which these form drag diagrams were taken was 34,800 and from figure 1.2B the coefficient of the total resistance of the nest to air flow at this Reynolds' number is seen to be 0.218.

$$\text{Therefore } \frac{\text{Form Drag}}{\text{Total Drag}} = \frac{0.2026}{0.218} = 0.93$$

Thus the form drag represents 93% of the total resistance and the tangential drag 7%

In comparing this estimate with the tangential drag of the parallel arrangement it should be remembered that this result is based upon seven typical form drag diagrams whereas the result of the parallel arrangement was calculated from eighty form drag diagrams.

DIAGRAMS ENLARGED TO CORRESPOND TO CATHETOMETER READING 2.34 CMS



| | $R_e = \frac{V_{max} d}{\nu}$ | MEAN ORDINATE $\bar{p} = 0.415 \rho V_{max}^2$ |
|--|-------------------------------|---|
| ◇ — CATHETOMETER READING 0.249 CMS | 15,650 | |
| □ — — — — — 0.321 " | 17,720 | = 0.417 " |
| × — — — — — 0.459 " | 21,220 | = 0.421 " |
| ○ — — — — — 1.179 " | 36,000 | = 0.428 " |
| W — — — — — WATER EXP ^T [EQUIVALENT C.R. 1.144] " | 16,750 | = 0.418 " |

10.4 Effect of speed on form drag diagram.

Diagrams were taken from the centre tube of the first row at Reynolds' numbers 15,630 to 36,000. These are shown plotted non-dimensionally in figure 10.4. The diagram is obtained by enlarging each of the separate diagrams until it corresponds to a cathetometer reading twice that of the standard, i.e. $2 \times 1.17 = 2.34$ Cms. of water. The diagrams are then superimposed so as to coincide at 0° . All the diagrams are remarkably similar in appearance and in fact the variation in mean ordinate lies between the limits of 0.415 and 0.428 $\rho V_{N,\max}^2$ with increasing speed. This result is interesting. It shows that the influence of Reynolds' number upon the coefficient of resistance of the nest as a whole is due almost entirely to the behaviour of those rows subsequent to the first. The first row is more analagous to an isolated cylinder.

10.5 Comparison of the form drag resistance of the first row of tubes with that of a single cylinder in a wind tunnel

The problem of an isolated cylinder in a wind tunnel and that of the first row of tubes in a nest are not geometrically similar and search must be made for some plausible basis of comparison. It is clear that the forces involved depend upon the flow pattern. This can be partially described by considering V_0 and V_{\max} . The latter has clearly the greater

influence and may perhaps rather crudely be taken as the basis of comparison.

With flow past an isolated cylinder at the speeds under consideration V_{\max} is approximately $1.5 V_0$ and it appears legitimate to use this value in computing corresponding Reynolds' numbers. Thus the range of $\frac{V_{N.\max} d}{\nu}$ of 15,000 to 36,000 in figure 1.2B (form drag for first row) may be compared with a range of $\frac{V_0 d}{\nu}$ of 10,000 to 24,000 for the isolated cylinder.

Data are available from Linke⁽¹⁾ who experimented in an open jet wind tunnel and from Relf's⁽²⁾ experiments in a closed wind tunnel as follows :-

| $\frac{V_{N.\max} d}{\nu}$ | Form drag coefficient | | | | |
|----------------------------|---|------------------------|-----------------------------|------------------------|-----------------------------|
| | Nest of Tubes First row $\frac{p}{\rho V_{N.\max}^2}$ | Isolated cylinder | | | |
| | | Linke | | Relf | |
| | | $\frac{p}{\rho V_0^2}$ | $\frac{p}{\rho V_{\max}^2}$ | $\frac{p}{\rho V_0^2}$ | $\frac{p}{\rho V_{\max}^2}$ |
| 15,000 | 0.4151 | 0.550 | 0.248 | 0.568 | 0.256 |
| 36,000 | 0.4285 | 0.597 | 0.269 | 0.590 | 0.266 |

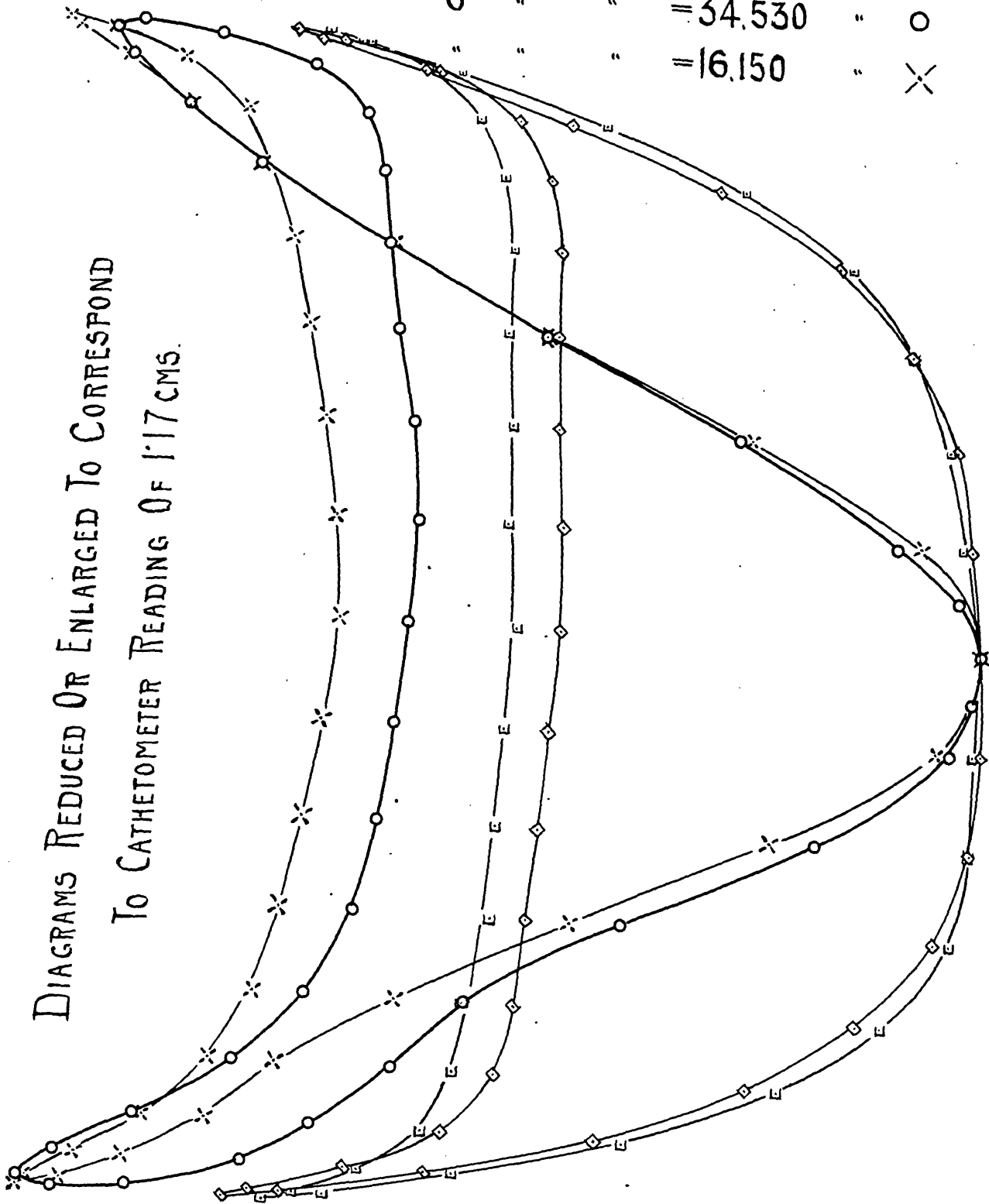
(1) Linke, W. Inaugural Dissertation. Leipzig (1931)

(2) Relf, E.F. R & M, 102, 1913-14, p.47.

COMPARISON OF FORM DRAGS AT VARYING AIR SPEED FIG. 10.6.

| | | | | |
|----------------------|---------------------|--------------------------|----------|---|
| PARALLEL ARRANGEMENT | 4 TH ROW | $V_{N, MAX. d} = 39,600$ | SHOWN | ◇ |
| " | " | " | = 21,100 | " |
| STAGGERED | 6 TH | " | = 34,530 | " |
| " | " | " | = 16,150 | " |

DIAGRAMS REDUCED OR ENLARGED TO CORRESPOND
TO CATHETOMETER READING OF 1.17 CMS.



It is seen that the values for the nest of tubes show the same tendency to increase with increasing Reynolds' number and further that they lie satisfactorily between the isolated cylinder values. They tend to lie closer to the V_0 values than might have been anticipated. This follows from the fact that on an isolated cylinder the upstream half experiences very little force whereas with a row of adjacent cylinders there is a definite upstream force exerted on the upstream half.

10.6 Influence of speed on the later rows.

Two typical diagrams taken at Reynolds' numbers of 16,150 and 34,530 are shown in figure 10.6. It is seen that there is less pressure recovery at the rear of the tube at the lower Reynolds' number. In other respects the diagrams are identical.

The drag coefficient decreased from 0.2538 to 0.2145 or roughly in proportion to the fall in resistance coefficient of the nest after the first row has been subtracted. Thus it may be said that these two diagrams demonstrate that the Reynolds' number influence is to be found at the rear of the tubes and only on rows subsequent to the first.

10.7 Comparison between later rows in parallel and staggered arrangements.

Two parallel arrangement diagrams are also shown on

figure 10.6. These were taken at Reynolds' numbers of 21,100 and 39,600 and so cover much the same speed range. Here again the Reynolds' number influence is seen in the different locations of the curves at the rear of the cylinder.

In comparison with the staggered arrangement the most marked feature is the differences on the upstream face and it is due to these that the form drag coefficient for the parallel arrangement is so much higher than the staggered.

Figure 10.6 makes it possible to account for the previously observed differences between the resistance laws for parallel and staggered nests as seen in figure 1.2B. The parallel arrangement gave higher resistance and less influence of Reynolds' number. The smaller influence of Reynolds' number is due to the fact that there were only four rows as compared with seven for the staggered nest. Therefore the first row with its nearly constant coefficient had a greater influence in the parallel arrangement.

On subtracting the first row, both nests show a similar Reynolds' number effect. This, as figure 10.6 shows, is due to changes at the rear of the tubes. A large numerical difference remains and this as shown by the figure is due to differences on the upstream faces.

11. CONFIRMATION THAT THE REYNOLDS' NUMBER
CHOSEN FOR THE MAJOR PORTION OF THE
EXPERIMENTS WAS NOT A CRITICAL NUMBER.

11.1 Considerations necessary to confirm that the
experiments and results are of a general nature.

In any research where the results from a limited number of experiments are used to investigate a wide range of phenomena, it is necessary to confirm that the results obtained and the laws discovered not only hold true for the particular set of conditions under which the experiments were carried out, but also that these conditions represent the general problem and are not a particular, unique, case. This confirmation is generally obtained by carrying out a few experiments at higher and lower Reynolds' numbers and ascertaining that there is no unaccountable change in these results. If the results are plotted against the varying Reynolds' numbers the curves obtained should be smooth curves without any indication of discontinuity.

The curves, figure 1.2B, showing the variation of total resistance of the nest with varying Reynolds' number had indicated that there was a continuous law connecting these two factors. The Reynolds' number at which the majority of the air experiments had been carried out was about 35,000 and

FORM DRAGS AT VARYING AIR SPEEDS.

FIG. 11'2.

PARALLEL ARRANGEMENT

4TH ROW

CENTRE TUBE

38 CMS. FROM BACK WALL

ATMOSPHERIC PRESSURE

$$\frac{V_{n, \max} d}{v} = 21,100$$

MEAN ORDINATE

$$\beta = 0.312 \rho V_{n, \max}^2$$

$$\frac{V_{n, \max} d}{v} = 27,000$$

$$\beta = 0.307 \rho V_{n, \max}^2$$

$$\frac{V_{n, \max} d}{v} = 35,700$$

$$\beta = 0.282 \rho V_{n, \max}^2$$

$$\frac{V_{n, \max} d}{v} = 39,500$$

$$\beta = 0.273 \rho V_{n, \max}^2$$

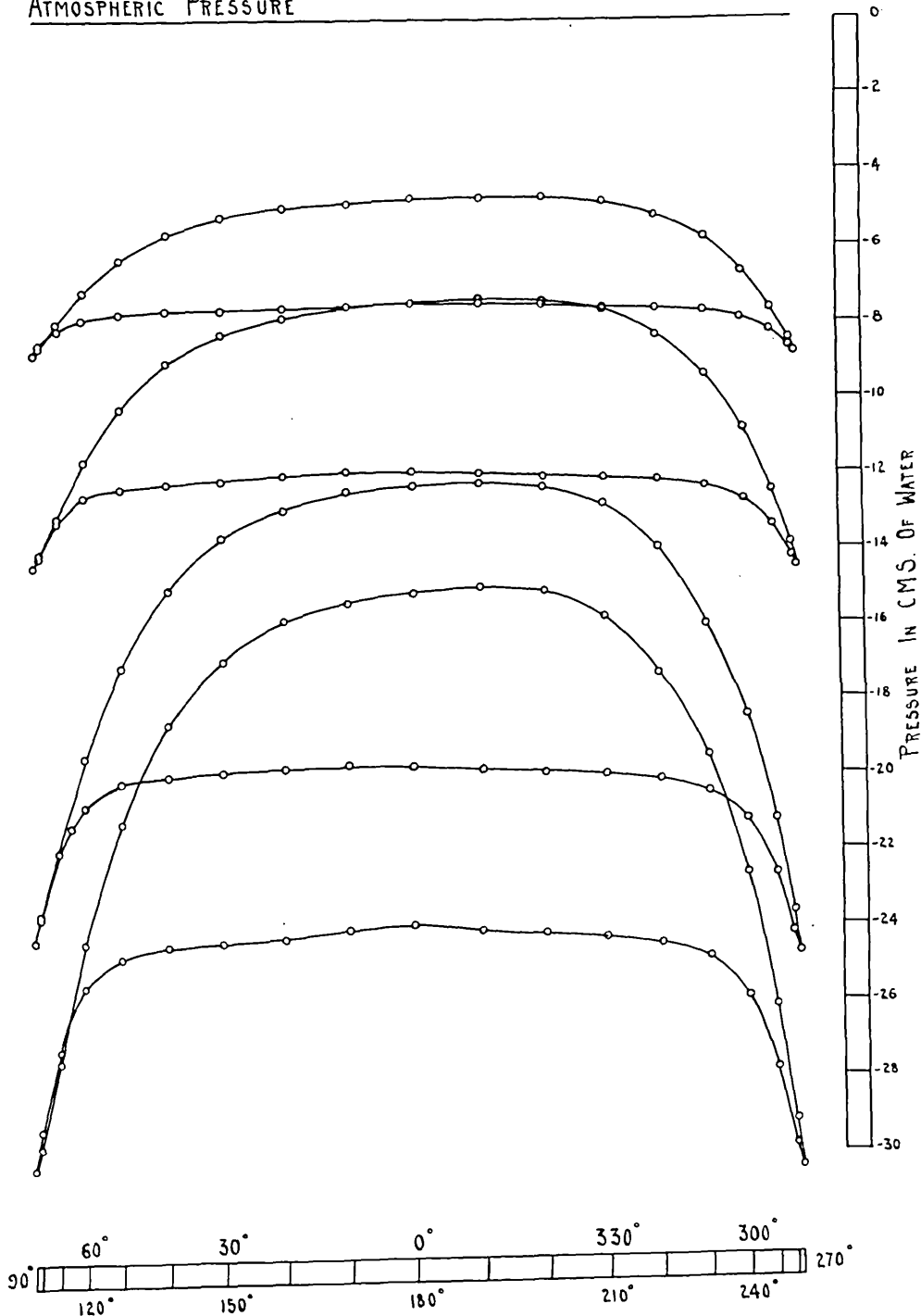


figure 1.2B gave no indication of this being a critical value.

Further evidence was available from figure 5.4C. This shows the relation between the air speed and the mean ordinate of the form drag diagram. However, the initial series of experiments was carried out on the centre tube of the first row and it was thought that it might not be truly representative. When the air impinges on the first row of tubes it is undisturbed whereas when it meets all other rows it is rendered turbulent by the preceding row. Therefore it was decided to carry out a series of experiments on the fourth row.

11.2 Form drags on the fourth row of tubes at varying air speeds - parallel arrangement.

Figure 11.2 shows a series of form drag diagrams taken from the centre tube of the last row. The mean ordinates of these various diagrams have been plotted against the corresponding cathetometer reading in figure 5.4C. From this curve it is seen that there is a continuous relation between the air speed and the mean ordinate of the drag on the fourth row as well as on the first row.

This was taken as conclusive evidence that the Reynolds' number of 35,000 was not a critical number and that the results obtained were general and not confined to the particular conditions of the experiments.

FORM DRAGS AT VARYING AIR SPEEDS.

FIG. 11*3.

STAGGERED ARRANGEMENT. 6TH ROW TUBE ABOVE CENTRE LINE
3.8 CMS. FROM BACK WALL

ATMOSPHERIC PRESSURE.

$$\frac{V_{R,MAX} d}{\nu} = 16,150.$$

MEAN ORDINATE
 $p = 0.254 \rho V_{R,MAX}^2$

$$\frac{V_{R,MAX} d}{\nu} = 25,400$$

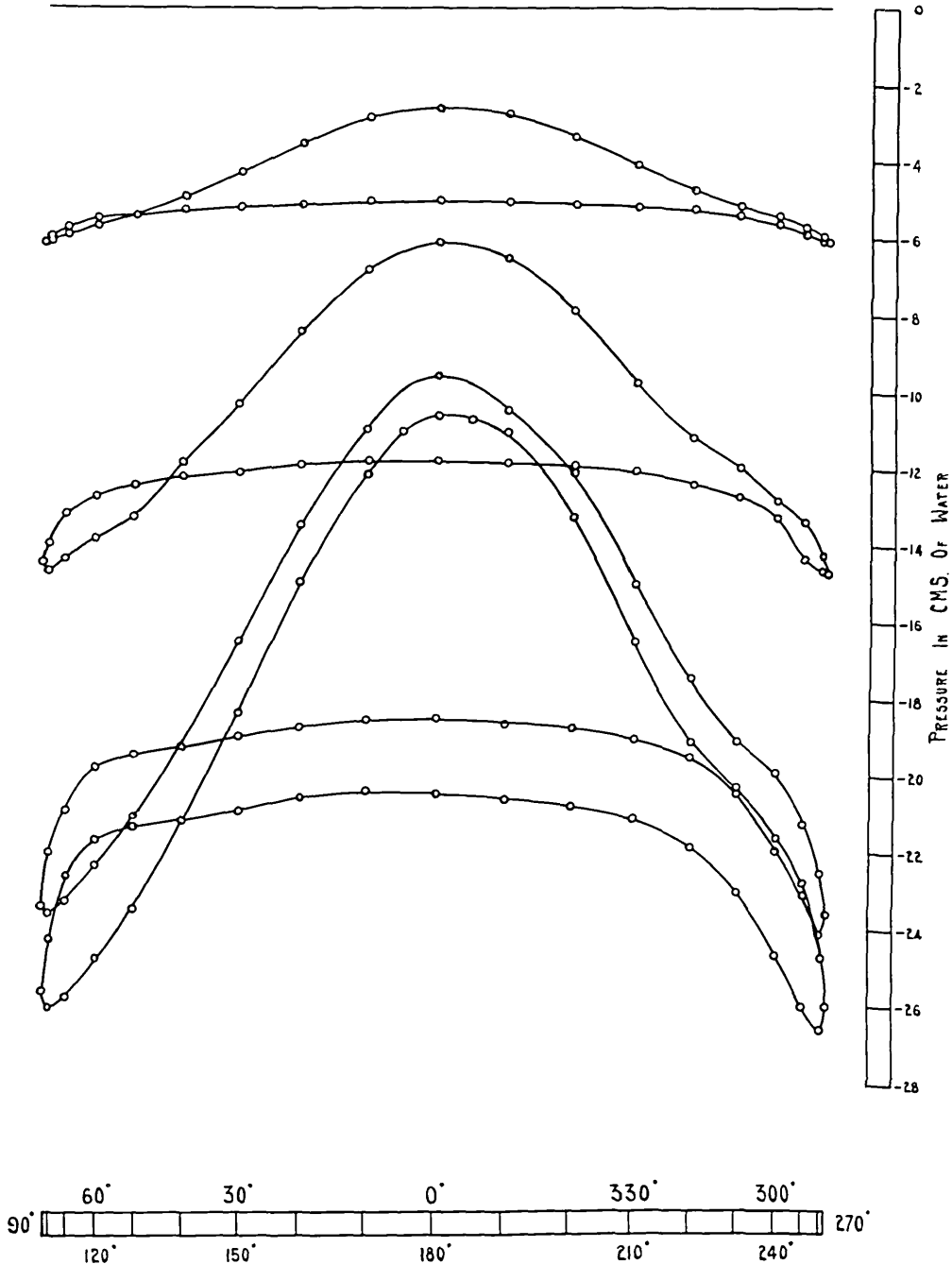
$$p = 0.222 \rho V_{R,MAX}^2$$

$$\frac{V_{R,MAX} d}{\nu} = 32,600$$

$$p = 0.211 \rho V_{R,MAX}^2$$

$$\frac{V_{R,MAX} d}{\nu} = 34,530.$$

$$p = 0.215 \rho V_{R,MAX}^2.$$



In figure 11.2 it is seen that the mean ordinate "p" decreases from $0.312 \rho V^2_{N,max}$ to $0.273 \rho V^2_{N,max}$ as Reynolds' number increases from 21,100 to 39,600. The largest and smallest of these series of form drag diagrams were used in the preparation of figure 10.6.

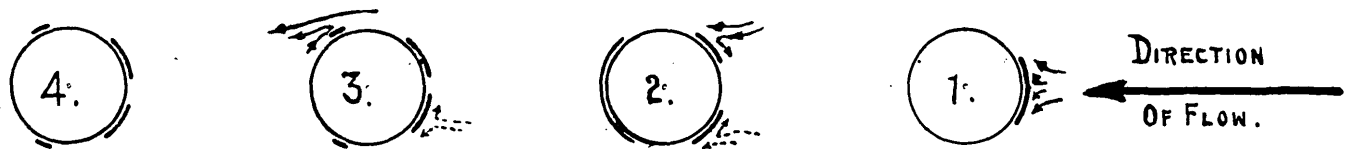
11.3 Form drags on the sixth row of tubes at varying air speeds - staggered arrangement.

In subsection 11.2 it is shown that as far as the parallel arrangement is concerned Reynolds' number 35,000 is not a critical condition of flow through the nest. It was considered advisable however to carry out a similar investigation with regard to the staggered arrangement. With this arrangement it was realised that the first, second and possibly last row of tubes differed materially from the remaining rows.

It was considered that the row preceding the last was likely to be most typical of the majority of rows within any large nest. A series of variable speed air tests was carried out on a central tube of the sixth row. These are shown in figure 11.3. Due to the limitation of the method of driving the Sturtevant fan it was impossible to exceed the Reynolds' number 35,000 but the four points obtained have been plotted on figure 5.4C and it is seen that within the experimental error they lie on a smooth curve without any indication of discontinuity at the upper limit.

DEPOSITION OF DUST ON TUBES. FIG. 12.1.

PARALLEL ARRANGEMENT.



$$\frac{V_{N.MAX.} d}{\nu} \approx 35,000$$

12. THE DEPOSITION OF SOLIDS ON THE OUTSIDE
OF THE TUBES

12.1 Position of dust deposits and explanation of the cause.

When dismantling the nest in order to clean the tubes it was noticed that the dust was not deposited uniformly on the surface but appeared to collect in straight lines along the length of the tubes. This would suggest that the deposition had a definite relation to the variation in pressure or velocity at the surface of the tube.

Figure 12.1 shows the deposition of dust on the tubes arranged in parallel. From this it will be seen that the main factor causing deposition is a change of direction of the stream. On the tubes of the first row the dust is deposited only on the upstream face of the tubes. Here the main stream divides and the centrifugal force caused by the change of direction of the stream apparently throws the dust on to the face of the tubes.

At the back of the first tube the air is not in rapid eddy motion and so no dust is deposited on this portion.

As has been seen in section 9.3 the main stream impinges first on one side of the face of the tube of the second row and a moment later on the other side of the face. Thus there

are two main stagnation points and in fig. 12.1 it is seen that there are two deposition points. In all probability the deposit is mainly from the inner stream which is entering the dead water region since this stream turns through a much more acute angle than the outer stream.

At the back of this tube there is a series of stagnation points which flicker from place to place. This causes the uniform and less marked deposition on the back of the tube.

The deposit on the tubes of the third and fourth rows is very similar. There are two wide patches on the front and two very clearly defined streaks at the back.

The front patches are comparable with those of the second row but the motion of the stream is of a less definite character and therefore the dust is deposited over a wider surface. In some cases on the third row the two front patches were joined together. It is interesting to compare this with the form drag diagrams figure 5.2 F.

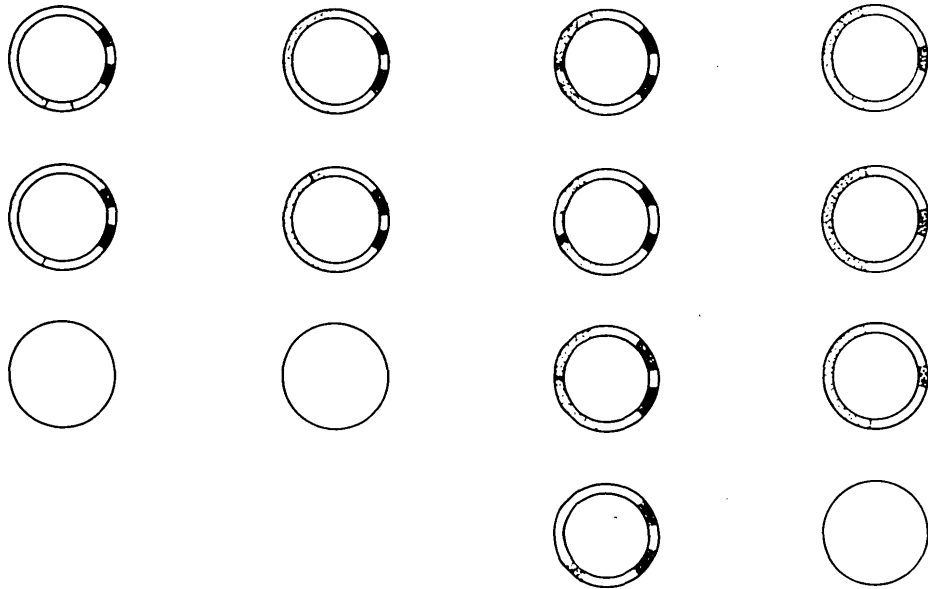
Deposition from the fluid in the angle between the main stream and the tube wall occurs just behind the point of breakaway. The eddy formed at the back of the tube runs out to a very acute angle, at the apex of which there is a sharp change of direction. The more acute this change of direction

DEPOSITION OF SOOT ON TUBES

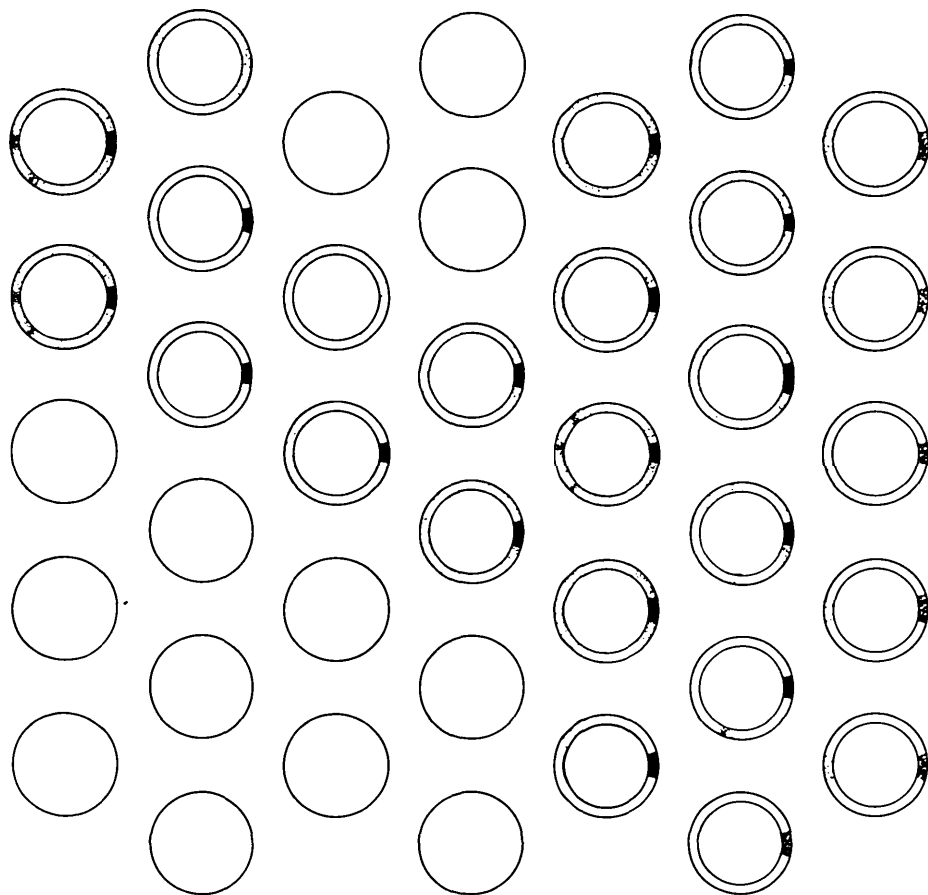
FIG. 12.2.

$$\frac{V_{n,MAX} d}{\nu} \approx 35,000$$

PARALLEL ARRANGEMENT



STAGGERED ARRANGEMENT



the greater the centrifugal force and the more marked the dust separation.

12.2 Experiments with the deposition of soot.

The foregoing records were made from visual observations and there was no possibility of recording the exact angular location of the deposits. The existence of regular deposits was not suspected and they were not observed until the nest was partially dismantled. New deposits of dust could not be obtained in the same manner since the time required would have been prohibitive.

In an attempt to accelerate the rate of growth of the deposits experiments were made in which powder or smoke was introduced into the air stream. Soot from burning camphor gave some measure of success but failed to give those clear cut definitions seen in the original air borne dust deposits. Nevertheless, the general location of the deposits showed marked similarity to the original ones, although the sharp clearly defined streaks at the rear of the back rows of tubes were absent or only found in isolated cases. This might have been due to the relative short time in which the soot was deposited. The effect of non-uniformity of temperature arising from the camphor flame was eliminated as far as possible by turning the nest through 90° so that the axes

of the tubes were vertical. The positions and intensities of the resulting deposits are recorded in figure 12.2. The tubes shown with single circles had insufficient deposits to yield any information of value.

With regard to the staggered arrangement the deposit on the first row consists of particularly coarse grains and was less in quantity than on succeeding rows. This is explained by the small speed and larger radius of curvature of the stream lines here. Only the heaviest particles were thrown out. A light bloom was found at the rear of this row of tubes showing that the heavier particles had been removed from the fluid before it found its way into the dead water region.

The main location of the deposits in all the rows was in the vicinity of the stagnation point at the upstream generator of the tubes; a very heavy deposit being found here even on the seventh row. The fact that deposit is found as far down the nest is consistent with the observed magnitude of the form drag curves since approximately only one sixth of the stream is degraded at each row.

So one obtains a general picture in which energy losses, soot deposits and presumably heat transfer all follow much the same laws.

REVIEW.

The work of previous investigators has in the main been restricted to the measurement of the overall resistance of a few specific nests. Such results cannot be correlated until the total resistance is separated into that of the various rows.

The first row, offers approximately $1\frac{1}{2}$ to $2\frac{1}{4}$ times the resistance of the later rows in the parallel and staggered arrangements respectively. The first row has a resistance coefficient, $\frac{P}{\rho V^2_{N.\max}}$, almost independent of the fluid speed, viscosity, and the tube diameter. It does however depend upon the transverse pitch/diameter ratio, varying from 0.42 in the case of closely spaced tubes to 0.58 in the case of extremely open spacing. The first rows both in rectangular and staggered arrangements have the same resistance.

The second rows both in parallel and staggered arrangements are subjected to pressure fluctuations which originate in the turbulent wake of the first row, and so exhibit the clinging boundary layer associated with much higher Reynolds' numbers. The resulting narrower wake reacts upon the third row, whose resistance accordingly is intermediate in value between the first and second. The subsequent rows,

including the last, exhibit but little variation.

The major difference between the resistance of rectangular and staggered arrangements is in the second row, the staggered having half the resistance of the parallel. This is due to a considerable upstream force found towards the sides of the tubes in the staggered arrangement.

On the third and subsequent rows in staggered arrangement the flow becomes somewhat asymmetrical and the upstream force is only found at one side of each tube. The resistances are correspondingly higher though they still remain 20% lower than the rectangular spacing. All rows except the first (both in rectangular and staggered arrangements) vary considerably with changing Reynolds' number, the form drag being approximately proportional to $Re^{-.25}$ (the numerical values quoted above refer to $Re = 36,000$). The appropriate index for the nest as a whole therefore depends upon the number of rows and varies from zero for one row to $-.25$ for an infinite number of rows.

The total resistance of the nest is made up of the combined totals of the pressure forces acting normally to the tube surface together with those acting tangentially along the tube surface. This tangential force is a relatively small factor, being of the order of 7% for staggered

and 2% of the total resistance for the rectangular arrangement.

The higher value in the case of the staggered arrangement is due, partly to the higher velocities in the region of 45° , partly to the later breakaway of the boundary layer and partly to the insignificance of the reverse flow at the back of the tube.

From the point of view of resistance the form drag is by far the more important factor.

As mentioned earlier viscosity or more generally the Reynolds' number has a considerable influence upon the value of the resistance coefficient but this influence arises in a rather indirect manner. The direct action of viscosity within the boundary layer contributes only a few per cent. of the total resistance and it follows that changes in this small amount could never be important were it not for the fact that the pressure at the rear of the tubes is very sensitive to the precise location of the point at which the motion within the boundary layer reverses. After local reversal has occurred the main stream ceases to follow the contour of the tubes and there is very little subsequent variation of pressure round the back of the tube. The form drag of any tube thus depends very much upon the value of the pressure obtaining at the point of reversal and

breakaway. Practically the whole of the variations of resistance with changing Reynolds' number are due to changes in form drag arising from such changes in the angular location of the point of breakaway.

Notwithstanding the constancy of pressure at the rear of the tubes the fluid near by is in vigorous motion. The velocities at the centre of the so called dead water regions sometimes approach half that prevailing in the gap between the tubes. The associated turbulent intermixing appears to be very vigorous and if judged by comparison with a jet issuing into unlimited still air gives rise to four times as great a mixing length or sixteen times as great a shear stress.

These values relate to the parallel arrangement and to that area where the main stream is rapidly entraining fluid from the dead water region. The relatively large values of the mixing length are necessary in order to permit the large dissipation of energy within the restricted space. Only 2% of the fluid actually enters the boundary layer and there can be subjected to the dissipative action of viscosity. Therefore it is in this turbulent intermixing downstream of each row of tubes that one finds the major dissipation of energy in those nests of rectangular arrangement with more or less conventional pitching.

With staggered arrangements however the general flow pattern is particularly sensitive to the longitudinal and transverse pitching. With certain geometrical arrangements, the point of maximum velocity usually found at 90° is replaced by two points, one in the vicinity of 40° and the other at 140° . In the case of close spacing breakaway is delayed until well after 140° and the subsequent dead water region is a triangle of insignificant dimensions. The flow pattern appears to be comparatively stable, only occasionally exhibiting asymmetrical tendencies.

With open spacing breakaway can occur immediately after the first constriction at 40° . The dead water region becomes wide and extends downstream for at least the longitudinal distance between two rows. Asymmetry becomes very noticeable.

With other staggered arrangements in which the constriction occurs at 90° the breakaway is only a few degrees later and the back of the form drag diagrams is similar to that for rectangular spacing. The dead water region is of limited extent sometimes being less than half a longitudinal pitch in length.

By using elliptical tubes in staggered formation the dead water can be reduced almost to vanishing point.

Gases flowing over surfaces tend to deposit any finely divided solids such as dust or soot that they may be carrying.

The particles of gas within the boundary layer have lost part of their initial velocity and therefore are less capable of pneumatically conveying the solid matter. The particles of gas in contact with the boundary wall are at rest and the finely divided solids associated with these gas particles are therefore also at rest. If these solid particles are of an adhesive nature they will cling to the boundary wall there forming a deposit.

In the nest of tubes, these deposits are by no means uniform but tend to become concentrated in certain well marked regions.

On the first row of tubes the deposit is mainly restricted to the upstream faces and is found close to the upstream generator. In addition a faint deposit may occur at the rear of the tube over that area embraced by the dead water region.

With rectangular spacing subsequent rows of tubes exhibit two regions of concentration on their upstream faces, heavy deposits being found in the vicinity of 30° and 330° . The rear of such tubes often exhibits very local, almost line deposits, occurring just behind the points of breakaway. In some cases there is also a slight uniform deposit at the rear.

In staggered arrangement the deposit on the upstream face appears to be restricted to the vicinity of 0° while three local deposits are found at the rear at 140° , 180° and 220° . The first and last of these correspond to the two points of breakaway while the deposit at 180° is associated with the rear stagnation point which occurs on the line of symmetry of the dead water region.

It seems that slight uniform deposits occur wherever dead water regions exist but the greatest deposits occur where the fluid makes an abrupt change of direction. Such abrupt changes occur where the stream divides at stagnation points and also where the flow reverses at breakaway. These deductions are based entirely on experiments with nests in which most of the boundary layer flow is essentially laminar. Where the surfaces are longer as in the case of fire tube boilers other causes, such as the motions of turbulence create a number of transitory stagnation and breakaway points which serve as starting points for deposits.

In conclusion it may be helpful to indicate where in the thesis reference is made to some of the more novel parts of the work.

With regard to new numerical data, that relating to the total resistance of nests of tubes is discussed in

section 1. and summarised in fig. 1.2B. In this diagram the total resistance has been separated into the form drag on the first and subsequent rows and from this it is possible to predict the resistance of nests having various numbers of rows. It is shown in section 5.7 that the total resistance is almost entirely due to the sum of the form drags on the various rows of tubes, thus indicating that the direct action of viscosity is almost negligible. The magnitude of the form drag is greatly dependent upon the point of breakaway for which data are given in table 9.4.

In certain fluid motion problems, e.g. in connection with scour of river beds below spillway dams it is desirable to be able to predict the velocities in dead water regions. The data relating to such regions are given in fig. 3.1 C and in section 7.6. A numerical coefficient is also given for the dispersion of the jet entering a highly turbulent region (section 9.2).

With regard to the application of the resistance data to nests having other geometrical forms the chief difficulty is in predicting to what extent the location of the point of breakaway depends upon the geometry of the nest. In this connection the Ahlborn photographs in section 7 considered in conjunction with the form drag diagrams of figures 5.2 F

and G may be of assistance. In any case these photographs reveal the flow pattern in typical nests and show how this is modified as the spacing and tube form is changed.

With regard to the technique of measurement, the method by which the form drag diagrams were plotted directly by using the manometer tube as a cylindrical lens may be found useful in other studies where a large number of pressure records have to be taken (see section 2.6).

In section 7 and figure 7.1 the arrangement used for photographing the flow patterns is described. This differs from normal Ahlborn tank practice in that in the present experiments water flowed continuously past the stationary model, thus avoiding the need for elaborate moving carriage arrangements for the camera and the model. This also gave less trouble from contamination of the water surface and made possible a method of cleaning the surface by the use of soap flakes. This overcame one of the most serious difficulties of the Ahlborn technique.

By the aid of fine grains of potassium permanganate dropped on to blotting paper semi-permanent records of stream lines close to a solid boundary were obtained. As described in section 7.23 these motions differ very materially from the general flow in the main stream.

Thoma, Lohrish, Powell and Griffiths have studied diffusion by the use of chemical action or of evaporation. In the present work a new method is described in which the rate of diffusion is assessed by the loss from the surface of a soluble model in a stream of water. Such experiments with a cylinder of shaving soap are described in section 7.7.

Relf and Taylor have used electrical models for the solution of hydrodynamic problems. This work has been extended and certain difficulties eliminated by the use of the electric tray described in section 8. The circuit shown in figure 8.2 A utilises a null A.C. method and yet gives direct readings for the stream velocity. This avoids the need of differentiation on the one hand or the use of a commutator on the other.

Another novel feature was the introduction of wakes (as shown in figure 8.3) to simulate the motion of a real as distinct from an ideal fluid, thus partially representing the effect of viscosity.

The location and reason of soot deposits is discussed in section 12 where it is shown that the deposition is mainly due to centrifugal force arising at points where there are marked changes of direction in the motion of the fluid. This is illustrated in figures 12.1 and 12.2.

APPENDIX No.1.

Effect of changes of atmospheric temperature, pressure and humidity.

Details of calculations of air flow in section 1.3.

When considering the flow of water the fluid can be considered incompressible and there is no difficulty in assigning a value to the density ρ or the maximum velocity $V_{N,max}$. With air the conditions are different and small though appreciable changes in ρ and $V_{N,max}$ accompany changes of temperature and pressure. Changes in humidity have also to receive consideration.

From table 1.3 it will be seen that at the highest air speed corresponding to 1.297 cms.of water the drop in pressure across the nest was 17.6 cms.of water. Thus with a barometric pressure of 30.04" Hg. i.e. 1035 cms.of water, the pressure at the entrance to the nest is 1033.7 cms.of water and at the outlet 1016.1 cms. This drop in pressure corresponds to 1.7% of the mean pressure in the nest. Thus neglecting humidity, the velocity of the air increases by 1.7% as it passes through the nest.

When comparing the results with those for water-flow the velocity and density of the air at the centre of the nest were used and 50% humidity was assumed. The effect of humidity is to lessen the density of the air. At 25°C and 760 mm. pressure the density of saturated air is 1.18% less than that of dry air. Thus if it is assumed that the air is 50% saturated the error cannot exceed 0.6% and will probably be considerably less. At a temperature of 8°C the corresponding possible error is less than 0.2%.

In order to obtain a clear conception of the effect of these variations and the condition of the air as it passes through the apparatus experiment (1) is analysed in detail.

The atmosphere conditions are (a) temperature 11.7°C and it is assumed that the air remain at this temperature during the passage through the nest, (b) atmospheric pressure 30.04" of mercury = 1035 cms.of water, (c) humidity assumed 50% saturated.

At the first pressure point, the inlet of the nest, the pressure has fallen 1.297 cms. to 1033.7 cms.of water. Since apart from 0.98 nozzle coefficient, the total energy at these two points is the same, this fall equals the velocity head at the inlet of the nest.

Appendix No.1, continued.

| | |
|---|--------------------------------------|
| Weight of dry air in 1 cu.meter at 0°C and 760 mm.pressure | = 1.293 kg. |
| ∴ " " " " " " " " "11.7°C " " " " | = $1.293 \times \frac{273}{284.7}$ |
| " " " " " 1 cu.meter of saturated air at | = 1.241 kg. |
| " " " " " " " " "11.7°C and 760 mm. " | = 1.2226 kg. |
| " " water vapour " " " " " " " " " " | = 0.0105 kg. |
| Total weight of " " " " " " " " " " | = 1.2331 kg. |
| Difference in weight between dry air and saturated air | |
| " " " " " " " " "11.7°C and 760 mm.pressure | = 1.241-1.2331 |
| | = 0.008 kg. |
| ∴ Weight of 1 cu.meter of 50% saturated air at 760 mm.pres. | = 1.237 kg. |
| " " " " " " " " " " " " 30.04" Hg. | = $\frac{30.04}{29.92} \times 1.237$ |
| | = 1.241 kg. |
| Weight of 1 cu.meter of water at 11.7°C | = 999.520 kg. |

$$\begin{aligned}
 V_{min}^2 &= 0.982 \times h_{water} \times \frac{\rho_{water}}{\rho_{air}} \times 2g. \\
 &= 0.96 \times \frac{999.52}{1.241} \times 2 \times 981 \times h. \\
 &= 0.96 \times 806 \times 1962 \times h. \\
 &= 1,518,000 h.
 \end{aligned}$$

$$V_{N.max}^2 = 1,518,000 \times 2.96^2 \times h = 13,300,000 h.$$

In experiment (1) $h = 1.297$ cms.

$$\therefore V_{min}^2 = 1,969,000 \quad \text{and} \quad V_{min} = 1,403 \text{ cms.per second.}$$

$$V_{N.max} = 2.96 V_{min}. \quad \therefore V_{N.max} = 4,150 \text{ cms.per second.}$$

∵ the kinematic viscosity of air at 11.7°C is 0.1417 C.G.S.units.

$$\frac{d}{\nu} = \frac{1.27}{0.1417} = 8.97$$

$$Re = \frac{d}{\nu} \cdot V_{N.max} = 8.97 \times 4,150 = 37.200$$

At the second pressure point, the outlet of the nest, the pressure has fallen 17.603 cms. to 1016.1 cms.of water.

The increase in volume and therefore the increase in velocity is practically inversely proportional to the pressure.

Appendix No.1, continued.

$$\begin{aligned} \therefore V_{\min} (\text{at outlet}) &= V_{\min} (\text{at inlet}) \times \frac{1033.7}{1016.1} \\ &= 1.403 \times \frac{1033.7}{1016.1} = 1,427 \text{ cms.per second.} \end{aligned}$$

$$V_{\min}^2 = 2,035,000$$

Weight of 1 cu.meter of 50% saturated air at 11.7°C and 760 mm. Hg.i.e.
 1030 cms.of water = 1.237 kg
 " " " " " " " " " " " " 11.7°C and 760 mm.Hg. at
 $1016.1 = 1.237 \times \frac{1016.1}{1030}$
 $= 1.220 \text{ kg.}$

$$\begin{aligned} \text{Head of water corresponding to } V_{\min} \text{ at outlet} &= \frac{V_{\min}^2}{2g} \cdot \frac{\rho_{\text{air}}}{\rho_{\text{water}}} \\ &= \frac{2,035,000}{1962} \times \frac{1,220}{999.5} \\ &= 1.266 \text{ cms.} \end{aligned}$$

$$\begin{aligned} \text{Head of water corresponding to } V_{\min} \text{ at inlet} &= \frac{1,969,000}{1962} \cdot \frac{1}{806} \\ &= 1.245 \text{ cms.} \end{aligned}$$

$$\begin{aligned} \text{Head required to cause increase in velocity of air} & \text{ cms} \\ &= 1.266 - 1.245 = 0.021 \text{ of water} \end{aligned}$$

The difference in pressure between the first and second pressure point is caused in overcoming the resistance of the nest of tubes and in increasing the velocity of the air. Since in a total resistance of 17.603cms only 0.021 cm. or 0.12% is utilised in increasing the velocity this factor can be neglected.

$$V_{\min} (\text{at outlet}) = 1,427 \text{ cm. per sec.}$$

$$\text{Therefore } V_{N,\max} (\text{at outlet}) = 2.96 \times 1,427 = 4,220 \text{ cms.per sec.}$$

The viscosity μ is independent of the pressure.

$$\text{Therefore } \frac{\mu}{\rho} \text{ at outlet} = 0.1417 \times \frac{1.241}{1.220} = 0.1443 = \nu$$

$$\frac{d}{\nu} = \frac{1.27}{0.1443} = 8.81$$

$$Re = \frac{d}{\nu} \cdot V_{N,\max} = 8.81 \times 4,220 = 37,200$$

Appendix No.1, continued.

From this it is seen that the Reynolds' number remains constant for as the velocity increases the kinematic viscosity also increases at the same rate.

In Table 1.3, $V_{N,max}$ at the centre of the nest is determined and the total resistance of the nest is expressed in non dimensional units with the square of this velocity in the denominator.

| | | |
|---|--------------------------------------|----------|
| Weight of 1 cu.meter of 50% saturated air at 11.7°C and 1030 cms. | of water | |
| | = 1.237 kg. | |
| " " " " " " " " " " | " 1024.9 cms. | of water |
| | = $1.237 \times \frac{1024.9}{1030}$ | |
| | = 1.231 | |
| " " " " " " " " " " | " 1033.4 cms. | of water |
| | = $1.237 \times \frac{1033.4}{1030}$ | |
| | = 1.241 | |

| | | | | | |
|-----------------------------------|----------------------------|---|------------------------|---|-----|
| $\frac{\rho_{water}}{\rho_{air}}$ | at a pressure of 1030 cms. | = | $\frac{999.52}{1.237}$ | = | 809 |
| " | " " " " " 1024.9 " | = | $\frac{999.52}{1.231}$ | = | 813 |
| " | " " " " " 1033.4 " | = | $\frac{999.52}{1.241}$ | = | 806 |

CYLINDRICAL PITOT WITH OBLIQUE FLOW.

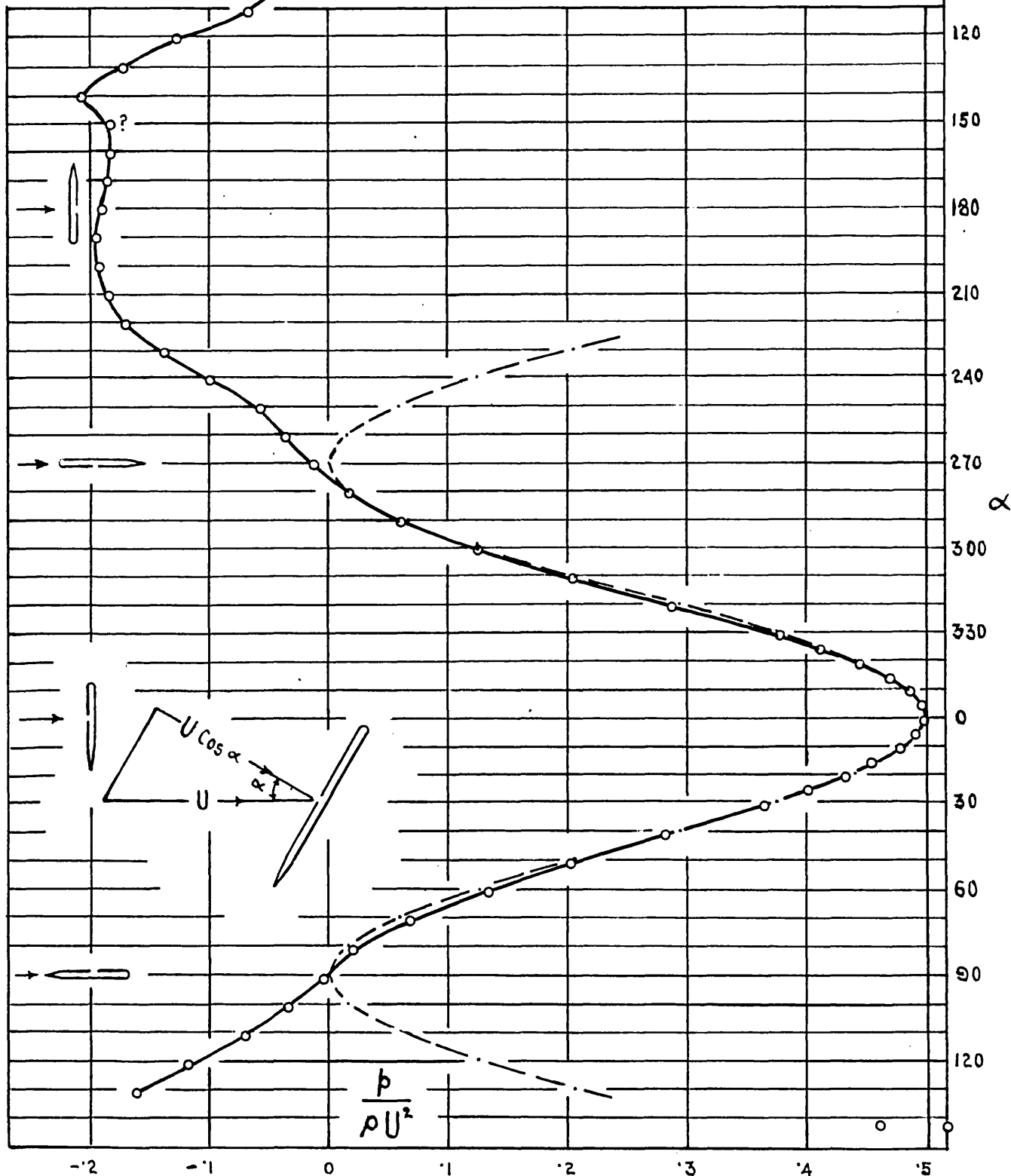
PITOT DIA. 0.127 CM.

PRESSURE HOLE 0.033 CM. DIA.

AIR 21.9°C

30.15 Hg

$U = 4.055 \text{ CMS./SEC.}$



APPENDIX No.2.

Pressure registered by a cylindrical pitot when placed at an angle to the direction of flow.

When carrying out the experiments for the orientation of the two hook shaped Pitot-static tubes shown in figs. 3.2A and B an opportunity was afforded to investigate the pressure registered by these tubes when placed at an angle to the stream.

The curve of variation in pressure with angle of rotation of the 0.127 cms. diameter tube is given in the figure.

The normal component of the velocity U is $U \cos \alpha$ and the corresponding pressure excess is $\frac{1}{2} \rho U^2 \cos^2 \alpha$. This value is shown with a dotted line and it will be seen that the observed values are in excellent agreement with the theoretical values.

This theoretical curve is based on the assumption that the tube functions correctly as an ordinary static tube i.e. that the reading at 90° is the true static pressure.

Table I gives the discrepancies between the observed and theoretical pressures as a percentage of that due to U and also $U \cos \alpha$ for the varying angles of obliquity.

Table I

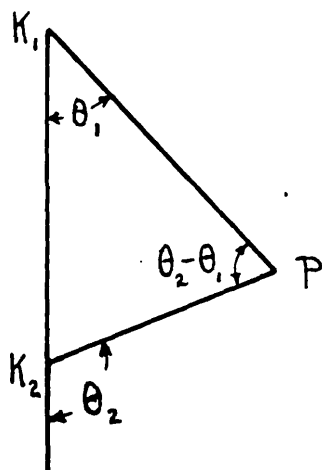
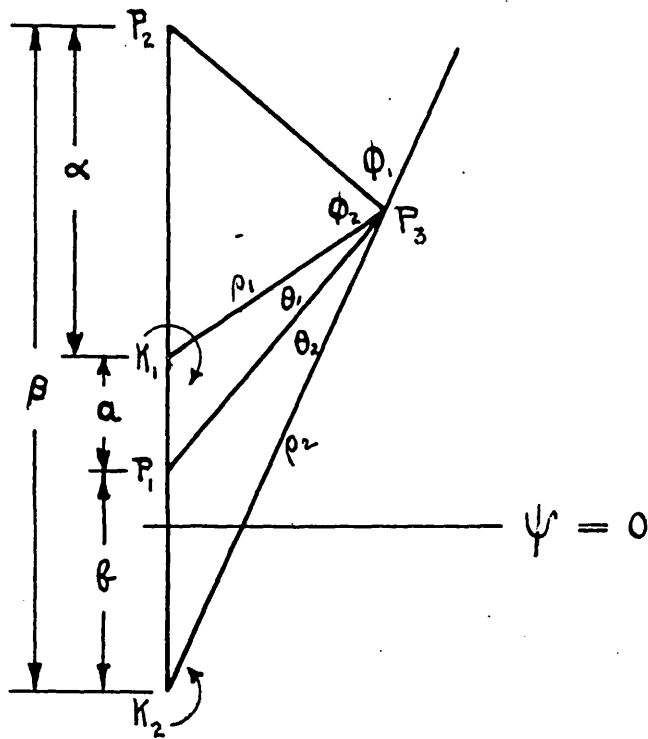
| Angle of Incidence | Amount by which Pitot reads higher than theoretical pressure | | |
|--------------------|--|--------------------------|--------------------------------------|
| | In Cms. of Water. | % of pressure due to "U" | % of pressure due to $U \cos \alpha$ |
| 50° | 0.15 | 1.42 | 2.21 |
| 60 | 0.24 | 2.27 | 4.55 |
| 70 | 0.35 | 3.32 | 9.70 |
| 80 | 0.22 | 2.08 | 12.02 |

From 0 to 40° the cylindrical pitot registered the theoretical pressure. The discrepancy increased steadily from 40° to a maximum at 70° when the error represents 3.3% of the pressure due to the stream velocity.

From 70 to 90° the discrepancy decreases steadily.

In the particular hooked pitot-static tubes under consideration a small flat surface was filed on the face of the tubes but from a comparison of the pressure recorded with truly cylindrical tubes this appears to have had little effect on the pressure indicated.

FLOW OF AN INVISCID FLUID BETWEEN PAIRS OF CYLINDERS.



APPENDIX No.3.

Flow of an inviscid fluid between pairs of cylinders. (see section 8.3).

Two point vortices placed $2a$ apart give rise to coaxial circular stream lines with centres lying on the line joining the vortex centres.

The problem is to find the position of the vortex centres, given the position of two circular stream lines viz. the surfaces of two adjacent tubes.

Let the circulation of the two point vortices be K_1 and $-K_2$ and let them be equal in strength but of opposite sign.

The stream function ψ for the vortex K_1 is $\frac{K_1}{2\pi} \log_e \rho_1$ where

ρ_1 is the distance of the point considered from the vortex centre. The combined stream function for the two vortices K_1 and $-K_2$ is

$$\psi = \frac{K}{2\pi} \log_e \rho_1 - \frac{K}{2\pi} \log_e \rho_2 + \text{constant.}$$

the constant arises from the fact that the origin for the two stream functions is not the same.

$$\text{Therefore } \psi = \frac{K}{2\pi} \log_e \frac{\rho_1}{\rho_2} + \text{const.}$$

Let the straight line passing through the point of symmetry be $\psi = 0$ therefore when $\rho_1 = \rho_2$ $\psi = 0$ and the constant = 0.

$$\text{We have } \psi = \frac{K}{2\pi} \cdot 2.3026 \log_{10} \frac{\rho_1}{\rho_2}$$

$$\text{Consider any particular stream line } \psi_r \quad \frac{\rho_1}{\rho_2} = \text{constant.}$$

The stream line is the locus of a point P which moves so that

$$\frac{\rho_1}{\rho_2} = \text{constant.} = N \dots \dots \dots (1)$$

Consider two particular locations of P from K_1 and K_2
 Firstly P_1 when P lies on the straight line $K_1 K_2$ and is between there two points.

Secondly P_2 When P lies on $K_2 K_1$ produced.

Let a, b and α, β be the distances of P_1 and P_2 from K_1 and K_2 respectively.

Appendix No.3 continued.

Now $\frac{a}{b} = N$ and $\frac{\alpha}{\beta} = N$.

Let P_3 be any other point complying with the relation (1).

Joining $P_3 K_1$ and $P_3 K_2$ we have

$$\frac{P_1}{P_2} = N.$$

Join $P_3 P_1$

We now have triangle $K_1 K_2 P_3$ in which parts of base are proportional to the sides. Therefore $P_3 P_1$ is the bisector of the apex angle (Euclid Book VI Prop. III.)

$$\text{So. } \theta_1 = \theta_2$$

Now produce $K_2 P_3$ and bisect the resulting external angle, this cuts the base produced in the ratio of the sides $\frac{P_1}{P_2}$ i.e. in the ratio $\frac{\alpha}{\beta}$

i.e. the bisector passes through P_2

$$\text{Now } 2\phi + 2\theta = 180^\circ$$

$$\text{Therefore } \phi + \theta = 90^\circ$$

So the locus of P_3 is a semicircle with $P_1 P_2$ as diameter.

Therefore all stream lines are circles with their centres on $K_1 K_2$ produced.

Consider the velocity potential ϕ

ϕ for the vortex $K_1 = \frac{K_1}{2\pi} \theta_1$, where θ_1 is the angle between the $P K_1$ and $K_1 K_2$.

The combined velocity potential for the two vortices K_1 and K_2 is

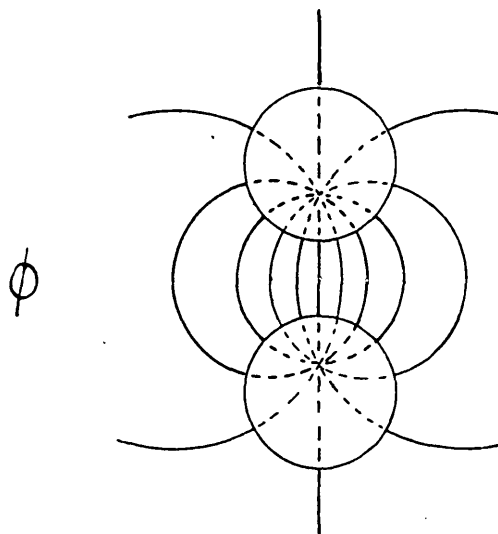
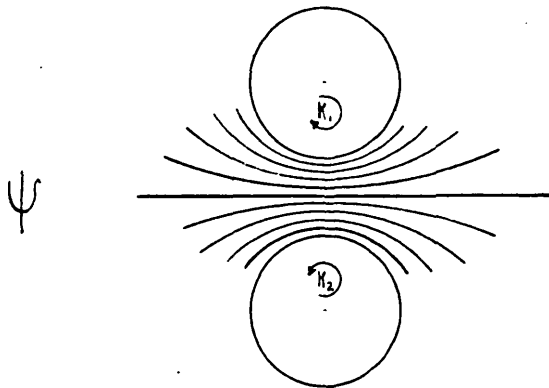
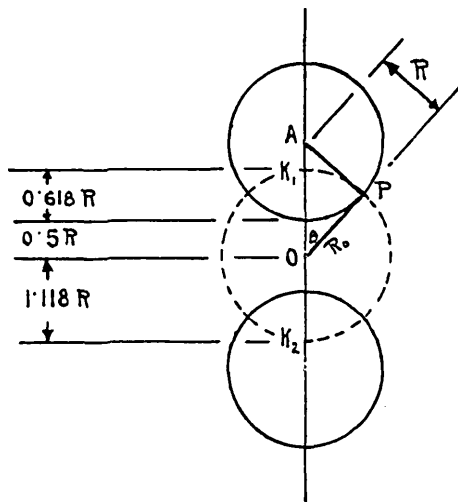
$$\phi = \frac{K}{2\pi} (\theta_1 - \theta_2) + \text{constant.}$$

the constant arises from the fact that the origin for the two velocity potentials is not the same.

$$\text{Let } \phi = 0 \text{ when } \theta_1 - \theta_2 = 0$$

Therefore constant = 0

FLOW OF AN INVISCID FLUID BETWEEN PAIRS OF CYLINDERS.



Appendix No.3 continued.

For equipotential lines $\phi = \text{constant}$.

Then $\theta_1 - \theta_2 = \text{constant}$. so $\theta_2 - \theta_1 = - \text{constant}$

But $\theta_2 - \theta_1$ is the angle $K_1 P K_2$

So the locus of P is a circle with $K_1 K_2$ as a chord (Euclid Book III. Prop. XXI.)

Consider case when $\theta_2 - \theta_1 = 90^\circ$

This equipotential line is circle with $K_1 K_2$ as diameter.

All stream lines cut it at right angles.

Therefore for nest of tubes K_1 and K_2 are the ends of the diameter of a circle which cuts the tube surfaces at right angles.

Erect perpendiculars at point of contact P. These respectively pass through O and the centre of the tube and they are at right angles to each other.

To determine the length OK_1 we have a right angled triangle with two sides known.

$$AP = \frac{1}{4} \text{ inch} \quad \text{and} \quad AO = \frac{3}{8} \text{ inch.}$$

$$\sin \theta = \frac{2}{3} = 0.667 \quad \text{therefore} \quad \theta = 41.8^\circ \quad \cos \theta = .7455$$

$$OK_1 = \frac{3}{8} \times .7455 = 0.28 \text{ inch}$$

$$= \frac{3}{2} R \times .7455 = 1.118 R$$

To plot stream lines for nest of tubes.

$$\psi = \frac{K}{2\pi} \cdot 2.3026 \log_{10} \frac{\rho_2}{\rho_1} \quad \text{or} \quad \frac{K}{2\pi} 2.3026 \log_{10} \frac{\rho_2}{\rho_1}$$

consider stream line on tube surface.

$$\psi_R = \frac{K}{2\pi} 2.3026 \log \frac{1.618}{.618} \quad \text{or} \quad \frac{K}{2\pi} 2.3026 \log \frac{.618}{1.618}$$

$$= \frac{K}{2\pi} 2.3026 \log 2.62 \quad \text{or} \quad \frac{K}{2\pi} 2.3026 \log \frac{1}{2.62}$$

$$= \frac{K}{2\pi} 2.3026 \left(\begin{array}{l} + \\ - \end{array} 0.418 \right)$$

$$\psi_R = \pm 0.418 \cdot \frac{K}{2\pi} 2.3026 \quad \text{These are the stream lines which represent the two tubes.}$$

Appendix No.3, continued.

In order to plot a series of stream lines between 0 and those corresponding to the tube surfaces, divide into ten equal increments of ψ , five on each side of zero.

$$\psi_n = 0.0836 \quad n \cdot \frac{K}{2\pi} \quad 2.3026$$

$$\rho_1 + \rho_2 = 2.236 \text{ on axis - internal point.}$$

$$\rho_1 = \frac{2.236}{1 + \rho_2/\rho_1}$$

$$\text{also } \rho_1 - \rho_2 = 2.236 \text{ on axis - external point.}$$

$$\rho_1 = \frac{2.236}{1 - \rho_2/\rho_1}$$

| n | log $\frac{\rho_1}{\rho_2}$ | $\frac{\rho_1}{\rho_2}$ | ρ_1 internal | ρ_1 external |
|---|-----------------------------|-------------------------|-------------------|-------------------|
| 0 | 0 | 1.0 | 1.118 | ∞ |
| 1 | 0.0836 | 1.213 | 1.011 | 10.5 |
| 2 | 0.1672 | 1.47 | 0.905 | 4.75 |
| 3 | 0.2508 | 1.78 | 0.805 | 2.87 |
| 4 | 0.3344 | 2.16 | 0.708 | 1.93 |
| 5 | 0.4180 | 2.62 | 0.617 | 1.38 |

Velocity distribution in the gap.

The velocity of the point P due to vortex K_1 is $\frac{K}{2\pi} \frac{1}{\rho_1} = q_1$
 " " " " " " " " " " K_2 is $\frac{K}{2\pi} \frac{1}{\rho_2} = q_2$

These are combined vectorially to give the resultant velocity q .

Since the velocity q_1 is at right angles to ρ_1 and the velocity q_2 is at right angles to ρ_2 the velocity triangle is similar to the triangle $K_1 P K_2$ but it is "reflected".

q corresponds to the side $K_1 K_2$ and equals $2a$
 q_1 " " " " " ρ_2
 q_2 " " " " " ρ_1

$$\frac{q}{q_1} = \frac{2a}{\rho_2}$$

$$\text{Therefore } q = \frac{2a}{\rho_2} \cdot q_1 = \frac{2a}{\rho_2} \cdot \frac{1}{\rho_1} \cdot \frac{K}{2\pi} = \frac{2a}{\rho_2^2} \cdot \frac{\rho_2}{\rho_1} \cdot \frac{K}{2\pi} \dots (2)$$

Appendix No.3, continued.

Along any stream line $\frac{\rho_2}{\rho_1}$ is constant.

Therefore $q \propto \frac{1}{\rho_2^2}$

From the fig. $R_0 = R \sqrt{1.5^2 - 1^2} = R \sqrt{1.25} = 1.118 R$

Consider the central stream line where $\psi = 0$

$$\rho_2^2 = x^2 + (1.118R)^2$$

$$\begin{aligned} \frac{\rho_2^2}{R^2} &= \left(\frac{x}{R}\right)^2 + 1.118^2 \\ &= \left(\frac{x}{R}\right)^2 + 1.25 \end{aligned}$$

From equation (2) $q = \frac{1}{\rho_2^2} \left(2a \frac{\rho_2}{\rho_1} \cdot \frac{K}{2\pi}\right)$

$$q = \frac{1}{\left(\frac{x}{R}\right)^2 + 1.25} \cdot \frac{2a}{R^2} \cdot \frac{\rho_2}{\rho_1} \cdot \frac{K}{2\pi}$$

$$q = \frac{1}{\left(\frac{x}{R}\right)^2 + 1.25} \cdot \text{const.}$$

If $q = 1$ when $x = 0$ i.e. on centre line of gap.

$$\frac{2a}{R^2} \cdot \frac{\rho_2}{\rho_1} \cdot \frac{K}{2\pi} = 1.25$$

On the central stream line $\rho_1 = \rho_2$

$$\text{Therefore } \frac{K}{2\pi} = \frac{1.25}{2a} \cdot R^2 = \frac{1.118^2}{2 \times 1.118} \frac{R^2}{R} = \frac{1.118R}{2}$$

$$\begin{aligned} \text{Therefore } q &= \frac{1}{\left(\frac{x}{R}\right)^2 + 1.25} \cdot 1.25 \\ &= \frac{1}{1 + 0.8 \left(\frac{x}{R}\right)^2} \end{aligned}$$

In the electric tray experiments $R = 5'' = 12.7$ cms. and reading in centre of gap was 624.5 and $V_{N,\max} = 676.5$

Appendix No.3, continued.

| | | | | | | | | | |
|-----------------------|-------|-------|-------|------|------|-------|------|------|-------|
| x | 0 | 1 | 2 | 4 | 6 | 8 | 10 | 12 | 14 |
| q | 624.5 | 621.5 | 612.5 | 579 | 530. | 474.5 | 417 | 364 | 316.5 |
| $\frac{q}{V_{N,max}}$ | .924 | .919 | .908 | .856 | .784 | .702 | .617 | .538 | .468 |

These values are plotted together with the experimental values in fig.83

Velocity distribution on centre line of gap.

$$q_1 = \frac{K}{2\pi} \cdot \frac{1}{\rho_1} \quad \text{and} \quad q_2 = \frac{K}{2\pi} \cdot \frac{1}{\rho_2}$$

When the point P lies on the line K, K₂ these two velocities act in the same straight line and in the same direction.

$$\text{Therefore } q = q_1 + q_2 = \frac{K}{2\pi} \left(\frac{1}{\rho_1} + \frac{1}{\rho_2} \right) \dots\dots\dots(3)$$

Let y = distance of P from centre 0

$$\text{Then } \rho_1 = 1.118R + y \quad \text{and} \quad \rho_2 = 1.118R - y.$$

$$\text{Therefore } q = \frac{K}{2\pi} \cdot \frac{2 \times 1.118 R}{\rho_1 \rho_2}$$

$$\text{but } \frac{K}{2\pi} = \frac{1.118 R}{2}$$

$$\text{Therefore } q = \frac{1.118R}{2} \cdot \frac{2 \times 1.118 R}{\rho_1 \rho_2}$$

$$= \frac{1.25R^2}{\rho_1 \rho_2}$$

$$= \frac{1.25 R^2}{1.25R^2 - y^2}$$

$$= \frac{1}{1 - \frac{y^2}{1.25R^2}}$$

$$\text{let } y_1 = \frac{y}{\text{gap}} = \frac{y}{R}$$

$$\text{Then } q = \frac{1}{1 - \frac{y_1^2 R^2}{1.25 R^2}} = \frac{1}{1 - \left(\frac{y_1}{1.118}\right)^2}$$

Appendix No.3, continued.

In the electric tray experiment the reading in the centre of the gap was 356 and $V_{N,max}$ 383.4 therefore the theoretical velocity distribution would be

| y | 0 | .1 | .2 | .3 | .4 | .45 | .5 |
|-----------------------|-------|-------|-------|-------|-------|-------|-------|
| y | | 18.55 | 17.28 | 16.01 | 14.75 | 14.08 | 13.41 |
| q | 19.82 | 21.09 | 22.36 | 23.67 | 24.90 | 25.55 | 26.17 |
| q | 356 | 359 | 368 | 384 | 408 | 425 | 445 |
| $\frac{q}{V_{N,max}}$ | .928 | .936 | .960 | 1.001 | 1.064 | 1.108 | 1.160 |

These values are plotted together with the experimental values in fig.8.3

$$\begin{aligned}
 \text{The mean velocity in the gap} &= V_{N,max} \frac{\psi_{R_1} - \psi_{R_2}}{\text{Gap}} \\
 &= \frac{K}{2\pi} \times 2.3026 (+0.418) - \frac{K}{2\pi} \times 2.3026(-0.418) \\
 &\qquad\qquad\qquad \text{Gap} \\
 &= \frac{K}{2\pi} \cdot \frac{2.3026 \times 0.836}{R} \\
 &= \frac{K}{2\pi} \cdot \frac{1.925}{R}
 \end{aligned}$$

From equation (2) Velocity in centre of gap.

$$\begin{aligned}
 V_{\text{centre of gap}} &= \frac{K}{2\pi} \left(\frac{1}{r_1} + \frac{1}{r_2} \right) \text{ where } r_1 = r_2 = 1.118 R \\
 &= \frac{K}{2\pi} \cdot \frac{2}{1.118R}
 \end{aligned}$$

$$\text{Therefore } \frac{V_{N,max}}{V_{\text{centre of gap}}} = \frac{\frac{K}{2\pi} \cdot \frac{1.925}{R}}{\frac{K}{2\pi} \cdot \frac{2}{1.118 R}} = 1.077$$

Velocity at the wall.

$$\begin{aligned}
 V_{\text{at wall}} &= \frac{K}{2\pi} \left(\frac{1}{r_1} + \frac{1}{r_2} \right) \\
 &= \frac{K}{2\pi} \cdot \left(\frac{r_2 + r_1}{r_1 r_2} \right)
 \end{aligned}$$

Appendix No.3, continued.

$$= \frac{K}{2\pi} \cdot \frac{2 \times 1.118R}{1.618R \times 0.618R}$$

$$= \frac{K}{2\pi} \cdot \frac{2 \times 1.118}{R}$$

Therefore

$$\frac{V_{\text{at wall}}}{V_{\text{centre of gap}}} = \frac{\frac{K}{2\pi} \cdot \frac{2 \times 1.118}{R}}{\frac{K}{2\pi} \cdot \frac{2}{1.118R}} = 1.250$$

$$\frac{V_{\text{at wall}}}{V_{N.\text{max}}} = \frac{\frac{K}{2\pi} \cdot \frac{2 \times 1.118}{R}}{\frac{K}{2\pi} \cdot \frac{1.925}{R}} = 1.162$$

APPENDIX No.4.

Estimation of the thickness of the boundary layer (See section 8.7).

From the original experiments on which fig.4.2 was obtained $\frac{v^2}{v_0^2}$ on the centre line of the first gap. = $\frac{10.55}{1.170}$

$$\text{Therefore } \frac{V}{V_{N.\max}} = \sqrt{\frac{10.55}{1.170 \times 8.76}} = 1.015$$

From the similar experiments with the sledge pitot-static tube fig.4.3B

$$\frac{v^2}{v_0^2} = \frac{9.57}{1.178} \text{ therefore } \frac{V}{V_{N.\max}} = \sqrt{\frac{9.57}{1.178 \times 8.76}} = 0.964$$

From the same figure and the experiments with the "leg" added to the sledge pitot-static tube.

$$\frac{v^2}{v_0^2} = \frac{9.70}{1.175} \text{ therefore } \frac{V}{V_{N.\max}} = \sqrt{\frac{9.70}{1.175 \times 8.76}} = 0.971$$

The average of these three values of $\frac{V}{V_{N.\max}}$ is 0.983

It will be seen that in the centre of the gap where these pressure differences are taken, there is a very large pressure gradient and it seems reasonable that a correction to compensate for the size of the static hole in the pitot-static tube should be applied. It is assumed that this correction is the same as that for the cylindrical pitot tube. Then the pressure indicated by the tube is not that at the geometrical centre of the pressure hole but that at a point half the hole radius towards the region of higher pressure.

This correction would reduce the pressure by 0.19 cms. of water and decrease the velocity in the gap by 0.95%.

$\frac{V}{V_{N.\max}}$ then becomes 0.9755.

The velocity on the centre line of the gap by the electric tray = $0.950 V_{N.\max}$ and the velocity on this line by air pressure measurements = $0.9755 V_{N.\max}$.

Appendix No.4., continued.

Let V_m be the actual mean velocity in the gap with air flow.

" δ^* be the effective thickness of the boundary layer.

" G = the width of the gap.

" Q = the volume of fluid flowing through the gap per second

$$Q = V_{N.\max} \times G = V_m (G - 2\delta^*)$$

$$G - 2\delta^* = \frac{V_{N.\max}}{V_m} \cdot G$$

$$2\delta^* = \left(1 - \frac{V_{N.\max}}{V_m}\right) G$$

Assuming for a first approximation that the shape of the pressure distribution curve is unaffected by the presence of the boundary layer.

Then we can replace the ratio $\frac{V_{N.\max}}{V_m}$ by the corresponding velocities on the centre line of the gap.

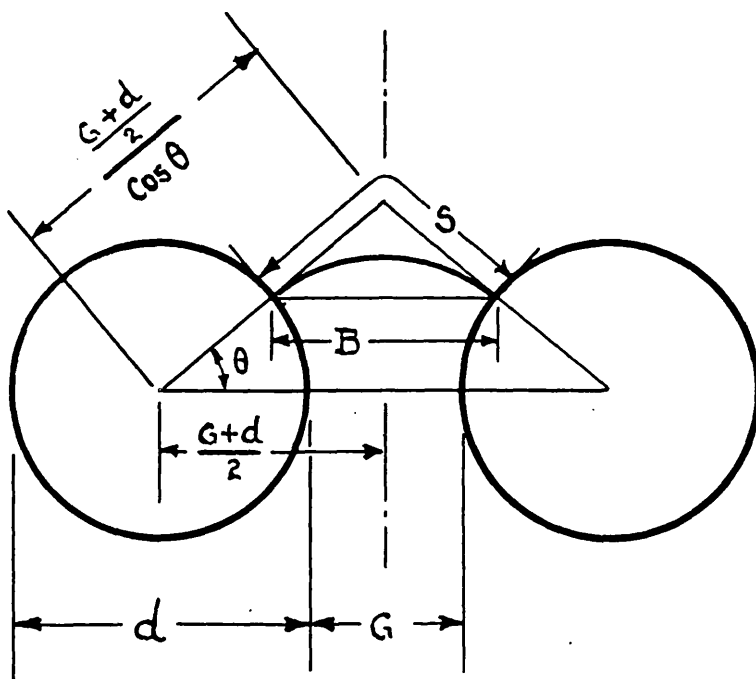
i.e. we can replace $\frac{V_{N.\max}}{V_m}$ by $\frac{0.950 V_{N.\max}}{0.9755 V_{N.\max}}$.

$$\text{Thus } 2\delta^* = \frac{0.9755 - 0.950}{0.9755} G$$

$$= \frac{0.0255}{0.9755} G$$

$$= 0.026 G$$

CALCULATION OF THEORETICAL POSITION OF BREAKAWAY FROM THE PRESSURE RECOVERY AT THE REAR OF THE TUBE



DIRECTION
OF FLOW

APPENDIX No.5.

Calculation of theoretical position of breakaway from the pressure recovery at the rear of a tube. (See section 9.3).

In the figure d = diameter of tubes = 1.270 cms.
 G = width of gap = 0.648 cms.

$$\frac{S}{G} = \frac{\frac{G+d}{2} / \cos \theta - \frac{d}{2}}{\frac{G}{2}}$$

$$= \frac{1 + \frac{d}{G}}{\cos \theta} - \frac{d}{G} \quad \left[\begin{array}{l} \text{Let } \cos \theta = 1 - \alpha \text{ where } \alpha \text{ is small} \\ \text{then } \frac{1}{1 - \alpha} = 1 + \alpha \end{array} \right]$$

$$= \left(1 + \frac{d}{G}\right) (1 + \alpha) - \frac{d}{G}$$

$$= 1 + \alpha + \frac{d}{G} + \alpha \frac{d}{G} - \frac{d}{G}$$

$$= 1 + \alpha + \frac{d}{G} \alpha \quad \text{but } \frac{d}{G} \text{ practically equals } 2$$

$$\text{Therefore } \frac{S}{G} = 1 + 3\alpha$$

$$B = d + G - \frac{2d}{2} \cos \theta$$

$$\text{Therefore } \frac{B}{G} = \frac{d}{G} + 1 - \frac{d}{G} \cos \theta$$

$$= \frac{d}{G} + 1 - \frac{d}{G} (1 - \alpha)$$

$$= 1 + \frac{d}{G} \alpha$$

$$= 1 + 2\alpha$$

But actual width of stream will lie between S and B

Therefore the ratio width of stream is taken as $1 + 2.5\alpha$
gap

Consider pressure recovery at rear of first row of tubes, parallel arrangement fig.5.2F.

$$\text{Pressure recovery} = \frac{0.66}{12.5} = 0.0528$$

Appendix No.5, continued.

Therefore kinetic energy = 0.9472 of K.E. in the gap.

Therefore velocity = $\sqrt{0.9472}$ = 0.9735

Therefore area of path = $\frac{1}{0.9735}$ = 1.028 = $1 + 2.5\alpha$

Therefore α = $\frac{.028}{2.5}$ = 0.0112

But $\cos \theta$ = $1 - \alpha$ = 0.9888

Therefore θ = $8\frac{1}{2}^\circ$

Therefore theoretical point of breakaway is $98\frac{1}{2}^\circ$

Table
Variation of Total Resistance of
Staggered

| Expt. No. | Q in ft. ³ per sec. | $V_{N.max.}$ $\frac{Q}{0.0638}$ ft./sec. | Re = $\frac{d}{v} \times V_{N.max}$ 3090 $V_{N.max}$ | $v^2_{N.max}$ $\left(\frac{ft.}{sec.}\right)^2$ |
|--------------|--------------------------------------|--|--|--|
| 1 | 0.317 | 4.97 | 15,350 | 24.68 |
| 2 | 0.280 | 4.38 | 13,540 | 19.2 |
| 3 | 0.228 | 3.57 | 11,040 | 12.76 |
| 4 | 0.135 | 2.116 | 6,535 | 4.47 |
| 5 | 0.100 | 1.567 | 4,840 | 2.455 |
| 6 | 0.370 | 5.80 | 17,830 | 33.63 |
| 7 | 0.424 | 6.65 | 20,540 | 44.2 |
| 8 | 0.455 | 7.13 | 22,040 | 50.85 |
| 9 | 0.480 | 7.52 | 23,250 | 56.55 |
| 10 | 0.505 | 7.92 | 24,490 | 62.7 |
| 11 | 0.562 | 8.81 | 27,230 | 77.6 |
| 12 | 0.695 | 10.89 | 33,650 | 118.6 |
| 13 | 0.830 | 13.02 | 40,200 | 169.6 |
| 14 | 0.895 | 14.03 | 43,340 | 197.0 |
| 15 | 0.975 | 15.28 | 47,250 | 233.5 |
| 16 | 0.825 | 12.94 | 39,970 | 167.5 |
| 17 | 0.715 | 11.21 | 34,620 | 125.6 |
| 18 | 0.535 | 8.38 | 25,900 | 70.2 |
| 19 | 0.460 | 7.21 | 22,280 | 52.0 |
| 20 | 0.430 | 6.74 | 20,820 | 45.4 |
| 21 | 0.340 | 5.33 | 16,460 | 28.4 |
| 22 | 0.133 | 2.09 | 6,452 | 4.36 |
| 23 | 0.077 | 1.207 | 3,730 | 1.455 |
| 24 | 0.295 | 4.590 | 14,500 | 21.08 |

$$d = \frac{1}{2}'' \quad \frac{1'}{24} = 0.0417'$$

$$v \text{ water at } 11.6^\circ\text{C} \quad v \text{ at } 10^\circ\text{C} = 1.41 \times 10^{-5} \text{ ft }^2/\text{sec}$$

Glauert p.104.

$$v \text{ at } 15^\circ\text{C} = \frac{1.23}{.18}$$

$$v \text{ at } 11.6^\circ = 1.35 \times 10^{-5} \text{ ft }^2/\text{sec}$$

$$\frac{d}{v} = \frac{0.0417}{1.35 \times 10^{-5}} = 3090$$

1.2 B.

Nest with varying water speed

Arrangement

| Expt. No. | Total Resistance of Nest = h ft. of water | $\frac{h}{V^2}$ N.max | $\frac{P}{nd1 \rho V^2 N.max}$ $6.94 \cdot \frac{h}{V^2 N.max}$ |
|--------------|--|--------------------------|--|
| 1 | 0.850 | 0.03448 | 0.2392 |
| 2 | 0.693 | 0.0361 | 0.2506 |
| 3 | 0.489 | 0.0383 | 0.2660 |
| 4 | 0.181 | 0.0405 | 0.2811 |
| 5 | 0.112 | 0.0457 | 0.3173 |
| 6 | 1.158 | 0.03445 | 0.2390 |
| 7 | 1.447 | 0.0327 | 0.2272 |
| 8 | 1.661 | 0.03265 | 0.2266 |
| 9 | 1.838 | 0.0325 | 0.2257 |
| 10 | 1.995 | 0.0318 | 0.2208 |
| 11 | 2.390 | 0.0308 | 0.2140 |
| 12 | 3.440 | 0.0290 | 0.2012 |
| 13 | 4.655 | 0.02745 | 0.1905 |
| 14 | 5.250 | 0.02665 | 0.1850 |
| 15 | 6.050 | 0.0259 | 0.1800 |
| 16 | 4.607 | 0.0275 | 0.1908 |
| 17 | 3.650 | 0.02905 | 0.2016 |
| 18 | 2.215 | 0.03155 | 0.2190 |
| 19 | 1.711 | 0.03288 | 0.2283 |
| 20 | 1.498 | 0.0330 | 0.2290 |
| 21 | 1.007 | 0.03547 | 0.2462 |
| 22 | 0.189 | 0.04335 | 0.3010 |
| 23 | 0.070 | 0.0481 | 0.3340 |
| 24 | 0.756 | 0.0359 | 0.2492 |

Table 1.2 B (Continued).

$p_1 - p_2 = h \rho g$ poundals per sq.ft. of flow area.

$P = A(p_1 - p_2)$ where $A = \text{flow area} = 0.189 \text{ sq.ft.}$

$$\frac{P}{ndl \rho v_{N.\max}^2} = \frac{0.189 h \rho g}{ndl \rho v_{N.\max}^2} \quad \text{where } n = \text{total number of tubes} = 42$$

$$d = \text{dia. of tube} = 0.0417 \text{ ft.}$$

$$l = \text{length of tube} = 0.5 \text{ ft.}$$

$$\frac{P}{ndl \rho v_{N.\max}^2} = \frac{0.189 \times 32.2}{42 \times 0.0417 \times 0.5} \times \frac{h}{v_{N.\max}^2}$$

$$= 6.94 \frac{h}{v_{N.\max}^2}$$

Probably a better method of regarding the ratio is to consider it as the pressure drop per row multiplied by the ratio

$\frac{\text{transverse pitch}}{\text{tube diameter}}$ and divided by $\rho v_{N.\max}^2$.

i.e.

$$\frac{p}{\text{No. of rows}} \times \frac{\left(\frac{\text{pitch}}{d}\right)}{\rho v_{N.\max}^2}$$

Table 1.3 A

See Appendix 1 and Fig.1.2B.

Variation of total resistance of nest with varying air speed.
Staggered Arrangement.

| 1 | 2 | 3 | 4 | 5 | 6 | 7 | 8 |
|-----------|--|---|---|--|---|--|--|
| Expt. No. | Chattock gauge Cms.of H ₂ O | Absolute pressure at inlet of nest Cms. of H ₂ O | Total Resistance of nest = H Cms. of H ₂ O | Absolute pressure at outlet of nest Cms. of H ₂ O | Mean Pressure in nest Cms.of H ₂ O | V ² _{N.max} at inlet $\left(\frac{\text{cms.}}{\text{sec}}\right)^2$ | V _{N.max} at inlet $\frac{\text{cms.}}{\text{sec}}$ |
| 1 | 1.154 | 1025.3 | 20.10 | 1005.2 | 1015.2 | 15.64x10 ⁶ | 3.95x10 ³ |
| 2 | 1.121 | 1025.4 | 19.63 | 1005.8 | 1015.6 | 15.20 | 3.90 |
| 3 | 1.030 | 1025.5 | 18.27 | 1007.2 | 1016.3 | 13.96 | 3.735 |
| 4 | 0.968 | 1025.5 | 17.18 | 1008.3 | 1016.9 | 13.13 | 3.622 |
| 5 | 0.814 | 1025.7 | 14.69 | 1011.0 | 1018.3 | 11.04 | 3.322 |
| 6 | 0.486 | 1026.0 | 9.31 | 1016.7 | 1021.3 | 6.59 | 2.568 |
| 7 | 0.278 | 1026.2 | 5.60 | 1020.6 | 1023.4 | 3.77 | 1.942 |
| 8 | 0.136 | 1026.4 | 2.91 | 1023.5 | 1024.9 | 1.844 | 1.358 |
| 9 | 0.0874 | 1026.4 | 1.943 | 1024.5 | 1025.4 | 1.185 | 1.088 |
| 10 | 0.0848 | 1026.4 | 1.753 | 1024.6 | 1025.5 | 1.150 | 1.072 |
| 11 | 0.06025 | 1026.4 | 1.389 | 1025.0 | 1025.7 | 0.817 | 0.904 |
| 12 | 0.0389 | 1026.5 | 0.976 | 1025.5 | 1026.0 | 0.528 | 0.727 |
| 13 | 0.03046 | 1026.5 | 0.816 | 1025.7 | 1026.1 | 0.413 | 0.643 |
| 14 | 0.02398 | 1026.5 | 0.666 | 1025.8 | 1026.1 | 0.3252 | 0.570 |
| 15 | 1.169 | 1034.3 | 20.64 | 1013.7 | 1024.0 | 15.72x10 ⁶ | 3.965x10 ³ |
| 16 | 1.041 | 1035.2 | 18.30 | 1016.9 | 1026.0 | 14.09 | 3.752 |
| 17 | 0.532 | 1035.6 | 11.73 | 1023.9 | 1029.7 | 8.55 | 2.925 |
| 18 | 0.2552 | 1035.9 | 5.14 | 1030.8 | 1033.3 | 3.45 | 1.857 |
| 19 | 0.459 | 1025.0 | 8.85 | 1016.2 | 1020.6 | 6.35 | 2.520 |
| 20 | 0.3211 | 1025.2 | 6.364 | 1018.8 | 1021.0 | 4.447 | 2.108 |
| 21 | 0.2492 | 1025.3 | 5.038 | 1020.3 | 1022.8 | 3.447 | 1.857 |

Air conditions 15.0°C . 29.82"Hg = 1026.5 cms.of water.

ρ_{air} at 15°C = 0.145 c.g.s.units. Griffiths & Awbery.Pro.Inst.of Mech. Eng.1933.

$$\frac{d}{V} = \frac{1.27}{0.145} = 8.76$$

$$P = (p_1 - p_2) A \text{ where } A = \text{flow area} = 11.509 \times 15.24 = 175.4 \text{ sq.cms.}$$

$$= 175.4 H_{\text{water}} \rho_{\text{water}} g.$$

$$\frac{P}{nd1 \rho_{\text{air}} V^2_{N.\text{max}}} = \frac{175.4 \times g}{nd1} \cdot \frac{\rho_{\text{water}}}{f_{\text{air}}} \cdot \frac{H_{\text{water}}}{V^2_{N.\text{max}}}$$

$$= \frac{175.4 \times 981}{42 \times 1.27 \times 15.24} \cdot \frac{\rho_{\text{water}}}{f_{\text{air}}} \cdot \frac{H_{\text{water}}}{V^2_{N.\text{max}}}$$

Total Resistance - Staggered Arrangement - Air Flow.

| | 9 | 10 | 11 | 12 | 13 | 14 | 15 | 16 |
|-----------|--|---|--|--|---------------------------------|------------|----------------------|---------------|
| Expt. No. | $Re = \frac{d V_{N.max}}{\nu}$ ($8.76 V_{N.max}$) | $V_{N.max}^2$ at centre of nest ($\frac{cms}{sec}$) ² | $\frac{H}{V_{N.max}^2}$ at centre of nest. | $\frac{\rho_{water}}{\rho_{air}}$ at centre of Nest. | $\frac{P}{ndl\rho V_{N.max}^2}$ | \sqrt{C} | $\frac{1}{\sqrt{C}}$ | $Re \sqrt{C}$ |
| 1 | 34,600 | 15.95x10 ⁶ | 1.260x10 ⁻⁶ | 830 | 0.2212 | .4702 | .2.125 | 16,270 |
| 2 | 34,200 | 15.49 | 1.267 | 830 | 0.2225 | .4717 | 2.118 | 16,130 |
| 3 | 32,700 | 14.21 | 1.285 | 829 | 0.2252 | .4745 | 2.106 | 15,520 |
| 4 | 31,700 | 13.35 | 1.286 | 829 | 0.2255 | .4748 | 2.104 | 15,060 |
| 5 | 29,100 | 11.20 | 1.311 | 828 | 0.2296 | .4790 | 2.087 | 13,940 |
| 6 | 22,470 | 6.65 | 1.421 | 825.7 | 0.2482 | .4982 | 2.006 | 11,180 |
| 7 | 17,000 | 3.79 | 1.478 | 824.2 | 0.2578 | .5075 | 1.968 | 8,625 |
| 8 | 11,890 | 1.849 | 1.573 | 823.2 | 0.2740 | .5232 | 1.910 | 6,220 |
| 9 | 9,520 | 1.187 | 1.636 | 822.8 | 0.2850 | .5338 | 1.873 | 5,080 |
| 10 | 9,395 | 1.152 | 1.522 | 822.7 | 0.2650 | .5145 | 1.942 | 4,835 |
| 11 | 7,920 | 0.818 | 1.697 | 822.5 | 0.2950 | .5430 | 1.841 | 4,300 |
| 12 | 6,365 | 0.5285 | 1.846 | 822.4 | 0.3204 | .5663 | 1.764 | 3,607 |
| 13 | 5,630 | 0.413 | 1.977 | 822.3 | 0.3440 | .5865 | 1.704 | 3,300 |
| 14 | 4,990 | 0.325 | 2.049 | 822.3 | 0.3565 | .5972 | 1.674 | 2,980 |
| 15 | 34,650 | 16.04x10 ⁶ | 1.286x10 ⁻⁶ | 823.8 | 0.2241 | | | |
| 16 | 32,400 | 14.34 | 1.276 | 827.7 | 0.2233 | | | |
| 17 | 25,270 | 8.65 | 1.356 | 824.7 | 0.2368 | | | |
| 18 | 16,040 | 3.467 | 1.482 | 821.9 | 0.2573 | | | |
| 19 | 21,270 | 6.405 | 1.382 | 842.3 | 0.2462 | | | |
| 20 | 17,780 | 4.475 | 1.422 | 842.0 | 0.2531 | | | |
| 21 | 15,670 | 3.464 | 1.453 | 840.5 | 0.2584 | | | |

$$211.5 \times \frac{\rho_{water}}{\rho_{air}} \cdot \frac{H_{water}}{V_{N.max}^2}$$

where n = total number of tubes
in nest = 42
d = dia. of tube = 1.27cms.
l = length of tube = 15.24 cm

Data for experiments 15 to 21 obtained from form drag diagrams with different air conditions.

Table 1.3 B See Appendix 1 and Fig.1.2 B.

Variation of total resistance of nest with varying air speed.

Parallel Arrangement.

| 1 | 2 | 3 | 4 | 5 | 6 | 7 | 8 |
|-----------|---|---|---|---|--|---|---------------------------------------|
| Expt. No. | Chattock gauge Cms. of H ₂ O | Absolute Pressure at inlet of nest Cms. of H ₂ O | Total Resistance of Nest = H Cms. of H ₂ O | Absolute Pressure at outlet of nest. Cms. of H ₂ O | Mean Pressure in nest Cms. of H ₂ O | V ² _{N.max} at inlet (cms/sec) ² | V _{N.max} at inlet Cms./sec. |
| 1 | 1.297 | 1033.7 | 17.803 | 1016.1 | 1024.9 | 17.25x10 ⁶ | 4.15x10 ³ |
| 2 | 1.210 | 1033.8 | 16.590 | 1017.2 | 1025.5 | 16.10 | 4.01 |
| 3 | 1.168 | 1033.8 | 16.082 | 1017.7 | 1025.7 | 15.54 | 3.94 |
| 4 | 1.103 | 1033.9 | 15.197 | 1018.7 | 1026.3 | 14.67 | 3.83 |
| 5 | 1.015 | 1034.0 | 14.085 | 1019.9 | 1026.9 | 13.50 | 3.675 |
| 6 | .932 | 1034.1 | 12.868 | 1021.2 | 1027.6 | 12.40 | 3.52 |
| 7 | .846 | 1034.2 | 11.854 | 1022.3 | 1028.2 | 11.25 | 3.353 |
| 8 | .760 | 1034.2 | 10.690 | 1023.5 | 1028.8 | 10.11 | 3.18 |
| 9 | .6835 | 1034.3 | 9.667 | 1024.6 | 1029.4 | 9.09 | 3.017 |
| 10 | .610 | 1034.4 | 8.690 | 1025.7 | 1030.0 | 8.11 | 2.848 |
| 11 | .531 | 1034.5 | 7.619 | 1026.9 | 1030.7 | 7.06 | 2.658 |
| 12 | .3985 | 1034.6 | 5.852 | 1028.7 | 1031.6 | 5.30 | 2.302 |
| 13 | .2943 | 1034.7 | 4.456 | 1030.2 | 1032.4 | 3.914 | 1.978 |
| 14 | .2178 | 1034.8 | 3.382 | 1031.4 | 1033.1 | 2.895 | 1.701 |
| 15 | .1520 | 1034.8 | 2.398 | 1032.3 | 1033.5 | 2.022 | 1.422 |
| 16 | .0961 | 1034.9 | 1.504 | 1033.4 | 1034.1 | 1.279 | 1.131 |

Air conditions 11.7°C

d = 1.27 cms.

V_{air} at 15°C = 0.145 C.G.S. units. Griffiths & Awbery. Pro. of Inst. of Mech. Eng. 1933.
 10°C = 0.140 " "
 ∴ at 11.7°C = 0.1417 " "

$$\frac{d}{\sqrt{V}} = \frac{1.27}{0.1417} = 8.97$$

P = (p₁ - p₂) A where A = flow area = 11.509 x 15.24 = 175.4 sq. cms.
 = 175.4 H_{water} ρ_{water} g.

$$\frac{P}{nd \rho_{air} V_{N,max}^2} = \frac{175.4 \times g.}{nd \rho_{air}} \cdot \frac{\rho_{water}}{\rho_{air} \text{ at centre of nest.}} \cdot \frac{H_{water}}{V_{N,max}^2}$$

$$= \frac{175.4 \times 981}{24 \times 1.27 \times 15.24} \cdot \frac{999.52}{1.231} \cdot \frac{H_{water}}{V_{N,max}^2}$$

370.5

Total Resistance. Parallel Arrangement. Air flow.

| | 9 | 10 | 11 | 12 | 13. | 14. | 15. | 16. |
|-----------|--|---|--|--|-----------------------------|------------|----------------------|---------------|
| Expt. No. | $Re = \frac{d}{\nu} V_{N.max}$ 8.97 $V_{N.max}$ | $V_{N.max}^2$ at centre of nest. ($\frac{cms.}{sec}$) ² | $\frac{H}{V_{N.max}^2}$ at centre of nest. | $\frac{\rho_{water}}{\rho_{air}}$ at centre of nest. | $\frac{P}{ndl/V_{N.max}^2}$ | \sqrt{C} | $\frac{1}{\sqrt{C}}$ | $Re \sqrt{C}$ |
| 1 | 37,200 | 17.54x10 ⁶ | 1.004x10 ⁶ | 813 | 0.3025 | .5498 | 1.819 | 20,460 |
| 2 | 35,900 | 16.36 | 1.014 | 813 | 0.3054 | .5524 | 1.808 | 19,840 |
| 3 | 35,350 | 15.78 | 1.019 | 812.5 | 0.3069 | .5539 | 1.805 | 19,580 |
| 4 | 34,330 | 14.89 | 1.021 | 812 | 0.3073 | .5542 | 1.803 | 19,030 |
| 5 | 32,950 | 13.68 | 1.030 | 811.5 | 0.3098 | .5564 | 1.796 | 18,340 |
| 6 | 31,600 | 12.55 | 1.025 | 811 | 0.3080 | .5550 | 1.801 | 17,540 |
| 7 | 30,100 | 11.38 | 1.042 | 810 | 0.3128 | .5590 | 1.788 | 16,840 |
| 8 | 28,500 | 10.21 | 1.047 | 810 | 0.3144 | .5606 | 1.783 | 15,960 |
| 9 | 27,050 | 9.17 | 1.054 | 809 | 0.3159 | .5620 | 1.778 | 15,200 |
| 10 | 25,530 | 8.18 | 1.062 | 809 | 0.3182 | .5641 | 1.771 | 14,400 |
| 11 | 23,830 | 7.11 | 1.072 | 809 | 0.3214 | .5670 | 1.763 | 13,500 |
| 12 | 20,650 | 5.33 | 1.098 | 808 | 0.3286 | .5733 | 1.743 | 11,840 |
| 13 | 17,740 | 3.931 | 1.133 | 808 | 0.3386 | .5820 | 1.717 | 10,330 |
| 14 | 15,250 | 2.904 | 1.165 | 807 | 0.3480 | .5900 | 1.694 | 8,990 |
| 15 | 12,750 | 2.027 | 1.183 | 807 | 0.3540 | .5950 | 1.679 | 7,580 |
| 16 | 10,140 | 1.281 | 1.174 | 806 | 0.3507 | .5922 | 1.687 | 6,000 |

where n = total number tube in nest = 24.

d = dia.of tube = 1.27 cms.

l = length of tube = 15.24 cms.

Table 2.1 A

Variation of pressure at the surface of the centre tube of the third row at a section $2\frac{3}{4}$ inches from the back wall - Staggered arrangement.

Venturi meter 2.1 ft. of water.

Temperature 15°C

| No. of Expt. | Angle | Pressure Tube | Inlet of Nest | Difference - ft. of H ₂ O | No. of Expt. | Angle | Pressure Tube | Inlet of Nest | Difference - ft. of H ₂ O |
|--------------|-------|---------------|---------------|--------------------------------------|--------------|-------|---------------|---------------|--------------------------------------|
| 1 | 340 | 0.670 | 0.851 | -0.181 | 35 | 135 | 0.526 | 0.986 | -0.460 |
| 2 | 345 | .700 | .822 | -.122 | 36 | 140 | .535 | .981 | -.446 |
| 3 | 350 | .720 | .798 | -.078 | 37 | 0 | | | -.045 |
| 4 | 355 | .736 | .787 | -.051 | 38 | 140 | .536 | .981 | -.445 |
| 5 | 0 | | | -.045 | 39 | 145 | .540 | .979 | -.439 |
| 6 | 5 | | | -.056 | 40 | 150 | .543 | .976 | -.433 |
| 7 | 10 | | | -.081 | 41 | 155 | .545 | .972 | -.427 |
| 8 | 15 | .695 | .825 | -.130 | 42 | 160 | .548 | .970 | -.422 |
| 9 | 20 | .665 | .853 | -.188 | 43 | 165 | .550 | .968 | -.418 |
| 10 | 25 | .635 | .885 | -.250 | 44 | 170 | .550 | .967 | -.417 |
| 11 | 30 | .605 | .913 | -.308 | 45 | 175 | .553 | .965 | -.412 |
| 12 | 0 | | | -.045 | 46 | 180 | .553 | .965 | -.412 |
| 13 | 35 | .582 | .933 | -.351 | 47 | 185 | .554 | .966 | -.412 |
| 14 | 40 | .567 | .951 | -.384 | 48 | 190 | .552 | .967 | -.415 |
| 15 | 45 | .552 | .962 | -.410 | 49 | 195 | .550 | .970 | -.420 |
| 16 | 50 | .545 | .971 | -.426 | 50 | 200 | .548 | .972 | -.424 |
| 17 | 55 | .536 | .980 | -.444 | 51 | 0 | .740 | .786 | -.046 |
| 18 | 60 | .532 | .985 | -.453 | 52 | 210 | .544 | .975 | -.431 |
| 19 | 65 | .520 | 1.000 | -.480 | 53 | 220 | .538 | .984 | -.446 |
| 20 | 70 | .504 | 1.010 | -.506 | 54 | 230 | .530 | .990 | -.460 |
| 21 | 75 | .495 | 1.020 | -.525 | 55 | 240 | .517 | 1.003 | -.486 |
| 22 | 80 | .485 | 1.030 | -.545 | 56 | 250 | .502 | 1.020 | -.518 |
| 23 | 85 | .475 | 1.040 | -.565 | 57 | 110 | .488 | 1.032 | -.544 |
| 24 | 90 | .470 | 1.045 | -.575 | 58 | 260 | .485 | 1.036 | -.551 |
| 25 | 0 | | | -.045 | 59 | 270 | .471 | 1.048 | -.577 |
| 26 | 90 | .471 | 1.045 | -.574 | 60 | 280 | .471 | 1.048 | -.577 |
| 27 | 95 | .469 | 1.046 | -.577 | 61 | 290 | .480 | 1.040 | -.560 |
| 28 | 100 | .471 | 1.045 | -.574 | 62 | 300 | .492 | 1.026 | -.534 |
| 29 | 105 | .476 | 1.039 | -.563 | 63 | 310 | .511 | 1.007 | -.496 |
| 30 | 110 | .483 | 1.030 | -.547 | 64 | 320 | .546 | .974 | -.428 |
| 31 | 115 | .499 | 1.020 | -.521 | 65 | 330 | .601 | .922 | -.321 |
| 32 | 120 | .505 | 1.010 | -.505 | 66 | 340 | .669 | .855 | -.186 |
| 33 | 125 | .514 | 1.003 | -.489 | 67 | 345 | .669 | .825 | -.126 |
| 34 | 130 | .522 | .993 | -.471 | 68 | 0 | .739 | .785 | -.046 |

Table 2.2 A and B.

Exploration of variation of pressure at the surface of the centre tubes of various rows at a section $2\frac{3}{4}$ inches from the back wall - Staggered arrangement.

1st Row.

| No. of Expt. | Angle | Pressure Tube. | In-let of Nest | Difference ft. of H ₂ O | Remarks. |
|--------------|-------|----------------|----------------|------------------------------------|---|
| 1 | 0 | | | +0.055 | Water Temperature 17.8°C Venturi Meter 2.1 ft. of water. |
| 2 | 5 | | | .054 | |
| 3 | 10 | | | .054 | |
| 4 | 15 | | | .048 | |
| 5 | 20 | | | .040 | |
| 6 | 30 | | | .0 | |
| 7 | 45 | 0.555 | 0.640 | -0.085 | ? |
| 8 | 50 | .540 | .658 | - .118 | |
| 9 | 55 | .515 | .680 | - .165 | |
| 10 | 60 | .495 | .695 | - .200 | |
| 11 | 65 | .476 | .717 | - .241 | |
| 12 | 70 | .451 | .745 | - .286 | |
| 13 | 75 | .435 | .760 | - .325 | |
| 14 | 90 | .410 | .778 | - .368 | |
| 15 | 0 | | | + .055 | |
| 16 | 105 | .430 | .760 | - .330 | |
| 17 | 120 | .435 | .756 | - .321 | |
| 18 | 135 | .435 | .756 | - .321 | |
| 19 | 150 | .430 | .761 | - .331 | |
| 20 | 165 | .430 | .760 | - .330 | |
| 21 | 180 | .430 | .755 | - .325 | |
| 22 | 0 | | | + .055 | Blown through. |
| 23 | 180 | .510 | .825 | - .315 | may be low. |
| 24 | 195 | .500 | .830 | - .330 | |
| 25 | 210 | .497 | .830 | - .333 | |
| 26 | 225 | .501 | .830 | - .329 | |
| 27 | 240 | .503 | .828 | - .325 | |

Table 2.2 A and B., continued.

| No. of Expt. | Angle | Pressure Tube | Inlet of Nest | Difference ft. of H ₂ O | Remarks. |
|--------------|-------|---------------|---------------|------------------------------------|----------|
| 28 | 255 | 0.500 | 0.835 | -0.335 | |
| 29 | 270 | .475 | .855 | - .380 | |
| 30 | 0 | | | +0.055 | |
| 31 | 285 | .500 | .835 | - .335 | |
| 32 | 290 | .521 | .815 | - .314 | |
| 33 | 295 | .535 | .800 | - .265 | |
| 34 | 300 | .557 | .780 | - .223 | |
| 35 | 305 | .583 | .750 | - .167 | |
| 36 | 310 | .600 | .735 | - .135 | |
| 37 | 315 | .621 | .720 | - .099 | |
| 38 | 330 | | | - .020 | |
| 39 | 335 | | | 0 | |
| 40 | 340 | | | +0.015 | |
| 41 | 345 | | | .035 | |
| 42 | 350 | | | .040 | |
| 43 | 355 | | | .050 | |
| 44 | 0 | | | .055 | |

3rd Row.

| | | | | | |
|----|-----|-------|-------|--------|---------------------------------|
| 1 | 0 | | | -0.045 | Water Temperature 14.5°C |
| 2 | 15 | 0.635 | 0.760 | - .125 | Venturi Meter 2.10 ft. of water |
| 3 | 30 | .540 | .845 | - .305 | |
| 4 | 45 | .635 | .735 | - .100 | Blown through |
| 5 | 0 | | | - .045 | |
| 6 | 45 | .506 | .916 | - .410 | |
| 7 | 60 | .485 | .938 | - .453 | |
| 8 | 75 | .445 | .975 | - .530 | Readings within ± 0.002 |
| 9 | 90 | .416 | 1.002 | - .586 | |
| 10 | 95 | .415 | 1.004 | - .589 | |
| 11 | 105 | .422 | .995 | - .573 | |
| 12 | 110 | .432 | .986 | - .554 | Manometer tube adjusted. |
| 13 | 110 | .342 | .897 | - .555 | |
| 14 | 80 | .342 | .900 | - .558 | |
| 15 | 85 | .335 | .908 | - .573 | |
| 16 | 120 | .360 | .880 | - .520 | |

Table 2.2 A and B, continued.

| No. of Expt. | Angle | Pressure Tube | Inlet of Nest. | Difference ft. of H ₂ O. | Remarks. |
|--------------|-------|---------------|----------------|-------------------------------------|----------------|
| 17 | 135 | 0.385 | 0.860 | -0.475 | Surge removed. |
| 18 | 150 | .402 | .842 | - .440 | |
| 19 | 165 | .410 | .835 | - .425 | |
| | 0 | | | - .045 | |
| 20 | 90 | .360 | .940 | - .580 | |
| 21 | 105 | .371 | .930 | - .559 | |
| 22 | 135 | .420 | .880 | - .460 | |
| 23 | 120 | .400 | .905 | - .505 | |
| 24 | 150 | .435 | .867 | - .432 | |
| 25 | 165 | .441 | .862 | - .421 | |
| 26 | 180 | .445 | .855 | - .410 | |
| 27 | 195 | .445 | .865 | - .420 | |
| 28 | 210 | .435 | .867 | - .432 | |
| 29 | 225 | .430 | .878 | - .448 | |
| 30 | 240 | .405 | .890 | - .485 | |
| 31 | 255 | .385 | .923 | - .538 | |
| 32 | 270 | .360 | .935 | - .575 | |
| 33 | 0 | | | -0.045 | |
| 34 | 285 | .365 | .933 | - .568 | |
| 35 | 300 | .385 | .915 | - .530 | |
| 36 | 315 | .420 | .885 | - .465 | |
| 37 | 330 | .496 | .810 | - .314 | |
| 38 | 345 | .595 | .720 | - .125 | |
| 39 | 0 | | | .045 | |
| 40 | 0 | | | - .044 | |
| 41 | 60 | .422 | .880 | - .458 | |
| 42 | 300 | .391 | .913 | - .522 | |
| 43 | 0 | | | - .045 | |
| 44 | 60 | .425 | .885 | - .460 | |
| 45 | 300 | .385 | .918 | - .533 | |

7th Row.

| | | | | | |
|----|-----|-------|-------|--------|---|
| 1 | 0 | 0.420 | 0.855 | -0.435 | Water Temperature 18.0°C Venturi Meter 2.10 ft. of water Indicated ⊙ on Fig. 2.2A |
| 2 | 15 | .380 | .901 | - .521 | |
| 3 | 30 | .290 | .988 | - .698 | |
| 4 | 45 | .241 | 1.030 | - .789 | |
| 5 | 60 | .215 | 1.060 | - .845 | |
| 6 | 75 | .180 | 1.090 | - .910 | |
| 7 | 90 | .145 | 1.125 | - .980 | |
| 8 | 0 | .420 | .860 | - .440 | |
| 9 | 90 | .138 | 1.140 | -1.002 | |
| 10 | 105 | .135 | 1.150 | -1.015 | |
| 11 | 120 | .162 | 1.120 | - .958 | |
| 12 | 135 | .190 | 1.097 | - .907 | |
| 13 | 150 | .200 | 1.086 | - .886 | |

Table 2.2 A and B, continued.

| No. of Expt. | Angle | Pressure Tube | Inlet of Nest. | Difference ft. of H ₂ O | Remarks. |
|--------------|-------|---------------|----------------|------------------------------------|----------------|
| 14 | 165 | 0.206 | 1.082 | -0.876 | |
| 15 | 180 | .210 | 1.065 | - .855 | |
| 16 | 0 | .420 | .856 | - .436 | |
| 17 | 180 | .212 | 1.060 | - .848 | |
| 18 | 195 | .215 | 1.070 | - .855 | |
| 19 | 210 | .210 | 1.070 | - .860 | |
| 20 | 225 | .205 | 1.075 | - .870 | |
| 21 | 240 | .194 | 1.100 | - .906 | |
| 22 | 255 | .175 | 1.105 | - .930 | |
| 23 | 270 | .150 | 1.135 | - .985 | |
| 24 | 0 | .421 | .865 | - .444 | |
| 25 | 270 | .150 | 1.140 | - .990 | |
| 26 | 285 | .140 | 1.150 | -1.010 | |
| 27 | 300 | .175 | 1.110 | - .935 | |
| 28 | 315 | .212 | 1.087 | - .875 | |
| 29 | 330 | .282 | 1.005 | - .723 | |
| 30 | 345 | .385 | .905 | - .620 | |
| 31 | 0 | .422 | .865 | - .443 | |
| 32 | 45 | .240 | 1.045 | - .805 | |
| 33 | 50 | .230 | 1.055 | - .825 | |
| 34 | 55 | .225 | 1.060 | - .835 | |
| 35 | 60 | .220 | 1.065 | - .845 | |
| 36 | 65 | .210 | 1.080 | - .870 | |
| 37 | 70 | .195 | 1.090 | - .895 | |
| 38 | 285 | .150 | 1.146 | - .996 | |
| 39 | 290 | .152 | 1.140 | - .988 | |
| 40 | 295 | .156 | 1.130 | - .974 | |
| 41 | 300 | .175 | 1.100 | - .925 | |
| 42 | 305 | .185 | 1.100 | - .915 | |
| 43 | 310 | .200 | 1.100 | - .900 | |
| 44 | 315 | .220 | 1.082 | - .862 | |
| 45 | 0 | .430 | .870 | - .440 | Speed varying. |


| | | | | | |
|----|-----|-------|-------|--------|--|
| 1 | 0 | 0.500 | 0.940 | -0.440 | Outlet cone adjusted concentrically Temperature of water 17.5°C Venturi Meter 2.1 ft. of water. Indicated  on Fig. 2.2A. |
| 2 | 15 | .445 | .980 | - .535 | |
| 3 | 30 | .365 | 1.070 | - .705 | |
| 4 | 40 | .325 | 1.105 | - .780 | |
| 5 | 50 | .310 | 1.127 | - .817 | |
| 6 | 60 | .295 | 1.145 | - .850 | |
| 7 | 70 | .270 | 1.160 | - .890 | |
| 8 | 80 | .240 | 1.195 | - .955 | |
| 9 | 90 | .220 | 1.215 | - .995 | |
| 10 | 0 | .500 | .940 | - .440 | |
| 11 | 100 | .215 | 1.220 | -1.005 | |
| 12 | 120 | .245 | 1.185 | - .940 | |
| 13 | 140 | .280 | 1.160 | - .880 | |

Table 2.2 A and B, continued.


| No. of Expt. | Angle | Pressure Tube | Inlet of Nest. | Difference ft. of H ₂ O | Remarks. |
|--------------|-------|---------------|----------------|------------------------------------|--|
| 14 | 160 | 0.285 | 1.145 | -0.860 | |
| 15 | 180 | .290 | 1.145 | - .855 | |
| 16 | 200 | .290 | 1.146 | - .856 | |
| 17 | 220 | .285 | 1.152 | - .867 | |
| 18 | 240 | .270 | 1.175 | - .905 | |
| 19 | 260 | .245 | 1.200 | - .955 | |
| 20 | 280 | .220 | 1.220 | -1.000 | |
| 21 | 0 | .500 | 0.940 | -0.440 | |
| 22 | 290 | .230 | 1.210 | - .980 | |
| 23 | 300 | .247 | 1.190 | - .943 | |
| 24 | 310 | .275 | 1.175 | - .900 | |
| 25 | 320 | .310 | 1.135 | - .825 | |
| 26 | 340 | .430 | 1.020 | - .590 | Blown through. |
| 27 | 0 | .430 | .870 | - .440 | |
| 28 | 320 | .240 | 1.070 | - .830 | |
| 29 | 330 | .297 | 1.010 | - .713 | |
| 30 | 340 | .365 | .950 | - .585 | |
| 31 | 350 | .415 | .900 | - .485 | |
| 32 | 0 | .430 | .870 | - .440 | |
| 33 | 0 | .510 | .950 | - .440 | Right hand side of outlet cone bent. |
| 34 | 50 | .325 | 1.135 | - .810 | Indicated  on Fig.2.2A. |
| 35 | 60 | .310 | 1.150 | - .840 | |
| 36 | 70 | .285 | 1.180 | - .895 | |
| 37 | 80 | .257 | 1.210 | - .953 | |
| 38 | 290 | .245 | 1.222 | - .977 | |
| 39 | 300 | .260 | 1.205 | - .945 | |
| 40 | 310 | .285 | 1.190 | - .905 | |
| 41 | 320 | .325 | 1.150 | - .825 | |
| 42 | 330 | .383 | 1.090 | - .707 | |
| 43 | 0 | .510 | .950 | - .440 | |

Table 2.4 A and B.

Nest of tubes rotated through 180° . Pressure distribution on the surface of the centre tubes of the 1st and 7th rows and on the first tube to the right of the centre line of the 2nd row.

Section $2\frac{3}{4}$ inches from back wall - Staggered arrangement.

1st Row.

| No. of Expt. | Angle | Pressure Tube | In-let of nest | Difference ft. of H ₂ O | Remarks. |
|--------------|-------|---------------|----------------|------------------------------------|---|
| 1 | 0 | 0.685 | 0.645 | +0.040 | Water temperature 18.4°C Venturi Meter 2.10 ft. of water |
| 2 | 10 | .680 | .645 | + .035 | |
| 3 | 20 | | | + .017 | |
| 4 | 30 | | | -0.015 | |
| 5 | 40 | .635 | .695 | - .060 | |
| 6 | 50 | .600 | .723 | - .123 | |
| 7 | 60 | .565 | .755 | - .190 | |
| 8 | 70 | .525 | .797 | - .272 | |
| 9 | 80 | .500 | .825 | - .325 | |
| 10 | 90 | .487 | .832 | - .345 | |
| 11 | 100 | .495 | .825 | - .330 | |
| 12 | 0 | .685 | .645 | | |
| 13 | 110 | .502 | .815 | - .313 | |
| 14 | 120 | .505 | .815 | - .310 | |
| 15 | 140 | .505 | .813 | - .308 | |
| 16 | 160 | .500 | .817 | - .317 | |
| 17 | 180 | .510 | .810 | - .300 | |
| 18 | 200 | .501 | .817 | - .316 | |
| 19 | 220 | .505 | .815 | - .310 | |
| 20 | 240 | .505 | .817 | - .312 | |
| 21 | 260 | .495 | .825 | - .330 | |
| 22 | 0 | .685 | .645 | | |
| 23 | 270 | .490 | .837 | - .347 | |
| 24 | 280 | .492 | .827 | - .335 | |
| 25 | 290 | .525 | .800 | - .275 | |
| 26 | 300 | .560 | .760 | - .200 | |
| 27 | 310 | .595 | .723 | - .128 | |
| 28 | 320 | .630 | .695 | - .065 | |
| 29 | 330 | | | - .017 | |
| 30 | 340 | | | + .015 | |
| 31 | 350 | | | + .032 | |
| 32 | 0 | .685 | .645 | + .040 | |

2nd Row.

| | | | | | |
|---|----|-------|-------|--------|---|
| 1 | 0 | | | +0.040 | Water temperature 18.4°C Venturi Meter 2.10 ft. of water |
| 2 | 10 | | | + .010 | |
| 3 | 20 | 0.685 | 0.807 | -0.122 | |

Table 2.4 A and B, continued.

| No. of Expt. | Angle | Pressure Tube | In-let of nest | Difference ft. of H ₂ O | Remarks. |
|--------------|-------|---------------|----------------|------------------------------------|----------------------|
| 4 | 30 | 0.600 | 0.890 | -0.290 | |
| 5 | 40 | .530 | .960 | - .430 | |
| 6 | 50 | .495 | .995 | - .500 | |
| 7 | 60 | .480 | 1.005 | - .525 | |
| 8 | 70 | .480 | 1.005 | - .525 | |
| 9 | 80 | .485 | 1.005 | - .520 | |
| 10 | 90 | .485 | 1.000 | - .515 | |
| 11 | 100 | .490 | .995 | - .505 | |
| 12 | 0 | .770 | .730 | | |
| 13 | 110 | .508 | .980 | - .472 | |
| 14 | 120 | .525 | .960 | - .435 | |
| 15 | 140 | .560 | .925 | - .365 | |
| 16 | 160 | .580 | .905 | - .325 | |
| 17 | 180 | .590 | .900 | - .310 | |
| 18 | 200 | .585 | .906 | - .321 | |
| 19 | 220 | .565 | .923 | - .358 | |
| 20 | 240 | .532 | .950 | - .418 | |
| 21 | 260 | .505 | .980 | - .475 | .500 - .985 = -.485. |
| 22 | 0 | | | +0.040 | |
| 23 | 270 | .495 | .992 | - .497 | |
| 24 | 280 | .495 | .995 | - .500 | |
| 25 | 290 | .495 | .990 | - .495 | |
| 26 | 300 | .497 | .990 | - .493 | ? |
| 27 | 310 | .500 | .990 | - .490 | |
| 28 | 320 | .530 | .955 | - .425 | |
| 29 | 330 | .598 | .890 | - .292 | |
| 30 | 340 | .690 | .805 | - .115 | |
| 31 | 350 | | | +0.010 | |
| 32 | 0 | | | + .042 | |

7th Row.

| | | | | | |
|----|-----|-------|-------|--------|---|
| 1 | 0 | 0.480 | 0.912 | -0.432 | Water temperature 18.0°C Venturi Meter 2.10 ft. of water |
| 2 | 10 | .460 | .930 | - .470 | |
| 3 | 20 | .410 | .980 | - .570 | |
| 4 | 30 | .350 | 1.035 | - .685 | |
| 5 | 40 | .300 | 1.085 | - .785 | |
| 6 | 50 | .280 | 1.112 | - .832 | |
| 7 | 60 | .255 | 1.130 | - .875 | |
| 8 | 70 | .235 | 1.145 | - .910 | |
| 9 | 80 | .215 | 1.170 | - .955 | |
| 10 | 90 | .205 | 1.180 | - .975 | |
| 11 | 100 | .215 | 1.165 | - .950 | |
| 12 | 0 | .480 | .910 | | |
| 13 | 110 | .230 | 1.160 | - .930 | |
| 14 | 120 | .242 | 1.145 | - .903 | |
| 15 | 140 | .260 | 1.130 | - .870 | |

Table 2.4 A and B, continued.

| No. of Expt. | Angle | Pressure Tube | In-let of Nest | Difference ft. of H ₂ O. | Remarks. |
|--------------|-------|---------------|----------------|-------------------------------------|---------------------|
| 16 | 160 | 0.270 | 1.120 | -0.850 | |
| 17 | 180 | .272 | 1.115 | - .843 | |
| 18 | 200 | .270 | 1.118 | - .848 | |
| 19 | 220 | .262 | 1.122 | - .860 | |
| 20 | 240 | .260 | 1.130 | - .870 | See later readings. |
| 21 | 260 | .255 | 1.132 | - .877 | " " " |
| 22 | 0 | .480 | .912 | - | |
| 23 | 270 | .200 | 1.195 | - .995 | |
| 24 | 280 | .205 | 1.190 | - .985 | |
| 25 | 290 | .220 | 1.170 | - .950 | |
| 26 | 300 | .245 | 1.150 | - .905 | |
| 27 | 310 | .260 | 1.125 | - .865 | |
| 28 | 320 | .295 | 1.100 | - .805 | |
| 29 | 330 | .345 | 1.043 | - .698 | |
| 30 | 340 | .410 | .985 | - .575 | |
| 31 | 350 | .460 | .930 | - .470 | |
| 32 | 0 | .480 | .913 | - .433 | |
| 33 | 0 | .435 | .865 | - .430 | |
| 34 | 180 | .230 | 1.067 | - .837 | may be low. |
| 35 | 200 | .225 | 1.070 | - .845 | |
| 36 | 220 | .217 | 1.090 | - .873 | unstable. |
| | | .217 | 1.080 | - .863 | |
| 37 | 240 | .200 | 1.120 | - .920 | unstable |
| | | .200 | 1.110 | - .900 | |
| 38 | 250 | .190 | 1.102 | - .912 | |
| 39 | 260 | .180 | 1.114 | - .934 | |
| 40 | 270 | .172 | 1.120 | - .952 | kink in pipe. |
| 41 | 270 | .155 | 1.145 | - .990 | |

Table 2.5 A.

Investigation of asymmetry of normal pressure at the surface of the centre tube of the 7th Row. - Staggered arrangement.

| Expt. No. | Distance from back wall. | Angle of Rotation | Inlet pressure Cms. of Water. | Outlet pressure Cms. of Water. | Total re-sistance of Nest. Cms. of Water. | Exploration Tube Pressure above atmosphere. Cms. of Water. | | |
|-----------|--------------------------|-------------------|-------------------------------|--------------------------------|---|--|-------|-------|
| 1 | $\frac{1}{2}$ " | 0 | -1.084 | -20.2 | 19.1 | -11.4 | | |
| 2 | | 180 | | -20.3 | 19.2 | -21.6 | | |
| 3 | | 60 | | | 19.2 | 23.1 -22.4 | | |
| 4 | $1\frac{1}{2}$ | 300 | | -20.5 | 19.4 | 22.7 -22.3 | | |
| 5 | | 90 | -1.093 | -20.6 | 19.5 | -24.8 | | |
| 6 | | 0 | -1.101 | -20.5 | 19.4 | -11.7 | | |
| 7 | $2\frac{1}{2}$ | 60 | | -20.6 | 19.5 | 21.4 -21.2 | | |
| 8 | | 90 | | | | -25.7 | | |
| 9 | | 180 | | -20.8 | 19.7 | -22.8 | | |
| 10 | $3\frac{1}{4}$ | 270 | -1.110 | -20.7 | 19.6 | 25.4 -25.0 | | |
| 11 | | 300 | | | | | | -24.2 |
| 12 | | 0 | | | | | -20.8 | 19.7 |
| 13 | $4\frac{1}{2}$ | 60 | | -20.9 | 19.8 | 22.7 -21.7 | | |
| 14 | | 90 | | | | 25.9 -25.3 | | |
| 15 | | 180 | | | | 23.1 -22.9 | | |
| 16 | $5\frac{1}{2}$ | 270 | | | | -25.0 | | |
| 17 | | 300 | | | | 24.9 -23.7 | | |
| 18 | | 0 | -1.128 | -21.1 | 20.0 | 13.7 -13.2 | | |
| 19 | $6\frac{1}{2}$ | 60 | | | | 25.2 -23.3 | | |
| 20 | | 90 | | | | 28.5 -28.1 | | |
| 21 | | 180 | -1.120 | | | 24.2 -23.5 | | |
| 22 | $7\frac{1}{2}$ | 270 | | | | 28.0 -27.5 | | |
| 23 | | 300 | | | | 27.2 -26.0 | | |
| 24 | | 0 | -1.128 | -21.1 | 20 | 14.0 -13.5 | | |
| 25 | $8\frac{1}{2}$ | 60 | | | | 27.2 -26.5 | | |
| 26 | | 90 | | | | 29.0 -28.2 | | |
| 27 | | 180 | | | | 24.2 -23.7 | | |
| 28 | $9\frac{1}{2}$ | 270 | | | | 28.2 -27.7 | | |
| 29 | | 300 | | | | 27.2 -25.2 | | |
| 30 | | 0 | -1.110 | -20.9 | 19.8 | 13.2 -12.5 | | |
| 31 | $10\frac{1}{2}$ | 60 | | | | 25.5 -25.0 | | |
| 32 | | 90 | | | | -25.0 | | |
| 33 | | 180 | | | | -22.7 | | |
| 34 | $11\frac{1}{2}$ | 270 | | | | -25.9 | | |
| 35 | | 300 | | | | 24.7 -23.0 | | |
| 36 | | 0 | -1.120 | -20.9 | 19.8 | -12.2 | | |
| 37 | $12\frac{1}{2}$ | 60 | | | | -25.7 | | |
| 38 | | 90 | | -21.0 | 19.9 | -25.9 | | |
| 39 | | 180 | | | | -23.3 | | |
| 40 | $13\frac{1}{2}$ | 270 | | | | -26.7 | | |
| 41 | | 300 | -1.128 | | 19.9 | -22.3 | | |
| 42 | | 0 | | | | -12.2 | | |
| 43 | $14\frac{1}{2}$ | 60 | | | | 25.7 -25.0 | | |
| 44 | | 90 | | | | -26.5 | | |
| 45 | | 180 | | | | -23.1 | | |
| 46 | $15\frac{1}{2}$ | 270 | | | | -26.7 | | |
| 47 | | 300 | | | | 24.7 -22.8 | | |

Table 2.5 B.

Investigation of asymmetry of normal pressure at surface of the centre tube of the 1st Row. - Staggered arrangement.

| Expt. No. | Distance from back wall in inches. | Angle of Rotation | Inlet Pressure. Cms. of Water. | Exploration Tube Pressure above atmosphere. Cms. of Water. | |
|-----------|------------------------------------|-------------------|--------------------------------|--|------|
| 1 | $\frac{1}{2}$ | 60° | 1.21 | -7.8 | -7.3 |
| 2 | $1\frac{1}{2}$ | | | -7.5 | -7.2 |
| 3 | $2\frac{1}{2}$ | | | -7.9 | -7.5 |
| 4 | $2\frac{3}{4}$ | | | -7.9 | -7.6 |
| 5 | 3 | | | -8.0 | -7.7 |
| 6 | $3\frac{1}{4}$ | | | -7.9 | -7.7 |
| 7 | $3\frac{3}{4}$ | | | -7.9 | -7.6 |
| 8 | $4\frac{1}{2}$ | | | -7.8 | -7.5 |
| 9 | $5\frac{1}{2}$ | | | -8.2 | -7.7 |
| 10 | $\frac{1}{2}$ | 300° | 1.21 | -7.4 | -6.8 |
| 11 | $1\frac{1}{2}$ | | | -7.5 | -6.9 |
| 12 | $2\frac{1}{2}$ | | | -7.9 | -7.0 |
| 13 | $2\frac{3}{4}$ | | | -7.7 | -6.7 |
| 14 | 3 | | | -7.2 | -6.8 |
| 15 | $3\frac{1}{4}$ | | | -7.2 | -6.7 |
| 16 | $3\frac{3}{4}$ | | | -7.3 | -7.1 |
| 17 | $4\frac{1}{2}$ | | | -7.3 | -6.9 |
| 18 | $5\frac{1}{2}$ | | | -7.4 | -6.8 |

Table 2.6

Normal pressure at surface of centre tube of 4th Row.
(i.e. last row) Parallel Arrangement. 21.6°C 30.34" H₂O

| Expt. No. | Distance from back wall. | Angle of Rotation. | Inlet pressure Cms. of Water. | Outlet pressure Cms. of Water. | Total resistance of Nest. Cms. of Water. | Exploration Tube Pressure above atmosphere. Cms. of Water. | | |
|-----------|--------------------------|--------------------|-------------------------------|--------------------------------|--|--|-------|-------|
| 1 | 1½" | 0 | -1.454 | -21.4 | 19.9 | -15.6 | | |
| 2 | | 10 | | -15.7 | | | | |
| 3 | | 20 | | -16.3 | | | | |
| 4 | | 30 | | -21.5 | | 20.0 | -17.4 | |
| 5 | | 40 | | -21.4 | | 19.9 | -19.1 | |
| 6 | | 50 | | | | | -21.6 | |
| 7 | | 60 | | -21.5 | | 20.0 | -24.8 | |
| 8 | | 70 | | | | | -28.2 | |
| 9 | | 80 | | | | | -30.6 | |
| 10 | | 90 | | | | | -31.4 | |
| 11 | | 100 | | | | | -30.4 | |
| 12 | | 110 | | | | | -28.4 | |
| 13 | | 120 | | | | | -26.6 | |
| 14 | | 130 | | | | | -25.8 | |
| 15 | | 140 | | | | | -25.5 | |
| 16 | | 150 | | | | | -25.5 | |
| 17 | | 160 | | | | | -25.4 | |
| 18 | | 170 | | | | | -25.1 | |
| 19 | | 180 | | | | | -25.1 | |
| 20 | | 190 | | | | -21.5 | 20.0 | -25.1 |
| 21 | | 200 | | | | | -25.3 | |
| 22 | | 210 | | | | | -25.5 | |
| 23 | | 220 | | | | | -25.6 | |
| 24 | | 230 | | | | | -26.0 | |
| 25 | | 240 | | | | | -26.9 | |
| 26 | | 250 | | | | | -28.9 | |
| 27 | | 260 | | | | | -30.9 | |
| 28 | | 270 | | -21.5 | | 20.0 | -31.7 | |
| 29 | | 280 | | | | | -30.5 | |
| 30 | | 290 | | | | | -27.6 | |
| 31 | | 300 | | | | | -24.0 | |
| 32 | | 310 | | | | | -20.7 | |
| 33 | | 320 | | | | | -18.3 | |
| 34 | | 330 | | | | | -16.6 | |
| 35 | | 340 | | | | | -15.9 | |
| 36 | | 350 | | | | | -15.7 | |
| 37 | | 360 | | -1.454 | | -21.5 | 20.0 | -15.6 |
| 1 | 3 | 0 | -1.445 | -21.5 | 20.1 | -15.75 | | |
| 2 | | 10 | | -15.8 | | | | |
| 3 | | 20 | | -16.1 | | | | |
| 4 | | 30 | | -17.0 | | | | |

Table 2.6, continued.

| Expt. No. | Distance from back wall. | Angle of Rotation | Inlet pressure Cms. of Water. | Outlet pressure Cms. of Water. | Total resistance of Nest. Cms. of Water. | Exploration Tube Pressure above atmosphere. Cms. of Water. | | | | |
|-----------|--------------------------|-------------------|-------------------------------|--------------------------------|--|--|--------|-------|--------|--------|
| 5 | 3" | 40 | -1.445 | -21.5 | 20.1 | -18.8 | | | | |
| 6 | | 50 | | | | -21.4 | | | | |
| 7 | | 60 | | | | -24.6 | | | | |
| 8 | | 70 | | | | -28.1 | | | | |
| 9 | | 80 | | | | -30.7 | | | | |
| 10 | | 90 | | | | -31.6 | | | | |
| 11 | | 100 | | | | -30.7 | | | | |
| 12 | | 110 | | | | -28.7 | | | | |
| 13 | | 120 | | | | -26.9 | | | | |
| 14 | | 130 | | | | -26.0 | | | | |
| 15 | | 140 | | | | -25.6 | | | | |
| 16 | | 150 | | | | -25.6 | | | | |
| 17 | | 160 | | | | -25.4 | | | | |
| 18 | | 170 | | | | -25.3 | | | | |
| 19 | | 180 | | | | -25.3 | | | | |
| 20 | | 190 | | | | -25.3 | | | | |
| 21 | | 200 | | | | -25.5 | | | | |
| 22 | | 210 | | | | -25.6 | | | | |
| 23 | | 220 | | | | -25.6 | | | | |
| 24 | | 230 | | | | -26.0 | | | | |
| 25 | | 240 | | | | -27.0 | | | | |
| 26 | | 250 | | | | -29.0 | | | | |
| 27 | | 260 | | | | -31.1 | | | | |
| 28 | | 270 | | | | -31.8 | | | | |
| 29 | | 280 | | | | -30.5 | | | | |
| 30 | | 290 | | | | -27.7 | | | | |
| 31 | | 300 | | | | -24.1 | | | | |
| 32 | | 310 | | | | -20.8 | | | | |
| 33 | | 320 | | | | -18.4 | | | | |
| 34 | | 330 | | | | -16.8 | | | | |
| 35 | | 340 | | | | -16.0 | | | | |
| 36 | | 350 | | | | -15.8 | | | | |
| 37 | | 360 | | | | -1.445 | -21.5 | 20.1 | -15.75 | |
| 1 | | 4 $\frac{1}{2}$ " | | | | 0 | -1.454 | -21.5 | 20.0 | -15.6 |
| 2 | | | | | | 10 | | | | -15.75 |
| 3 | | | | | | 20 | | | | -21.5 |
| 4 | 30 | | -17.2 | | | | | | | |
| 5 | 40 | | -18.8 | | | | | | | |
| 6 | 50 | | -21.4 | | | | | | | |
| 7 | 60 | | -21.4 | 19.9 | -24.5 | | | | | |
| 8 | 70 | | -28.0 | | | | | | | |
| 9 | 80 | | -21.4 | 19.9 | -30.6 | | | | | |
| 10 | 90 | | -21.5 | 20.0 | -31.8 | | | | | |
| 11 | 100 | | -30.7 | | | | | | | |

Table 2.6, continued.

| Expt. No. | Distance from back wall. | Angle of Rotation | Inlet pressure Cms. of Water. | Outlet pressure Cms. of Water. | Total resistance of Nest. Cms. of Water. | Exploration Tube Pressure above atmosphere. Cms. of Water. | | | | | |
|-----------|--------------------------|-------------------|----------------------------------|-----------------------------------|---|---|-------|------|-------|------|-------|
| 12 | 4½" | 110 | -1.454 | -21.5 | 20.0 | -28.7 | | | | | |
| 13 | | 120 | | | | -26.9 | | | | | |
| 14 | | 130 | | | | -25.9 | | | | | |
| 15 | | 140 | | | | -1.454 | -21.4 | 19.9 | -25.6 | | |
| 16 | | 150 | | | | | | | -25.4 | | |
| 17 | | 160 | | | | | | | -25.3 | | |
| 18 | | 170 | | | | | | | -25.3 | | |
| 19 | | 180 | | | | | | | -25.1 | | |
| 20 | | 190 | | | | | | | -25.1 | | |
| 21 | | 200 | | | | | | | -21.3 | 19.8 | -25.3 |
| 22 | | 210 | | | | | | | | | -25.4 |
| 23 | | 220 | | | | | | | | | -25.6 |
| 24 | | 230 | | | | | | | | | -26.0 |
| 25 | | 240 | -27.2 | | | | | | | | |
| 26 | | 250 | -29.1 | | | | | | | | |
| 27 | | 260 | -31.1 ? | | | | | | | | |
| 28 | | 270 | -31.8 | | | | | | | | |
| 29 | | 280 | -21.4 | 19.9 | -30.5 | | | | | | |
| 30 | | 290 | | | -27.5 | | | | | | |
| 31 | | 300 | | | -23.9 | | | | | | |
| 32 | | 310 | | | -20.5 | | | | | | |
| 33 | | 320 | | | -18.0 | | | | | | |
| 34 | | 330 | | | -16.5 | | | | | | |
| 35 | | 340 | | | -15.75 | | | | | | |
| 36 | | 350 | | | -15.5 | | | | | | |
| 37 | | 360 | -1.454 | -21.4 | 19.9 | -15.5 | | | | | |

Table 3.3.

Determination of "shift" of velocity distribution curve for an air jet 2 cms.diameter when recorded with cylindrical Pitot tube.

Standard Pitot tube 0.09 inside diameter 0.244 external diameter.

Cylindrical Pitot tube 0.635 cms.external diameter - Pressure hole 0.165 cms. diameter.

Air Velocity $U_0 = 3,900$ cms.per second. 24.5°C

Standard Pitot $1\frac{1}{2} D = 3$ cms., from nozzle.

| Expt. No. | Total Head | Zero. | Total Head - Zero = H. | y Cms. | y - 39.25 | Pitot Tube. | Pitot Tube - Zero = h. | $\frac{h}{H}$ | $\frac{u}{u_0} = \sqrt{\frac{h}{H}}$ |
|-----------|------------|-------|------------------------|--------|-----------|-------------|------------------------|---------------|--------------------------------------|
| 1 | 75.8 | 10.50 | 65.3 | 37.5 | -1.75 | 10.5 | 0 | | |
| 2 | | | | 37.8 | -1.45 | 10.45 | -0.05 | | |
| 3 | | | | 38.0 | -1.25 | 16.50 | 6.0 | .0919 | .303 |
| 4 | 75.2 | | 64.7 | 38.1 | -1.15 | 24.1 | 13.6 | .209 | .457 |
| 5 | | | | 38.2 | -1.05 | 37.3 | 26.8 | .414 | .644 |
| 6 | | | | 38.3 | -.95 | 53.7 | 43.2 | .667 | .817 |
| 7 | | | | 38.4 | -.85 | 66.0 | 55.5 | .855 | .925 |
| 8 | | | | 40.1 | +.85 | 66.5 | 56.0 | .862 | .928 |
| 9 | | | | 40.2 | .95 | 53.0 | 42.5 | .654 | .809 |
| 10 | 75.6 | | 65.1 | 40.3 | 1.05 | 39.0 | 28.5 | .438 | .662 |
| 11 | | | | 40.4 | 1.15 | 26.0 | 15.5 | .238 | .488 |
| 12 | | | | 40.5 | 1.25 | 18.9 | 8.4 | .129 | .359 |
| 13 | | | | 40.6 | 1.35 | 13.7 | 3.2 | .049 | .222 |
| 14 | | | | 40.8 | 1.55 | 10.6 | .1 | .0015 | .012 |
| 15 | | | | 41.0 | 1.75 | 10.45 | -.05 | | |
| 16 | | | | 41.5 | 2.25 | 10.5 | 0 | 0 | 0 |
| 17 | | | | 75.6 | | 65.1 | 38.5 | -.75 | 73.6 |
| 18 | 38.6 | -.65 | 75.1 | | | | 64.6 | .984 | .992 |
| 19 | 38.7 | -.55 | 75.5 | | | | 65.0 | .984 | .992 |
| 20 | 39.4 | +.15 | 75.0 | | | | 64.5 | .972 | .986 |

Table 3.3, continued.

| Expt. No. | Total Head | Zero. | Total Head - Zero = H. | y Cms. | y -39.25 | Pitot Tube. | Pitot Tube - Zero = h | $\frac{h}{H}$ | $\frac{u}{u_0} = \sqrt{\frac{h}{H}}$ |
|-----------|------------|-------|------------------------|--------|----------|-------------|-----------------------|---------------|--------------------------------------|
| 21 | 75.6 | 10.50 | 65.1 | 39.9 | +0.65 | 75.0 | 64.5 | 0.968 | 0.984 |
| 22 | | | | 39.0 | - .25 | 76.8 | 66.3 | .993 | .996 |
| 23 | 77.6 | | 67.1 | 39.4 | + .15 | 76.0 | 65.5 | .977 | .988 |
| 24 | 75.7 | | 65.2 | 40.0 | .75 | 72.0 | 61.5 | .944 | .972 |
| 25 | | | | 39.8 | .55 | 75.1 | 64.6 | .991 | .995 |
| 26 | 75.6 | | 65.1 | 39.7 | .45 | 74.9 | 64.4 | .989 | .994 |
| 27 | | | | 37.8 | -1.45 | 10.8 | .3 | .0046 | .068 |
| 28 | | | | 37.7 | -1.55 | 10.4 | -.1 | | |
| 29 | | | | 37.9 | -1.35 | 12.4 | 1.9 | .029 | .171 |

Cylindrical Pitot. 3 cm. from nozzle.

| | | | | | $\bar{y} = 42.13$ | | | | |
|----|------|------|------|------|-------------------|-------|------|-------|------|
| 1 | 75.0 | 10.5 | 64.5 | 40.5 | -1.63 | 13.6 | 3.1 | 0.048 | .219 |
| 2 | | | | 40.7 | -1.43 | 19.9 | 9.4 | .146 | .382 |
| 3 | | | | 43.8 | 1.67 | 12.8 | 2.3 | .035 | .189 |
| 4 | | | | 44.0 | 1.87 | 11.7 | 1.2 | .019 | .136 |
| 5 | | | | 44.5 | 2.37 | 11.0 | .5 | .008 | .088 |
| 6 | | | | 45.0 | 2.87 | 10.7 | .2 | .003 | .055 |
| 7 | | | | 45.5 | 3.37 | 10.5 | 0 | | |
| 8 | | 10.5 | | 46.0 | 3.87 | 10.5 | 0 | | |
| 9 | | | | 38.7 | -3.43 | 10.55 | .05 | .0008 | .028 |
| 10 | | | | 38.9 | -3.23 | 10.55 | .05 | | .028 |
| 11 | | | | 39.2 | -2.93 | 10.6 | .1 | .0015 | .039 |
| 12 | | | | 39.4 | -2.73 | 10.7 | .2 | .003 | .055 |
| 13 | | | | 39.7 | -2.43 | 11.0 | .5 | .007 | .088 |
| 14 | 75.5 | | 65.0 | 39.9 | -2.23 | 11.3 | .8 | .0123 | .111 |
| 15 | | | | 40.0 | -2.13 | 11.5 | 1.0 | .0153 | .124 |
| 16 | | | | 40.1 | -2.03 | 11.65 | 1.15 | .0175 | .132 |
| 17 | | | | 40.3 | -1.83 | 12.0 | 1.5 | .0228 | .151 |
| 18 | | | | 40.5 | -1.63 | 13.4 | 2.9 | .044 | .210 |
| 19 | | | | 40.7 | -1.43 | 20.2 | 9.7 | .146 | .385 |
| 20 | | | | 40.8 | -1.33 | 27.8 | 17.3 | .260 | .510 |
| 21 | | | | 43.6 | +1.47 | 18.3 | 7.8 | .117 | .342 |
| 22 | | | | 43.5 | 1.37 | 22.9 | 12.4 | .185 | .431 |
| 23 | 77.5 | | 67.0 | 43.4 | 1.27 | 31.6 | 21.1 | .315 | .561 |

Table 3.3, continued.

| Expt. No. | Total Head. | Zero. | Total Head - Zero = H | y Cms | y -42.13 | Pitot Tube | Pitot Tube - Zero = h | $\frac{h}{H}$ | $\frac{u}{u_0} = \sqrt{\frac{h}{H}}$ |
|-----------|-------------|-------|-----------------------|-------|----------|------------|-----------------------|---------------|--------------------------------------|
| 24 | | | 67.0 | 43.3 | 1.17 | 42.0 | 31.5 | .470 | .685 |
| 25 | | | | 43.2 | 1.07 | 53.4 | 42.9 | .640 | .800 |
| 26 | | | | 43.1 | .97 | 62.3 | 51.8 | .771 | .878 |
| 27 | 77.8 | | 67.3 | 43.0 | .87 | 67.6 | 57.1 | .849 | .921 |
| 28 | | | | 40.8 | -1.33 | 27.5 | 17.0 | .252 | .503 |
| 29 | | | | 40.9 | -1.23 | 38.2 | 27.7 | .412 | .642 |
| 30 | | | | 41.0 | -1.13 | 50.5 | 40.0 | .595 | .772 |
| 31 | 77.8 | | 67.3 | 41.1 | -1.03 | 61.2 | 50.7 | .754 | .868 |
| 32 | | | | 41.2 | -.93 | 68.0 | 57.5 | .855 | .925 |
| 33 | | | | 41.3 | -.83 | 71.7 | 61.2 | .909 | .952 |
| 34 | | | | 41.4 | -.73 | 73.8 | 63.3 | .941 | .970 |
| 35 | | | | 41.5 | -.63 | 74.5 | 64.0 | .948 | .974 |
| 36 | | | | 41.6 | -.53 | 75.7 | 65.2 | .974 | .987 |
| 37 | | | | 41.7 | -.43 | 76.1 | 65.6 | .981 | .990 |
| 38 | 77.2 | | 66.7 | 41.8 | -.33 | 76.2 | 65.7 | .986 | .993 |
| 39 | | | | 42.0 | -.13 | 76.6 | 66.1 | .992 | .996 |
| 40 | | | | 42.2 | +.07 | 76.5 | 66.0 | .995 | .998 |
| 41 | | | | 42.4 | .27 | 75.7 | 65.2 | .984 | .992 |
| 42 | | | | 42.5 | .37 | 75.4 | 64.9 | .979 | .990 |
| 43 | | | | 42.6 | .47 | 74.5 | 64.0 | .967 | .984 |
| 44 | | | | 42.7 | .57 | 73.5 | 63.0 | .950 | .975 |
| 45 | | | | 42.8 | .67 | 72.1 | 61.6 | .927 | .963 |
| 46 | | | | 42.9 | .77 | 70.0 | 59.5 | .907 | .953 |
| 47 | 76.2 | 10.5 | 65.7 | 43.0 | .87 | 66.7 | 56.2 | .856 | .926 |
| 48 | | | | 44.2 | 2.07 | 11.4 | .9 | .0137 | .117 |

Cylindrical Pitot. 3.D = 6 cms.from nozzle.

| | | | | | | | | | |
|----|------|------|------|------|------------------|------|------|-------|------|
| 1 | 76.0 | 10.5 | 65.5 | 39.5 | y-42.15 -2.65 | 10.8 | .3 | .0046 | .068 |
| 2 | | | | 39.7 | -2.45 | 11.0 | .5 | .0076 | .087 |
| 3 | | | | 40.0 | -2.15 | 11.3 | .8 | .0122 | .110 |
| 4 | | | | 40.3 | -1.85 | 12.9 | 2.4 | .0367 | .191 |
| 5 | | | | 40.5 | -1.65 | 16.0 | 5.5 | .084 | .290 |
| 6 | | | | 40.7 | -1.45 | 22.2 | 11.7 | .179 | .423 |
| 7 | | | | 40.8 | -1.35 | 27.1 | 16.6 | .253 | .503 |
| 8 | | | | 40.9 | -1.25 | 33.2 | 22.7 | .347 | .589 |
| 9 | 76.1 | | 65.6 | 41.0 | -1.15 | 40 | 29.5 | .450 | .670 |
| 10 | | | | 43.2 | +1.05 | 45.1 | 34.6 | .527 | .726 |
| 11 | | | | 43.3 | 1.15 | 38.3 | 27.8 | .424 | .651 |
| 12 | | | | 43.4 | 1.25 | 32.3 | 21.8 | .332 | .577 |
| 13 | | | | 43.5 | 1.35 | 27.0 | 16.5 | .252 | .502 |
| 14 | | | | 43.6 | 1.45 | 22.5 | 12.0 | .183 | .428 |
| 15 | | | | 43.7 | 1.55 | 19.2 | 8.7 | .133 | .364 |
| 16 | | | | 43.8 | 1.65 | 16.5 | 6.0 | .092 | .303 |

Table 3.3, continued.

| Expt. No. | Total Head | Zero. | Total Head - Zero = H. | y Cms. | y -42.15 | Pitot Tube. | Pitot Tube - Zero = h. | $\frac{h}{H}$ | $\frac{u}{u_0} = \sqrt{\frac{h}{H}}$ |
|-----------|------------|-------|------------------------|--------|----------|-------------|------------------------|---------------|--------------------------------------|
| 17 | 76.1 | 10.5 | 65.6 | 43.9 | 1.75 | 14.8 | 4.3 | .066 | .256 |
| 18 | | | | 44.0 | 1.85 | 13.4 | 2.9 | .044 | .210 |
| 19 | | | | 44.2 | 2.05 | 11.8 | 1.3 | .0198 | .141 |
| 20 | | | | 44.4 | 2.25 | 11.1 | .6 | .0092 | .096 |
| 21 | | | | 44.6 | 2.45 | 10.9 | .4 | .0061 | .078 |
| 22 | | | | 45.0 | 2.85 | 10.7 | .2 | .0031 | .055 |
| 23 | 75.9 | | 65.4 | 45.5 | 3.35 | 10.5 | 0 | 0 | 0 |
| 24 | | | | 43.2 | 1.05 | 45.3 | 34.8 | .532 | .730 |
| 25 | | | | 43.1 | .95 | 52.2 | 41.7 | .638 | .798 |
| 26 | | | | 43.0 | .85 | 58.5 | 48.0 | .734 | .857 |
| 27 | | | | 42.9 | .75 | 63.5 | 53.0 | .810 | .900 |
| 28 | | | | 42.8 | .65 | 67.3 | 56.8 | .870 | .933 |
| 29 | | | | 42.7 | .55 | 70.0 | 59.5 | .910 | .954 |
| 30 | | | | 42.6 | .45 | 72.1 | 61.6 | .942 | .971 |
| 31 | | | | 42.5 | .35 | 73.1 | 62.6 | .957 | .978 |
| 32 | | | | 42.4 | .25 | 73.9 | 63.4 | .970 | .985 |
| 33 | | | | 42.3 | .15 | 74.2 | 63.7 | .974 | .987 |
| 34 | | | | 42.2 | .05 | 74.6 | 64.1 | .980 | .990 |
| 35 | | | | 42.1 | -.05 | 74.8 | 64.3 | .982 | .991 |
| 36 | | 10.55 | 65.65 | 42.0 | -.15 | 74.7 | 64.15 | .977 | .989 |
| 37 | | | | 41.9 | -.25 | 74.5 | 63.95 | .975 | .988 |
| 38 | 76.2 | | | 41.8 | -.35 | 74.2 | 63.65 | .970 | .985 |
| 39 | | | | 41.7 | -.45 | 73.2 | 62.65 | .954 | .977 |
| 40 | | | | 41.6 | -.55 | 72.3 | 61.75 | .941 | .970 |
| 41 | | | | 41.5 | -.65 | 70.2 | 59.65 | .909 | .954 |
| 42 | | | | 41.4 | -.75 | 66.9 | 56.35 | .858 | .926 |
| 43 | | | | 41.3 | -.85 | 61.6 | 51.05 | .778 | .882 |
| 44 | | | | 41.2 | -.95 | 55.3 | 44.75 | .682 | .826 |
| 45 | | | | 41.1 | -1.05 | 47.9 | 37.35 | .569 | .754 |
| 46 | | | | 41.0 | -1.15 | 39.9 | 29.35 | .447 | .669 |
| 47 | | | | 39.0 | -3.15 | 10.7 | .15 | .0023 | .048 |
| 48 | | | | 38.5 | -3.65 | 10.55 | 0 | | |
| 49 | | 10.55 | | 38.0 | -4.15 | 10.55 | 0 | | |

Standard Pitot. 3.D = 6 cms. from nozzle.

| | | | | | y-39.3 | | | | |
|---|------|-------|-------|------|--------|------|-------|-------|------|
| 1 | 76.2 | 10.55 | 65.65 | 37.3 | -2.0 | 10.6 | .05 | .0008 | .028 |
| 2 | | | | 37.5 | -1.8 | 10.9 | .35 | .0053 | .073 |
| 3 | | | | 37.7 | -1.6 | 12.6 | 2.05 | .031 | .177 |
| 4 | | | | 37.9 | -1.4 | 17.5 | 6.95 | .107 | .326 |
| 5 | | | | 38.0 | -1.3 | 21.5 | 10.95 | .168 | .410 |
| 6 | | | | 38.1 | -1.2 | 26.8 | 16.25 | .251 | .500 |
| 7 | | | | 38.2 | -1.1 | 33.9 | 23.35 | .361 | .601 |
| 8 | | | | 38.3 | -1.0 | 42.0 | 31.45 | .488 | .699 |

Table 3.3, continued.

| Expt. No. | Total Head. | Zero. | Total Head - Zero = H. | y Cms. | y -39.3 | Pitot Tube. | Pitot Tube - Zero = h. | $\frac{h}{H}$ | $\frac{u}{u_0} = \sqrt{\frac{h}{H}}$ |
|-----------|-------------|-------|------------------------|--------|---------|-------------|------------------------|---------------|--------------------------------------|
| 9 | | | | 38.4 | - .9 | 50.5 | 39.95 | .621 | .788 |
| 10 | 74.8 | | 64.25 | 38.5 | - .8 | 59.6 | 49.05 | .764 | .874 |
| 11 | 76.2 | | 65.65 | 38.5 | - .8 | 60.6 | 50.05 | .762 | .873 |
| 12 | | | | 40.0 | + .7 | 62.8 | 52.25 | .794 | .891 |
| 13 | | | | 40.1 | .8 | 56.1 | 45.55 | .689 | .830 |
| 14 | | | | 40.2 | .9 | 47.7 | 37.15 | .560 | .749 |
| 15 | | | | 40.3 | 1.0 | 39.5 | 28.95 | .435 | .660 |
| 16 | | | | 40.4 | 1.1 | 32.9 | 22.35 | .335 | .579 |
| 17 | | | | 40.5 | 1.2 | 26.5 | 15.95 | .238 | .488 |
| 18 | | | | 40.6 | 1.3 | 22.1 | 11.55 | .172 | .415 |
| 19 | 78.0 | | 67.45 | 40.7 | 1.4 | 18.3 | 7.75 | .115 | .339 |
| 20 | 76.0 | | 65.45 | 40.7 | 1.4 | 18.0 | 7.45 | .114 | .337 |
| 21 | | | | 40.8 | 1.5 | 15.3 | 4.75 | .073 | .270 |
| 22 | | | | 41.0 | 1.7 | 12.1 | 1.55 | .024 | .154 |
| 23 | | | 65.00 | 41.2 | 1.9 | 10.9 | .35 | .0054 | .073 |
| 24 | | | | 41.4 | 2.1 | 10.6 | .05 | .0008 | .028 |
| 25 | | | | 41.6 | 2.3 | 10.5 | - .05 | | |
| 26 | | 10.55 | | 42.0 | 2.7 | 10.55 | 0 | 0 | 0 |
| 27 | 74.9 | | 64.35 | 39.2 | - .1 | 74.9 | 64.35 | 1.000 | 1.000 |
| 28 | 76.1 | | 65.55 | 39.2 | - .1 | 75.8 | 65.25 | .997 | .999 |
| 29 | | | | 39.0 | - .3 | 75.8 | 65.25 | .997 | .999 |
| 30 | | | | 38.8 | - .5 | 74.2 | 63.65 | .972 | .986 |
| 31 | | | | 38.6 | - .7 | 66.6 | 56.05 | .854 | .924 |
| 32 | | | | 38.6 | - .7 | 67.0 | 56.45 | .861 | .928 |
| 33 | | | | 38.7 | - .6 | 71.9 | 61.35 | .934 | .966 |
| 34 | | | | 38.5 | - .8 | 59.4 | 48.85 | .744 | .862 |
| 35 | | | | 39.4 | + .1 | 75.7 | 65.15 | .977 | .989 |
| 36 | | | | 39.5 | .2 | 75.5 | 64.95 | .989 | .995 |
| 37 | | | | 39.6 | .3 | 75.0 | 64.45 | .980 | .990 |
| 38 | | | | 39.7 | .4 | 73.8 | 63.25 | .962 | .981 |
| 39 | | | | 39.8 | .5 | 71.6 | 61.05 | .927 | .963 |
| 40 | | | | 39.9 | .6 | 68.2 | 57.65 | .874 | .935 |
| 41 | 76.6 | | 66.05 | 40.0 | .7 | 62.9 | 52.35 | .793 | .890 |

Table 5.4C (See also table 11.2 and 11.3).

Effect of variation of air speed on mean ordinate of form drag diagram.

Experiments were carried out on the first row, centre tube at a distance of 3.8 cms. from the back wall - Parallel arrangement.

1st Row.

| Expt. No. | Cathetometer Reading. | Tachometer | Anemometer | Mean Ordinate |
|-----------|-----------------------|-------------|-------------|---------------|
| 1 | 1.021cms | 1940 R.P.M. | 98.5 m.p.h. | 7.342 cms. |
| 2 | 1.074 | 1999 | 101.75 | 7.735 |
| 3 | 1.160 | 2065 | 106.25 | 8.397 |
| 4 | 1.193 | 2110 | 109.0 | 8.825 |
| 5 | 1.218 | 2140 | 110.5 | 9.060 |
| 6 | 1.275 | 2182 | 113.25 | 9.447 |
| 7 | 1.325 | 2220 | 115.75 | 9.782 |

Table 5.5

Relationship between "central ordinate" and "mean ordinate" of form drag diagrams.

Parallel arrangement.

First Row, centre tube.

Variable speed test - section 5.4

| | | | | | | | |
|------------------|-------|-------|-------|-------|-------|-------|-------|
| Mean Ordinate. | 7.342 | 7.735 | 8.397 | 8.825 | 9.06 | 9.447 | 9.78 |
| Central Ordinate | 10.18 | 10.71 | 11.65 | 12.25 | 12.60 | 13.06 | 13.57 |

Other Diagrams.

| | | | | | | |
|-------------------|-------|-------|-------|-------|-------|-------|
| Mean Ordinate. | 8.35 | 8.787 | 8.405 | 8.167 | 8.505 | 8.875 |
| Central Ordinate. | 11.53 | 12.15 | 11.65 | 11.16 | 11.73 | 12.25 |

1st Row - Top tube.

| | | | | | | |
|-------------------|-------|-------|-------|-------|-------|-------|
| Mean Ordinate. | 7.905 | 7.955 | 8.15 | 8.112 | 7.882 | 8.037 |
| Central Ordinate. | 11.15 | 11.27 | 11.55 | 11.36 | 11.20 | 11.37 |

Second Row - centre tube.

| | | | | | | |
|-------------------|-------|-------|-------|-------|-------|-------|
| Mean Ordinate. | 5.132 | 5.082 | 5.153 | 5.243 | 4.992 | 4.780 |
| Central Ordinate. | 5.40 | 5.30 | 5.07 | 5.14 | 4.86 | 4.47 |

Third Row - centre tube.

| | | | | | |
|-------------------|------|-----|------|------|------|
| Mean Ordinate. | 5.14 | 5.0 | 5.18 | 5.27 | 5.38 |
| Central Ordinate. | 6.7 | 6.4 | 6.87 | 6.88 | 6.7 |

Fourth Row - centre tube.

Variable speed test - section 10.2

| | | | | |
|-------------------|------|------|-------|------|
| Mean Ordinate. | 6.51 | 5.46 | 3.395 | 2.11 |
| Central Ordinate. | 8.75 | 7.40 | 4.45 | 2.76 |

Other Diagrams.

| | | | | | |
|-------------------|------|------|-------|-------|------|
| Mean Ordinate. | 5.57 | 5.44 | 5.497 | 5.367 | 5.65 |
| Central Ordinate. | 7.43 | 6.91 | 7.4 | 7.12 | 7.45 |

Fourth Row - Top Tube.

| | | | | | | | |
|-------------------|-------|-------|-------|-------|-------|-------|-------|
| Mean Ordinate. | 6.182 | 5.877 | 5.782 | 6.135 | 5.987 | 6.092 | 6.215 |
| Central Ordinate. | 7.6 | 7.58 | 7.32 | 7.29 | 7.5 | 7.65 | 7.85 |

Table 5.8.

The Effect of Initial Turbulence in the Air-Stream.

These experiments were carried out before the slide damper was fitted to the fan outlet. The air speed was controlled by placing a sack or a sieve or both over the fan discharge.

Air Temperature 10°C.

Free Inlet.

| Expt. No. | Total Friction | Central Ordinate | Remarks. |
|-----------|----------------|------------------|---|
| 1 | 15.2 cms. | 11.51 cms. | With sack and sieve on outlet of fan. Sack removed. Sieve removed. Plotted ⊙ |
| 2 | 13.76 | 10.21 | |
| 3 | 11.8 | 8.61 | |
| 4 | 9.25 | 6.56 | |
| 5 | 9.30 | 6.61 | |
| 6 | 8.40 | 5.96 | |
| 7 | 6.75 | 4.62 | |
| 8 | 6.13 | 4.19 | |
| 9 | 10.50 | 7.68 | |
| 10 | 12.02 | 8.88 | |
| 11 | 13.39 | 9.95 | |
| 12 | 15.21 | 11.46 | |
| 13 | 16.97 | 13.00 | |
| 14 | 18.02 | 13.90 | |
| 15 | 18.42 | 14.39 | |
| 16 | 16.26 | 12.50 | |

With cords over inlet of nest.

| | | | |
|----|---------------|---------------|--------------------|
| 1 | 16.1 | 12.26 | Plotted with dots. |
| 2 | 16.82 | 12.8 | |
| 3 | 17.18 | 13.13 | |
| 4 | 17.70 | 13.65 | |
| 5 | 18.85 | 14.56 | |
| 6 | 18.20 | 14.09 | |
| 7 | 17.82 | 13.70 | |
| 8 | 17.59 | 13.48 | |
| 9 | 16.8 to 16.91 | 12.8 to 12.92 | |
| 10 | 16.38 | 12.43 | |
| 11 | 16.05 | 12.15 | |
| 12 | 15.08 | 11.40 | |
| 13 | 13.97 | 10.43 | |
| 14 | 13.07 | 9.70 | |

Table 5.8, continued.

With cords and circular sieve over inlet.

| Expt. No. | Total Friction | Central Ordinate | Remarks. |
|-----------|----------------|------------------|-----------|
| 1 | 17.70 cms. | 13.42 cms. | Plotted x |
| 2 | 16.39 | 12.22 | |
| 3 | 15.35 | 11.40 | |
| 4 | 14.48 | 10.62 | |
| 5 | 13.37 | 9.70 | |

With cords and perforated zinc over inlet.

| | | | |
|---|-------|-------|--------------------|
| 1 | 16.68 | 12.65 | Plotted \diamond |
| 2 | 16.09 | 12.01 | |
| 3 | 15.30 | 11.51 | |
| 4 | 14.55 | 10.90 | |
| 5 | 13.55 | 10.12 | |
| 6 | 12.20 | 8.90 | |

With perforated zinc 8.25 cms.in front of first row of tubes.

| | | | |
|---|-------|------|-------------------|
| 1 | 10.78 | 7.26 | Plotted \square |
| 2 | 9.90 | 6.65 | |
| 3 | 9.32 | 6.20 | |
| 4 | 8.85 | 5.83 | |
| 5 | 8.13 | 5.32 | |

Tables 7.5 A and B.

Velocity distribution in eddy A of figure 7.3 B'

| | A | B | A/B | Length of Streak. |
|----|---------|---------|-------|-------------------|
| 1 | 0.35cms | 2.8 cms | 0.125 | 0.2 cms. |
| 2 | .5 | 3.0 | .167 | .2 |
| 3 | .7 | 3.4 | .21 | .3 |
| 4 | .8 | 3.2 | .25 | .6 |
| 5 | .75 | 2.75 | .27 | .65 |
| 6 | .6 | 3.55 | .17 | .3 |
| 7 | .55 | 4.6 | .12 | .2 |
| 8 | .5 | 4.2 | .12 | .35 |
| 9 | .8 | 4.2 | .19 | .4 |
| 10 | 1.3 | 4.6 | .28 | .25 |
| 11 | 1.55 | 4.6 | .34 | .25 |
| 12 | 1.9 | 4.1 | .46 | .7 |
| 13 | 2.3 | 4.2 | .55 | .9 |
| 14 | 1.5 | 2.85 | .53 | 1.1 |
| 15 | 1.85 | 2.8 | .66 | .95 |
| 16 | 2.05 | 2.8 | .73 | .85 |
| 17 | 1.4 | 4.2 | .33 | .6 |
| 18 | 1.7 | 4.2 | .40 | .8 |
| 19 | 2.3 | 4.1 | .56 | 1.4 |
| 20 | 3.0 | 4.3 | .70 | 1.1 |
| 21 | 3.3 | 4.2 | .79 | 1.15 |
| 22 | 3.3 | 3.9 | .85 | 1.0 |
| 23 | 2.3 | 4.6 | .50 | 1.0 |
| 24 | 1.5 | 4.0 | .37 | .7 |
| 25 | 1.0 | 4.2 | .24 | .45 |
| 26 | .8 | 2.9 | .28 | .65 |
| 27 | .9 | 3.2 | .28 | .6 |
| 28 | 1.1 | 3.1 | .35 | .7 |
| 29 | 1.2 | 2.8 | .43 | .85 |
| 30 | 1.4 | 2.8 | .50 | .85 |
| 31 | 2.1 | 3.4 | .62 | .85 |
| 32 | 1.5 | 2.8 | .53 | 1.0 |
| 33 | 2.1 | 3.0 | .70 | 1.05 |
| 34 | 2.3 | 3.0 | .77 | 1.2 |
| 35 | 2.5 | 2.75 | .91 | 1.15 |
| 36 | 2.8 | 3.0 | .93 | 1.1 |
| 37 | 3.2 | 3.4 | .94 | 1.2 |
| 38 | 4.6 | 4.6 | 1.00 | 1.5 |
| 39 | 3.5 | 3.5 | 1.00 | 1.4 |
| 40 | 2.95 | 4.6 | .64 | .55 |
| 41 | 4.2 | 4.55 | .92 | .75 |
| 42 | 4.5 | 4.5 | 1.00 | .7 |
| 43 | 2.8 | 3.7 | .76 | .65 |
| 44 | 3.1 | 4.1 | .76 | .7 |
| 45 | 3.6 | 4.0 | .90 | .55 |
| 46 | 3.7 | 4.4 | .84 | .85 |
| 47 | 4.2 | 4.5 | .93 | .65 |
| 48 | 4.4 | 4.4 | 1.00 | .75 |

Tables 7.5 A and B. continued.

Velocity distribution in eddy B of figure 7.3 B'

| | A | B | A/B | Length of Streak. |
|----|---------|---------|------|-------------------|
| 1 | 0.3 cms | 3.0 cms | 0.10 | 0.5 cms. |
| 2 | .6 | 3.0 | .20 | .4 |
| 3 | .7 | 3.2 | .22 | .4 |
| 4 | .9 | 3.4 | .26 | .35 |
| 5 | 1.1 | 3.3 | .33 | .6 |
| 6 | 1.0 | 3.2 | .31 | .8 |
| 7 | 1.1 | 3.1 | .35 | .9 |
| 8 | 1.2 | 3.0 | .40 | .9 |
| 9 | 1.5 | 2.9 | .52 | .9 |
| 10 | 1.9 | 2.7 | .70 | 1.0 |
| 11 | 2.1 | 2.7 | .78 | 1.1 |
| 12 | 2.1 | 3.4 | .62 | .9 |
| 13 | 2.5 | 3.2 | .78 | .8 |
| 14 | 2.5 | 3.1 | .81 | 1.0 |
| 15 | 3.1 | 3.1 | 1.00 | 1.2 |
| 16 | 3.0 | 3.3 | .91 | .8 |
| 17 | 3.4 | 3.4 | 1.00 | 1.0 |
| 18 | 1.5 | 3.4 | .44 | .8 |
| 19 | 1.6 | 3.4 | .47 | .85 |
| 20 | 1.9 | 3.4 | .60 | .9 |
| 21 | 1.6 | 3.0 | .53 | 1.2 |
| 22 | 1.7 | 3.0 | .57 | 1.2 |
| 23 | 2.6 | 3.2 | .81 | .9 |
| 24 | 2.7 | 3.1 | .87 | 1.0 |
| 25 | 2.0 | 2.8 | .71 | 1.1 |
| 26 | .7 | 3.1 | .22 | .4 |
| 27 | 1.1 | 3.1 | .35 | .5 |
| 28 | 1.6 | 3.0 | .53 | 1.1 |
| 29 | 1.9 | 2.9 | .65 | 1.0 |
| 30 | 2.0 | 2.9 | .69 | 1.0 |
| 31 | 2.1 | 2.9 | .72 | 1.0 |
| 32 | 1.5 | 3.1 | .48 | .55 |
| 33 | 1.3 | 3.2 | .41 | .5 |
| 34 | .8 | 3.3 | .24 | .3 |
| 35 | .45 | 3.3 | .14 | .3 |
| 36 | .2 | 2.8 | .07 | .4 |
| 37 | 1.7 | 3.3 | .52 | .5 |
| 38 | 2.1 | 3.2 | .66 | 1.0 |
| 39 | 2.5 | 3.2 | .78 | 1.0 |
| 40 | 2.7 | 3.2 | .84 | 1.0 |
| 41 | 1.2 | 3.2 | .37 | .5 |
| 42 | 1.8 | 3.4 | .53 | .6 |
| 43 | 1.9 | 3.3 | .57 | .7 |
| 44 | 2.2 | 3.3 | .67 | 1.0 |
| 45 | 2.3 | 3.3 | .70 | .6 |
| 46 | 2.9 | 3.1 | .94 | 1.0 |

Table 7.5 A and B, continued.

| | A | B | A/B | Length of Streak. |
|----|---------|---------|------|-------------------|
| 47 | 3.3 cms | 3.3 cms | 1.00 | 0.8 cms |
| 48 | 1.6 | 3.0 | .53 | .65 |
| 49 | 1.7 | 2.9 | .59 | .75 |
| 50 | 2.0 | 2.9 | .69 | 1.1 |
| 51 | 2.5 | 2.9 | .86 | 1.2 |
| 52 | 2.7 | 2.7 | 1.00 | 1.5 |

Table 8.6

Velocity at the tube surface as determined by the electric tray experiment with wakes in position.

In air flow experiments for centre tube of first row shown in fig.5.2F. cathetometer reading was 1.171 cms. of water.

$$\frac{\rho V_o^2}{2} = 1.171 \times \text{nozzle coefficient } 0.96 \text{ (in cms.of water).}$$

$$= 1.124 \quad \text{'' '' '' ''}$$

$$\left(\frac{V_{N.\max}}{V_o}\right)^2 = 8.76$$

Therefore $\frac{\rho V_{N.\max}^2}{2} = 1.124 \times 8.76$

$$= 9.85 \text{ cms.of water.}$$

On the electric tray $V_{N.\max}$ was represented by a reading of 705 and the head of water "h" is proportional to q^2

At 60° $q = 657$ therefore $h = \left(\frac{657}{705}\right)^2 \times 9.85 = 8.55$

Sensitivity 80 - Perfect phase.

| | | |
|--|---------------------------|-------|
| $V_{N.\max}$ from 1.048 $V_{\text{centre line}}$ | = | 705 |
| $V_{N.\max}$ from 2.97 V_o | = | 705 |
| θ | $\frac{705q}{V_{N.\max}}$ | h. |
| 90° | 817.5 | 13.24 |
| 85 | 825 | 13.48 |
| 80 | 811 | 13.03 |
| 70 | 744 | 10.96 |
| 60 | 657 | 8.55 |
| 50 | 533 | 5.63 |
| 40 | 438 | 3.80 |
| 30 | 323 | 2.07 |
| 20 | 211 | .88 |
| 10 | 106 | .22 |
| 0 | 0 | 0 |
| $V_{c.l.}$ | 673 | |
| $V_y = 16.5$ | 703 | |
| $V_y = 24.3$ | 702.5 | |
| V_o | 237.5 | |

Table 9.2 Curve plotted on fig. 3.1C

$$\sqrt[3]{20^2} = 0.209$$

$$\eta = \frac{y}{x} = \frac{y}{.6605} \quad \text{where } y \text{ is in inches.}$$

$$\text{Therefore } y = 0.6605\eta = 0.1381 \frac{\eta}{\sqrt[3]{20^2}}$$

| $\frac{\eta}{\sqrt[3]{20^2}}$ | y _{side} in inches. | $\frac{u}{U_0}$ | u in cms/sec. |
|-------------------------------|---------------------------------|-----------------|---------------|
| 0.981 | 0.1355 | 1.000 | 4260 |
| 0.731 | 0.1009 | .969 | 4127 |
| 0.481 | 0.0664 | .895 | 3811 |
| 0.231 | 0.0319 | .791 | 3370 |
| -0.019 | -0.0026 | .668 | 2844 |
| -0.269 | -0.0371 | .538 | 2291 |
| -0.519 | -0.0717 | .411 | 1750 |
| -0.769 | -0.1061 | .296 | 1261 |
| -1.019 | -0.1407 | .193 | 822 |
| -1.269 | -0.1752 | .112 | 477 |
| -1.519 | -0.2098 | .049 | 209 |
| -1.769 | -0.2442 | .012 | 51 |
| -2.019 | -0.2788 | 0.0 | 0 |
| -2.039 | -0.2815 | 0.0 | 0 |

$$U_0 = 1,242\sqrt{h} \quad \text{and } h = 11.75 \text{ cms.}$$

Therefore $U_0 = 4260$ cms.per sec.

Table 10.3 (See also tables 11.2 and 11.3).

Effect of variation of air speed on mean ordinate of form drag diagrams.

Staggered arrangement. - First Row - Centre Tube 3.8 cms. from back wall.

Air Conditions 20.5°C 29.79"Hg.

| Expt. No. | Cathetometer cms. of water. | $V_{N.max}$ cm. per sec. | $\frac{V_{N.max.d}}{V}$ | $\frac{p}{\rho V_{N.max}^2}$ | $h' =$ mean ordinate cms. of water. | $p = h' \rho V_{N.max}^2$ |
|-----------|-----------------------------|--------------------------|-------------------------|------------------------------|-------------------------------------|---------------------------|
| 1 | 0.2492 | 1,857 | 15,630 | 0.2385 h' | 1.74 | 0.4155 $\rho V_{N.max}^2$ |
| 2 | 0.3211 | 2,107 | 17,720 | 0.1853 h' | 2.25 | 0.4172 $\rho V_{N.max}^2$ |
| 3 | 0.459 | 2,522 | 21,220 | 0.1296 h' | 3.245 | 0.4210 $\rho V_{N.max}^2$ |
| 4* | 1.179 | 3,950 | 36,000 | 0.0505 h' | 8.48 | 0.4285 $\rho V_{N.max}^2$ |
| 5 ϕ | 1.144 | 139.8 | 16,730 | 1.528 h' | 8.33 | 0.4176 $\rho V_{N.max}^2$ |

* Air conditions 9.0°C 29.83"Hg

ϕ Water Flow Water 17.8°C

Table 11.2 (See also table and figure 5.4C)

Effect of variation of air speed on mean ordinate of form drag diagrams.

Parallel arrangement - Fourth row - Centre Tube - 3.8 cms. from back wall.

Air conditions 10.6°C 30.13" Hg.

| Expt. No. | Cathetometer Cms. of water | $V_{N,max}$ cms. per sec. | $\frac{V_{N,max} d}{\nu}$ | $\frac{p}{\rho V_{N,max}^2}$ | $h' =$ mean ordinate cms of water | $p = h' \rho V_{N,max}^2$ |
|-----------|----------------------------|---------------------------|---------------------------|------------------------------|-----------------------------------|---------------------------|
| 1 | 1.432 | 4,355 | 39,600 | 0.04195 h' | 6.51 | $0.2732 \rho V_{N,max}^2$ |
| 2 | 1.163 | 3,921 | 35,700 | 0.0517 h' | 5.46 | $0.2825 \rho V_{N,max}^2$ |
| 3 | 0.665 | 2,966 | 27,000 | 0.0905 h' | 3.395 | $0.3075 \rho V_{N,max}^2$ |
| 4 | 0.406 | 2,319 | 21,100 | 0.1478 h' | 2.11 | $0.3120 \rho V_{N,max}^2$ |

Table 11.3

Effect of variation of air speed on mean ordinate of form drag diagrams.

Staggered arrangement - Sixth Row - Tube above centre line - 3.8 cms. from back wall.

Air conditions 17.0°C 30.10" Hg.

| Expt. No. | Cathetometer Cms. of Water | $V_{N,max}$ cms. per sec. | $\frac{V_{N,max} d}{\nu}$ | $\frac{p}{\rho V_{N,max}^2}$ | $h' =$ mean ordinate cms of water | $p = h' \rho V_{N,max}^2$ |
|-----------|----------------------------|---------------------------|---------------------------|------------------------------|-----------------------------------|---------------------------|
| 1 | 1.168 | 3,973 | 34,530 | 0.0509 h' | 4.215 | $0.2146 \rho V_{N,max}^2$ |
| 2 | 1.040 | 3,753 | 32,600 | 0.0571 h' | 3.690 | $0.2108 \rho V_{N,max}^2$ |
| 3 | 0.632 | 2,924 | 25,400 | 0.0942 h' | 2.362 | $0.2225 \rho V_{N,max}^2$ |
| 4 | 0.2552 | 1,858 | 16,150 | 0.2332 h' | 1.088 | $0.2538 \rho V_{N,max}^2$ |

BIBLIOGRAPHY.

BREAKAWAY.

The air flow around a circular cylinder in the region where the boundary layer separates from the surface. A.Fage. R & M.No.1179,1928-29 Vol.1. p.148.

Breakaway of boundary layer on a cylinder and an aerofoil J.J.Green. R & M.1396. 1930.

BOUNDARY LAYER AND TANGENTIAL DRAG.

Measurements of the distribution of the velocity of a fluid in the immediate neighbourhood of a plane smooth surface. J.M.Burgers and Van der Hegge Zijnen. Thesis Delft.1924.

The viscous layer associated with a circular cylinder. J.J.Green. R & M.1313 1929-30.Vol.1. p.256.

Experimental investigation of boundary layer flow. L.F.G.Simmons and A.F.C.Brown. R & M.1547. 1934.

Steady flow in the boundary layer near the surface of a cylinder in a stream. L.Howarth. R & M.1632.

Skin friction. L.Bairstow. Jour.Roy.Aero.Soc. 1925. Vol.29. p.3.

The boundary layer and recent developments. L.Bairstow. Jour.Roy.Aero.Soc. Feb.1936.

DIFFUSION.

Experiments on heat transmission based upon the diffusion method developed by H.Thoma. W.L.Lohrisch. Forschungsarbeiten. No.322. 46-68.

Extracts of Inst.of Civil Engineers. 139. April 1930.

The evaporation of water from plane and cylindrical surfaces. R.W.Powell and E.Griffiths. Trans.Inst.Chem. Eng.Vol.13 - 1935, p.175.

Bibliography, continued.

EDDIES & VORTICES.

Eddies and the diffusion of momentum. A.Mallock. R & M.314
1916-17 Vol.1. p.13.

On eddies in air. H.Nisi and A.W.Porter. Phil.Mag.Vol.46.
1923, p.754.

On eddies formed behind apertures through which air is
streaming. A.L.Griffith and A.W.Porter. Phil.Mag.Vol.49.
1925 p.649.

Vortex motion: Preliminary report upon an experimental
method of investigation by the aid of kinematograph
photography, the history of eddying flow past a model
immersed in water. J.L.Nayler and R.A.Frazer. R & M.332.
1917-18 Vol.1. p.18.

- (a) On the sound emitted by wires of circular section when
exposed to an air current. E.F.Relf. Phil.Mag.1921.
Vol.42 p.173.
- (b) On the frequency of the eddies generated by the motion
of circular cylinders through a fluid. E.F.Relf and
L.F.G.Simmons. Phil.Mag.1925, Vol.49. p.509.
- (c) On the system of vortices generated by a circular cylinder
in steady motion through a fluid. C.N.Lock. R & M.986.
1925.

N.B. Works (a) (b) and (c) should be read in this order.

- (d) The effect of upwind disturbances in the air current of
the channel upon the forces on models with special refer-
ence to the effect on the drag of an airship model.
E.F.Relf and T.Lavender. R.& M.597. 1918-19 Vol.1.p.79.
- (e) On the dissipation of eddies. G.I.Taylor. R & M.598.
1918-19. Vol.1. p.73.
- (f) The decay of eddies. H.A.Webb. R & M. 609
1918-19.

N.B. Works (d) (e) and (f) should be read in this order.

ELECTRIC TRAY.

An electrical method of tracing stream lines for the
two dimensional motion of a perfect fluid. E.F.Relf.
R & M.905. 1924.

Bibliography, continued.

A mechanical method for solving problems of flow in compressible fluids. G.I.Taylor and C.F.Sharman. R.& M.1195. 1928.

Report on progress during 1927-28 in calculation of flow of compressible fluid and suggestions for further work. G.I.Taylor. R.& M.1196. 1928.

ENTRAINMENT.

The discharge of air through small orifices and the entrainment of air by the issuing jet. J.S.G.Thomas. Phil.Mag.1922 Vol.44 p.969.

The entrainment of air by a jet of gas issuing from a small orifice in a thin plate. J.S.G.Thomas and E.V.Evans. Phil.Mag.1923 Vol.46. p.785.

Calculation of turbulent spreading flow. W.Tollmien. Zeitschrift für angewandte Mathematik und Mechanik 1926. Vol.6. p.468.

FORM DRAG AND TOTAL DRAG OF CYLINDERS.

Determination of the pressure distribution round a cylinder. A.Fage. R.& M. 106, 1913-14. p.65.

Discussion of the results of measurements of the resistance of wires, with some additional tests on the resistance of wires of small diameter. E.F.Relf. R.& M. 102. 1913-14, p.47.

An investigation of fluid flow in two dimensions. A.Thom. R.& M.1194. 1928-29, Vol.1. p.166.

The drag of circular cylinders and spheres at high values of Reynolds numbers. A.Fage. R.& M.1370. 1930-31.Vol.1. p.172.

HEAT TRANSFER.

Fluid friction and its relation to heat transfer. C.M.White. Inst.Chem.Ens. 1932, Vol.10, p.66.

The mechanism of heat transmission; distribution of heat flow about the circumference of a pipe in a stream of fluid. T.B.Drew and W.P.Ryan. Amer.Inst.of Chem.Ens. 1931, Vol.26, p.118.

Bibliography, continued.

The average and local rates of heat transfer from the surface of a hot cylinder in a transverse stream of fluid. J.Small. Phil.Mag. 1935, p.251.

The melting of an ice cylinder in a transverse hot air stream V.Klain. Archiv.fur Wärmewirtschaft. June 1934.

PITOT AND STATIC TUBES.

The development and theory of the Pitot tube. A.H.Gibson. The Engineer, July 10th and 17th. 1914., p.29.and 59.

Notes on the Pitot tube. J.Airey. Engineering News 1913. Vol.69, p.782. The Pitot tube: its formula. W.Monroe White. Association of Engineering Societies 1901. Vol.27, p.35.

The motion of gases in pipes and the use of gauges to determine the delivery. R.Threlfall. Pro.Inst.Mech.Engs.1904, parts 1 and 2, p.245.

On a determination of the Pitot-static tube factor at low Reynolds' numbers with special reference to the measurement of low air speeds. E.Ower and F.C.Johansen. R.& M.1437,1931-32 Vol.2, p.1049.

On the determination on the whirling arm of the pressure - velocity constant for a Pitot (velocity head and static pressure) tube and on the absolute measurement of velocity in aeronautical work. F.H.Bramwell, E.F.Relf and A.Fage. R.& M.71, 1912, p.35.

The design of Pitot-static tubes, E.Ower and F.C.Johansen, R.& M.981, 1925, p.985.

On the conditions at the boundary of a fluid in turbulent motion (including account of specially designed surface tube) T.E.Stanton, D.Marshall and C.N.Bryant. Pro.Roy.Soc.,A 1920. Vol,97. p.413.

On the use of very small Pitot tubes for measuring wind velocities M.Barker. Pro.Roy.Soc.1922, Vol.101, p.435.

The measurement of fluid velocity and pressure. J.R.Pannell. Pub.Edward Arnold & Co., 1924.

RESISTANCE OF NESTS.

Pressure drop across tube banks. T.H.Chilton and R.P.Genereaux Contribution No.127 from the Experimental Station. E.l. du Pont de Nemours & Co.

Bibliography, continued.

STREAM FUNCTION AND VELOCITY POTENTIAL.

The elements of aerofoil and airscrew theory. H.Glauert
Chapter 3 and 5. Pub.University Press. Cambridge 1930.

TURBULENCE.

The behaviour of fluids in turbulent motion. A.Fage.
Pro.Roy.Aero.Soc. 1933.

Turbulent flow in a circular pipe. A. Fage. Phil.Mag.
Vol.21. 1936, p.80.

The effect of up-wind disturbances in the air current of
the channel upon the forces on models with special reference
to the effect on the drag of an airship model. E.F.Relf
and T.Lavender. R & M.597. 1918-19 Vol.1. p.79.

The effect of turbulence and surface roughness on the
drag of a cylinder. A.Fage and J.H.Warsap. R.& M.1283
1929.

Comparative measurement of turbulence by three methods
Simmons, Fage and Townend. R.& M.1651. 1934.

Statistical Theory of Turbulence.
Parts I,II and III. Distribution of dissipation of energy
in a pipe over its cross-section.
Part IV. Diffusion in a turbulent air stream.
G.I.Taylor. Pro. Roy.Soc.A. Vol.151, Sep.1935., p.421.

VISCOSITY.

"The Viscosity of Liquids" by Emil Hatschik.

VISIBILITY OF FLOW.

(1) Colour bands in water.

Osborne Reynolds. Phil.Trans.A.Roy.Soc.1883., p.935.

(2) Smoke in Air

Smoke photographs of turbulent flow in boundary layer
L.F.G.Simmons and N.S.Dewey. R.& M.1335. 1930-31,
Vol.1, p.141.

Experiments in which air flow is made visible with the
white smoke from titanium tetrachloride. W.S.Farren.
Jour.Roy.Aero.Soc.1932.,Vol.36, p.451.

(3) Aluminium powder in solution of glycerine.

On the motion of a sphere in a viscous fluid. W.E.Wil-
liams. Phil.Mag.1915.,Vol 29., p.526.

Bibliography, continued.

- (4) Condensed milk or a mixture of one part of carbon tetra chloride with four parts xylene.
Vortex motion. J.L.Nayler and R.A.Fraser. R & M.332. 1917-18, Vol.1.,p.18.
- (5) Aluminium dust on the surface of water flowing in an open channel.
Applied hydro and aeromechanics. O.G.Tietjens. Pub.McGraw-Hill Book Co.,1934.
- (6) Ultra microscope.
The behaviour of fluids in turbulent motion. A.Fage. Roy.Aero.Soc.1933.

On eddies formed behind apertures through which air is streaming. A.L.Griffith and A.W.Porter. Phil.Mag.1925, Vol.49, p.649. (smoke produced by burning magnesium ribbon).

VORTICITY.

The elements of airfoil and airscrew theory. H.Glauert. Chapter 4. Pub.University Press. Cambridge 1930.

The structure of vortex sheets. Fage,A. and F.C.Johansen. Phil.Mag.1928, Vol.5.,p.417.

On the flow of air behind an inclined flat plate of infinite span. A.Fage and F.C.Johansen. Pro.Roy.Soc.A. 1927, Vol.116, p.170.

The characteristics of a Karman vortex street in a channel of finite breadth. H.Glauert. R.& M.1151, 1928-29,Vol.1., p.62.

WIND TUNNELS.

Aerodynamical research and hydraulic practice. Fage A. Trans.Inst.Mech.Engs.1935.

INDEX.

A

| | |
|--|---------------|
| Ahlborn, F. | 7.1 |
| Allen - resistance of nest | Fig.1.7 |
| Aluminium dust - explanation of shape of form drag diagrams | 9.3 |
| - used in Ahlborn tank | 7.1 |
| Ames dial indicator | 8.2 |
| Anemometer - 107 miles per hour | 5.2 |
| Atmospheric temperature, pressure and humidity | Appendix No.1 |

B

| | |
|---|---------|
| Benzoin - tincture of benzoin as Ahlborn tank indicator | 7.3 |
| Blasius - boundary layer on first row of tubes | 8.5,8.7 |
| - estimation of boundary layer on bottom of Ahlborn tank | 7.21 |
| Boundary layer - estimation of thickness in Appendix No.4 air experiments | |
| - for isolated cylinder | 8.81 |
| - motion in boundary layer at bottom of Ahlborn tank | 7.23 |
| - thickness at bottom of Ahlborn tank | 7.21 |
| Breakaway - controlled by fluctuations of pressure more than variations of energy | 10.1 |

| | |
|--|--------------------|
| Breakaway - Karman Pohlhausen expression | |
| $\frac{dU}{dx} \cdot \frac{\xi^2}{\nu} \longrightarrow -12$ | 9.4 |
| - later on second and subsequent rows | 9.3 |
| - point of breakaway investigated with titanium-tetra-chloride | 6.3 |
| - point of breakaway investigated with magnetic rod | 6.3 |
| - relation of pressure recovery to point of breakaway | 9.4, Appendix No.5 |
| Burr-walnut flow pattern | 7.22 |
| C | |
| Camphor - burning camphor to produce soot | 12.2 |
| Carrier - resistance of nests | Fig. 1.7 |
| Cathetometer - 1.17 Cms. | 1.3, 5.2 |
| Celluloid box | 6.1 |
| Central ordinate - defined | 5.5 |
| Chattock tilting gauge | 1.3 |
| Chezy resistance formula | 1.6 |
| Chilton and Genereaux - resistance of nests | 1.7 |
| Circular sieve used to create artificial turbulence | 5.8 |
| Colour bands | 7.21, 7.24 |
| Copper Sulphate electrolite | 8.2 |
| Cylindrical lens | 2.6 |

D

| | |
|---|----------|
| "Dead water" defined | 9.1 |
| Dehn - resistance of nests | Fig. 1.7 |
| Diffusion experiments by Lohrisch | 7.7 |
| Diffusion from the surface of soap cylinder | 7.7 |
| Disc static tube | 3.2 |
| Dissipation of energy in dead water region | 9.6 |
| Drew and Ryan - flow pattern practically the same with non-isothermal conditions. | 7.24 |
| Dummy replacing dead water region | 2.6 |
| Dust - deposition of dust | 12.1 |

E

| | |
|---|-----|
| Eagle and Ferguson - necessity for cleaning the surfaces of the tubes | 5.8 |
| Elliptical tubes. | 7.3 |
| Entrainment in jets - Tollmien | 9.2 |

F

| | |
|---|------|
| Fage, A - Drop in resistance coefficient of cylinder at $R_e = 200,000$ | 9.3 |
| Form drag of isolated cylinder | 2.1 |
| Relation between shear stress and variation from mean velocity | 9.7 |
| Fage and Johansen - production of vortex sheets | 7.91 |
| velocity of eddy down stream = $0.8V_0$ | 7.22 |

| | | |
|-----------------|--|-----|
| Fage and Warsap | - reduction of drag due to initial turbulence | 5.7 |
| | reduction of drag due to irregularities on the surface | 9.3 |
| Farren, W.S. | - Air flow indicated with titanium-tetra-chloride | 6.2 |
| Free vortex | | 7.5 |

G

| | | |
|--------------|-----------------------------|------------|
| Gibson, A.H. | - Pitot and static tubes | 3.1 |
| Glauert, H. | - $p = \frac{1}{2}\rho V^2$ | 3.1 |
| | viscosity of water | Table 1.2B |

H

| | | |
|---|--|-----------|
| Heat transfer and tangential drag | | 5.9 |
| | and diffusion | 7.7 |
| Hiemenz pressure distribution around a cylinder | | 8.82 |
| Honeycomb | | 1.3 |
| Hooked Pitot-static tubes | | 3.2 |
| Howarth, L. | - boundary layer of constant thickness | 8.5 |
| | boundary layer for isolated cylinder. | Fig. 8.81 |
| | calculation of boundary layer | 9.4 |
| Hydrochloric acid and ammonia fumes | | 6.2 |

I

| | |
|---|---------------|
| Inviscid flow between a pair of cylinders | Appendix No.3 |
|---|---------------|

J

| | |
|---|------|
| Johansen and Fage - Production of vortex sheets | 7.91 |
| Velocity of eddy down stream = $0.8V_0$ | 7.22 |
| Johansen and Ower - Effect of position of hole and stem in static tubes | 4.2 |

K

| | |
|---|-----------|
| Karman-Pohlhausen expression for point of breakaway | 9.4 |
| Karman street | 7.3, 7.91 |
| Kinetic energy - distribution of K.E. throughout the nest | 9.5, 10.2 |

L

| | |
|--|------|
| Lavender and Relf - effect of initial turbulence in air stream | 5.8 |
| Latex as Ahlborn tank indicator | 7.3 |
| Linke, W. - Resistance coefficient of isolated cylinder in wind tunnel | 10.5 |
| Lohrisch diffusion experiments | 7.7 |
| Lux - used to remove oil in Ahlborn tank experiments | 7.21 |
| Lycopodium powder as Ahlborn tank indicator | 7.3 |

M

| | |
|---|-----|
| Mean ordinate = 0.72 of central ordinate | 5.5 |
| Milk - cow's milk as Ahlborn tank indicator | 7.3 |

| | |
|---|-----|
| Milk - condensed milk as Ahlborn tank indicator | 7.3 |
| - mixture of milk and tincture of benzoin | 7.3 |
| Mischungsweg - relation to shear stress | 9.2 |

N

| | |
|--|------|
| Nisi and Porter - eddies behind cylinder | 3.1 |
| velocity distribution in eddies | 7.5 |
| Nominal maximum velocity $V_{N,max}$ defined | 1.2 |
| Non-isothermal conditions | 7.24 |

O

| | |
|--|---------------------|
| Oblique flow over static tube | 3.2 & Appendix No.2 |
| Orientation of Pitot tube | 3.1 |
| Ower and Johansen - Effect of position of static hole and stem in static tubes | 4.2 |

P

| | |
|--|---------------|
| Paltz and Starr heat transfer from cylinder | 7.7 |
| Parabolic mirror | 2.6 |
| Perforated zinc to create artificial turbulence | 5.8, 9.3 |
| Pitot tube - correction in steep velocity gradient $\frac{d_i + 2d_o}{10}$ from geometrical centre towards region of higher pressure | 3.3 |
| cylindrical Pitot with oblique flow | Appendix No.2 |
| Hooked design | 3.2 |

| | |
|--|---------------|
| Pitot tube - "Shift" for cylindrical Pitot tube | 3.3 |
| Sledge Pitot-static tube | 4.2 |
| Pohlhausen - Karman Pohlhausen expression for point of breakaway | 9.4 |
| Polar diagrams | 2.3 |
| Potassium permanganate colour bands | 7.21, 7.24 |
| crystals | 7.23 |
| Potential function ϕ | Appendix No.3 |
| Prandtl - relation between shear stress and "mischungsweg" | 9.2 |
| Prandtl-Karman pipe resistance | 1.6 |
| Pressure tube with two holes at 60° | 5.2 |

R

| | |
|--|----------|
| Reiher - resistance of nests | Fig. 1.7 |
| Relf,E.F. - resistance coefficient of isolated cylinder in wind tunnel | 10.5 |
| - use of electric tray | 8.1 |
| Relf and Lavønder - effect of initial turbulence in air stream | 5.8 |
| Relf and Simmons - formation of eddies at high Reynolds' numbers | 7.4 |
| Resistance of nest compared with roughened pipes | 1.5 |
| Reynolds' analogy between change of momentum and heat transfer | 5.1 |
| analogy between change of momentum and diffusion | 7.7 |

Reynolds' numbers

| | | | |
|-----------|-----------------------------------|---|-------------|
| 11.6 | $= \frac{V_o d}{\nu}$ | for Nisi and Porter's experiments | 3.1 and 7.5 |
| 100 | $< Re$ | effect of viscosity on Pitot tube reading is not detectable - Thom | 3.1 |
| 286 | $= \frac{V_{N,max}.d}{\nu}$ | for breakaway experiments using latex as indicator | 7.3 |
| 1,500 | $\approx \frac{V_{N,max}.d}{\nu}$ | for most Ahlborn tank experiments | 7.6 |
| 2,800 | $= \frac{V_o d}{\nu}$ | for shaving soap diffusion experiment | 7.7 |
| 16,000 | $\approx \frac{V_{N,max}.d}{\nu}$ | for water flow over staggered nest | 1.2 and 2.1 |
| 18,544 | $= \frac{U_o d}{\nu}$ | for Hiemenz isolated cylinder | 8.82 |
| 35,000 | $\approx \frac{V_{N,max}.d}{\nu}$ | for most air experiments | |
| 39,600 | $= \frac{V_o d}{\nu}$ | for Paltz and Starr heat transfer experiments | 7.7 |
| 70,000 | $= \frac{V_o d}{\nu}$ | reduction of drag coefficient of isolated cylinders by slight irregularities on surface | 9.3 |
| 100,000 | $= \frac{V_o d}{\nu}$ | Relf and Simmons suggest a dead air region fringed with small eddies | 7.4 |
| 200,000 | $= \frac{V_o d}{\nu}$ | reduction in drag coefficient of isolated cylinder from 0.6 to 0.2 | 9.3 |
| Rietschel | - | resistance of nests | Fig. 1.7 |

Shaving soap diffusion experiment 7.7

Surface tension effects - oil on surface of water 7.21, 7.24

T

Tachometer - about 2100 r.p.m. 5.2 & Table 5.4C

Tangential drag - parallel arrangement
1.8% of total drag 5.7

staggered arrangement
7% of total drag 10.3

up to point of break-
away of first row of
tubes 8.84

Taylor, G.I. - on the causes of the dis-
sipation of eddies 7.92

on the rate of dissipation
of eddies 5.8

Thom, A. - correction for size of pressure
hole 3.1

- effect of viscosity on Pitot
tube reading 3.1

- tangential drag on isolated cylinder 5.7

Tietjens - recommendation to cover Ahlborn tank
models with paraffin wax 7.24

Titanium-tetra-chloride smoke 6.3

Tollmien, W. - entrainment in jets 9.2

Turbine draught tubes - loss of energy compared
with loss after last
row of tubes in nest 9.53

Turbulence - initial turbulence in air stream 5.8

V

| | |
|---|---------------------------|
| Variable air speed experiments | 5.4 |
| Velocity in eddies | Fig. 3.1C, 7.5, 7.6, 9.52 |
| Venturi meter - constant at 2.1 ft. of water | Fig. 2.1A |
| - loss of energy compared with loss after last row of tubes in nest | 9.53 |
| Vibration galvanometer | 8.2 |
| Vorticity - form drag dependent on the shedding of vorticity | 10.1 |

W

| | |
|---|------|
| Warsap, J.H. and Fage, A. - reduction in resist- ance coefficient by slight irregularities on the surface of a cylinder | 9.3 |
| Wax models of dead water regions or wakes | 8.5 |
| Webb, H.A. - on the causes of the dissipation of eddies | 7.92 |
| White, C.M. - tangential and form drag | 5.1 |
| tangential drag and heat transfer | 5.8 |
| Williams, W.E. - motion of a sphere through a solution of glycerine | 7.4 |
| - velocity distribution in an eddy | 7.5 |